AFFTC-TIM-08-06

TG-14A PARAMETER IDENTIFICATION (PROJECT HAVE MOTO)

WG CDR GYANDEEP SINGH
MAJ ROTEM MARIL
MAJ DEVIN TRAYNOR
CAPT MIKE MARLIN
CAPT ELLIOTT LEIGH

AFFTC

MAY 2008

FINAL REPORT

Approved for public release; distribution is unlimited.

AIR FORCE FLIGHT TEST CENTER
EDWARDS AIR FORCE BASE, CALIFORNIA
AIR FORCE MATERIEL COMMAND
UNITED STATES AIR FORCE

This Technical Information Memorandum (AFFTC-TIM-08-06, TG-14A Parameter Identification (Have MOTO) was prepared and submitted under Job Order Number M08C0200 by the Have MOTO test team, US Air Force Test Pilot School (USAFTPS), Edwards Air Force Base, CA 93524-6485.

Prepared by:

ELLIOTT J. LEIGH
Capt, USAF
Project Manager/Project Engineer

GYANDEEP SINGH
Wg Cdr, IAF (India)
Project Engineer

ROTEM MARIL
Maj, IAF (Israel)
Project Test Pilot

DEVIN S. TRAYNOR
Maj, USAF
Project Test Pilot

MICHAEL J. MARLIN
Capt, USAF
Project Engineer

Reviewed By:

CHAD E. RYTHER
Maj, USAF
Staff Monitor, USAF TPS

BRIAN A. KISH
Lt Col, USAF, PhD
Education Branch, USAF TPS

This report has been approved for publication:

TERRY M. LUALLEN
Col, USAF
Commandant, USAF TPS

AUG 25 2008

REPORT DOCUMENTATION PAGE

Form Approved
OMB No. 0704-0188

Public reporting burden for this collection of information is estimated to average 1 hour per response, including the time for reviewing instructions, searching existing data sources, gathering and maintaining the data needed, and completing and reviewing this collection of information. Send comments regarding this burden estimate or any other aspect of this collection of information, including suggestions for reducing this burden to Department of Defense, Washington Headquarters Services, Directorate for Information Operations and Reports (0704-0188), 1215 Jefferson Davis Highway, Suite 1204, Arlington, VA 22202-4302. Respondents should be aware that notwithstanding any other provision of law, no person shall be subject to any penalty for failing to comply with a collection of information if it does not display a currently valid OMB control number. **PLEASE DO NOT RETURN YOUR FORM TO THE ABOVE ADDRESS.**

1. REPORT DATE	2. REPORT TYPE	3. DATES COVERED *(From – To)*
May 2008	Final Technical Information Memorandum	14 to 28 March 2008

4. TITLE AND SUBTITLE
TG-14A Parameter Investigation

5a. CONTRACT NUMBER

6. AUTHOR(S)
Leigh, Elliott J., Captain, USAF
Traynor, Devin S., Major, USAF
Singh, Gyandeep, Wing Commander, IAF (India)
Maril, Rotem, Major, IAF (Israel)
Marlin, Michael J., Captain, USAF

5b. GRANT NUMBER

5c. PROGRAM ELEMENT NUMBER

5d. PROJECT NUMBER

5e. TASK NUMBER

5f. WORK UNIT NUMBER

7. PERFORMING ORGANIZATION NAME(S) AND ADDRESS(ES)
Air Force Flight Test Center
412th Test Wing
USAF Test Pilot School
220 South Wolfe Ave.
Edwards AFB CA 93524-6485

8. PERFORMING ORGANIZATION REPORT NUMBER
AFFTC-TIM-08-06

9. SPONSORING / MONITORING AGENCY NAME(S) AND ADDRESS(ES)
AFRL/AFOSR
POC: Dr. John Schmisseur
Arlington, VA
Commercial: (703) 696-6962

10. SPONSOR/MONITOR'S ACRONYM(S)

11. SPONSOR/MONITOR'S REPORT NUMBER(S)

12. DISTRIBUTION / AVAILABILITY STATEMENT
Approved for public release; distribution is unlimited.

13. SUPPLEMENTARY NOTES
CA: Air Force Flight Test Center, Edwards AFB CA CC: 012100

14. ABSTRACT
This report presents the results of Project Have MOTO which used parameter estimation to determine TG-14A stability derivatives. This test program demonstrated the ability to determine the stability derivatives using airborne flight test techniques. The USAF Test Pilot School (TPS), Class 07B, conducted 20 flight tests totaling 27.1 hours at Edwards AFB, California, from 17 to 25 March 2008.

15. SUBJECT TERMS
Parameter Identification,Stability Derivatives,Dynamic Scaling,SIDPAC (System Identification Programs for Aircraft),TG-14 Motorglider,Flight Testing,
Piccolo II

16. SECURITY CLASSIFICATION OF:			17. LIMITATION OF ABSTRACT	18. NUMBER OF PAGES	19a. NAME OF RESPONSIBLE PERSON
a. REPORT	b. ABSTRACT	c. THIS PAGE			Dr. John Schmisseur
UNCLASSIFIED	UNCLASSIFIED	UNCLASSIFIED	SAME AS REPORT	143	19b. TELEPHONE NUMBER *(include area code)* (703) 696-6962

Standard Form 298 (Rev. 8-98)
Prescribed by ANSI Std. 239.18

This page intentionally left blank.

PREFACE

The test team would like to thank everyone who worked in support of this project: Jim Murray, John Barbachano, David Hamilton, and Chris Valdivia. Thank you for getting our instrumented glider airborne.

This page intentionally left blank.

EXECUTIVE SUMMARY

This project used parameter estimation techniques to investigate dynamic scaling with an operational motorglider at the Test Pilot School. The Aeromot AMT 200S Super Ximango (TG-14A) was modified with a data acquisition system to record 3-axis accelerations, angular rates, angle of attack and sideslip, Euler angles, airspeed, altitude, temperature, and control positions of the rudder, ailerons, and elevators.

The primary objective was to estimate aircraft stability and control derivatives from flight test data. The secondary objective was to compare the derivatives to those measured and dynamically scaled during flight test of a one-fifth scale model. Flight testing of the full scale aircraft was accomplished at Test Pilot School from 14-24 March 2008. Flight test included Pitot-static calibration, angle of attack and sideslip calibration, and pitch and yaw-roll doublets for parameter estimation. The stability and control derivatives were estimated using a computational toolset called Systems IDentification Programs for AirCraft (SIDPAC), a collection of algorithms for parameter estimation.

The primary objective was met, though some of the data were scattered. The secondary objective was not met. Some of the parameter estimates were determined with a high level of confidence, while for others the data were scattered and difficult to interpret. Nevertheless, reconstruction of time histories using the final model estimates produced data very similar to the measurements. Without smooth conditions normally used for this type of data collection and programmed test inputs (PTIs), it would be difficult to improve the quality of data.

TABLE OF CONTENTS

LIST OF ILLUSTRATIONS

LIST OF TABLES

INTRODUCTION

Background

The University of Arizona and Air Force Office of Scientific Research (AFOSR) collaborated in a research program to investigate control strategies for boundary-layer separation of lifting surfaces through a combined approach of theory development, numerical simulations, laboratory experiments and free-flight test experiments. Successful control of boundary-layer separation had the potential to lead to major performance gains for many Air Force applications.

For their research, the University of Arizona constructed a flight-ready dynamically scaled 1/5 scale model of the TG-14A for wind/water tunnel and free-flight test experiments. The University of Arizona wanted to compare experimental data from the 1/5 scale to flight test data of a full size TG-14A to determine the "scalability" of their boundary-layer flow control strategies over a wide range of Reynolds numbers. The HAVE MOTO test team used established static stability and control derivative estimation and flight test techniques to determine the TG-14A's stability and control derivatives for comparison to experimental test results from the 1/5 scale model as conducted by the University of Arizona.

Chronology

The USAF Test Pilot School (TPS), Class 07B, conducted 20 flight tests totaling 27.1 hours at Edwards AFB, California, from 14 to 25 March 2008.

Test Item Description

The TG-14A (Figure 1) was a two place (side by side) T-tail motorglider built by Grupo Aeromot of Porto Alegre, Brazil, designed for soaring, pilot instruction, and training. The civilian designation for the TG-14A was the "AMT 200S Super Ximango." In addition to the standard aileron, elevator and rudder control surfaces, the TG-14A was equipped with spoilers on the main wing's upper surface, retractable main landing gear, and removable wingtip extensions (winglets) to increase the effective wingspan. The TG-14A was powered by a Bombardier-ROTAX (912S4) four cylinder, liquid cooled, horizontally opposed engine. The engine was rated at 100 horsepower at 5800 RPM , sea level. Engine controls consisted of a throttle, choke, and Propeller Pitch Control Lever (PPCL). For a more detailed description of the TG-14A refer to the aircraft flight manual (reference 1).

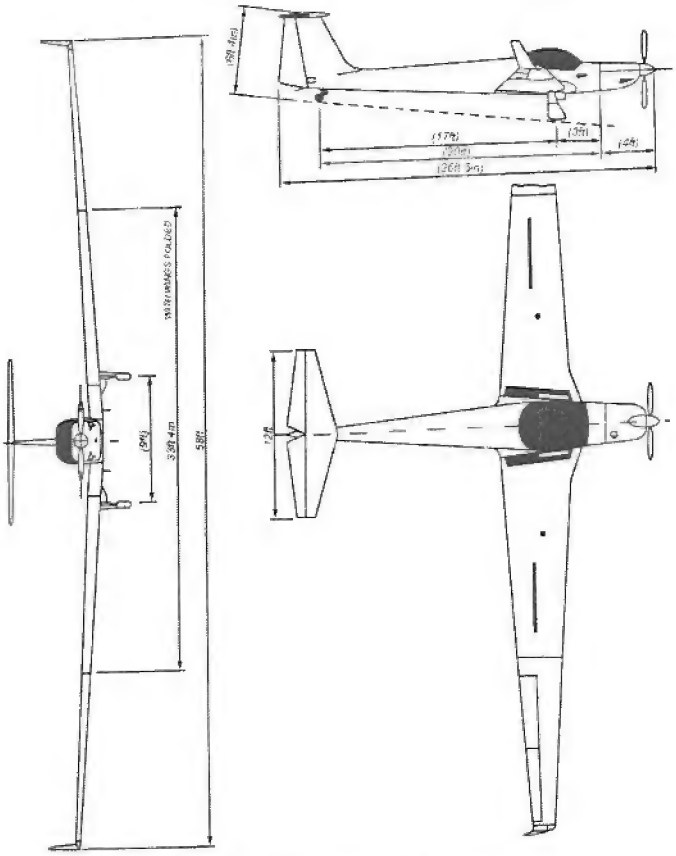

Figure 1. TG-14A Dimensions

The TG-14A used for the HAVE MOTO TMP was #02-0149 and was modified with flight test instrumentation to provide time histories of select data parameters required for calculating stability and control derivatives. The instrumentation consisted of a Cloud Cap Technologies Piccolo II data collection system installed between the aircrew seats, two additional air data probes (with angle of attack and sideslip vanes) installed at the folding joints of the two main wings and string potentiometer transducers installed on the main control surfaces. The Piccolo II was linked to a laptop computer onboard the aircraft and acted as the central data acquisition system for all data products. The Piccolo II also had the capability to relay data to a ground station via a 900MHz transmitter. A complete list of the data parameters recorded by the Piccolo II is available in appendix A.

Test Objectives

The overall objective of the HAVE MOTO TMP was to determine the stability and control derivatives of the TG-14A for comparison to dynamically scaled stability and control derivatives from a one-fifth scale model of the aircraft.

Objective 1 – Determine aircraft instrumentation accuracy.

Objective 2 – Determine stability and control derivatives.

Objective 3 – Compare stability and control derivatives to the one-fifth scale model.

Objective 4 – Determine the 3-dimensional center of gravity of the test aircraft.

All objectives were accomplished with the exception of objective 3. No data were obtained for the scale model, and therefore no comparison was done.

Limitations

The University of Arizona was unable to fly the one-fifth scale TG-14 model as a result of Federal Aviation Administration limitations. Consequently, objective 3 (compare stability and control derivatives to the one-fifth scale model) was not fulfilled.

This page intentionally left blank.

TEST AND EVALUATION

Aircraft Instrumentation Accuracy

In order to obtain accurate results for stability and control derivatives, the dynamic pressure and angle of attack and sideslip needed to be accurate. The pitot-static system was calibrated using the cloverleaf FTT and assuming zero total pressure error. Tower flyby and low altitude speed course FTTs were flown but the data were considered too noisy due to poor conditions. Angle of attack and sideslip vane corrections were obtained first by correcting the vane angles to the aircraft body axis, then using flight path reconstruction on data from pitch and yaw roll doublets. Additionally, Piccolo II measurements for angular rates (roll, pitch, and yaw) and body axis accelerations were checked for correct sense and magnitude using level turns, push over pull up, and bank to bank roll FTTs and comparing accelerometer and gyro measurements to handheld data.

A laser survey was performed in hangar 1600 at Edwards AFB. This survey used precision laser measurement equipment to determine the relative angles of each boom with respect to the aircraft body axis, as well as the position and orientation of the Piccolo relative to the center of gravity. The measurements of the Piccolo can be taken with confidence, however the booms were extremely flexible and were disturbed by the measurement equipment. Therefore, the numbers for boom offsets were not used. Instead, an inclinometer was used to measure the angle of the body axis and the angles of each boom, and the difference was used for the bias. The inclinometer was less intrusive to the measurement than the laser equipment, and no boom movement was observed while taking the measurements. The biases were subtracted from the measurements to correct them to the body axis. However, this was only possible for angle of attack. Yaw offsets from the laser survey were approximately zero, and no other method was used to estimate them. Consequently, the sideslip offsets were assumed to be zero. Therefore, they are a potential source of error in the data. There was not time to accomplish the measurement using any other method. **The yaw offsets for each boom should be determined using a non-intrusive measurement technique. (R1)**[1]

Table 1: Boom Angle Correction Results

Inclinometer	**Left Boom**	**Right Boom**
Angle of Attack Offset	2.0 deg	2.9 deg
Laser Survey	**Left Boom**	**Right Boom**
Angle of Attack Offset	1.5 deg	2.3 deg
Angle of Sideslip Offset	-0.79 deg	0.29 deg

Note: Inclinometer results were used for data reduction, and angle of sideslip offset was assumed zero.

[1] Numerals preceded by an R within parenthesis at the end of a sentence correspond to the recommendation numbers tabulated in the Conclusions and Recommendations section of this report.

Airspeed and Altitude Corrections

Airspeed and altitude correction data were collected using the Cloverleaf flight test technique (FTT) as described reference 2. Cloverleaf test points were flown over a range of airspeeds from 50 KIAS to 90 KIAS and a range of altitudes from 5,000 feet MSL to 10,000 feet MSL. Position error corrections for airspeed, ΔV_{pc}, and altitude, ΔH_{pc}, were calculated using methods also described in reference 2. Data are presented in appendix B and consist of plots of airspeed and altitude position error corrections as a function of instrument corrected velocity, Vic, for each wing mounted air data probe.

As shown in each figure of appendix B the position error corrections were small in magnitude and scattered about zero. A linear regression curve was fit to the data in each plot with 95% confidence intervals. For the right air data probe the maximum and minimum ΔV_{pc} and ΔH_{pc} values were +0.78/-0.76 knots and +7.0/-6.8 feet occurring at airspeeds of 86 and 77 KIAS respectively. For the left air data probe the maximum and minimum ΔV_{pc} and ΔH_{pc} values were +1.04/-0.42 knots and +8.4/-4.0 feet occurring at airspeeds of 86 and 77 KIAS respectively.

In general, the position error corrections were not significant for calculating stability control derivatives. The right air data probe tended to have a slight negative bias while the left air data probed tended to have slight positive bias. For calculating stability control derivatives the left and right air data were average which further reduced the effect of any position errors.

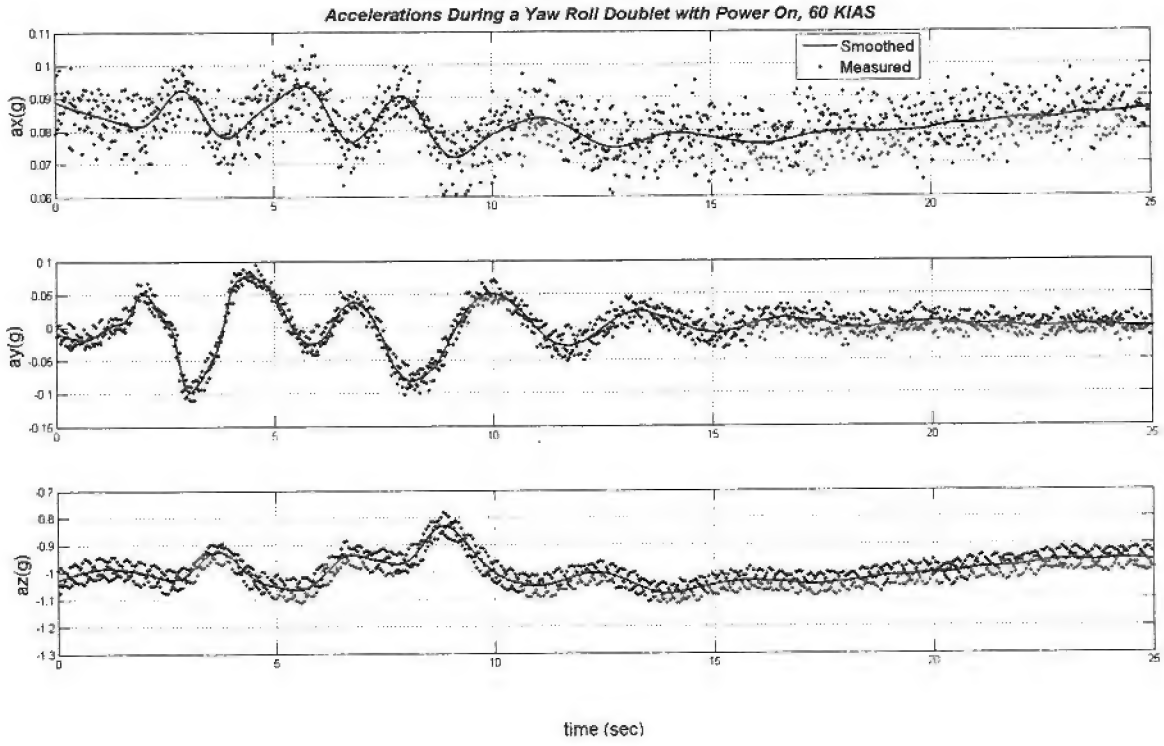

Figure 2: Measured Accelerations vs. Smoothed Accelerations with Power On

Angle of Attack and Angle of Sideslip Corrections

In order to determine accurate angle of attack and sideslip, the angles were first corrected to the body axis system and then a scale factor and bias for each were determined using flight path reconstruction on data from pitch and yaw roll doublets. This analysis was accomplished using an algorithm from SIDPAC (System Identification Programs for Aircraft), a MATLAB ® program, to generate estimates for stability and control derivatives (reference 3). Measured velocity, angle of attack, sideslip, angular rates, Euler angles, and accelerations were smoothed using an optimal global Fourier smoothing algorithm from SIDPAC. The smoothed inputs were treated as the actual inputs during the rest of the analysis. An example of smoothed inputs is shown in figure 2. The most noise in the data occurred with the accelerometers while the engine was running.

Next, the angle of attack and sideslip of each vane were corrected for pitch, roll, and yaw rates. Accelerations were also corrected for angular rates based on the c.g. position relative to the Piccolo. Finally, the algorithm determined if the accelerations, Euler angles, and angular rates were consistent with the air data using kinematic relationships. This is also called a data compatibility check. If the measurements were perfect, they would be completely satisfied by the equations of motion. The algorithm determined the scale factors and biases for the measurements using an output error method, and reconstructed the data using these correction factors. The measurements were corrected using the following formula:

$$x_{corrected} = x_{bias} + \frac{x_{measured}}{(1 + x_{scalefactor})}$$

Table 2: Angle of Attack Bias and Scale Factors

Power	Wingtips	Airspeed (KIAS)	α scale factor		α bias	
			Mean	Std Dev	Mean	Std Dev
Off	On	60	0.154	0.077	0.053	0.254
Off	On	80	0.215	0.016	0.0240	0.043
Off	Off	60	0.206	0.055	-0.342	0.225
On	On	60	0.133	0.103	-0.270	0.603
On	Off	60	0.230	0.018	-0.003	0.003

Note: Scale factors are unitless and biases are in degrees

The flight path reconstruction analysis was accomplished using doublets from each of the flight conditions tested. For angle of attack, the results from both vanes were averaged to generate a single angle of attack before the data compatibility analysis. The angles of sideslip were kept separate and analyzed separately to determine individual bias

and scale factors for each vane, and then the two vanes were averaged after the separate corrections were applied. Results are shown in appendix C. Tables 2 and 3 contain the means for each data set which were used for subsequent analysis. The bias for both angle of attack and sideslip was about zero, but the data were noisy. The scale factors were positive and easier to determine.

Table 3: Sideslip Bias and Scale Factors

Power	Wingtips	Airspeed (KIAS)	Left Boom				Right Boom			
			β scale factor		β bias		β scale factor		β bias	
			Mean	Std Dev	Mean	Std Dev	Mean	Std Dev	Mean	Std Dev
Off	On	60	0.202	0.016	-0.003	1.051	0.127	0.010	0.003	0.529
Off	On	80	-0.049	0.060	-0.302	1.217	0.151	0.007	-0.084	0.363
Off	Off	60	0.243	0.010	-1.279	0.177	0.116	0.015	-0.383	0.420
Off	Off	80	0.051	0.034	-0.124	1.371	0.124	0.013	0.515	0.364
On	On	60	0.253	0.026	-0.255	0.891	0.158	0.012	-0.126	0.743
On	Off	60	0.240	0.038	-0.534	0.590	0.160	0.003	-0.288	0.366

Note: Scale factors are unitless and biases are in degrees

Stability and Control Derivatives

Three static stability derivatives, three control power derivatives, and three damping derivatives were determined using parameter estimation techniques on data from pitch and yaw roll doublets. There were many contributors to noise which induced scatter in the data. The lateral data had less scatter overall than the longitudinal data, and some of the derivatives had very good estimates while others were questionable. At the end of the analysis, the final model was used to predict longitudinal and lateral-directional responses and determine how close the model matched the flight test data. The characteristic responses were the same, although there were some unexplained differences.

All test points were flown with the stick and rudders fixed during the free response. Rudder was defined as positive trailing edge left. Aileron deflection was defined as one half of the left minus the right aileron deflection, where trailing edge down was positive deflection. Elevator was defined as positive trailing edge down. Two different values of dynamic pressure were tested by flying two different values of calibrated airspeed, 60 KIAS and 80 KIAS. Flying constant calibrated airspeed kept dynamic pressure constant as altitude changed. Data were taken with wingtips on and off, and also with the engine on and off. The majority of the test points were flown at 60 KIAS with wingtips on, which was the primary test condition where the most confidence in the data was desired. Maneuvers with power off were flown in a steady glide, and power on points were obtained with maximum power while climbing back up to the top of the data band. Data were collected from 5,000 to 10,000 ft pressure altitude. Appendix A lists the parameters recorded by the Piccolo.

Measurements were smoothed using an algorithm in SIDPAC and corrected for the c.g. offset, boom offsets, and angular rates. To determine the position of the Piccolo with respect to the c.g., a laser survey was accomplished. The reference datum for all measurements was the tip of the propeller spinner, and the aircraft level reference was determined from the flight manual. Results are in table 4.

After correcting for c.g. offsets, bias and scale factor corrections were applied to the angle of attack, sideslip, and acceleration measurements. The stability and control derivatives were estimated for each maneuver using an output error algorithm. A confidence interval was generated on the means of each parameter for each condition. The results for each derivative at each condition are shown in appendix F. Standard Cramér-Rao boundaries are shown without any correction factors applied. These values are typical for a high aspect ratio, lightweight glider, and were successful in modeling the actual outputs from the flight data.

Table 4: Laser Survey Results for Piccolo II Placement

Piccolo Position Offsets	
X	-23.36 in
Y	3.21 in
Z	-9.34 in
Piccolo Angular Offsets	
Roll	1.35 deg
Pitch	-0.79 deg
Yaw	-0.53 deg

Note: these results are measured from the c.g. to the Piccolo

Longitudinal Stability and Control Derivatives

Longitudinal data were collected from pitch doublets. The characteristic response of the TG-14 in pitch was highly damped with no overshoots. A typical maneuver length was 6 seconds from pitch input to stable trimmed flight. Several strategies were used to estimate longitudinal parameters. First, the algorithm was set up to match only three states (α, q, a_z) and include only C_z and C_m parameters in the model. The resulting data were scattered, and resulted in poor results for V, θ, and a_x when reconstructing the data. Next, the algorithm was set up to match all six states (V, α, q, θ, a_x, a_z) using C_x, C_z, and C_m parameters in the model. For most cases, this condition was too strict and the algorithm could not converge on a solution. The best results were obtained by including C_x, C_m, and C_z parameters in the model and matching only five of the states (V, α, q, θ, a_z). Here, good results were obtained when reconstructing the data, with the exception of a_x, which was generally small in magnitude and not of concern. In some cases this caused the velocity to drift when reproducing responses from other inputs. However, it improved angle of attack, pitch rate, and g response and the data were more consistent than previous attempts. Therefore, this technique was applied to all of the data for the final analysis.

Standard, uncorrected Cramér-Rao boundaries were estimated for each maneuver and are shown in appendix F. The individual maneuvers had tight tolerances on these boundaries, but between maneuvers there was some scatter on the parameter estimates. Appendix D contains sample time histories of pitch doublet responses and model estimates. These estimates are based on the parameters determined for that particular maneuver.

Since the flight operations took place in March during warm weather over the lakebeds, there was always a small amount of turbulence present. Turbulence introduced some noise into the data, some of which was removed using smoothing techniques. However, large amplitude inputs were used to increase the signal to noise ratio and maximize the effectiveness of the smoothing techniques. This could have introduced nonlinear effects due to the range of angle of attack and sideslip that was experienced during the maneuvers. Additionally, there was no mechanism for a programmed test input (PTI), so every square wave input was slightly different. Low weathercock stability and yaw damping made it difficult to maintain trimmed flight without sideslip, so only maneuvers with less than +/- 1.5 degrees of sideslip were used. Pitch doublets often excited the Dutch roll mode in the data because of small aileron inputs. These were not observed in flight but traces could be seen in the data. Only data with good trim conditions and inputs were analyzed, but there were still some variations within those data for sideslip and pilot inputs.

To determine a final estimate for each derivative, the T statistic was computed for a 95 percent confidence interval on the mean of each data set. Some of the time histories from previous maneuvers were reconstructed using the final results to determine how successful the parameter estimation was. The results are in appendix G. The final model has similar characteristics as the flight data, including damping ratio and frequency, but the oscillations vary in amplitude and phase.

Overall, the longitudinal results were noisy and inconsistent. The longitudinal static stability was difficult to estimate, and data from engine on runs resulted in approximately neutral stability. Since the airplane did not fly as if it were neutrally stable, these estimates are incorrect. Nevertheless, the predicted response still follows that of the actual aircraft. Predicted responses were based on a state space model where the A and B matrices contained the stability and control derivatives. More accurate predictions could be obtained with the full set of nonlinear equations of motion, and may provide some insight into this situation. Insight into the results may be gained by using the full nonlinear set of equations of motion, and by using a nonlinear aeromodel for parameter estimation.

The pitch damping derivatives also had a lot of scatter. There does not appear to be significant difference between power on and off, or wingtips on and off conditions, but it would be difficult to tell with the scatter in the data. The elevator control power derivative was the most consistent, with the exception of the power on, wingtips off configuration, where only three runs were useable. It appeared to be constant at all flight conditions. The z force coefficients, which are related to the lift curve of the aircraft, were also determined and are contained in appendix F with the other data for completeness. Despite the poor data quality, the reconstructed outputs had the same characteristics of the flight data, and were successful at predicting the airplane response.

Lateral-Directional Stability and Control Derivatives

Lateral-directional data were collected from yaw roll doublets. A two second pause was observed between the two control inputs. The response was lightly damped and exhibited more yaw than roll. A typical maneuver was 25 seconds from the initial rudder input to stable trimmed conditions. Lateral directional derivative estimates were determined by matching five states (p, r, β, φ, a_y) and including C_n, C_l, and C_y parameters in the model. The data were more consistent than the longitudinal parameters, both in the scatter of the data and also in the ability to reproduce other maneuvers using different initial conditions and inputs. They also varied less with changes in conditions. Therefore, all five states were estimated and no changes were made to the initial output error algorithm.

Similar to the longitudinal response, uncorrected Cramér-Rao boundaries were estimated for each maneuver and are shown in appendix F. Appendix E contains sample time histories of yaw roll doublet responses and model estimates. These estimates are based on the parameters determined for that particular maneuver. In general, they match better than the longitudinal response. Potential sources of noise are the same as in the longitudinal case. Additionally, the rudder pedals were more difficult to center than the stick, making it difficult to obtain perfect trim conditions before and after the maneuver. Aileron inputs had a tendency to affect the elevator, and some maneuvers ended out of trim. The tolerance for sideslip was +/- 1.5 degrees, and the tolerance for bank angle (trim) was +/- 5 degrees. Variations in these conditions as well as input forms could account for scatter in the data.

To determine a final estimate for each derivative, a 95 percent confidence interval on the mean was computed using the T statistic for each data set. Some of the previous maneuvers were reconstructed using the final model to determine data quality. The results are in Appendix G. Like the longitudinal response, these were developed using a state space model provided by SIDPAC, and are therefore based on linearized equations of motion. The parameters exhibit less variation between flight conditions, and match the data well in frequency and damping ratio.

The dihedral ($C_{l\beta}$) had the worst scatter of all of the lateral-directional data. It was difficult to determine if there was an effect between flight conditions because of the scatter. The Cramér-Rao boundaries on individual maneuvers were worse than the other derivatives, and the individual results were scattered. The data suggest that the aircraft was stable, which was expected, and the magnitude is similar to other lightweight, high aspect ratio gliders. The results for both C_{lp} and $C_{l\delta a}$ were consistent between maneuvers and also did not change between flight conditions, which was expected. The Cramér-Rao boundaries were very tight on individual maneuvers. The yaw damping derivative (C_{nr}) was more difficult to estimate, and for most conditions only three or four useable doublets were obtained. Consequently, there is less confidence in these results. The means suggest that the parameter may be consistent over all flight conditions, but the standard error is too large to make this conclusion. The rudder control power ($C_{n\delta r}$) estimates were good, and were mostly consistent among all flight conditions. The data suggest that there may be a power effect, although only three points were accomplished with the power on and wingtips off. The weathercock stability ($C_{n\beta}$) was the most consistent static stability derivative. The Cramér-Rao boundaries were small, and the results were consistent. Sideforce derivatives were estimated and the results are

contained in appendix F for completeness. Overall, there were insufficient runs to make significant conclusions given the scatter observed in the data.

3-Dimensional Center of Gravity

The test aircraft was positioned on three calibrated scales with each wheel resting on a separate scale. Aircrew were present in the aircraft cockpit. The scales supporting the two main landing gear wheels were level with each other and the scale supporting the rear wheel was positioned above or below the horizontal plane of the main landing gear as shown in figure 3.

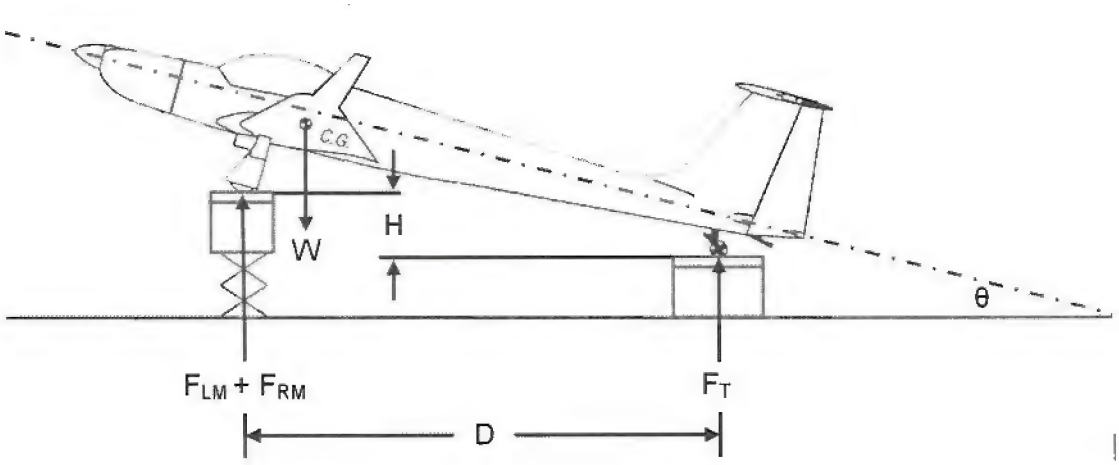

Figure 3. TG-14A CG Determination

W is total aircraft weight.
H is the vertical displacement between the surfaces of the two scales.
D is the lateral displacement between the aircraft main and tail wheels.
F_{LM} and F_{RM} are the measured forces from the scales at the main landing gear wheels.
F_T is the measured force from the scale at the tail wheel.
Θ is the longitudinal incline of the aircraft.

The aircraft location of the center of gravity in the X-Z plane was determined by setting the sum of the forces and moments equal to zero at multiple inclination angles. The resulting system of simultaneous equations was solved to give the location of the center of gravity. The center of gravity was assumed to be at the lateral centerline of the aircraft, and only x and z positions were determined. The results are shown in Table 6. The reference datum was the tip of the prop spinner, and all c.g. positions were determined with 360 lb of pilot weight. For all aircrew and equipment combinations, less than 20 lb of variation was observed in the pilot weight. The c.g. moved less than one

inch in both directions from full to empty fuel. These values were used to determine the relative position of the Piccolo with respect to the center of gravity.

Table 5. Center of Gravity Location

	Number of Measurements	Mean	95% Confidence Interval	
X zero fuel (in)	13	98.57	98.15	98.98
Z zero fuel (in)	13	9.84	8.12	11.46
X full fuel (in)	12	97.87	97.69	98.05
Z full fuel (in)	12	8.61	7.75	9.47

Note: Distances are measured with respect to the tip of the prop spinner

This page intentionally left blank

CONCLUSIONS AND RECOMMENDATIONS

The primary objective was met. Some of the parameter estimates were determined with a high level of confidence, while for others the data were scattered and difficult to interpret. Nevertheless, good results were obtained using data reconstruction with the mean values for each parameter at each flight condition. Contributing factors to the noise were lack of pure pilot inputs, variations in sideslip during maneuvers and at trimmed conditions, and atmospheric instabilities. Without smooth conditions normally used for this type of data collection and programmed test inputs (PTIs), it would be difficult to improve the quality of data. The c.g., air data calibration, and angle of attack and sideslip calibration were accomplished with one exception. Due to lack of confidence in the laser survey results for the boom measurements, an inclinometer was used to recalculate the angle of attack offset, and the sideslip offsets were assumed zero. **The yaw offsets for each boom should be determined using a non-intrusive measurement technique. (R1, page 5)**

Despite the scatter in the data, reconstruction of time histories using the final model estimates produced data very similar to the measurements. The angle of attack and sideslip matches were shifted in phase and slightly in magnitude, although they exhibited the same frequency and damping characteristics. However, the results for static stability did not make sense with power on for this aircraft. It is possible that the linear state space model is not adequately addressing the effect of this term, and a fully nonlinear model may reveal more accurate comparison of predicted to flight test data. Additionally, since large pilot inputs were used to increase the signal to noise ratio and account for the effects of turbulence, the use of a nonlinear aero model may be more appropriate for estimating the parameters.

REFERENCES

1. *Flight Manual, USAF Series Aircraft, TG-14A, Technical Order 1G-14(T)A-1*, ASC/YT, Wright Patterson AFB, OH, 2 June 2004.
2. *PF 701B Pitot Statics Textbook*, USAF Test Pilot School, Edwards AFB, CA, 1 March 2005.
3. *Aircraft System Identification: Theory and Practice*, Vladislav Klein and Eugene A. Morelli. June 2006.

APPENDIX A – LIST OF TG-14A DATA PARAMETERS

Parameter	Description	Sample Rate	Range	Resolution
a_x	Body axis acceleration	50Hz	-1g to 1g	0.001 ft/sec^2
a_y	Body axis acceleration	50Hz	-1g to 1g	0.001 ft/sec^2
a_z	Body axis acceleration	50Hz	-2g to 6g	0.001 ft/sec^2
p	Roll rate	50Hz	-100 to +100 degrees /second	0.01 deg/sec
q	Pitch rate	50Hz	-30 to +30 degrees /second	0.01 deg/sec
r	Yaw rate	50Hz	-60 to +60 degrees /second	0.01 deg/sec
P_t	Total Pressure	50Hz	1000 lb/ft^2 to 2500 lb/ft^2	0.1 lb/ft^2
P_s	Static Pressure	50Hz	1000 lb/ft^2 to 2500 lb/ft^2	0.1 lb/ft^2
δ_e	Elevator Position	50Hz	-20 to +20 degrees	0.05 deg
δ_r	Rudder Position	50Hz	-20 to +20 degrees	0.05 deg
δ_{al}	Left Aileron Position	50Hz	-20 to +20 degrees	0.05 deg
δ_{ar}	Right Aileron Position	50Hz	-20 to +20 degrees	0.05 deg
α_l	Left wing angle of attack	50Hz	-5 to 15 degrees	0.05 deg
α_r	Right wing angle of attack	50Hz	-5 to 15 degrees	0.05 deg
β_l	Left wing side slip	50Hz	-10 to +10 degrees	0.05 deg
β_r	Right wing sideslip	50Hz	-10 to +10 degrees	0.05 deg
P_{dl}	Differential Pressure Left wing	50Hz	0-300 lb/ft^2	0.5 lb/ft^2
P_{dr}	Differential Pressure Right wing	50Hz	0-300 lb/ft^2	0.5 lb/ft^2
P_{sl}	Static Pressure Left wing	50Hz	1000 lb/ft^2 to 2500 lb/ft^2	1.5 lb/ft^2
Psr	Static Pressure right wing	50Hz	1000 lb/ft^2 to 2500 lb/ft^2	1.5 lb/ft^2
OAT_l	Outside Air Temperature left wing	50Hz	-20^0 C to 50^{0}C	0.1^{0}C

APPENDIX B – AIR DATA CORRECTIONS

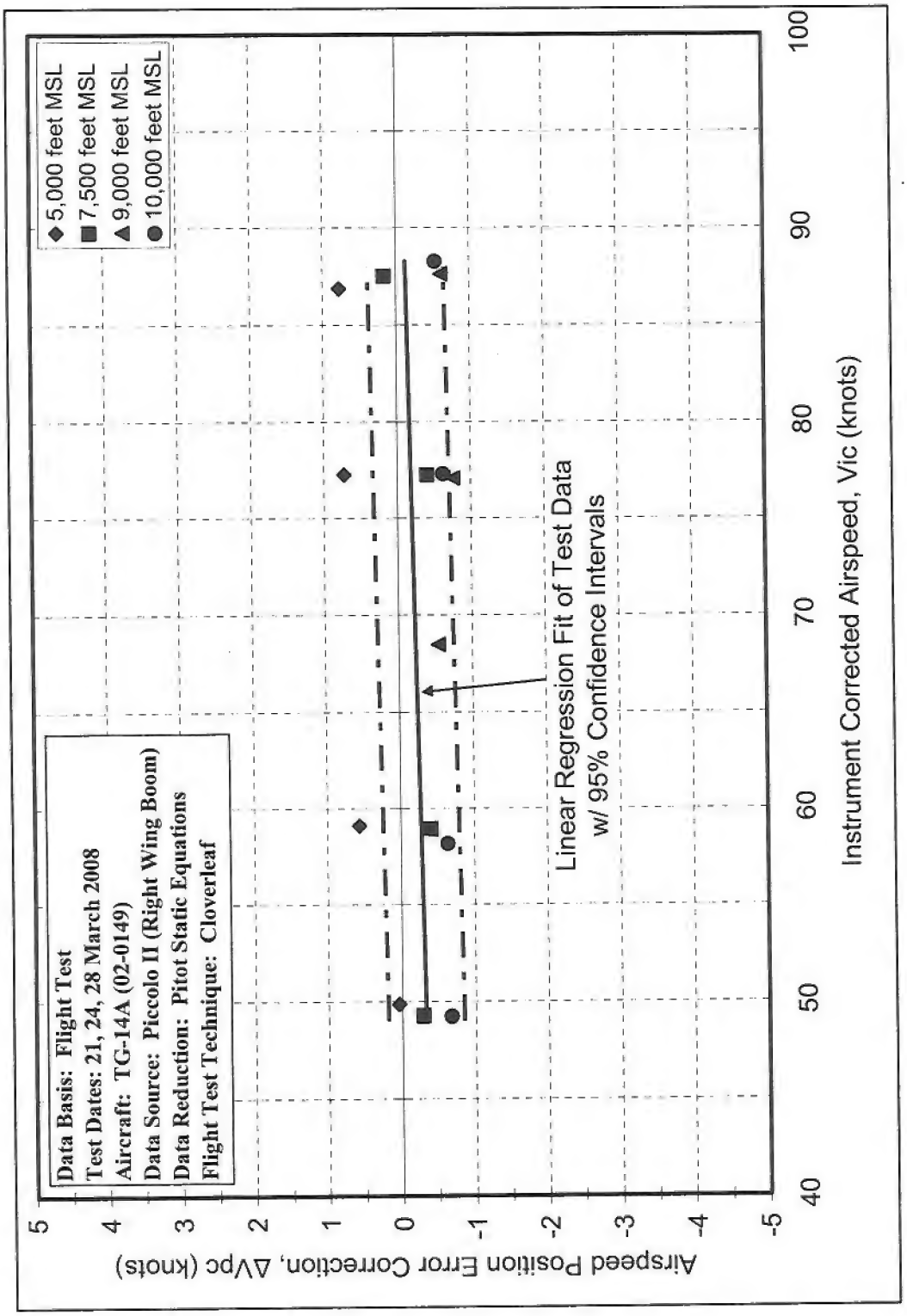

Figure B-1: Airspeed Position Error Correction as Function of Airspeed (Right Boom)

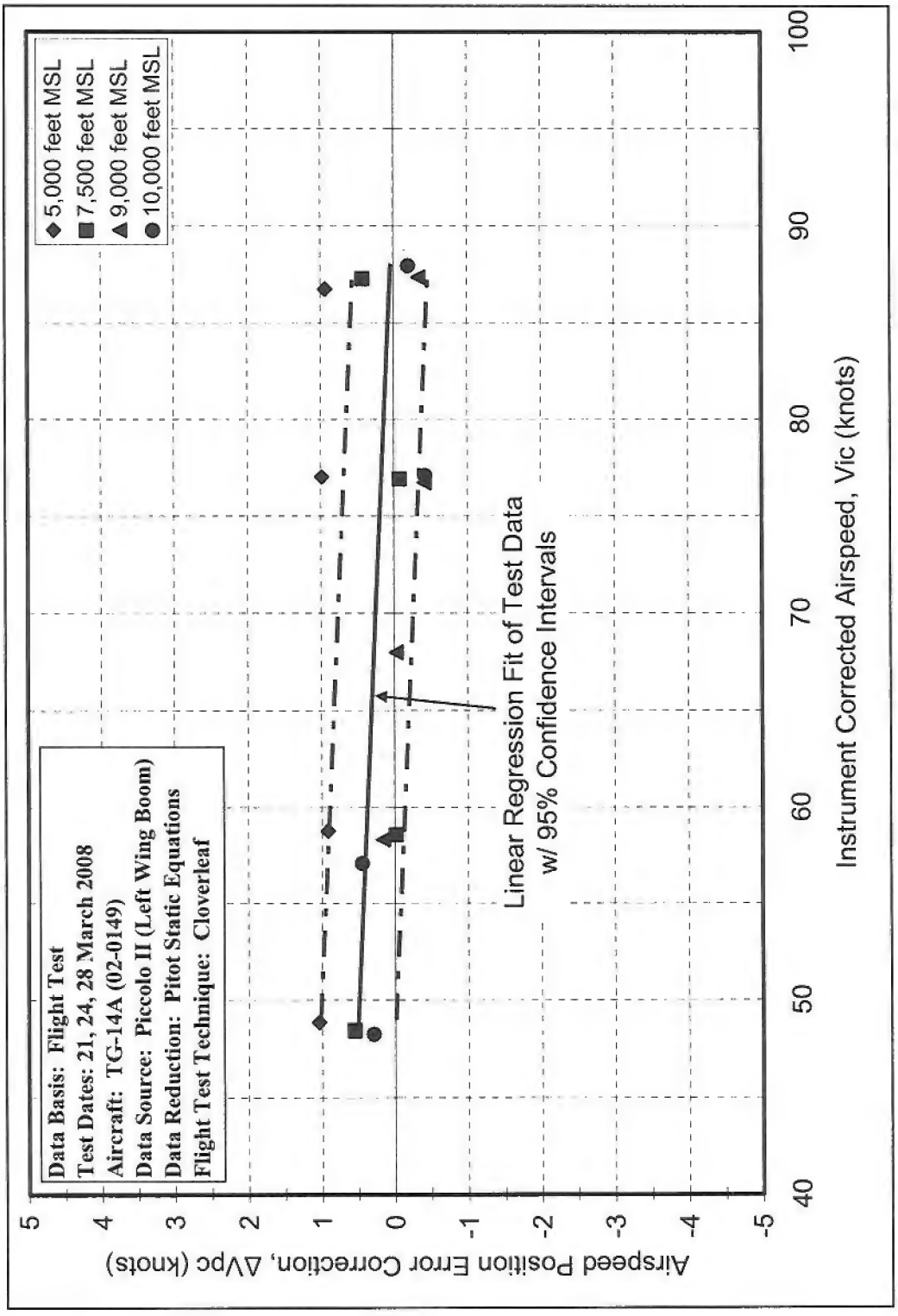

Figure B-2: Airspeed Position Error Correction as Function of Airspeed (Left Boom)

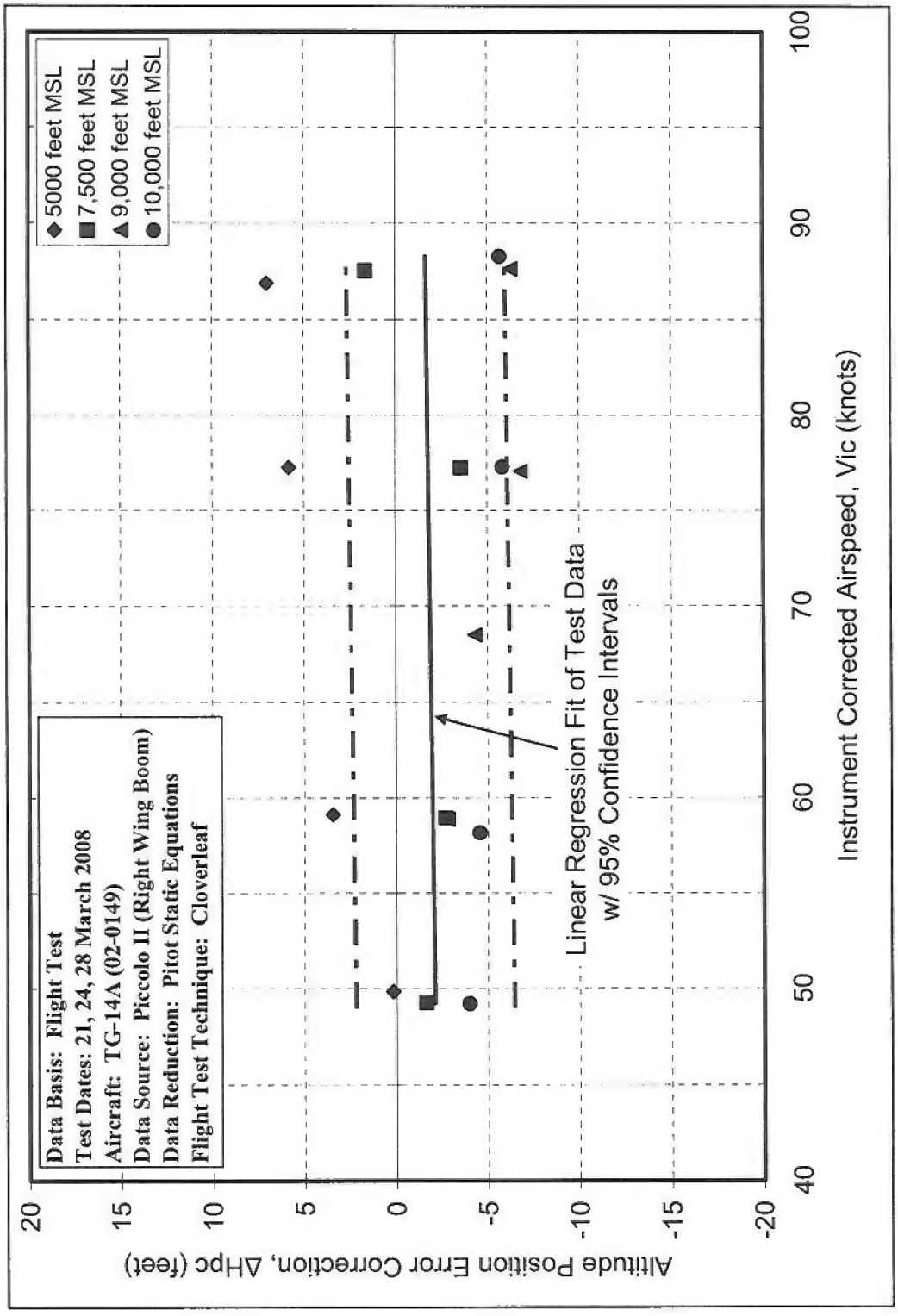

Figure B-3: Altitude Position Error Correction as Function of Airspeed (Right Boom)

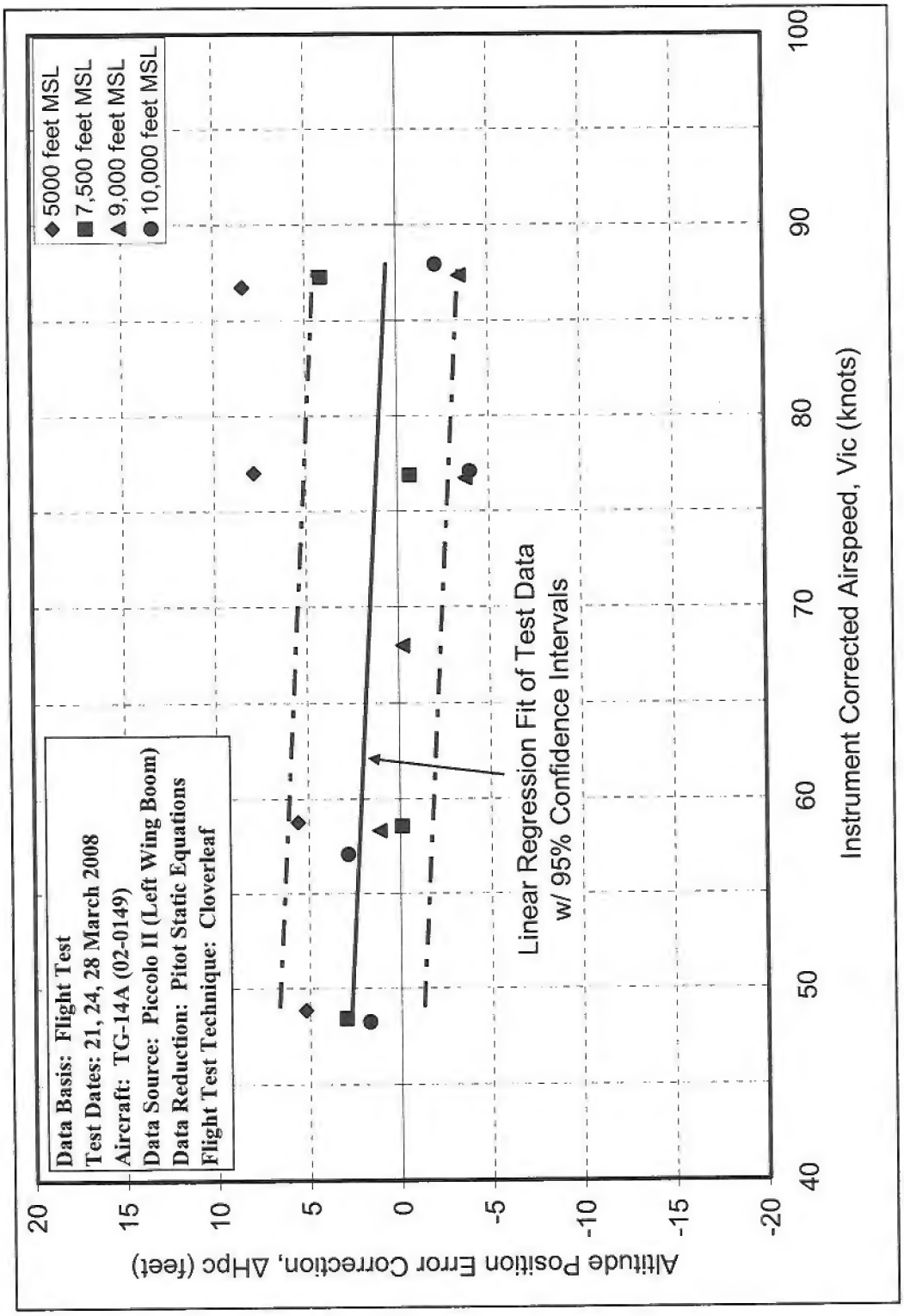

Figure B-4: Altitude Position Error Correction as Function of Airspeed (Left Boom)

APPENDIX C – AOA AND SIDESLIP CORRECTIONS

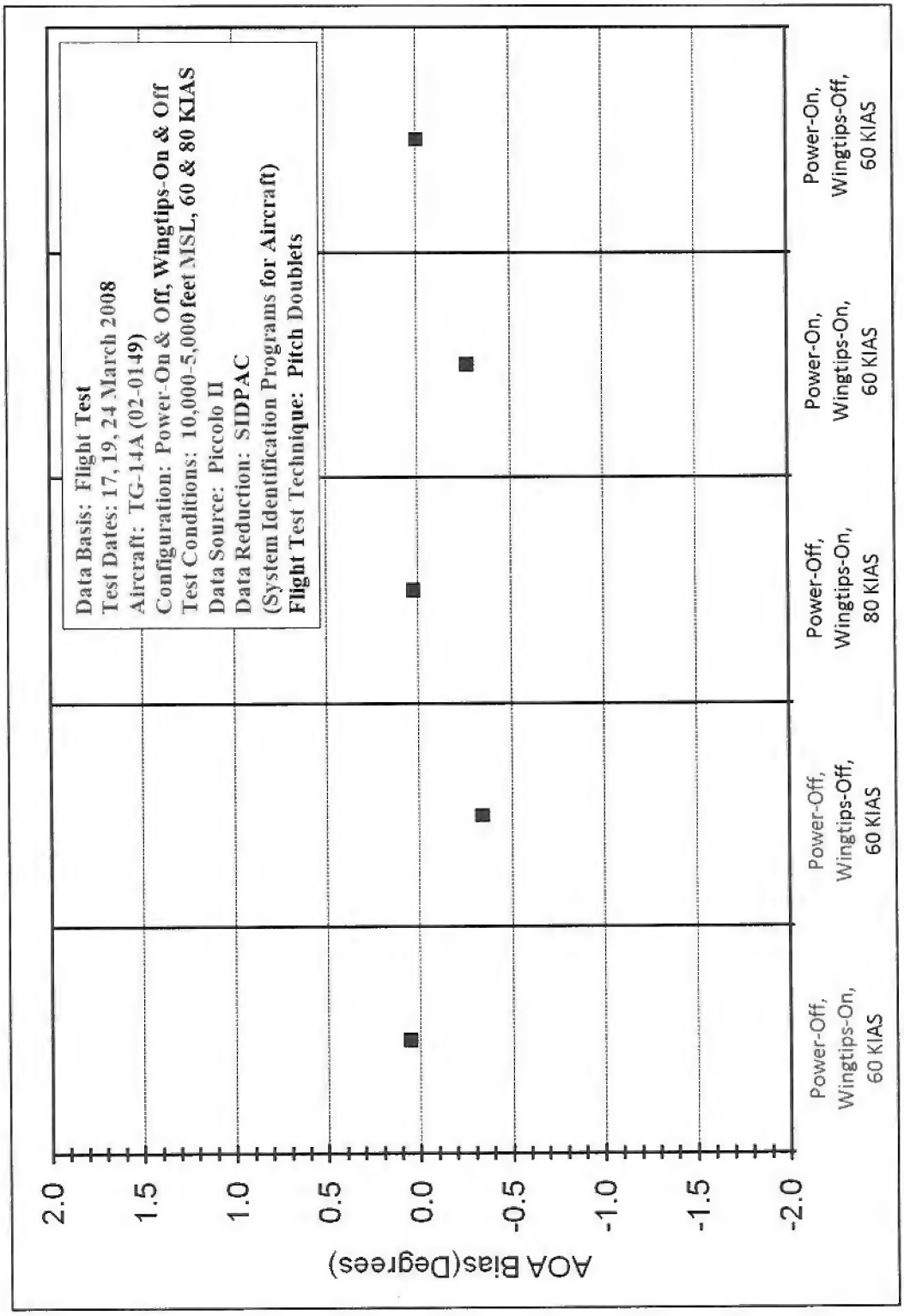

Figure C-1: Angle of Attack Bias

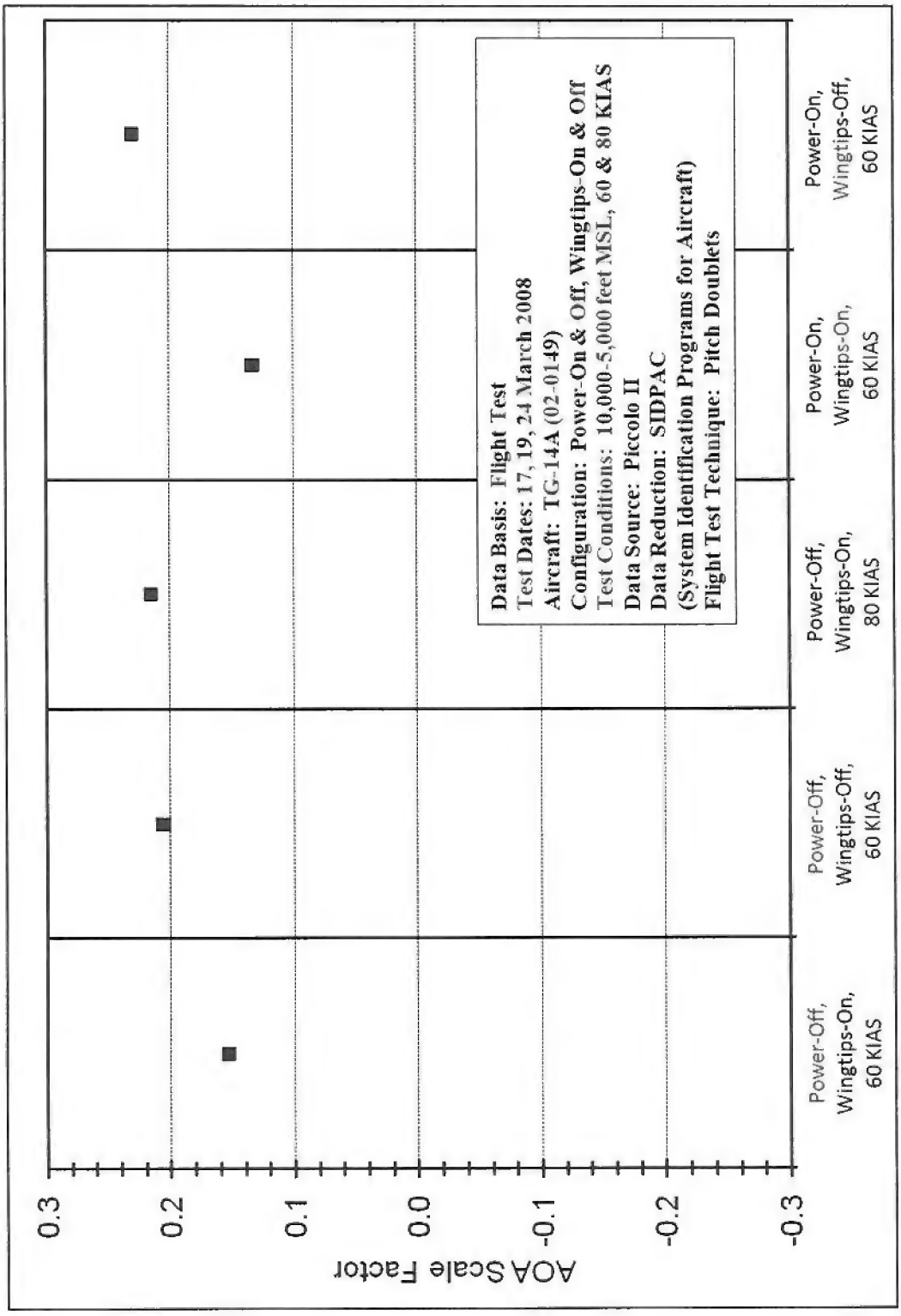

Figure C-2: Angle of Attack Scale Factor

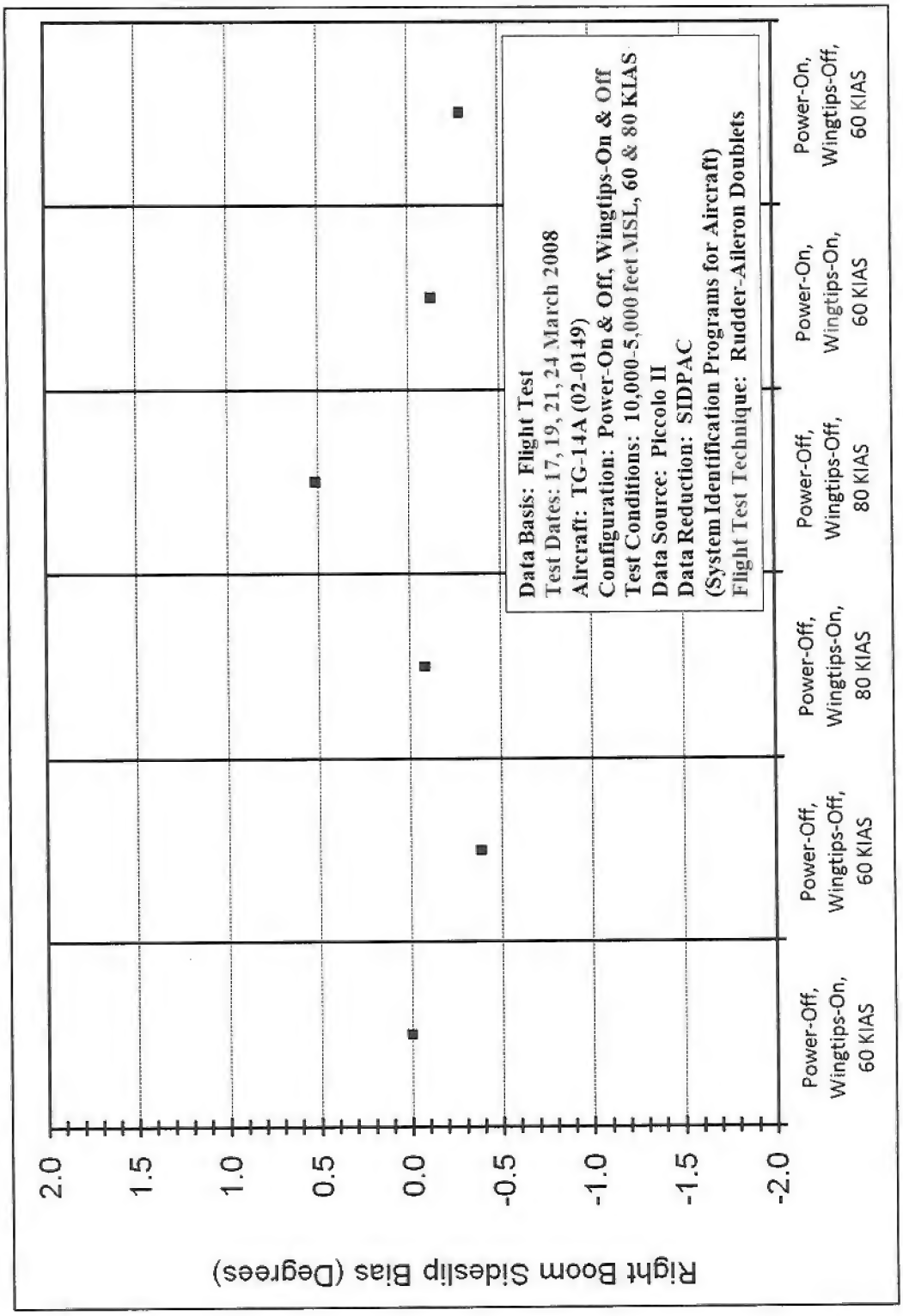

Figure C-3: Right Wing Air Data Boom Sideslip Bias

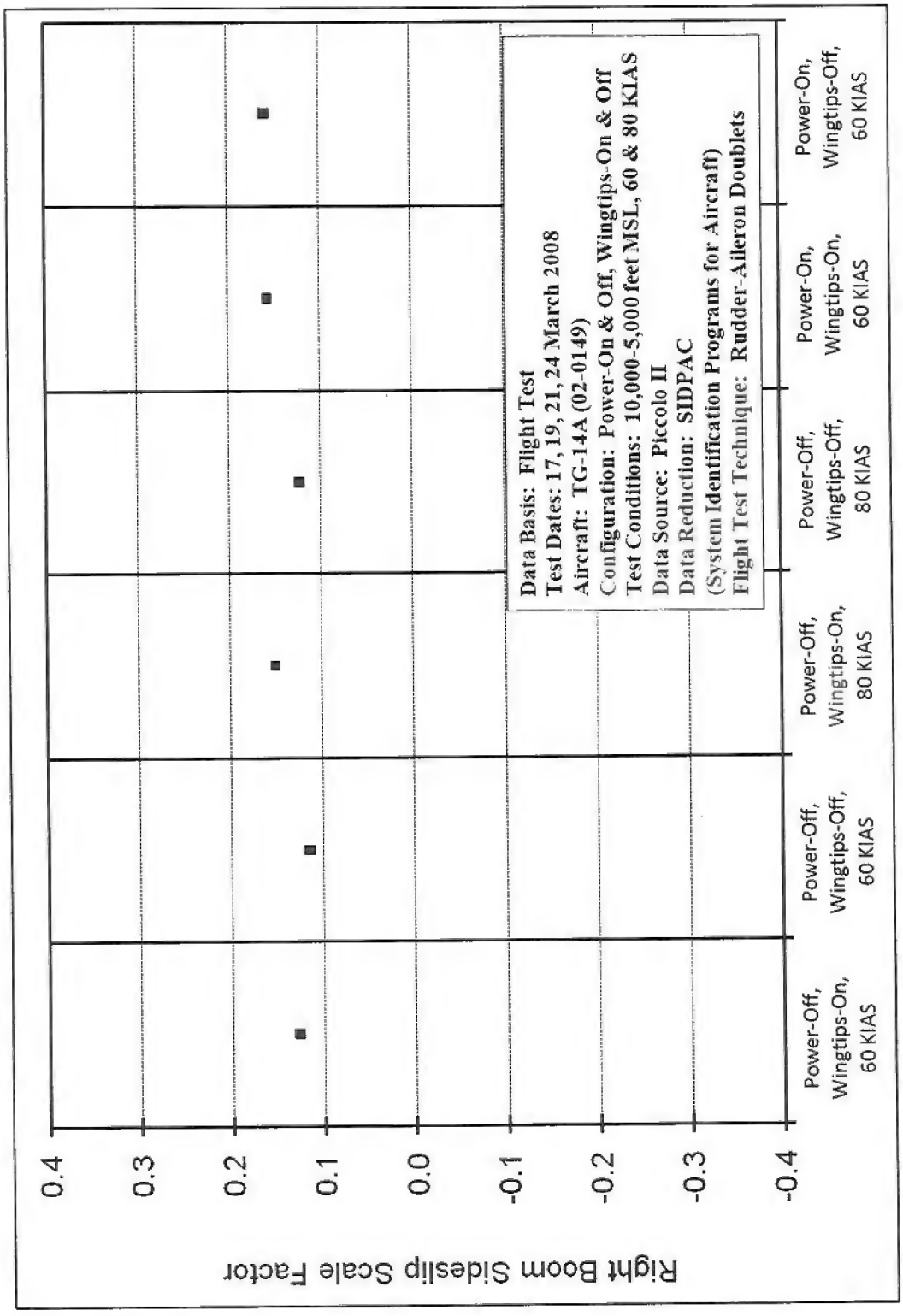

Figure C-4: Right Wing Air Data Boom Sideslip Scale Factor

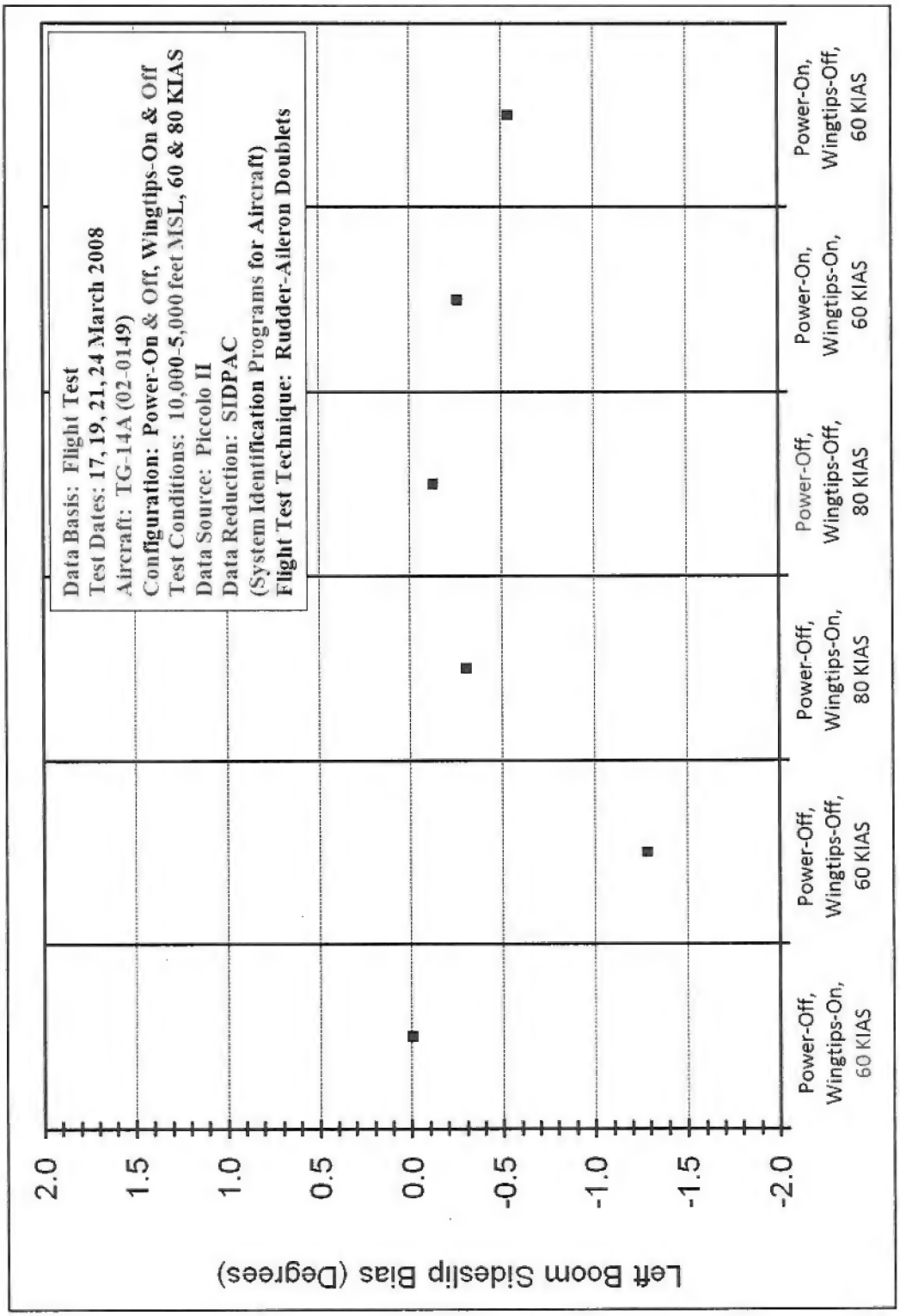

Figure C-5: Left Wing Air Data Boom Sideslip Bias

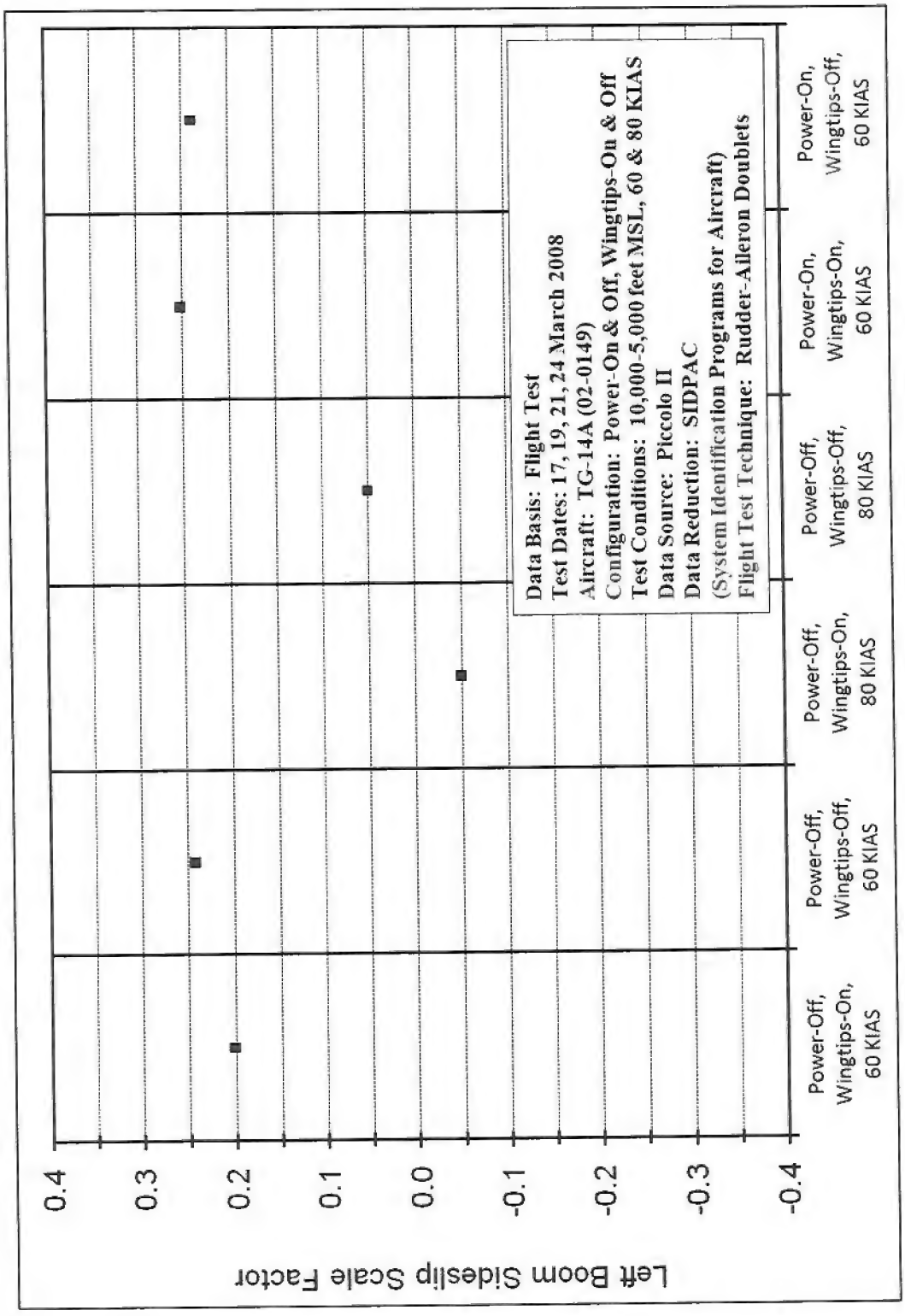

Figure C-6: Left Wing Air Data Boom Sideslip Scale Factor

APPENDIX D – SAMPLE LONGITUDINAL DATA

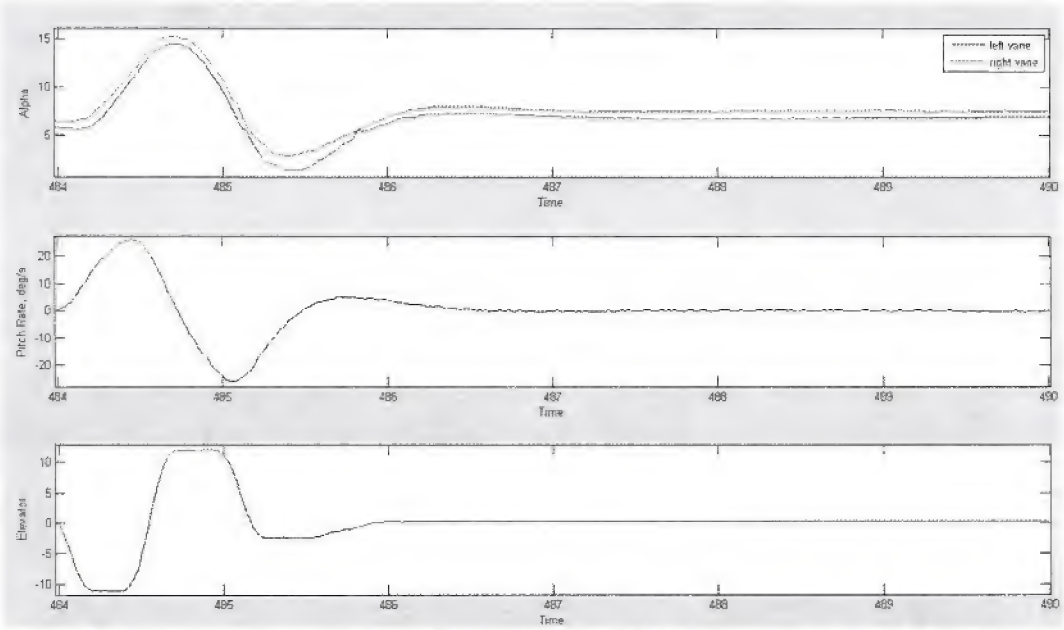

Figure D-1: Sample Time History for a Pitch Doublet (Wingtips on, Glide, 60 KIAS)

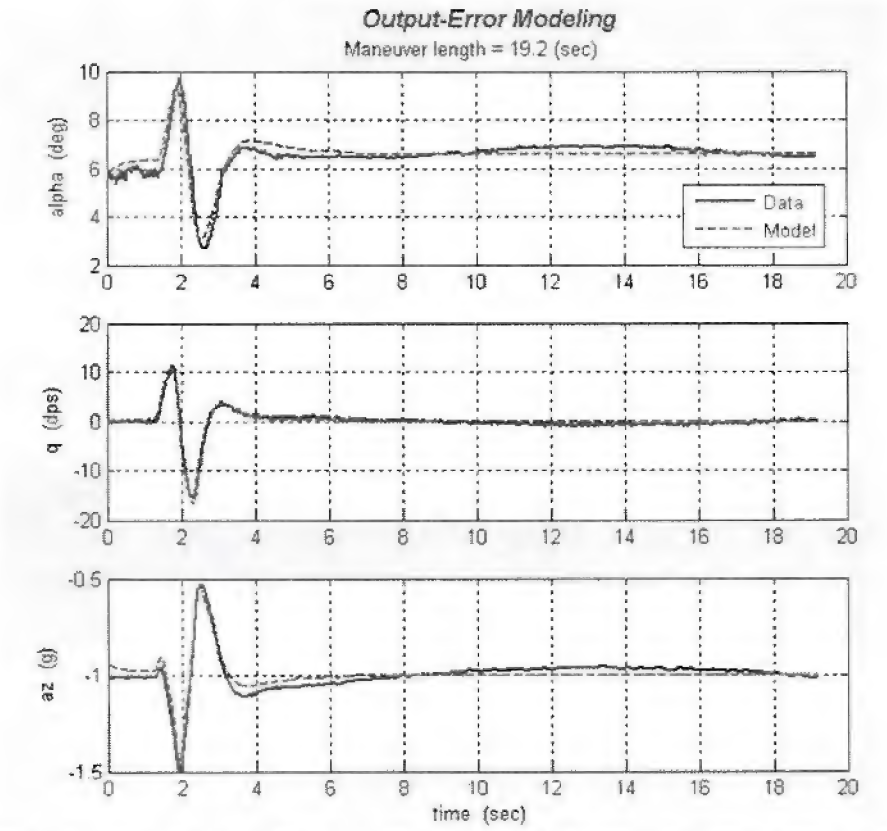

Figure D-2: Sample Results from a Pitch Doublet (Wingtips On, Glide, 60 KIAS)

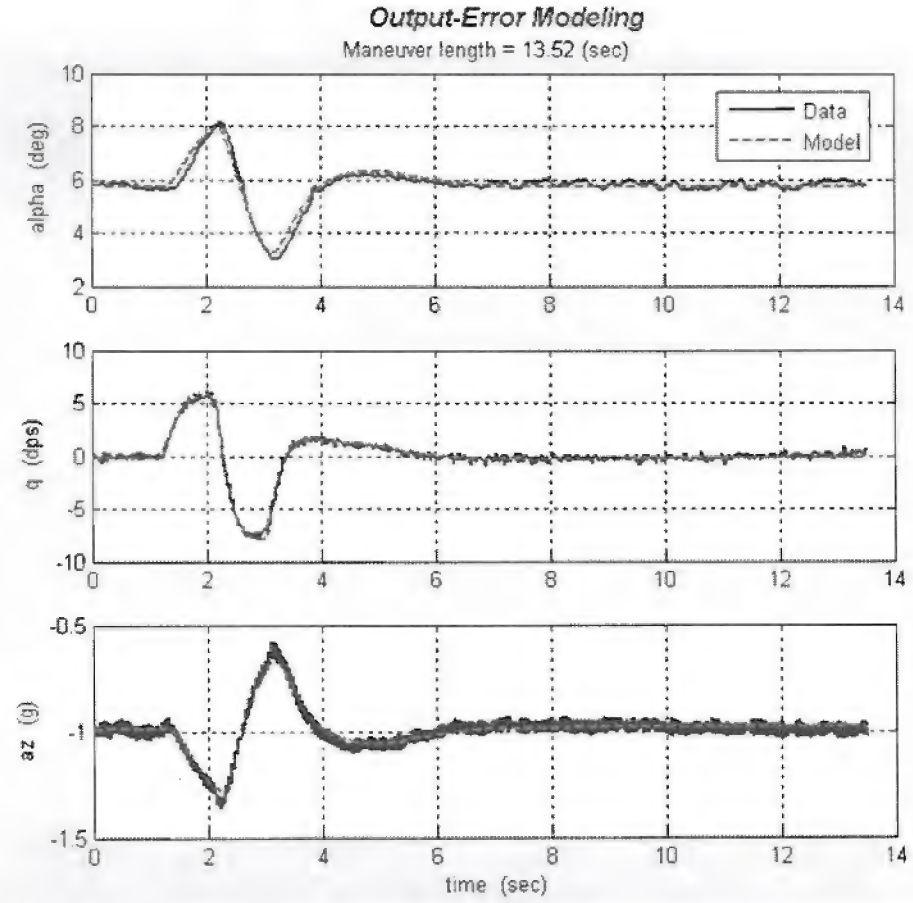

Figure D-3: Sample Results from a Pitch Doublet (Wingtips On, Power On, 60 KIAS)

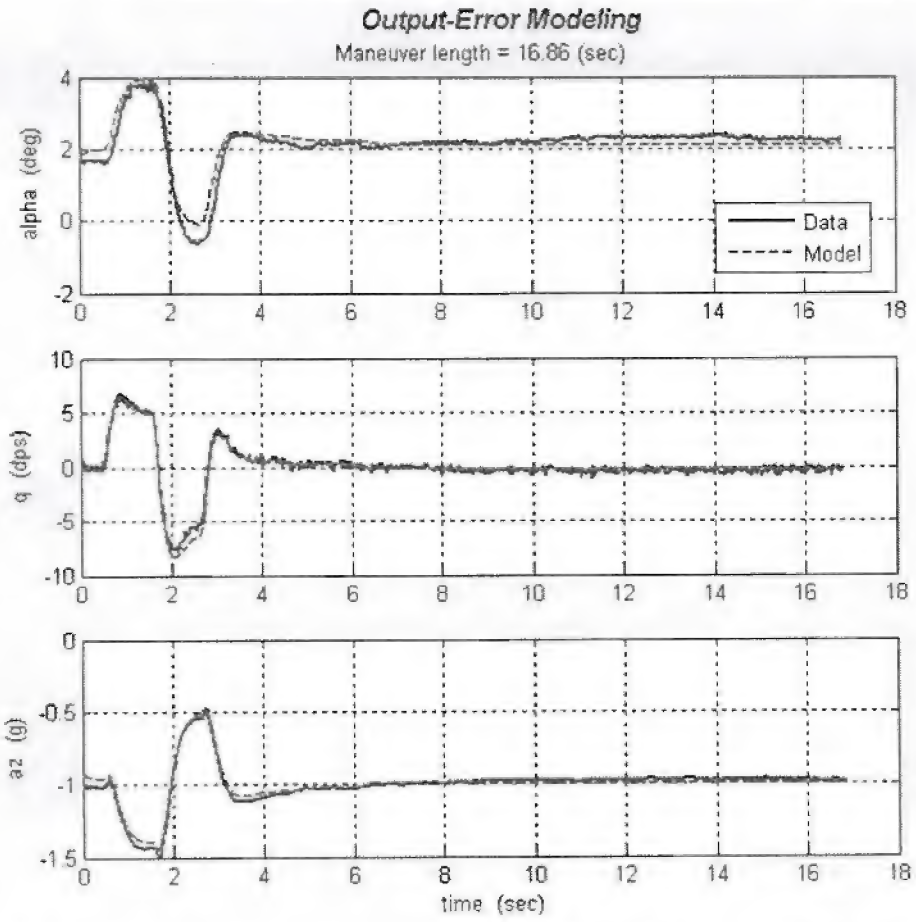

Figure D-4: Sample Results from a Pitch Doublet (Wingtips On, Glide, 80 KIAS)

APPENDIX E – SAMPLE LATERAL DATA

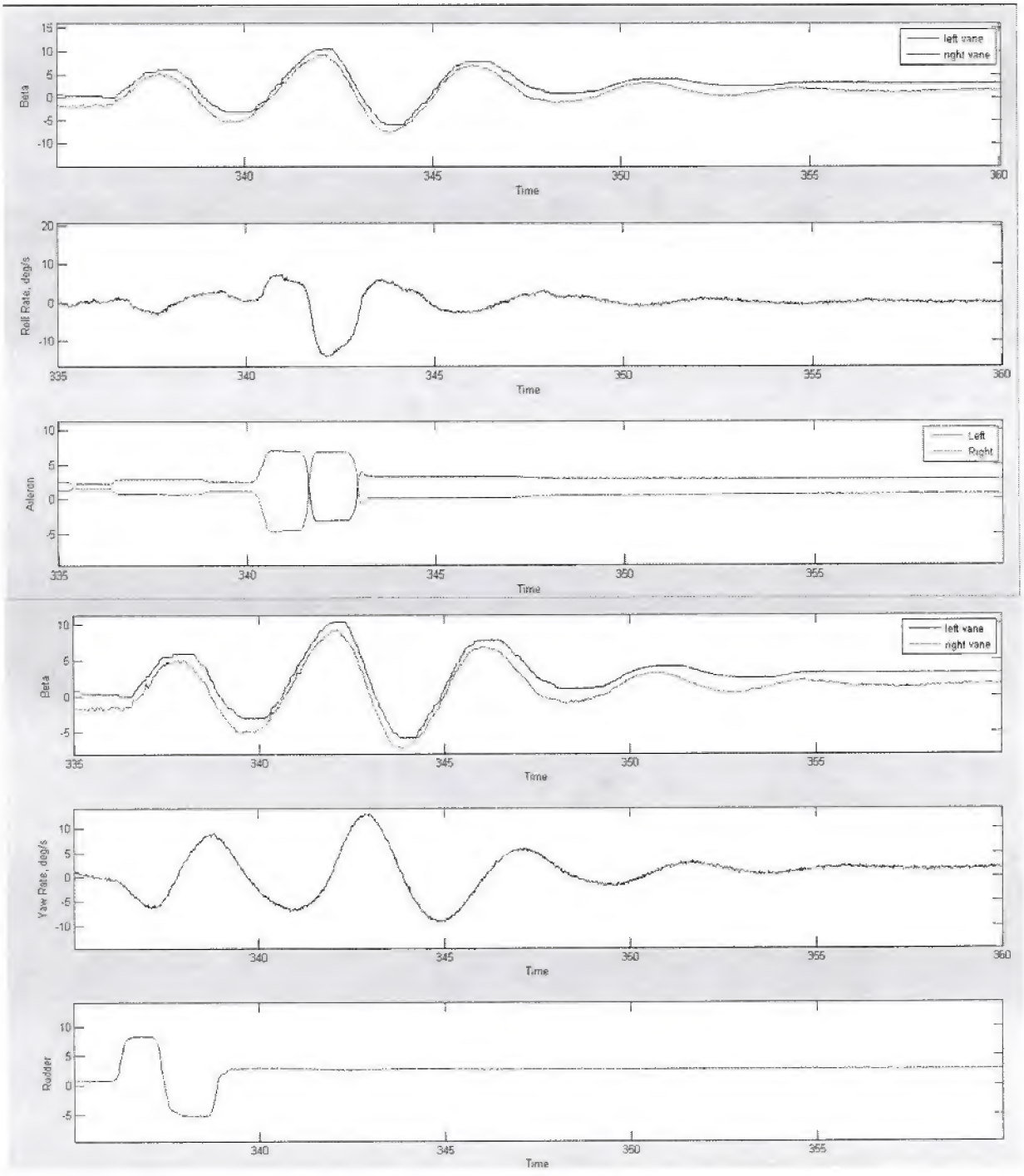

Figure E-1: Sample Time History for a Yaw Roll Doublet (Wingtips on, Glide, 60 KIAS)

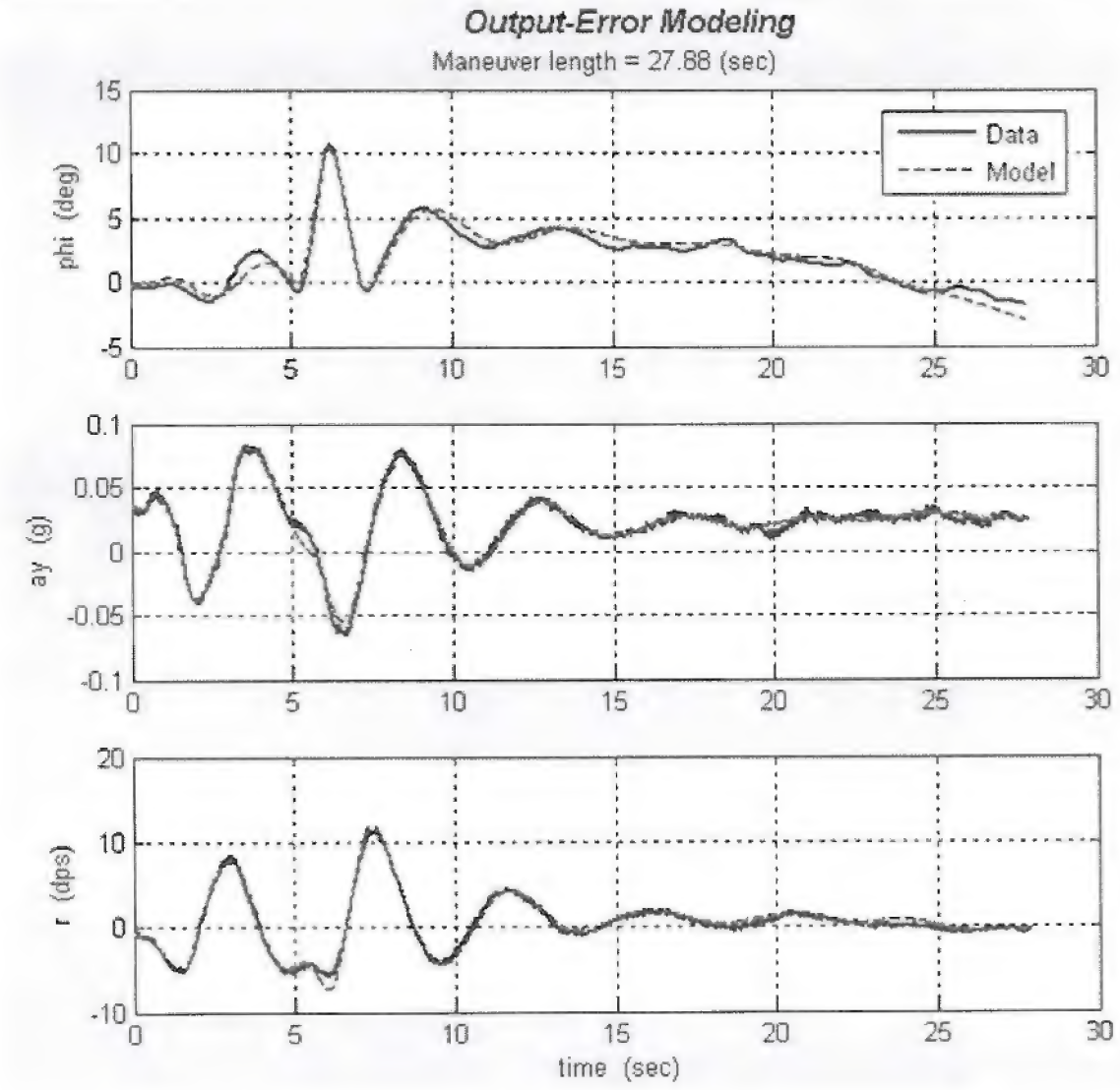

Figure E-2: Sample Results from a Yaw Roll Doublet (Wingtips On, Glide, 60 KIAS)

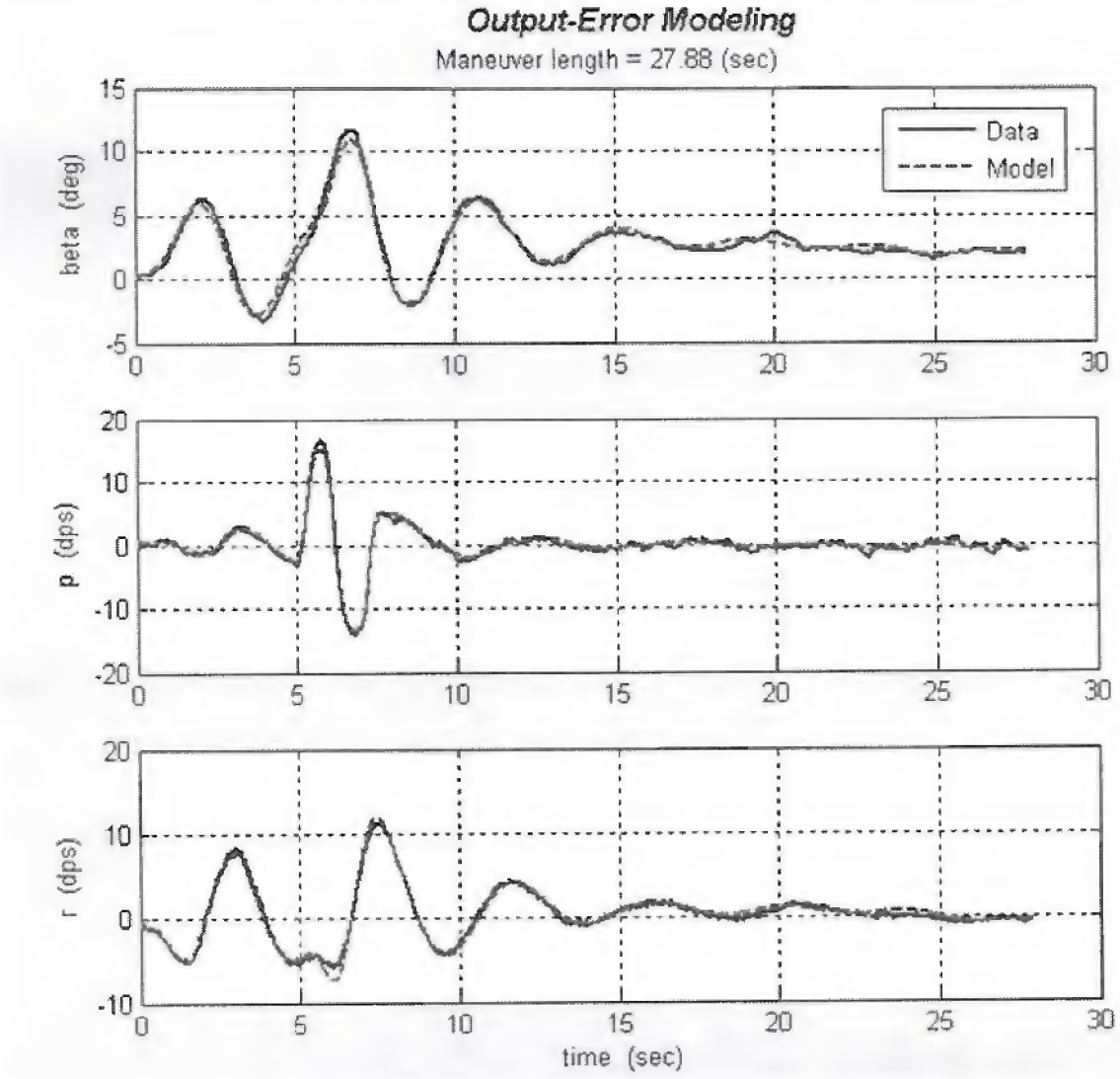

Figure E-3: Sample Results from a Yaw Roll Doublet (Wingtips On, Glide, 60 KIAS)

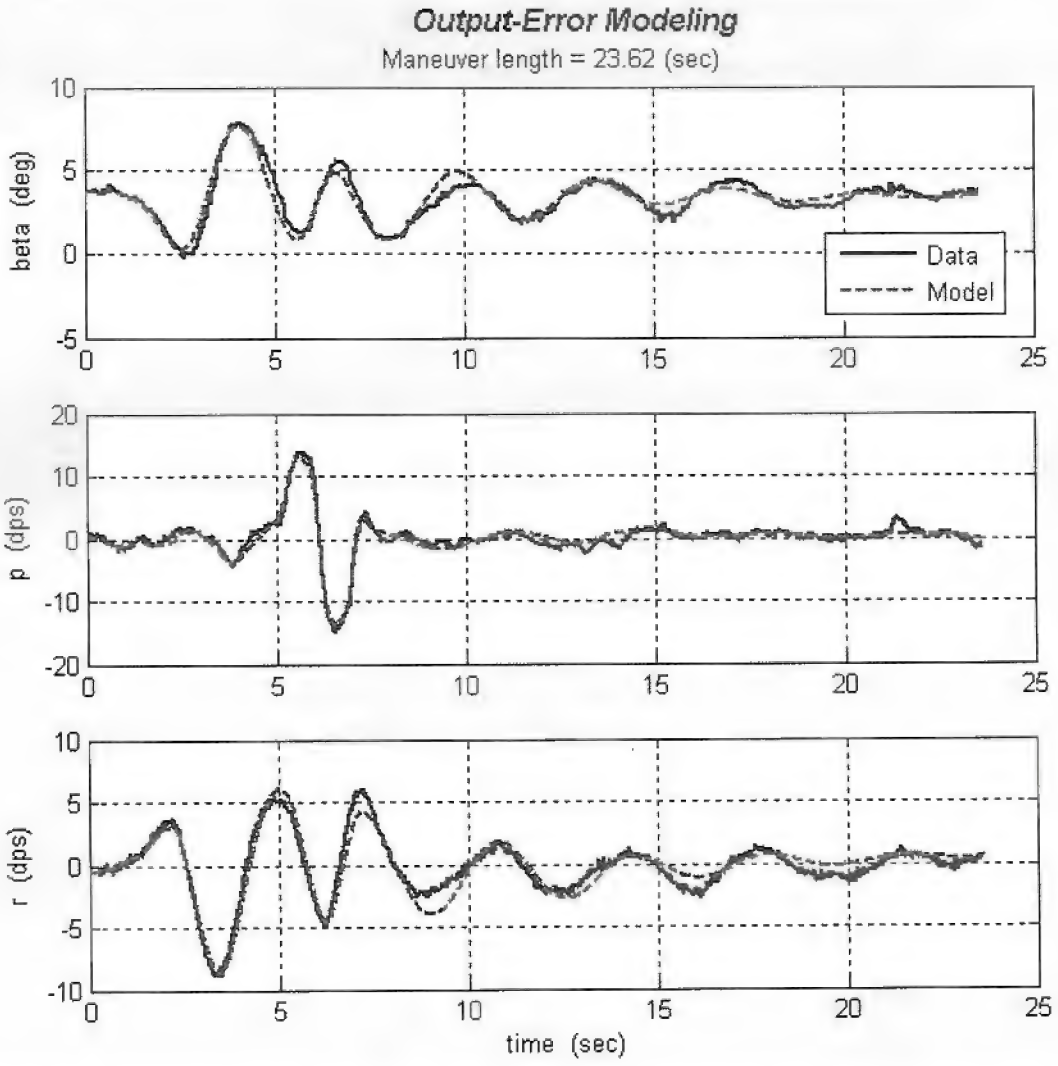

Figure E-4: Sample Results from a Yaw Roll Doublet (Wingtips On, Power On, 60 KIAS)

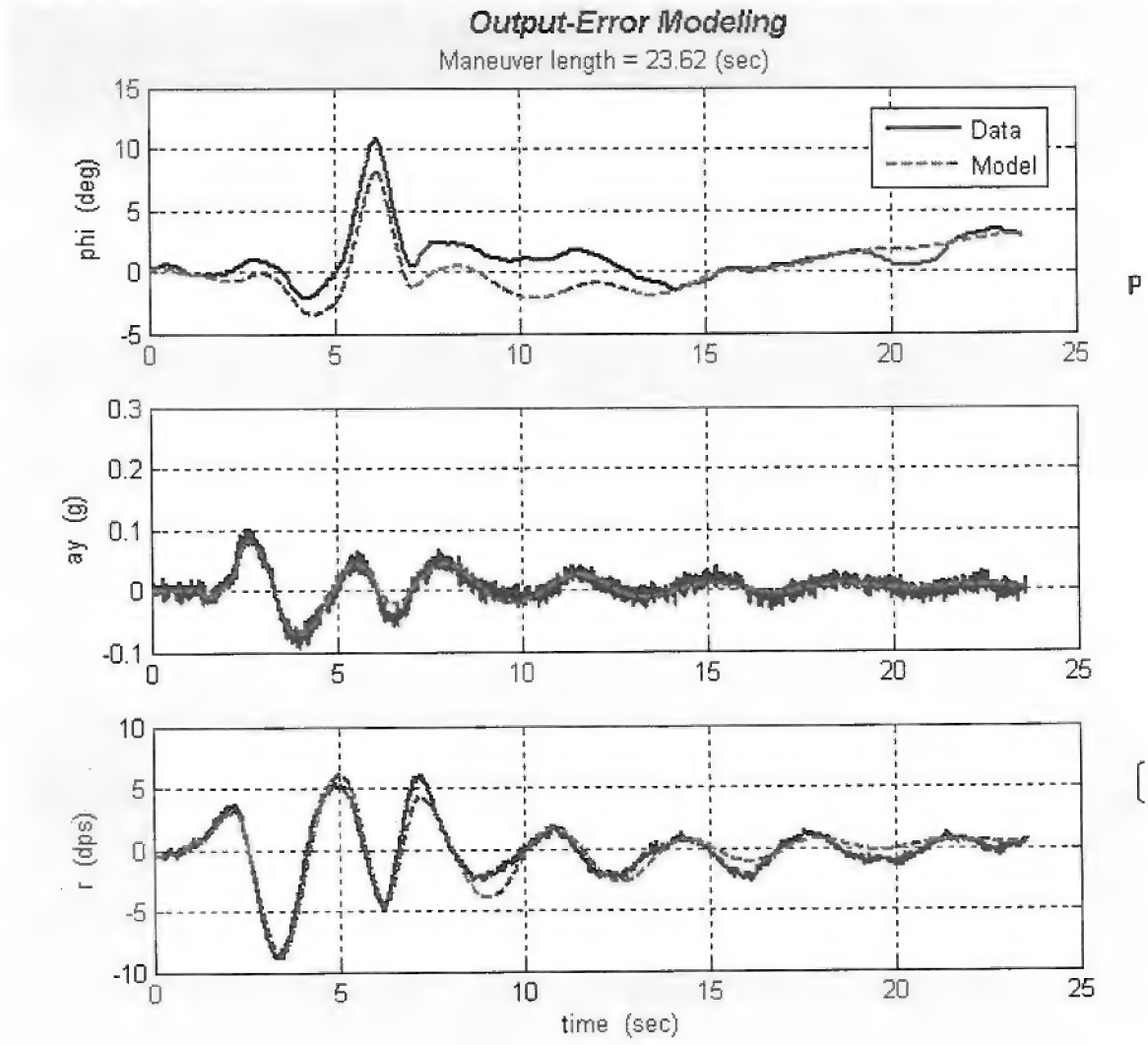

Figure E-5: Sample Results from a Yaw Roll Doublet (Wingtips On, Power On, 60 KIAS)

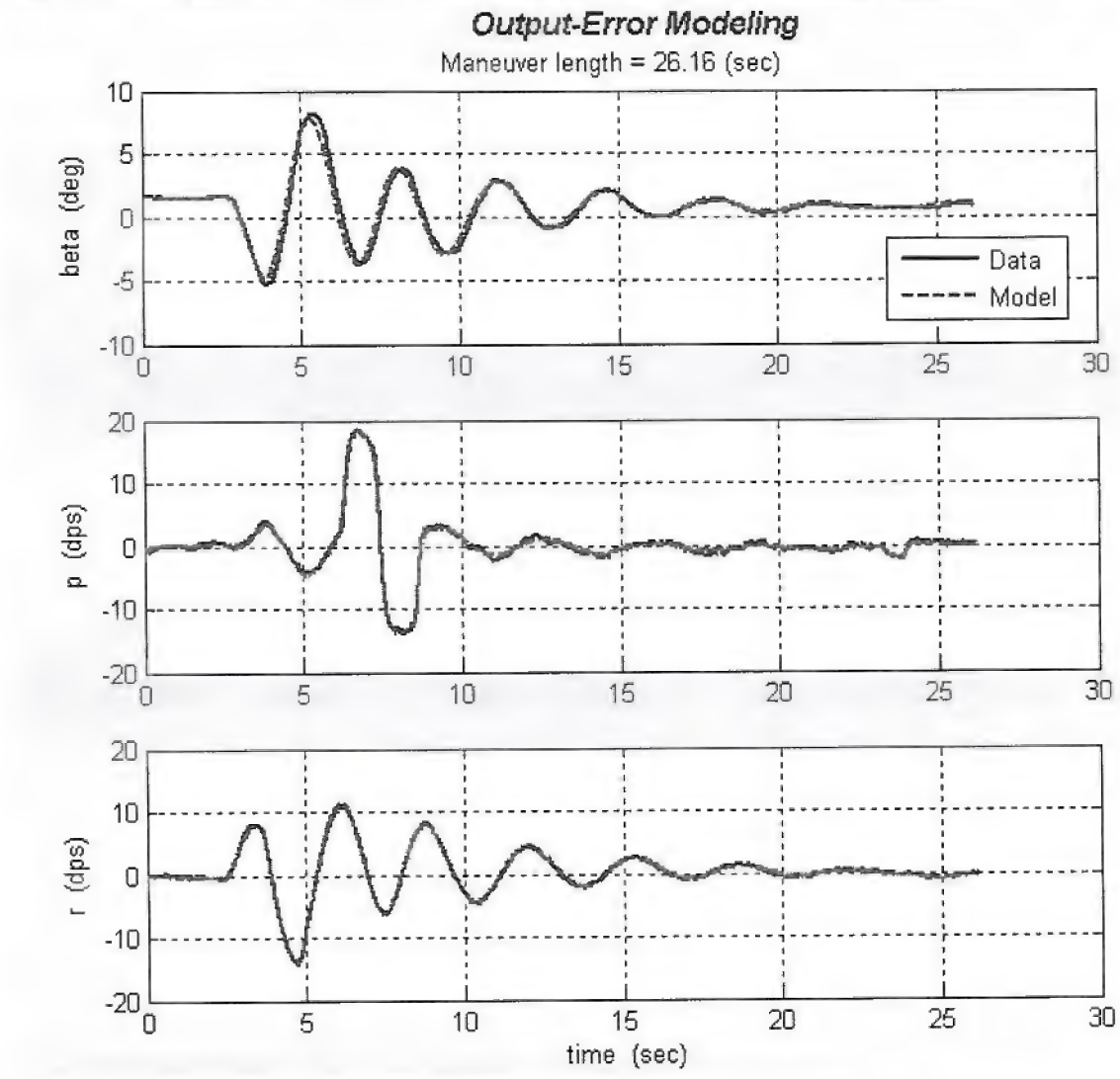

Figure E-6: Sample Results from a Yaw Roll Doublet (Wingtips On, Glide, 80 KIAS)

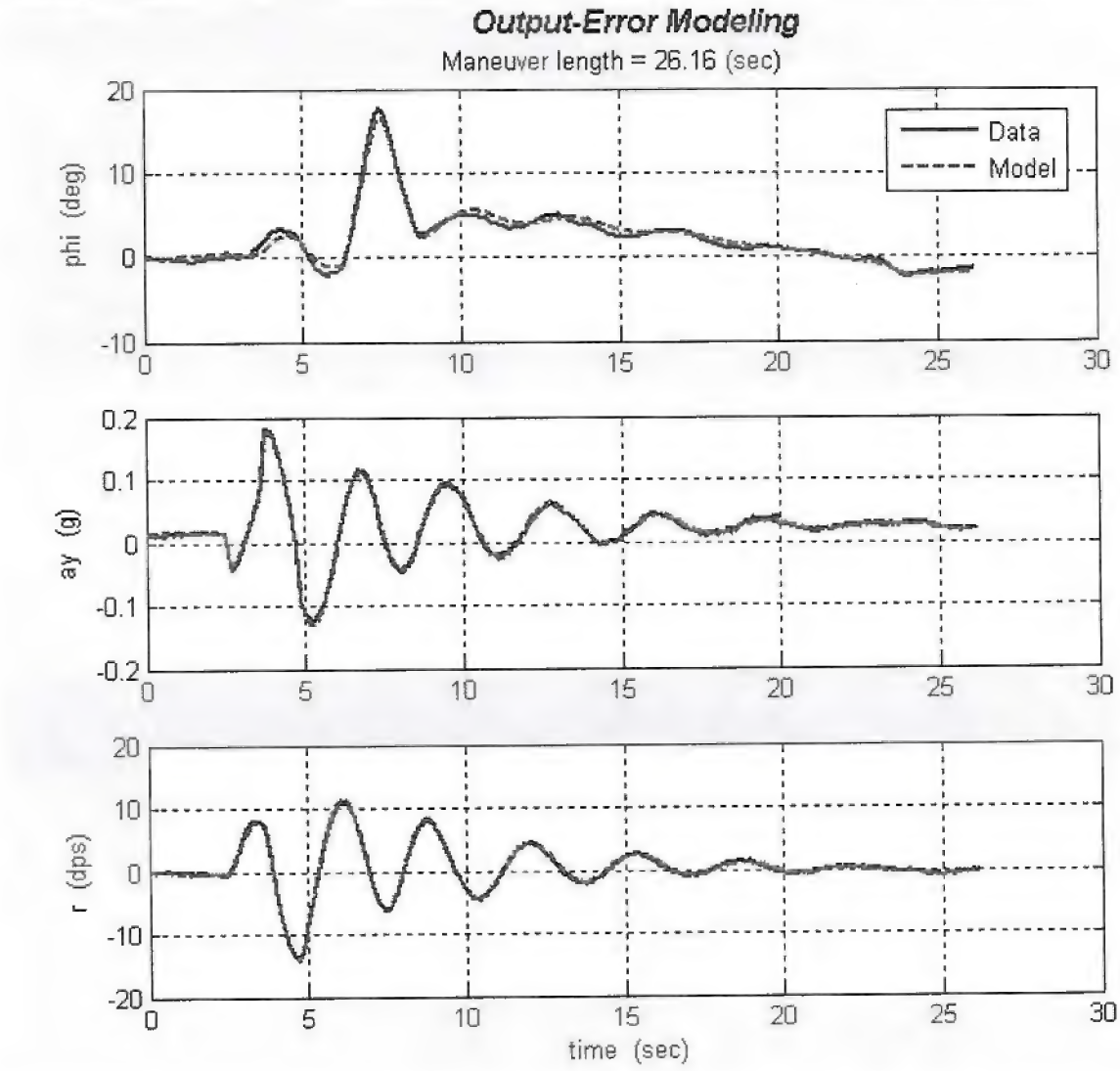

Figure E-7: Sample Results from a Yaw Roll Doublet (Wingtips On, Glide, 80 KIAS)

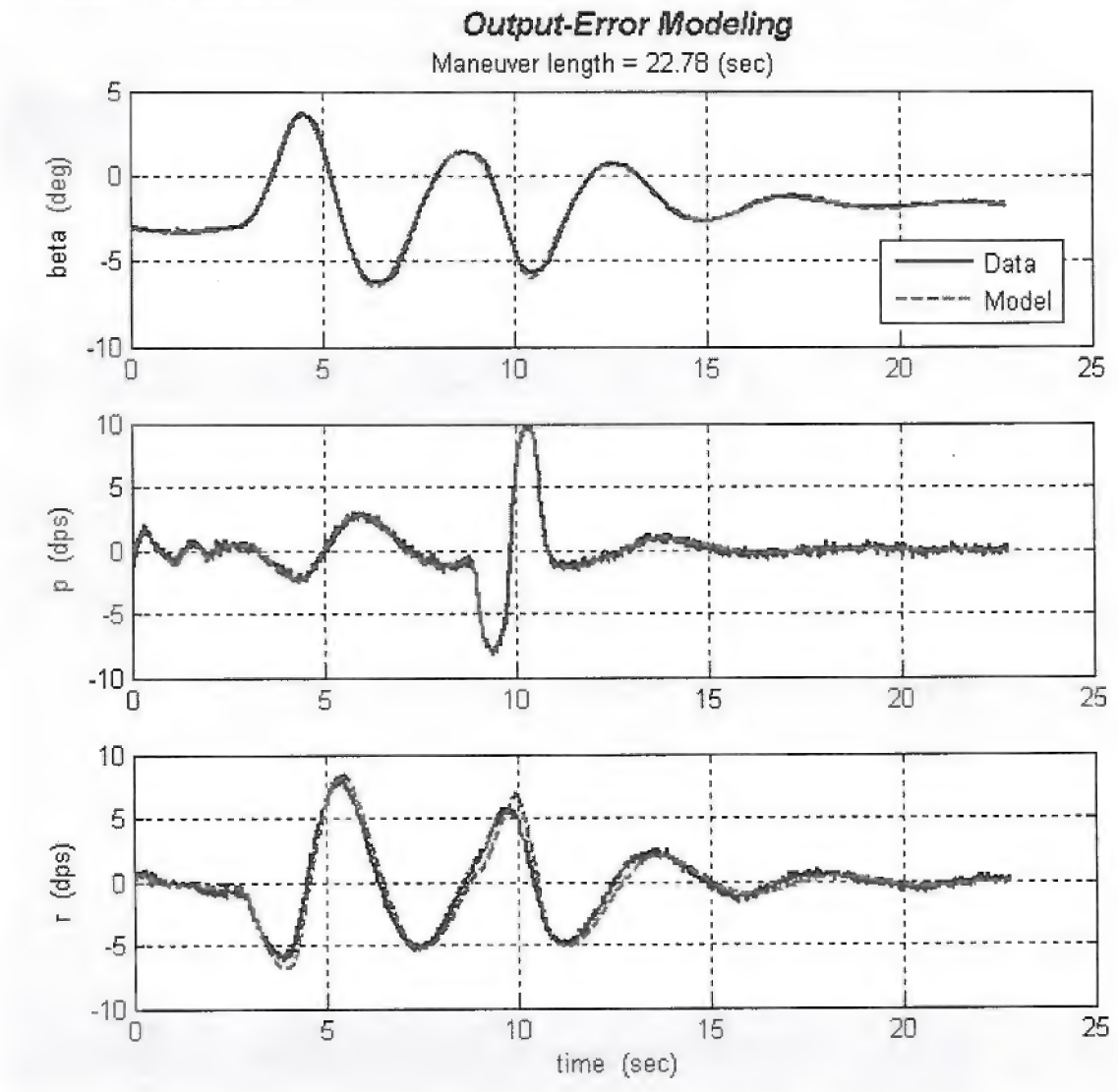

Figure E-8: Sample Results from a Yaw Roll Doublet (Wingtips Off, Glide, 60 KIAS)

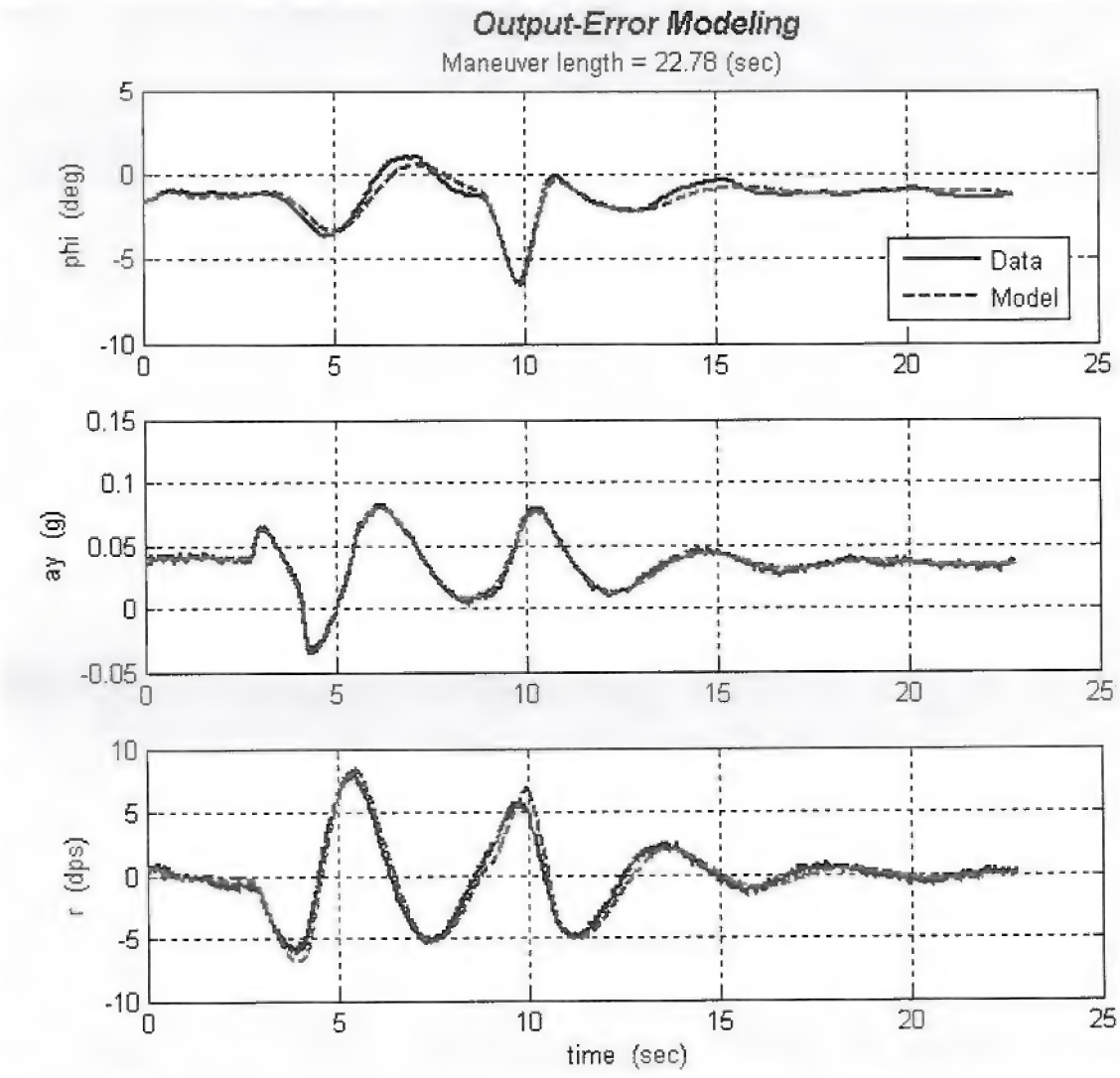

Figure E-9: Sample Results from a Yaw Roll Doublet (Wingtips Off, Glide, 60 KIAS)

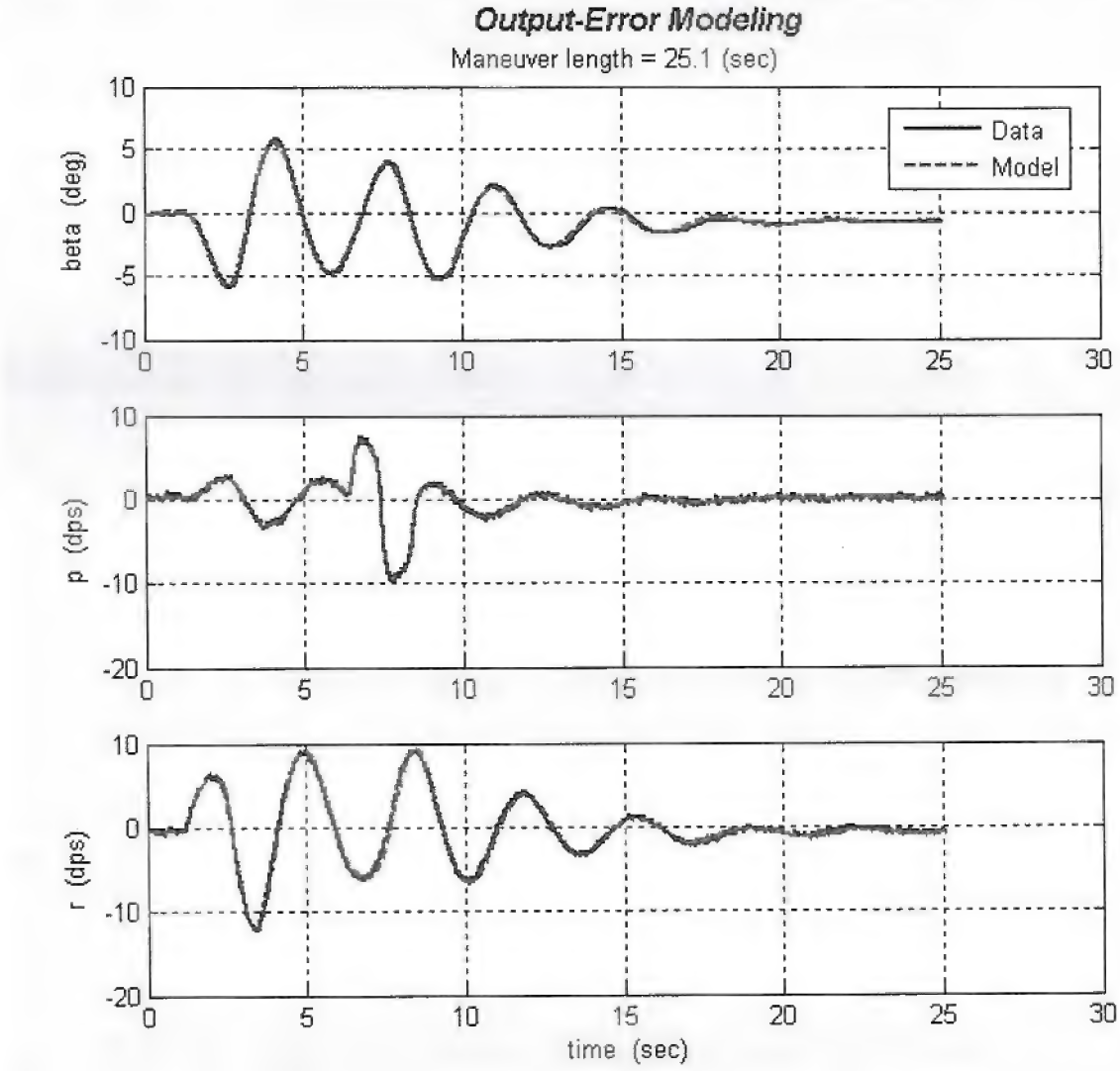

Figure E-10: Sample Results from a Yaw Roll Doublet (Wingtips Off, Glide, 80 KIAS)

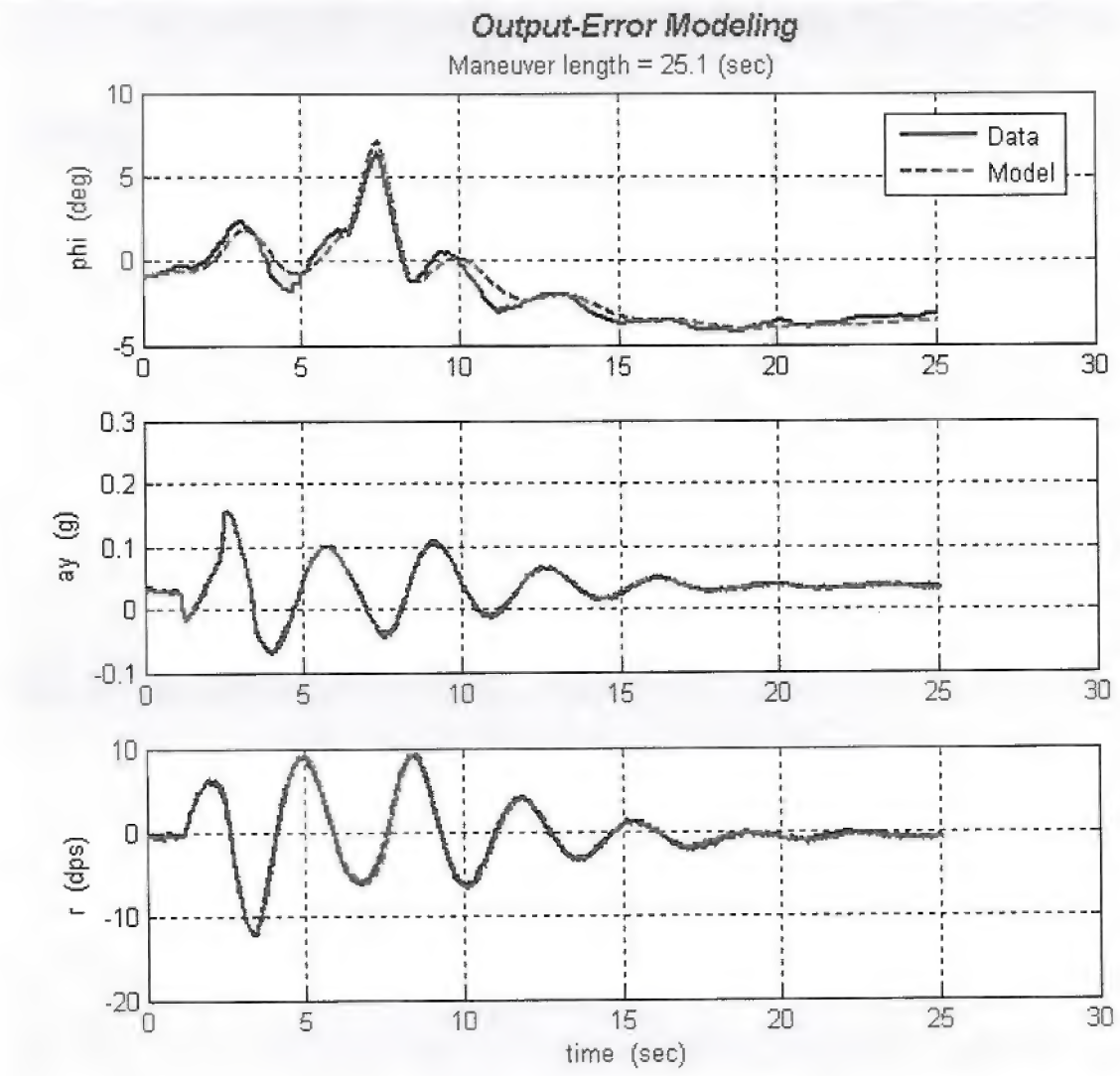

Figure E-11: Sample Results from a Yaw Roll Doublet (Wingtips Off, Glide, 80 KIAS)

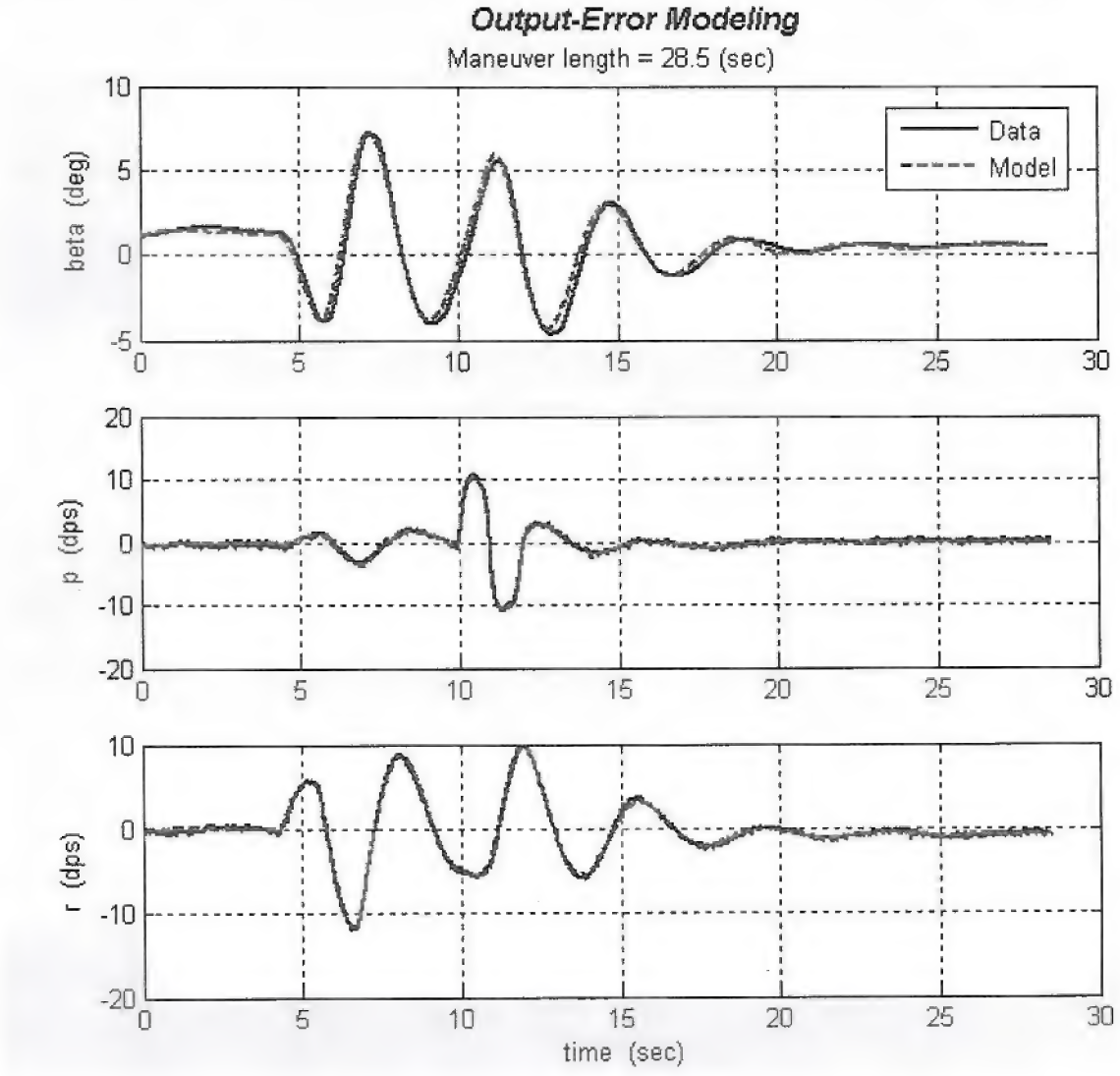

Figure E-12: Sample Results from a Yaw Roll Doublet (Wingtips Off, Power On, 60 KIAS)

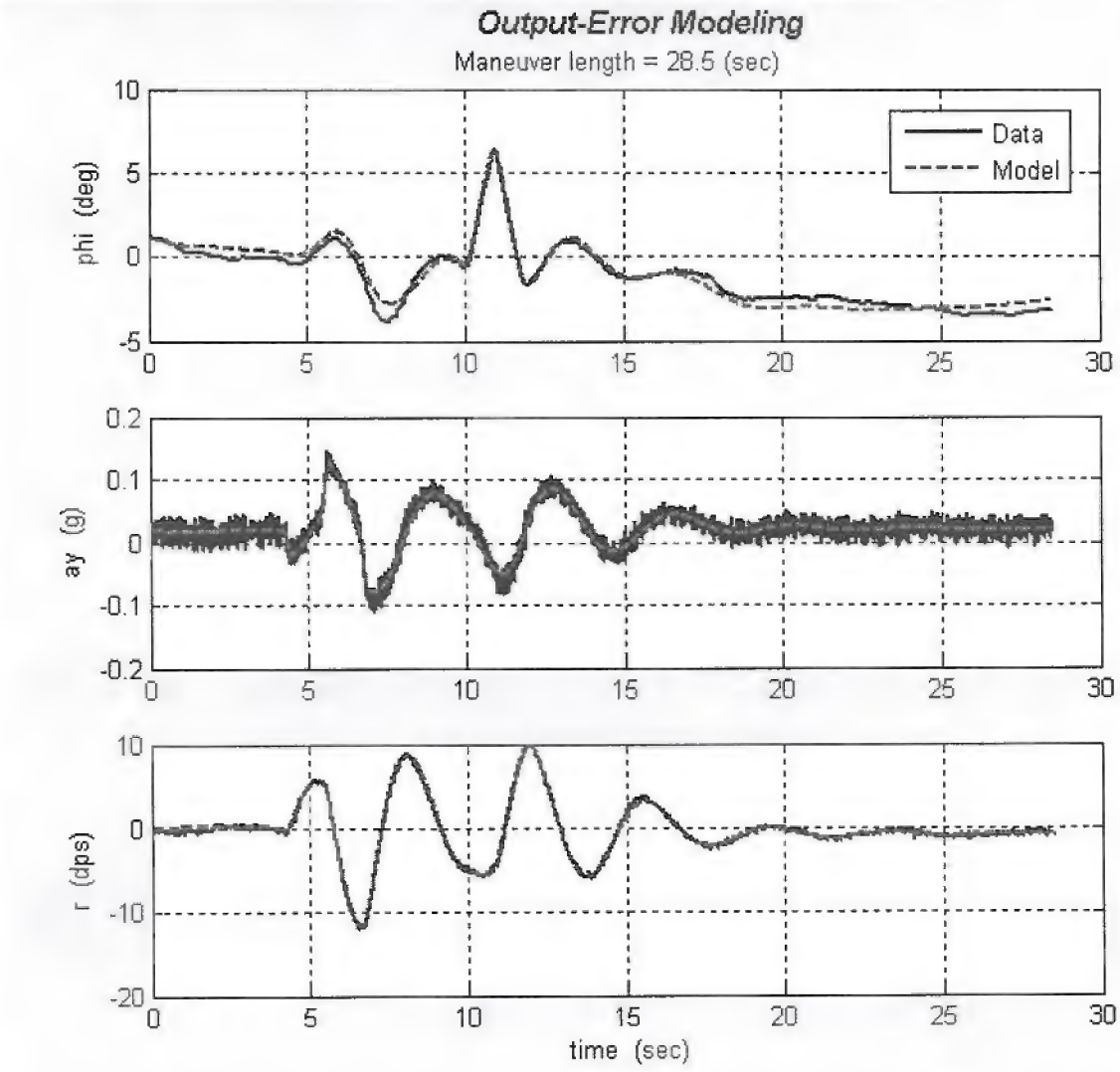

Figure E-13: Sample Results from a Yaw Roll Doublet (Wingtips Off, Power On, 60 KIAS)

APPENDIX F – STABILITY AND CONTROL DERIVATIVES

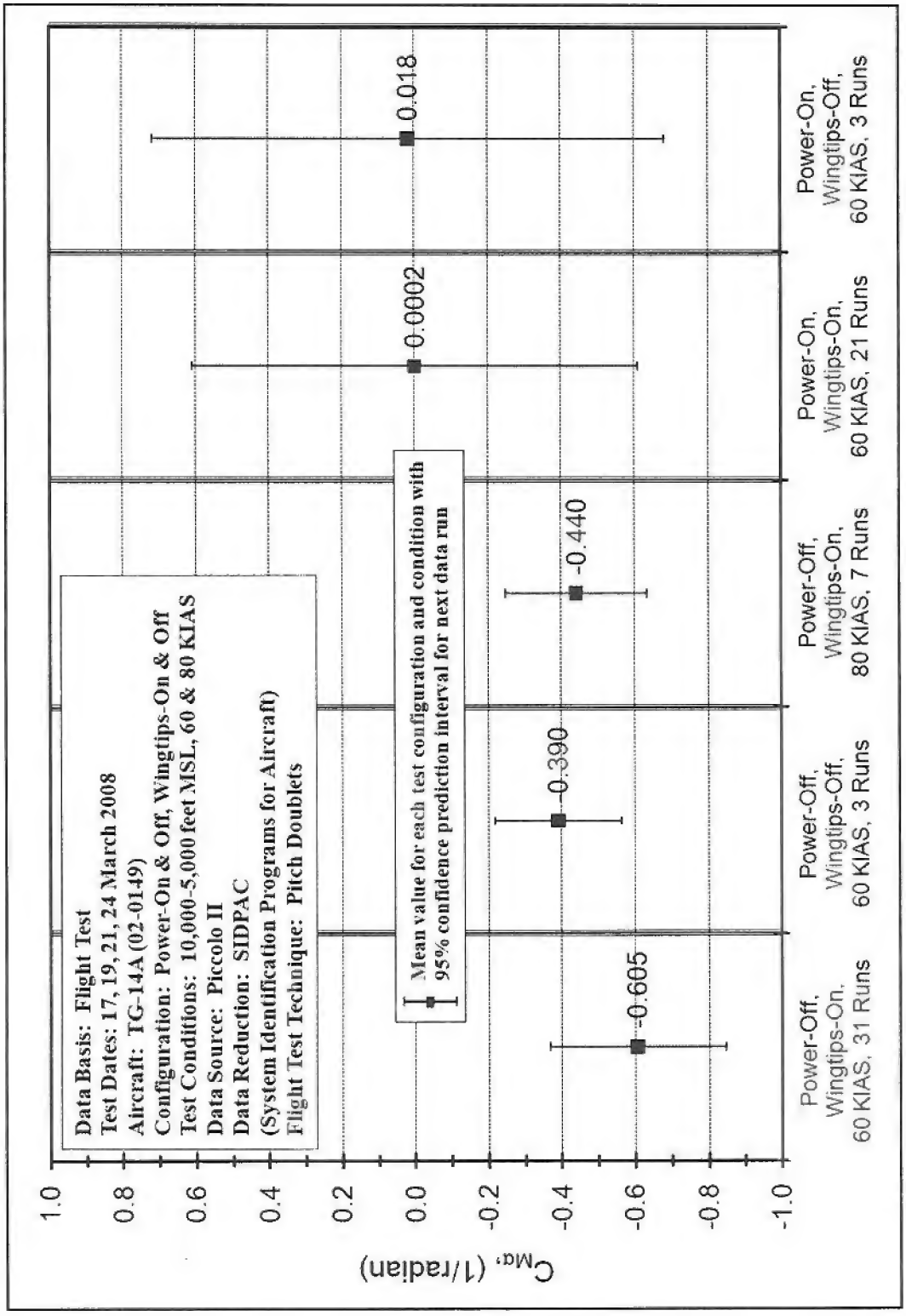

Figure F-1. $C_{M\alpha}$ from all test conditions with 95% confidence intervals

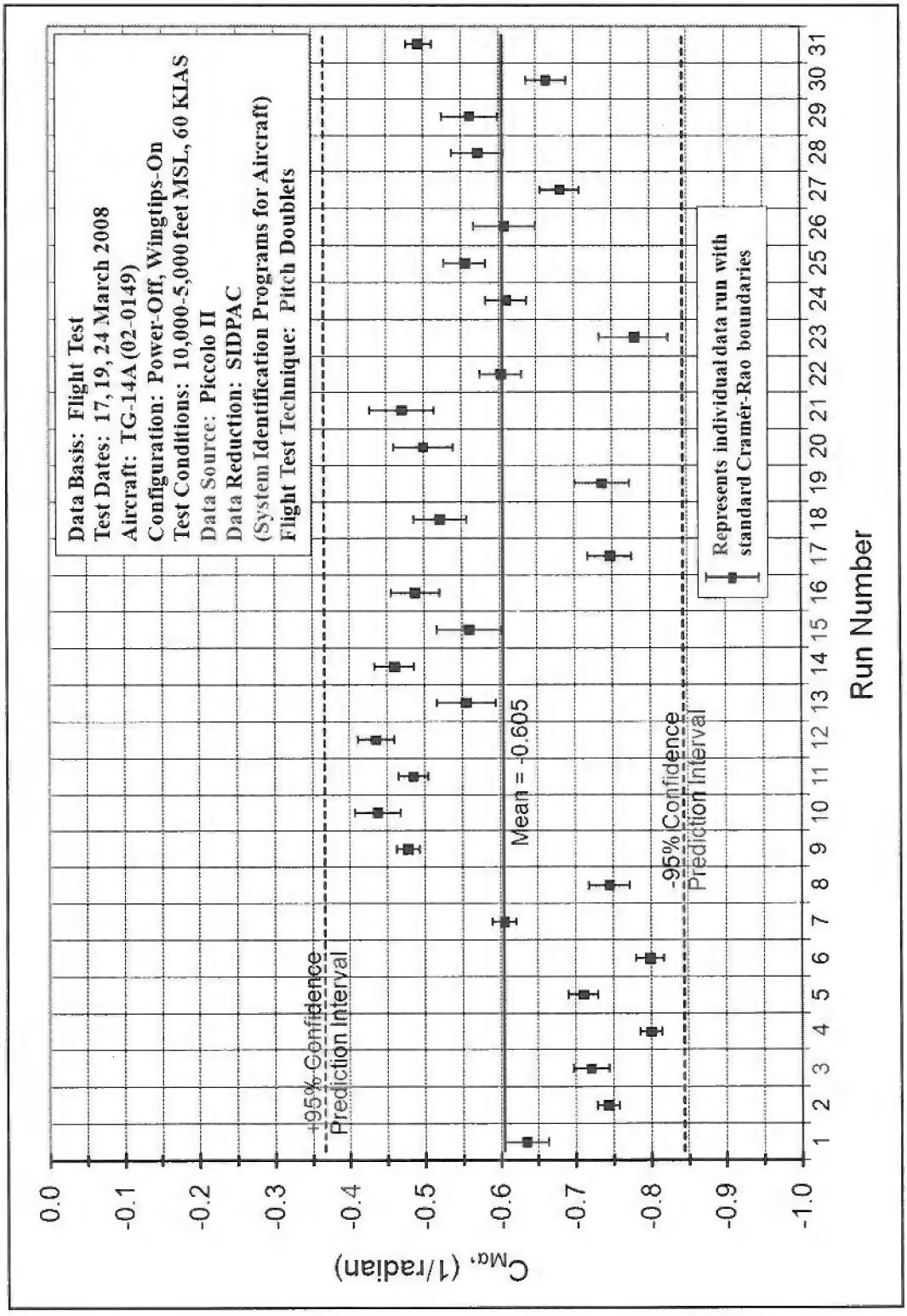

Figure F-2. $C_{M\alpha}$ (Power-Off, Wingtips-On, 60 KIAS)

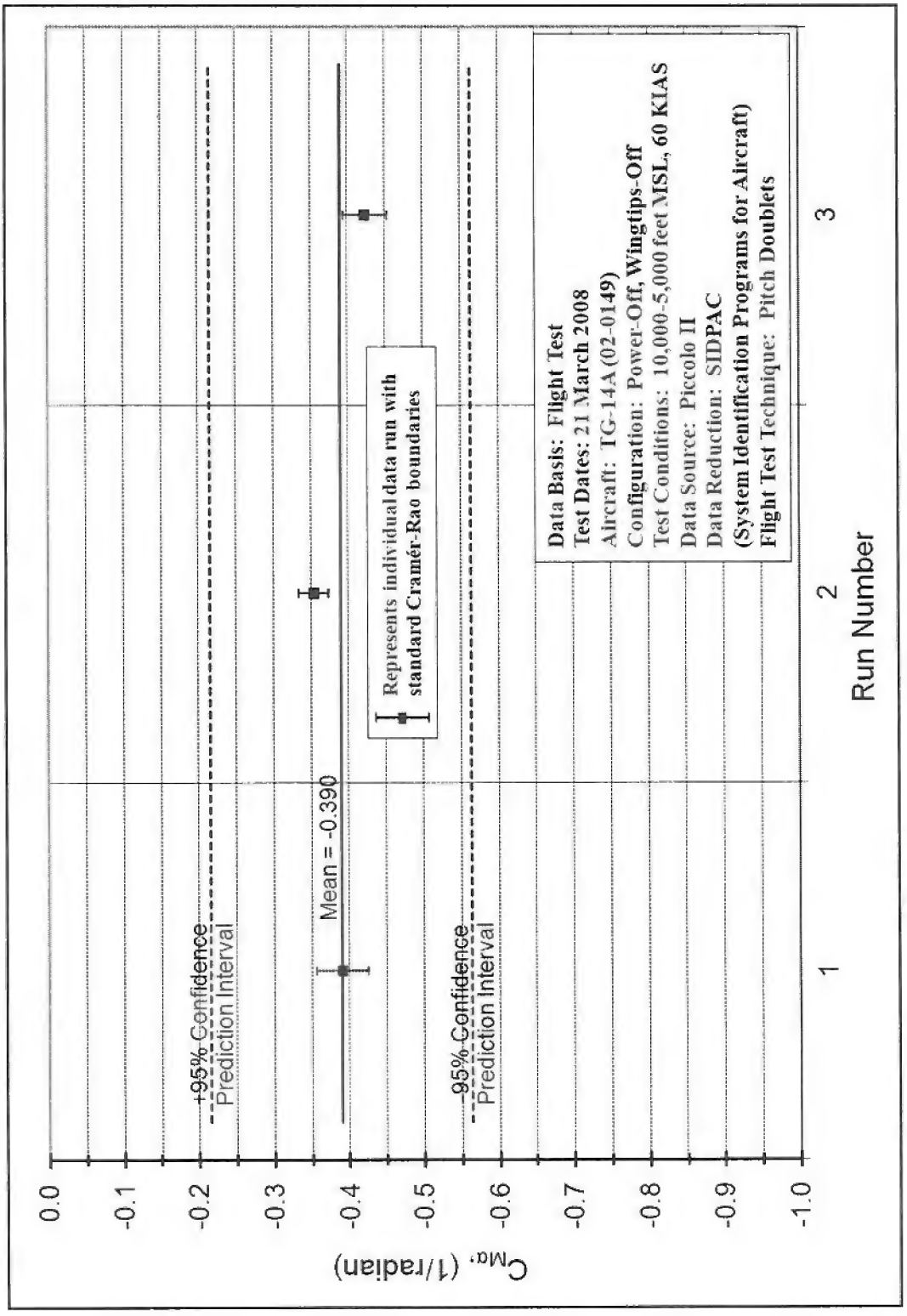

Figure F-3. $C_{M\alpha}$ (Power-Off, Wingtips-Off, 60 KIAS)

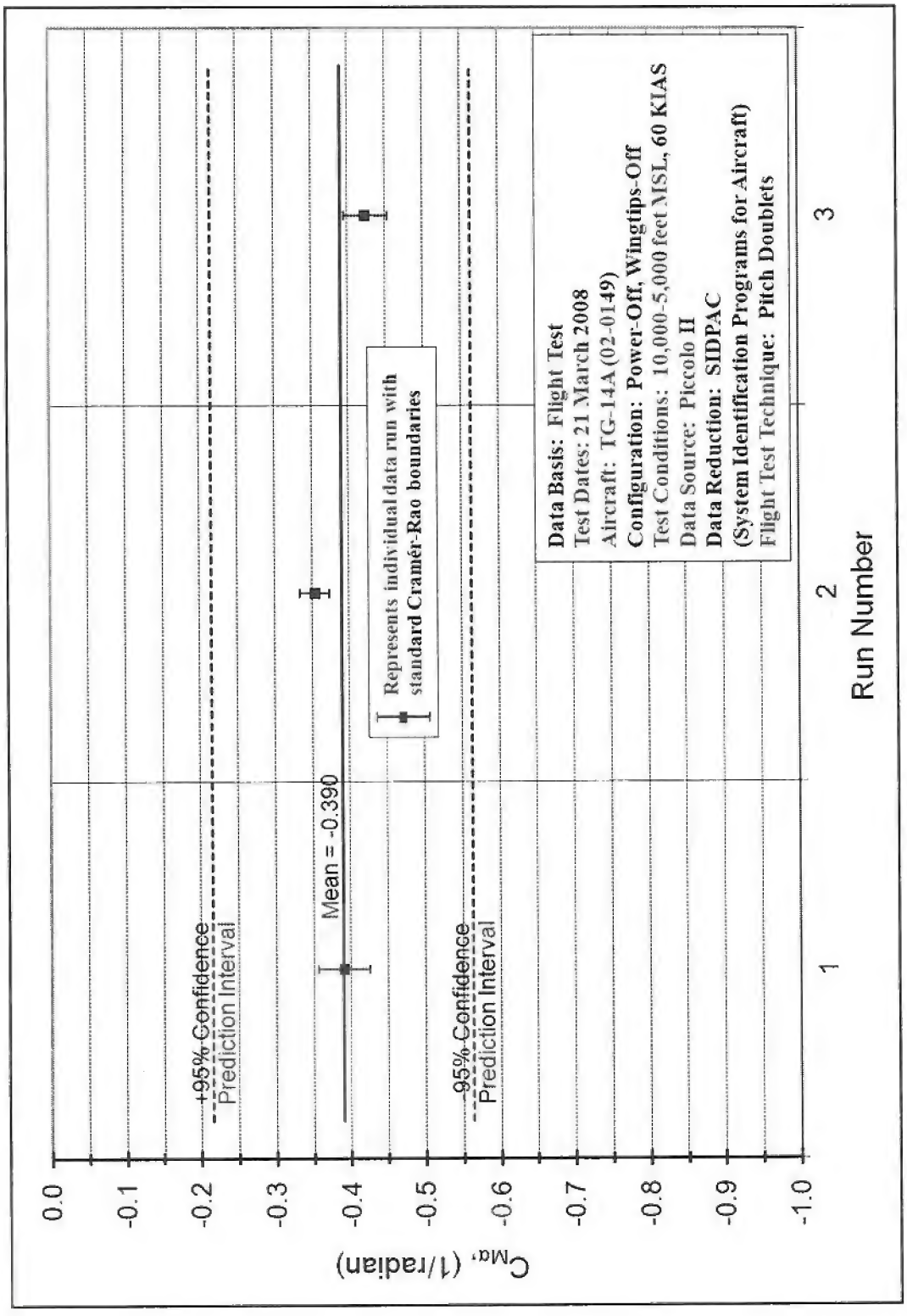

Figure F-4. $C_{M\alpha}$ (Power-Off, Wingtips-On, 80 KIAS)

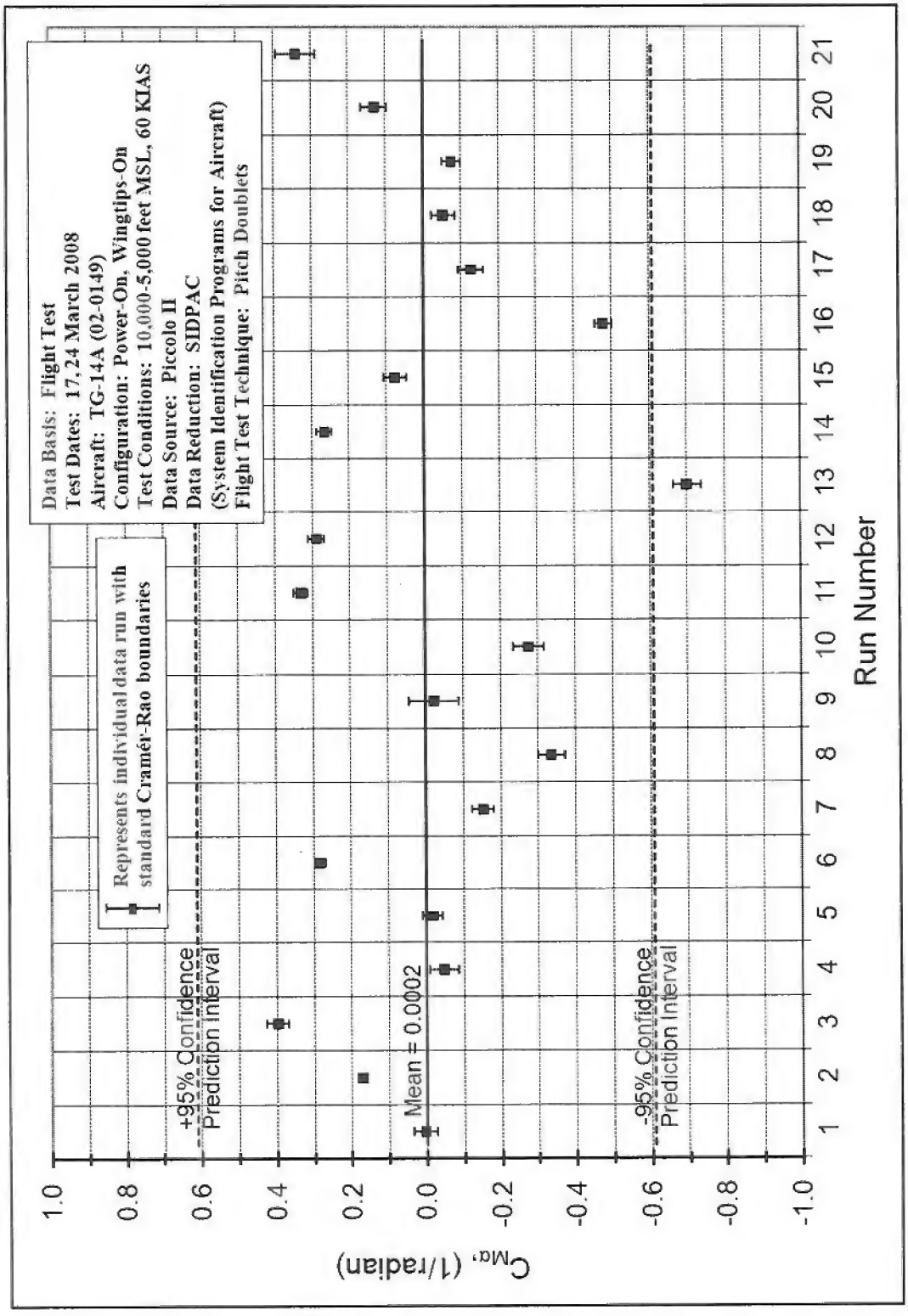

Figure F-5. $C_{M\alpha}$ (Power-On, Wingtips-On, 60 KIAS)

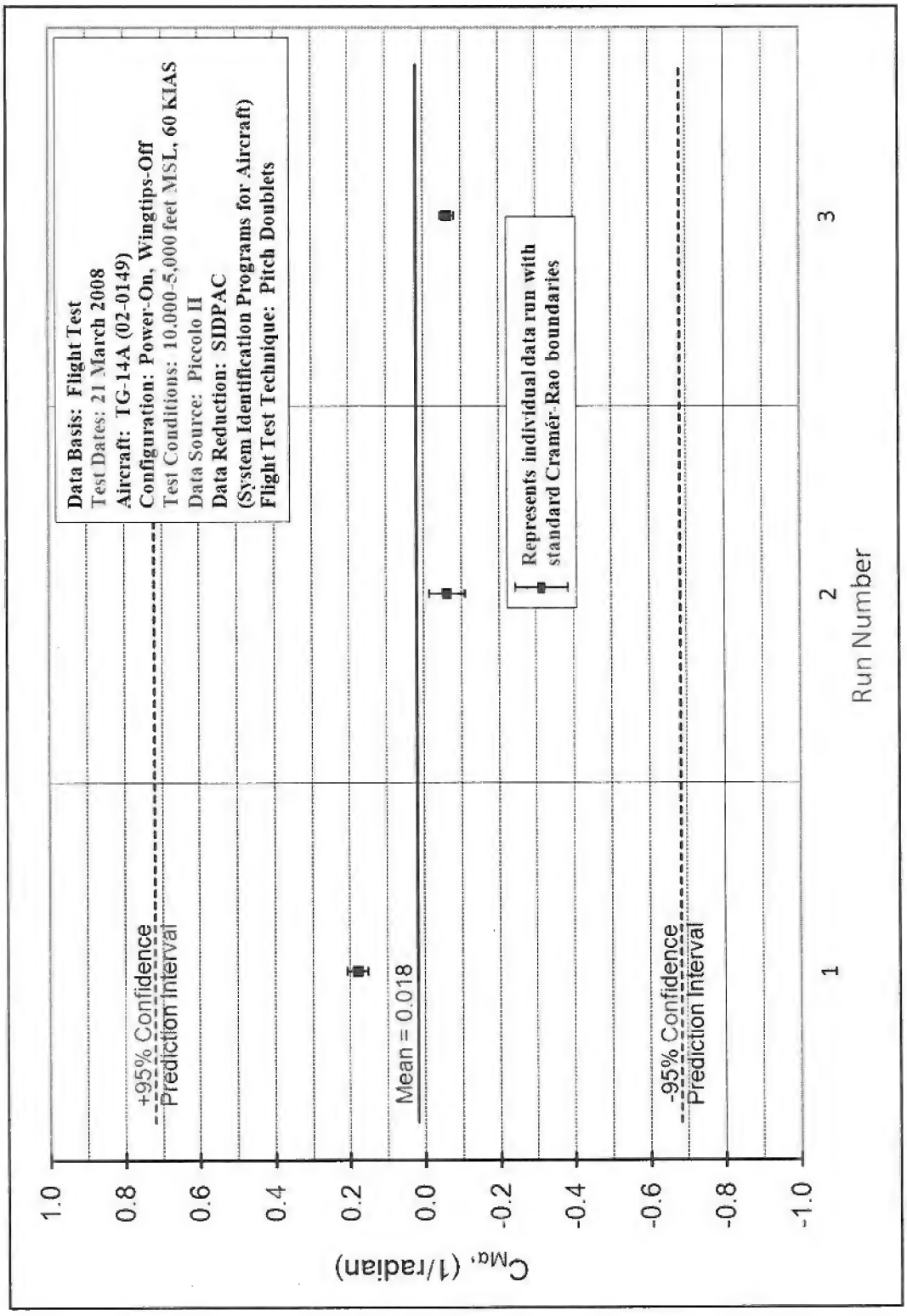

Figure F-6. $C_{M\alpha}$ (Power-On, Wingtips-Off, 60 KIAS)

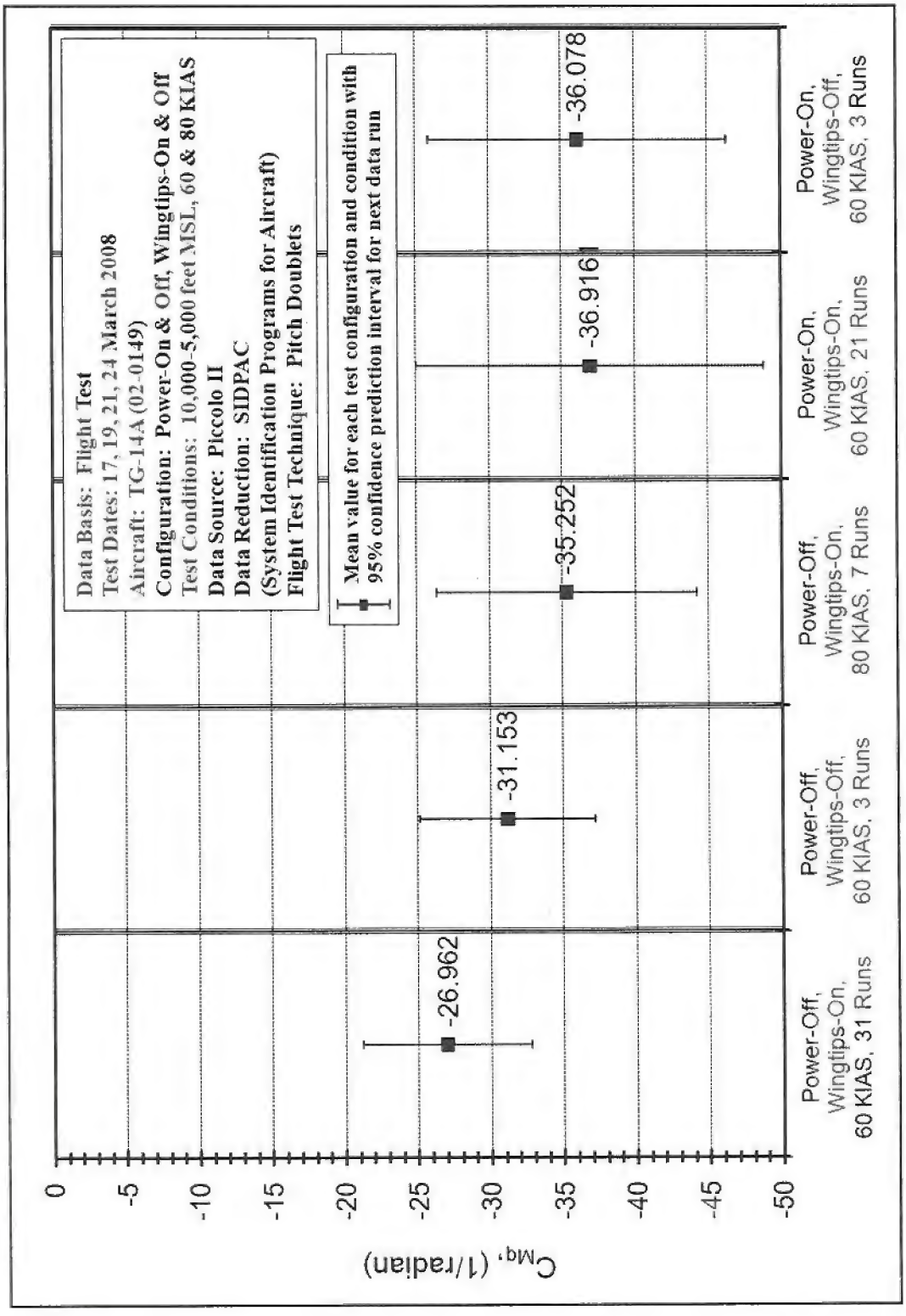

Figure F-7. C_{Mq} from all test conditions with 95% confidence intervals

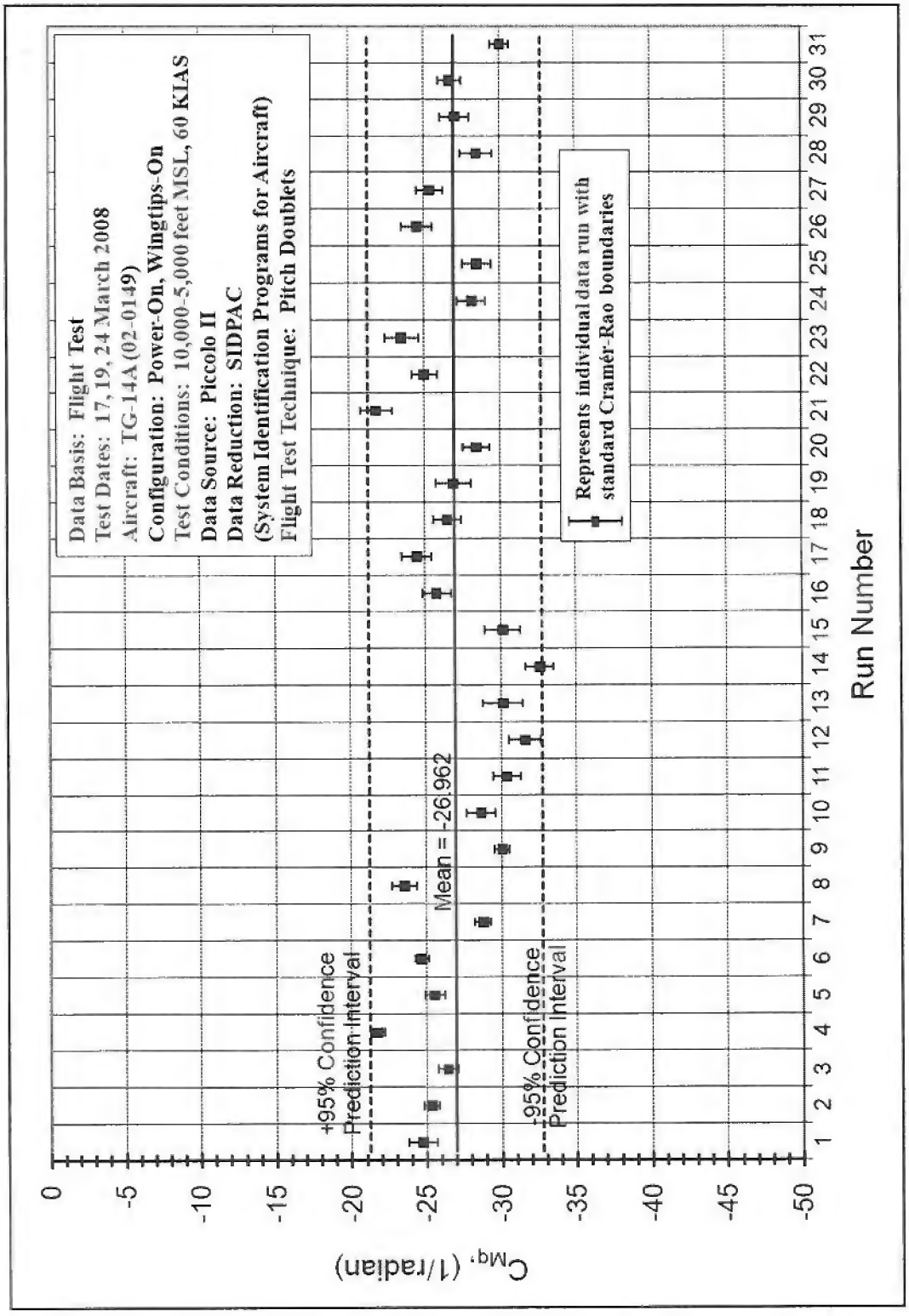

Figure F-8. C_{Mq} (Power-Off, Wingtips-On, 60 KIAS)

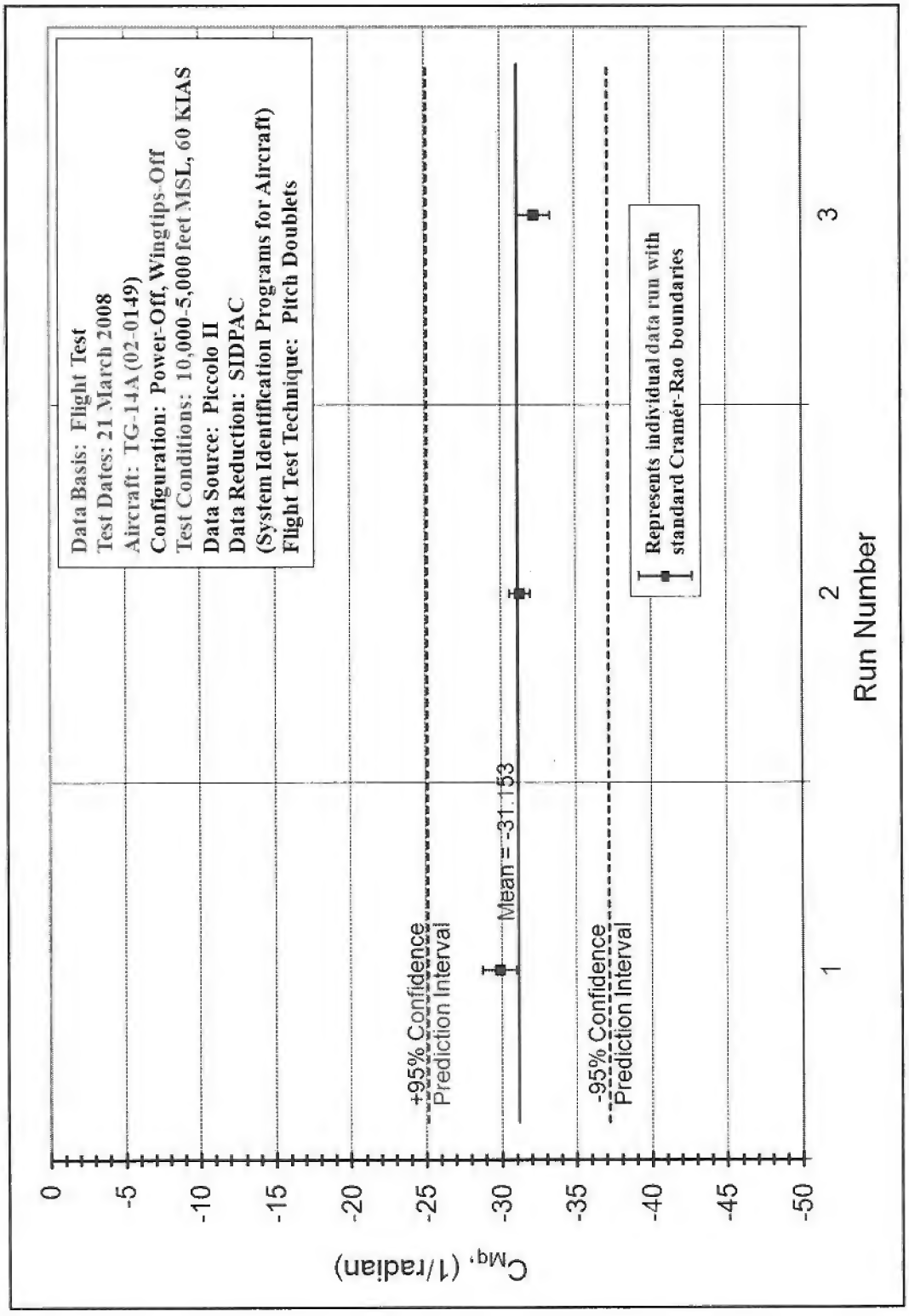

Figure F-9. C_{Mq} (Power-Off, Wingtips-Off, 60 KIAS)

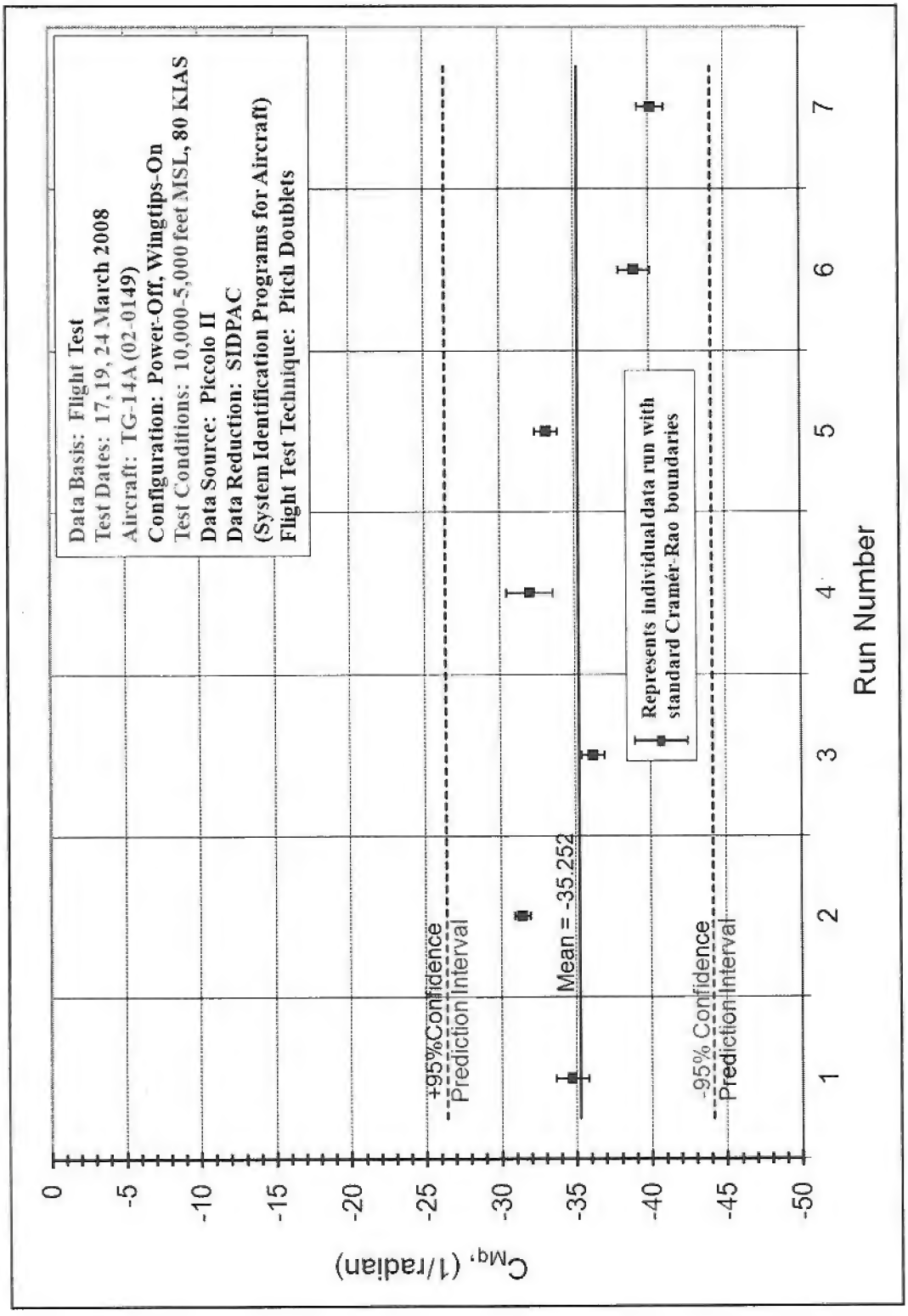

Figure F-10. C_{Mq} (Power-Off, Wingtips-On, 80 KIAS)

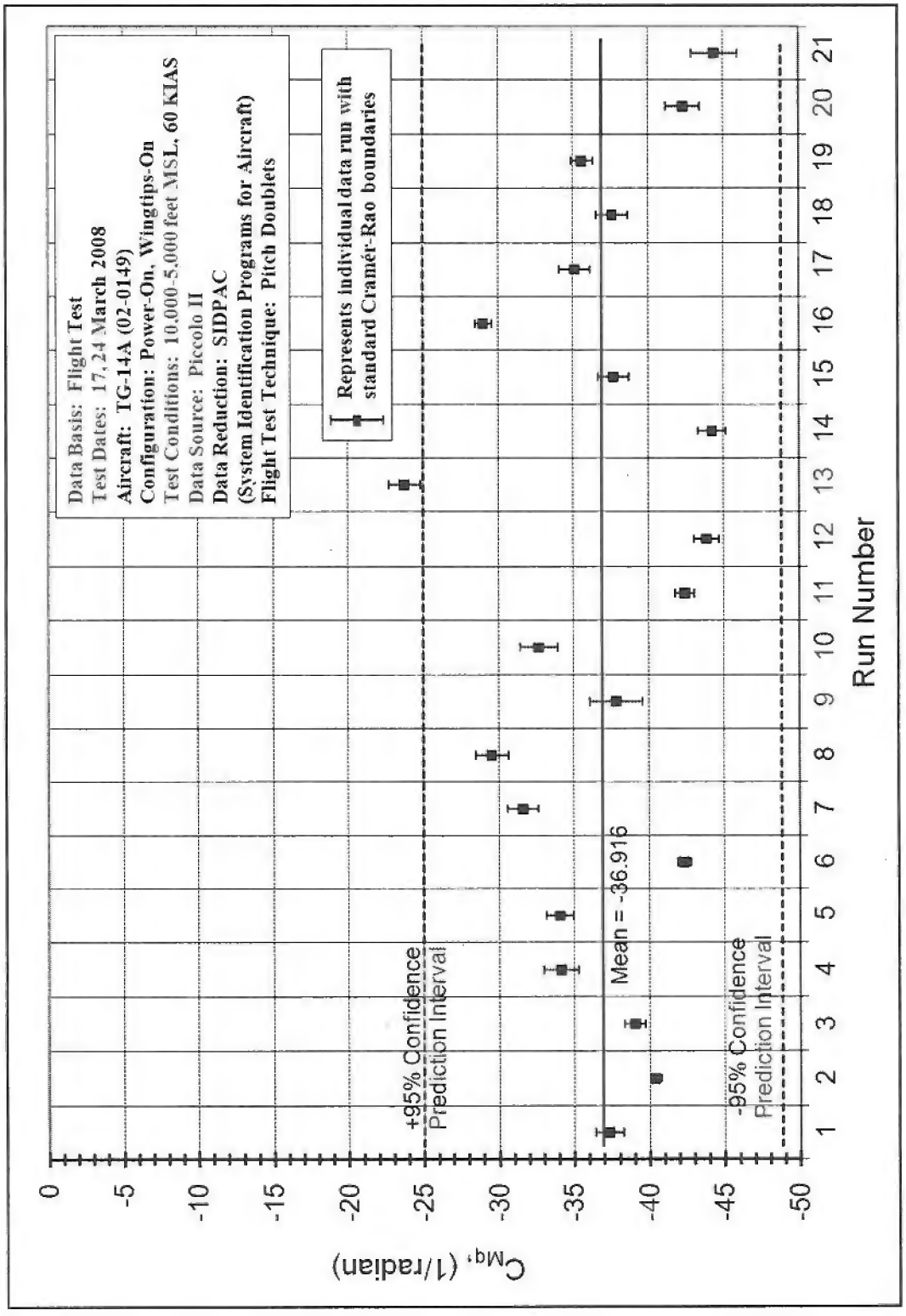

Figure F-11. C_{Mq} (Power-On, Wingtips-On, 60 KIAS)

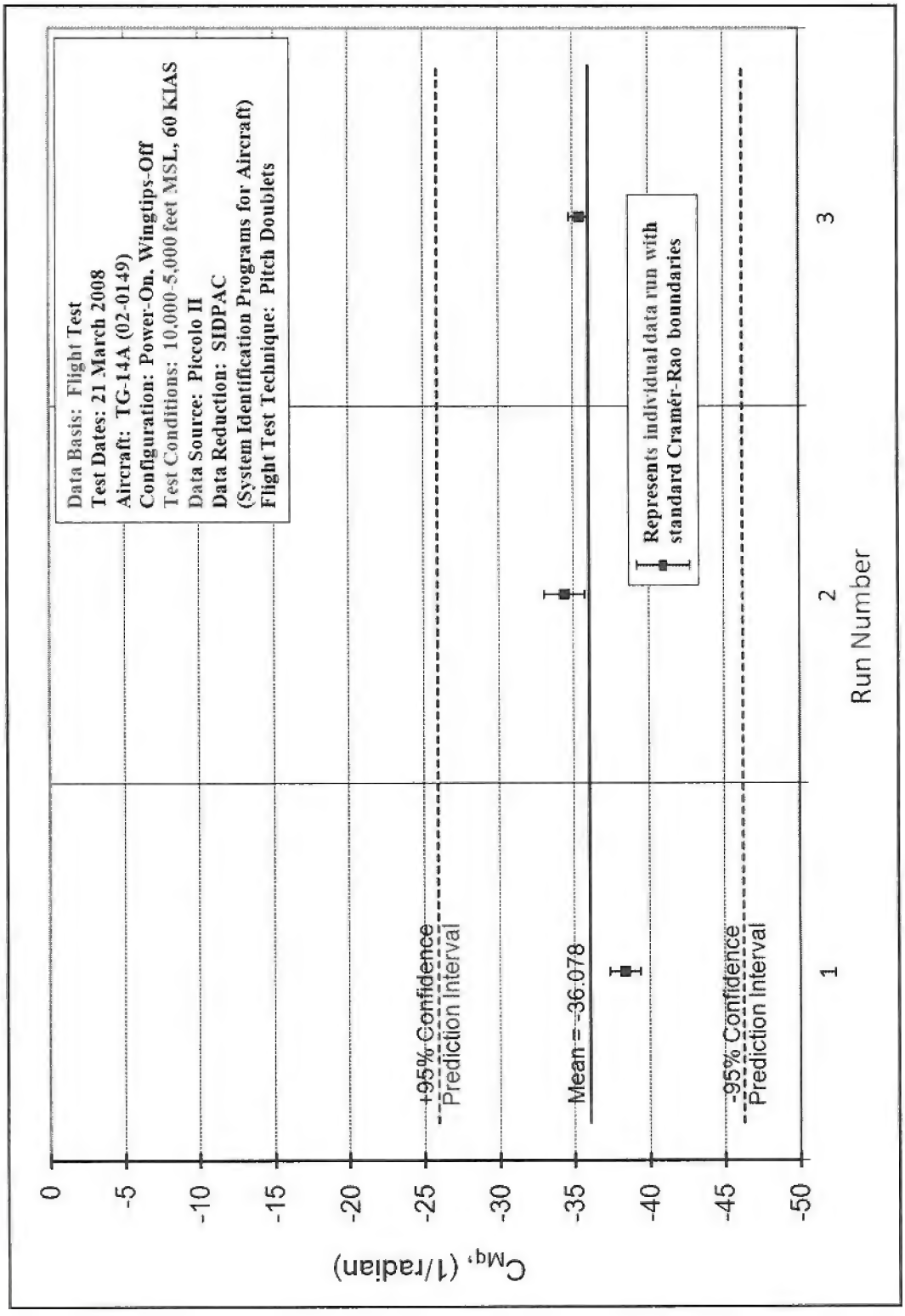

Figure F-12. C_{Mq} (Power-On, Wingtips-Off, 60 KIAS)

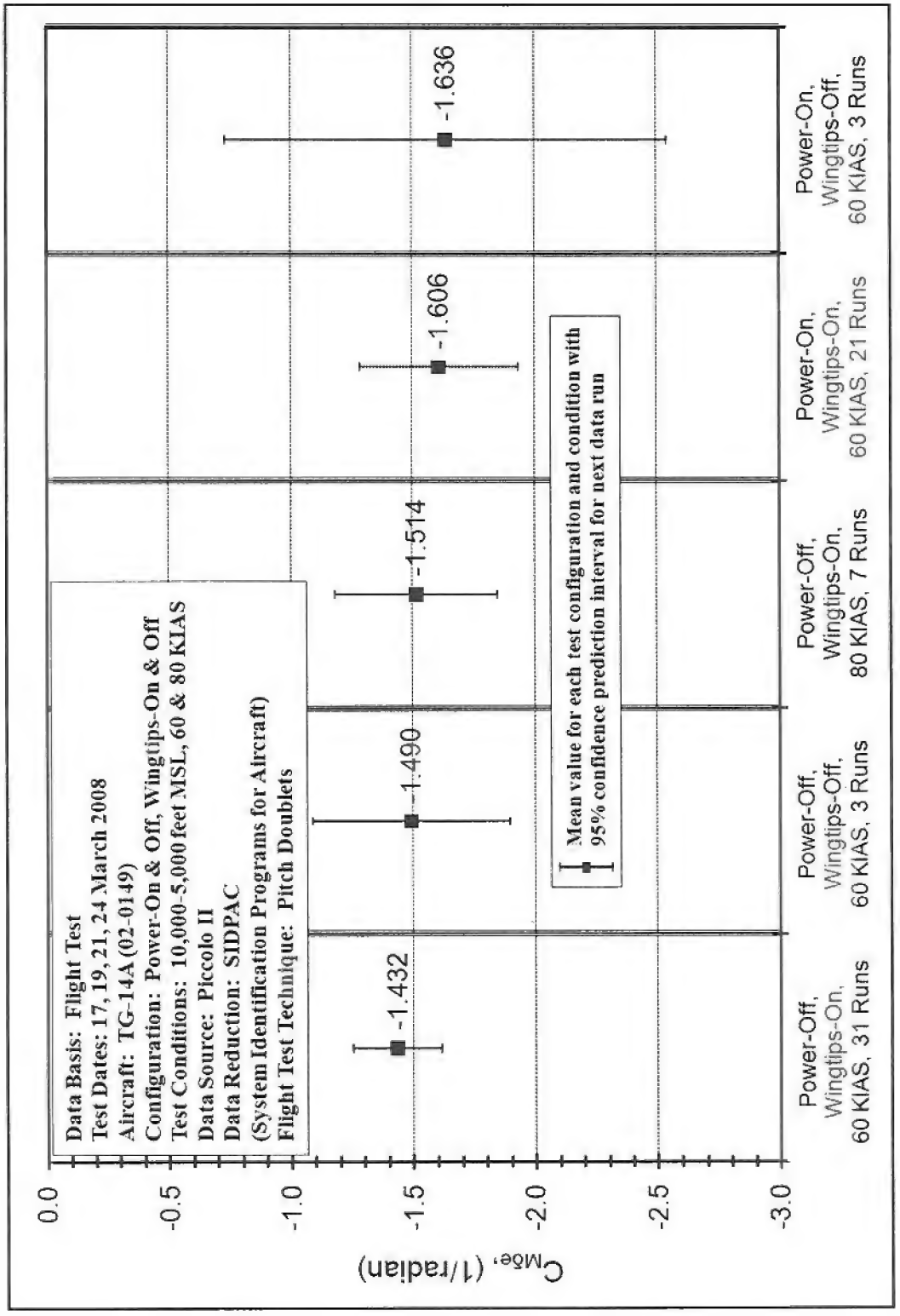

Figure F-13. $C_{M\delta e}$ from all test conditions with 95% confidence intervals

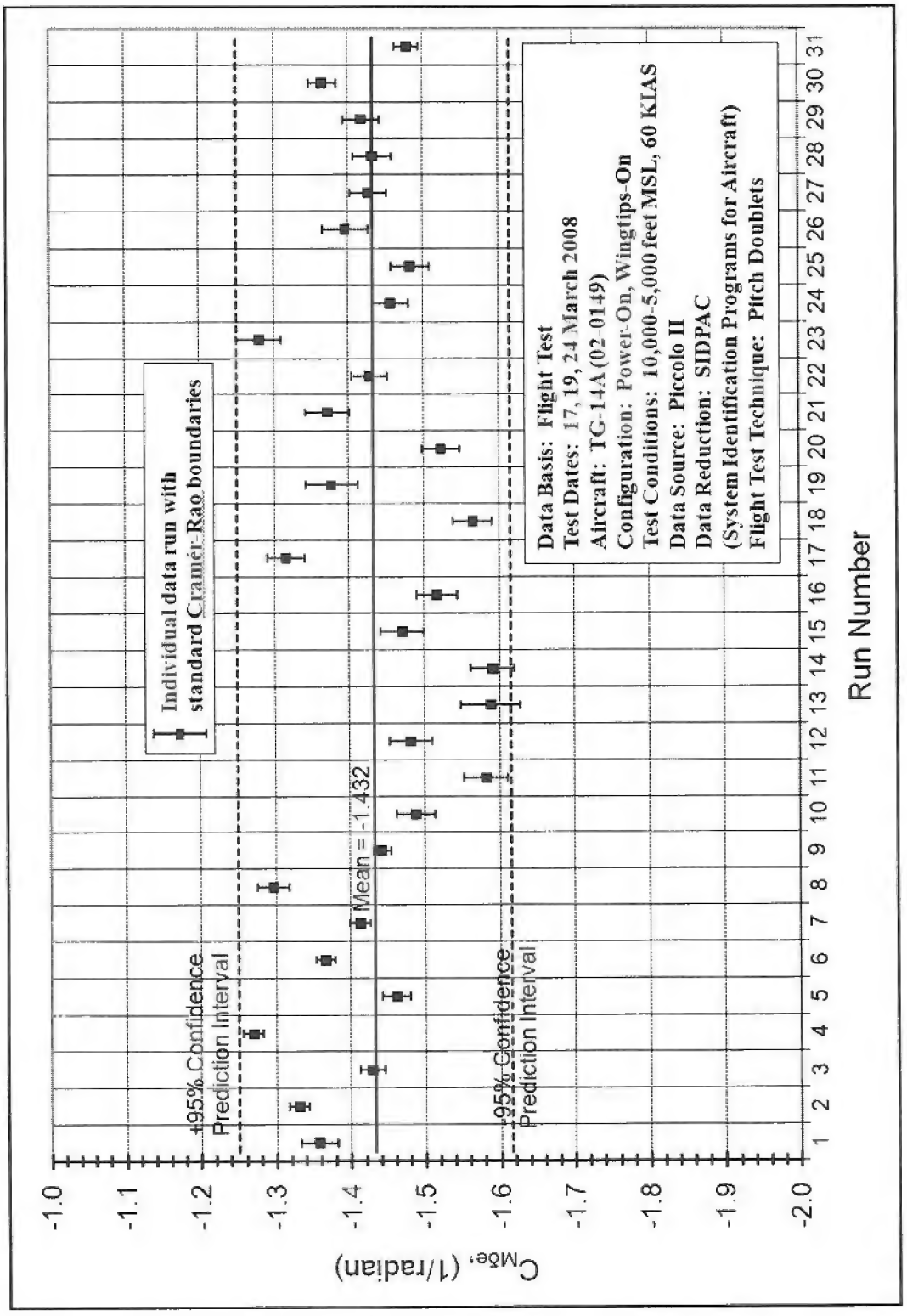

Figure F-14. $C_{M\delta e}$ (Power-Off, Wingtips-On, 60 KIAS)

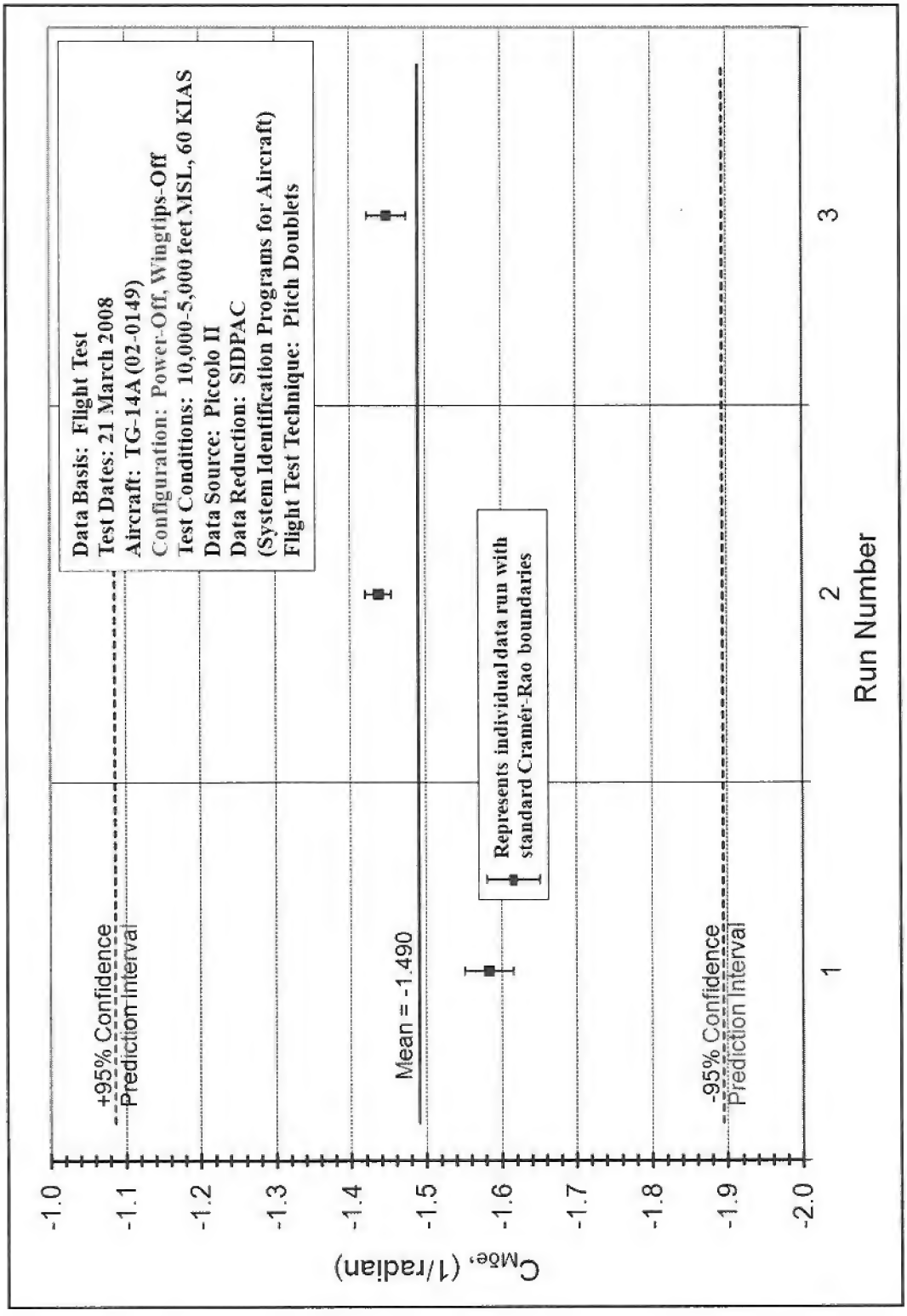

Figure F-15. $C_{M\delta e}$ (Power-Off, Wingtips-Off, 60 KIAS)

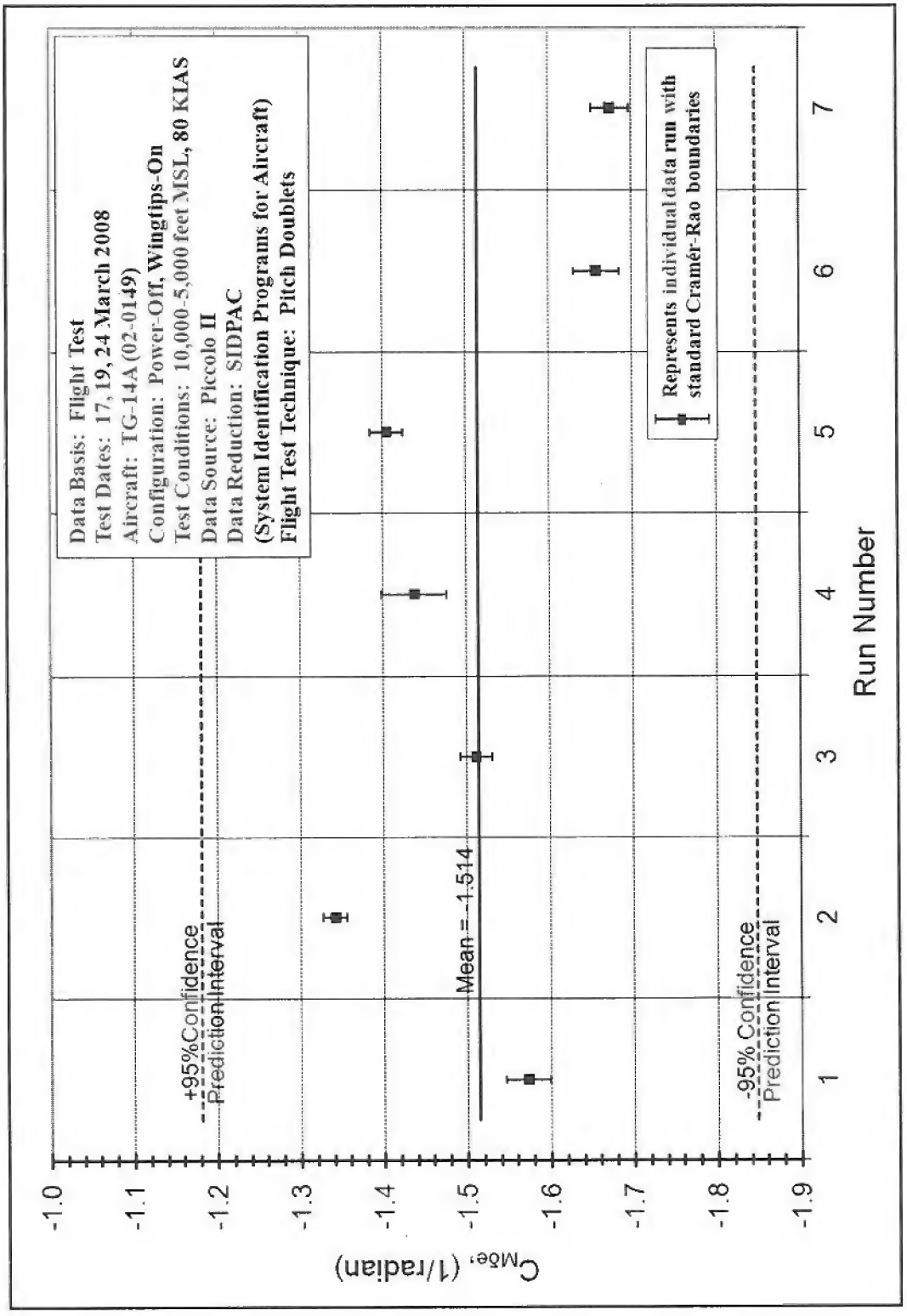

Figure F-16. $C_{M\delta e}$ (Power-Off, Wingtips-On, 80 KIAS)

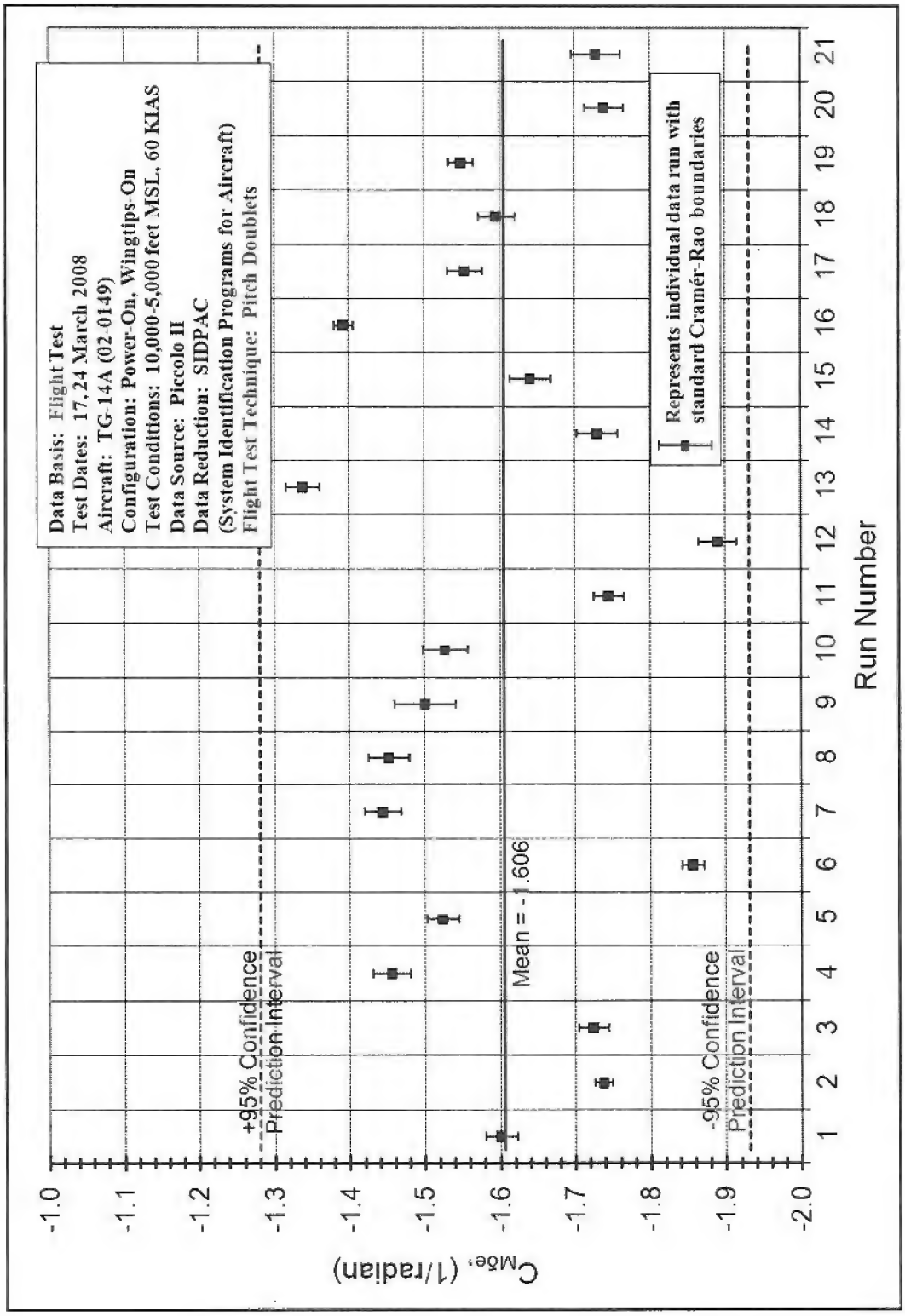

Figure F-17. $C_{M\delta e}$ (Power-On, Wingtips-On, 60 KIAS)

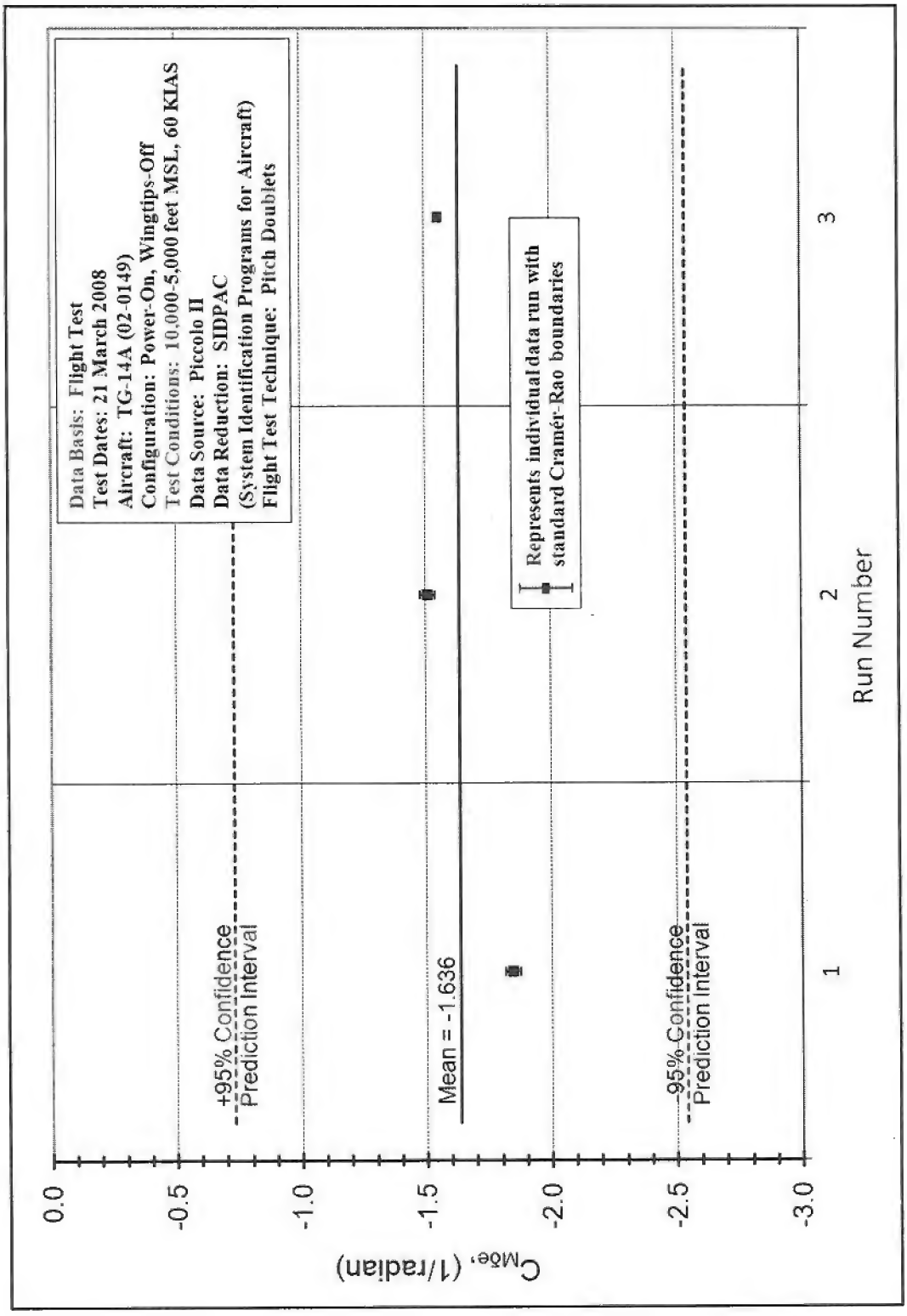

Figure F-18. $C_{M\delta e}$ (Power-On, Wingtips-Off, 60 KIAS)

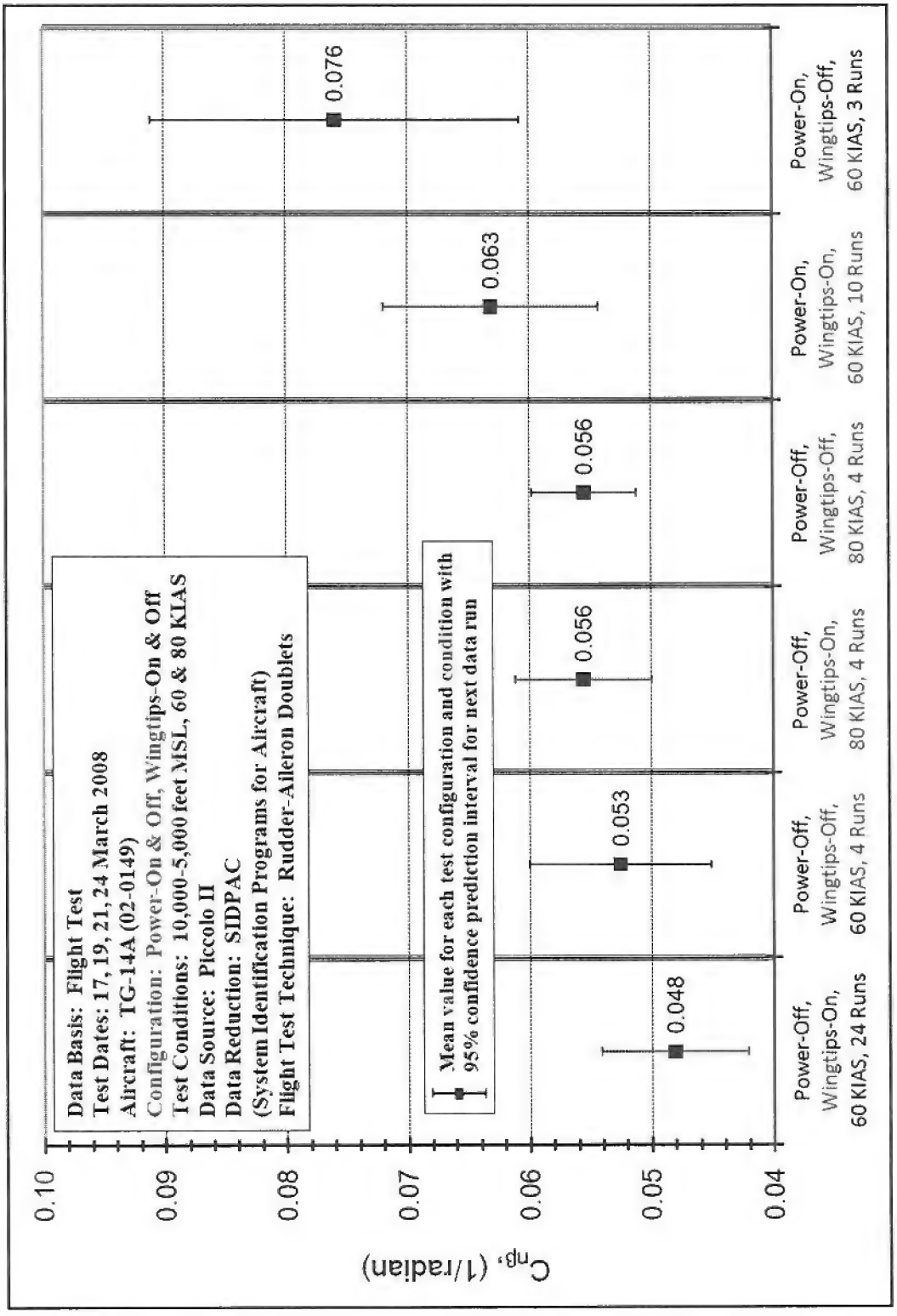

Figure F-19. $C_{n\beta}$ from all test conditions with 95% confidence intervals

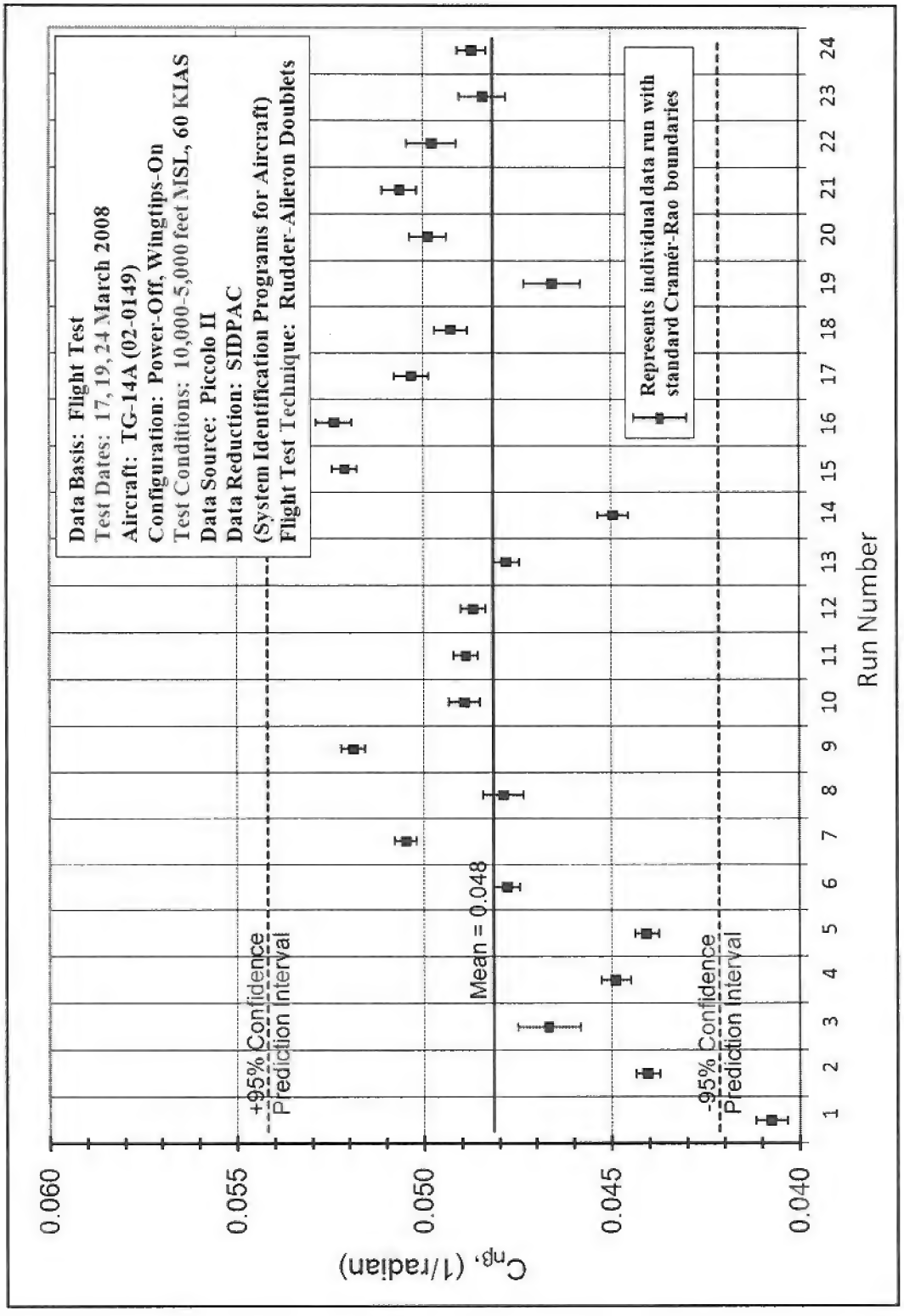

Figure F-20. $C_{n\beta}$ (Power-Off, Wingtips-On, 60 KIAS)

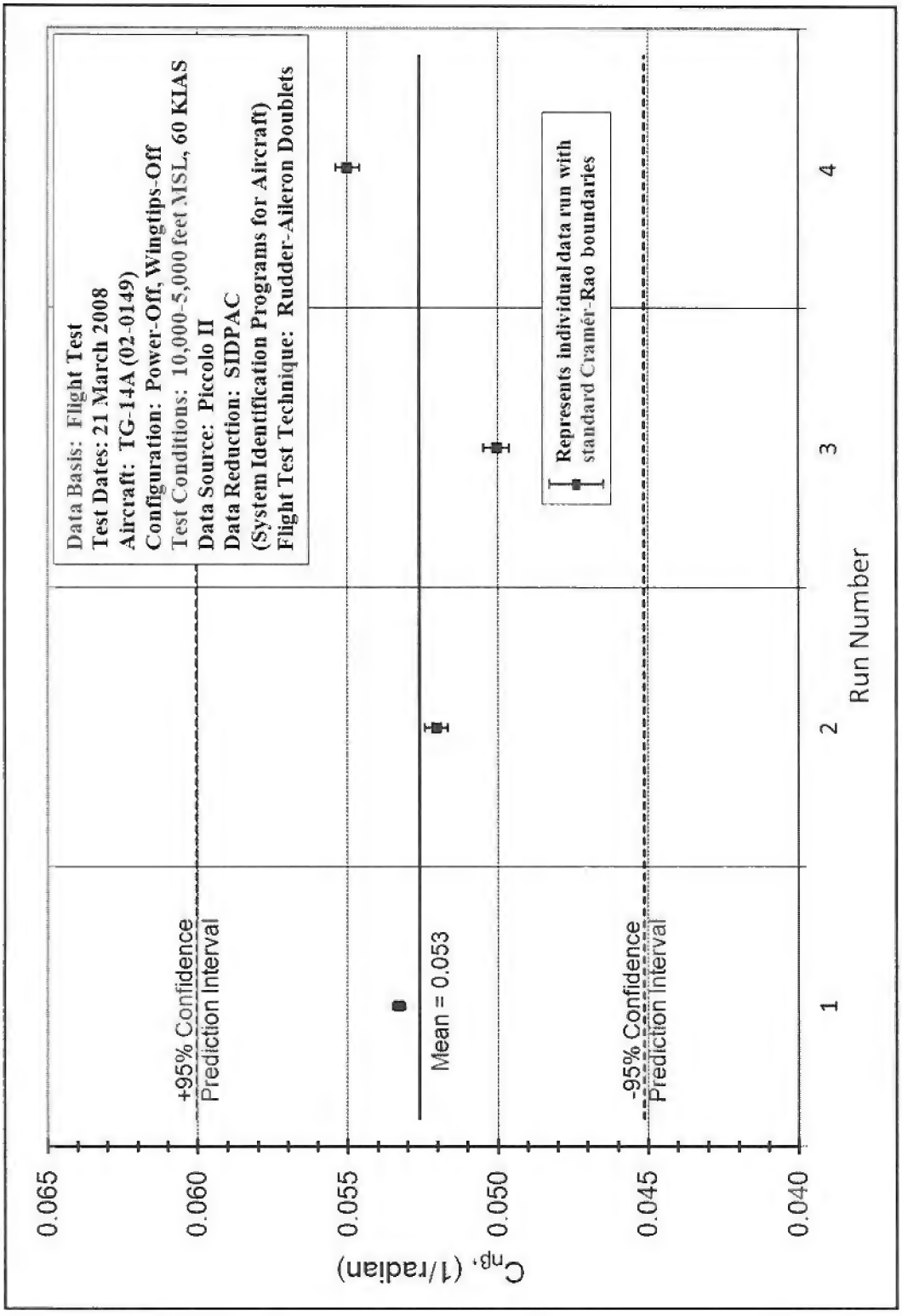

Figure F-21. $C_{n\beta}$ (Power-Off, Wingtips-Off, 60 KIAS)

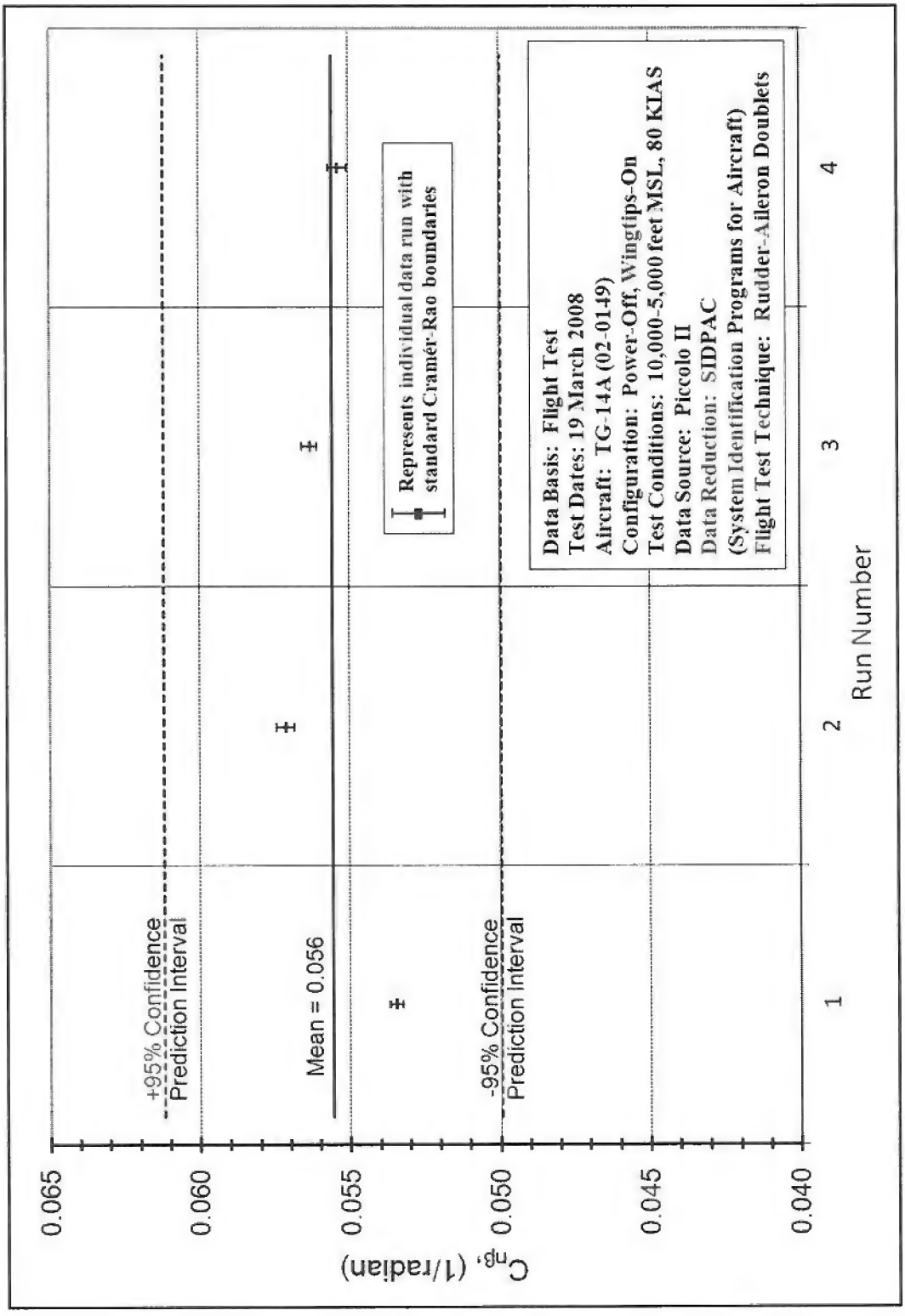

Figure F-22. C_{n_β} (Power-Off, Wingtips-On, 80 KIAS)

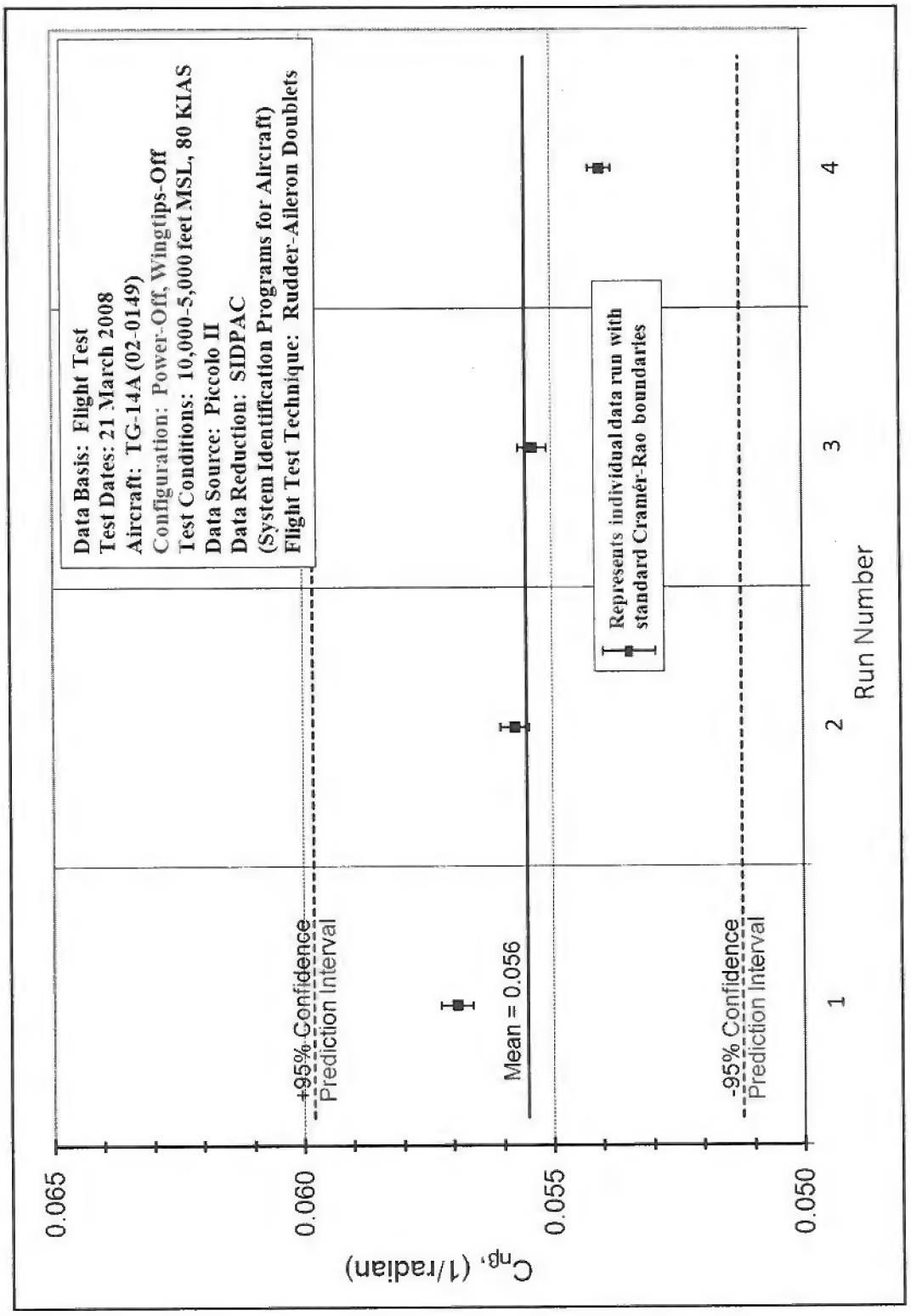

Figure F-23. $C_{n\beta}$ (Power-Off, Wingtips-Off, 80 KIAS)

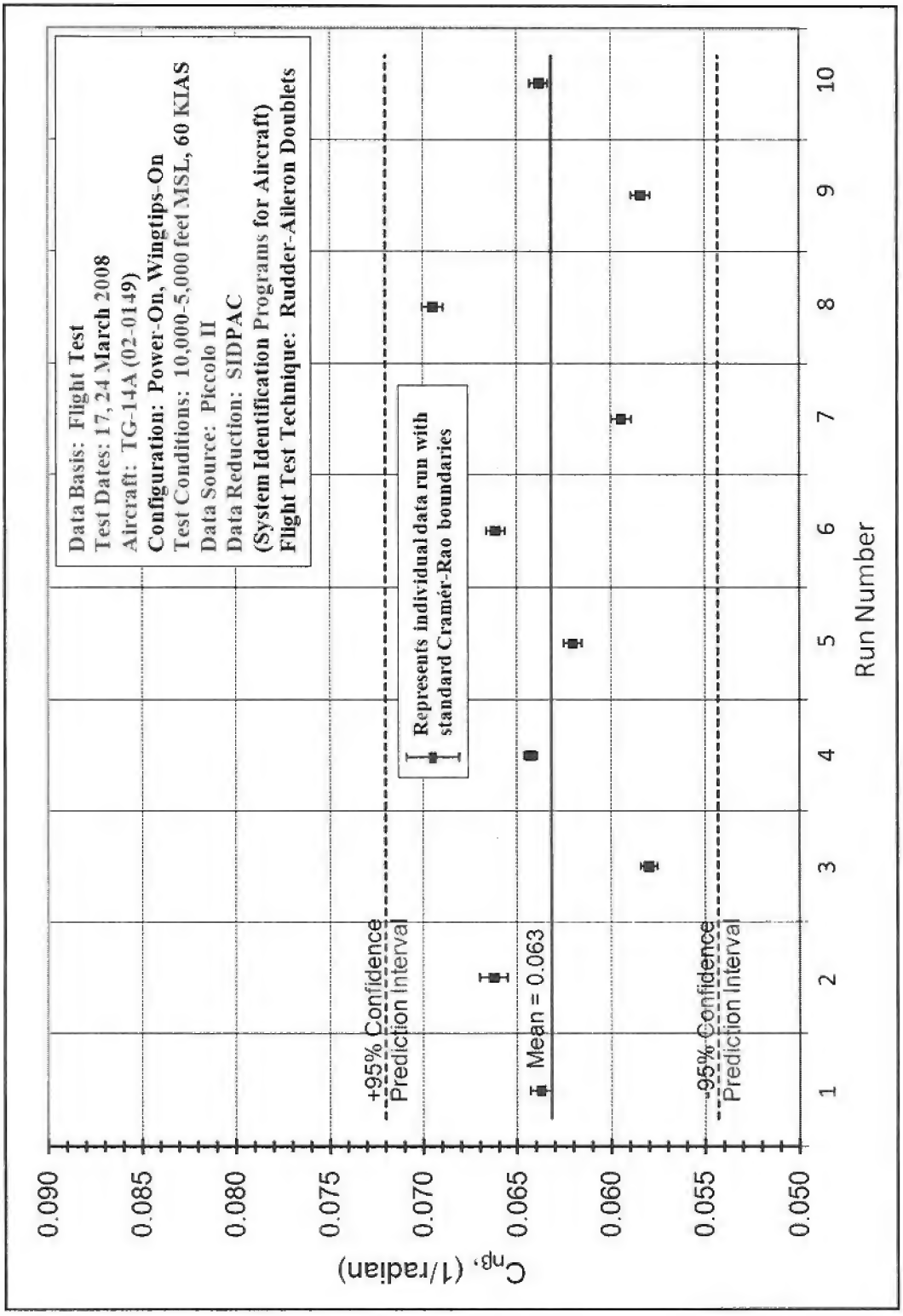

Figure F-24. $C_{n\beta}$ (Power-On, Wingtips-On, 60 KIAS)

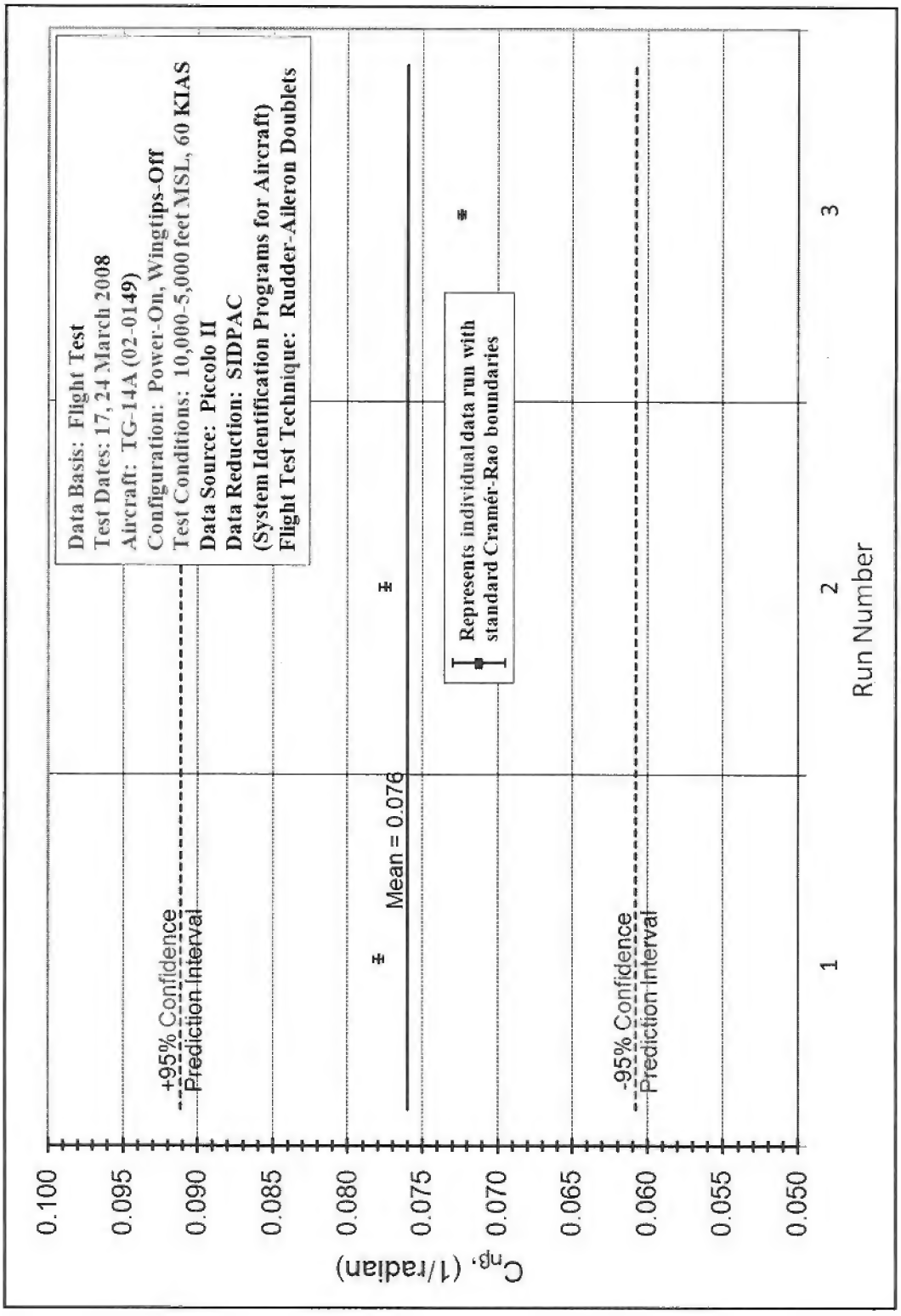

Figure F-25. $C_{n\beta}$ (Power-On, Wingtips-Off, 60 KIAS)

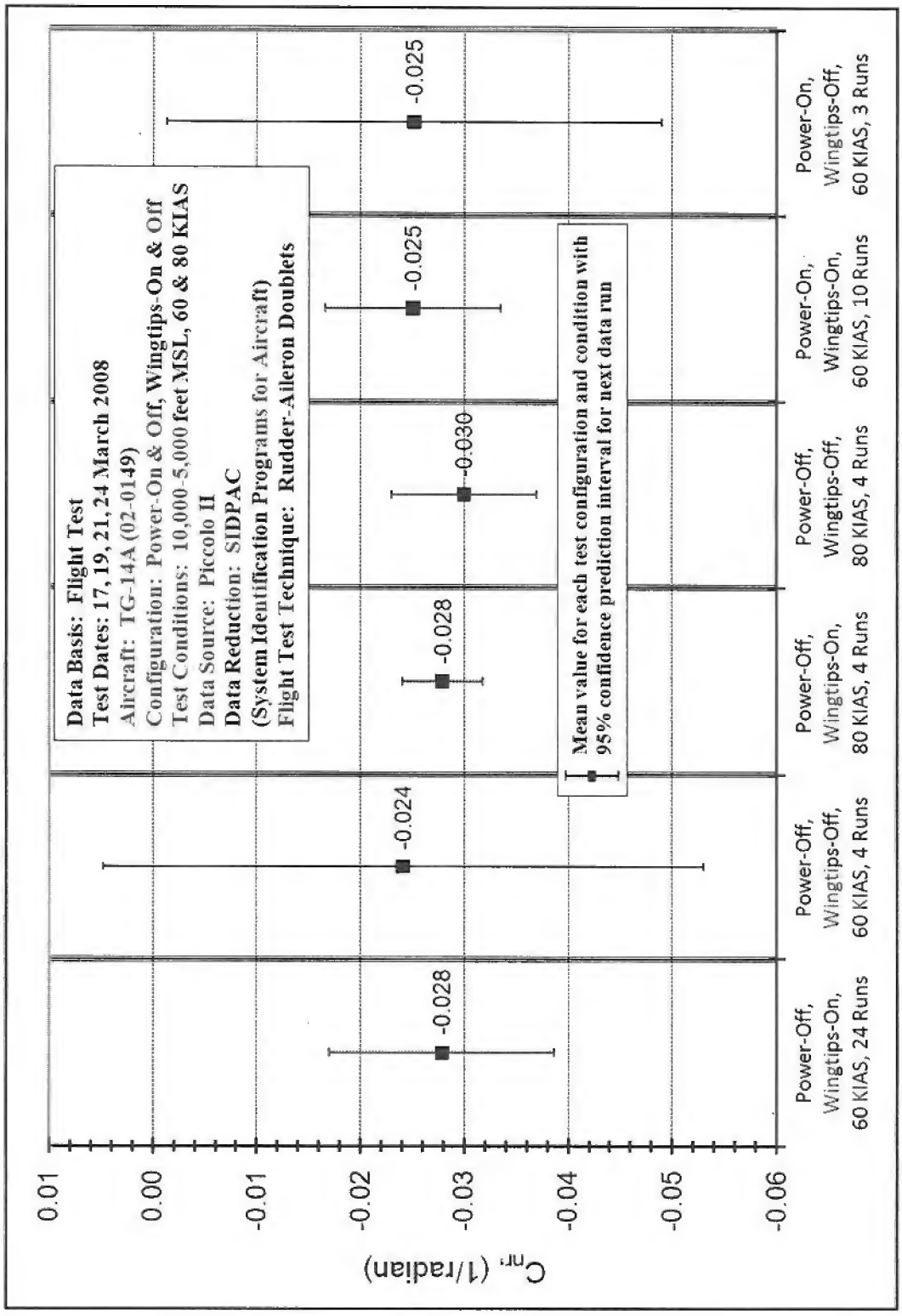

Figure F-26. C_{nr} from all test conditions with 95% confidence intervals

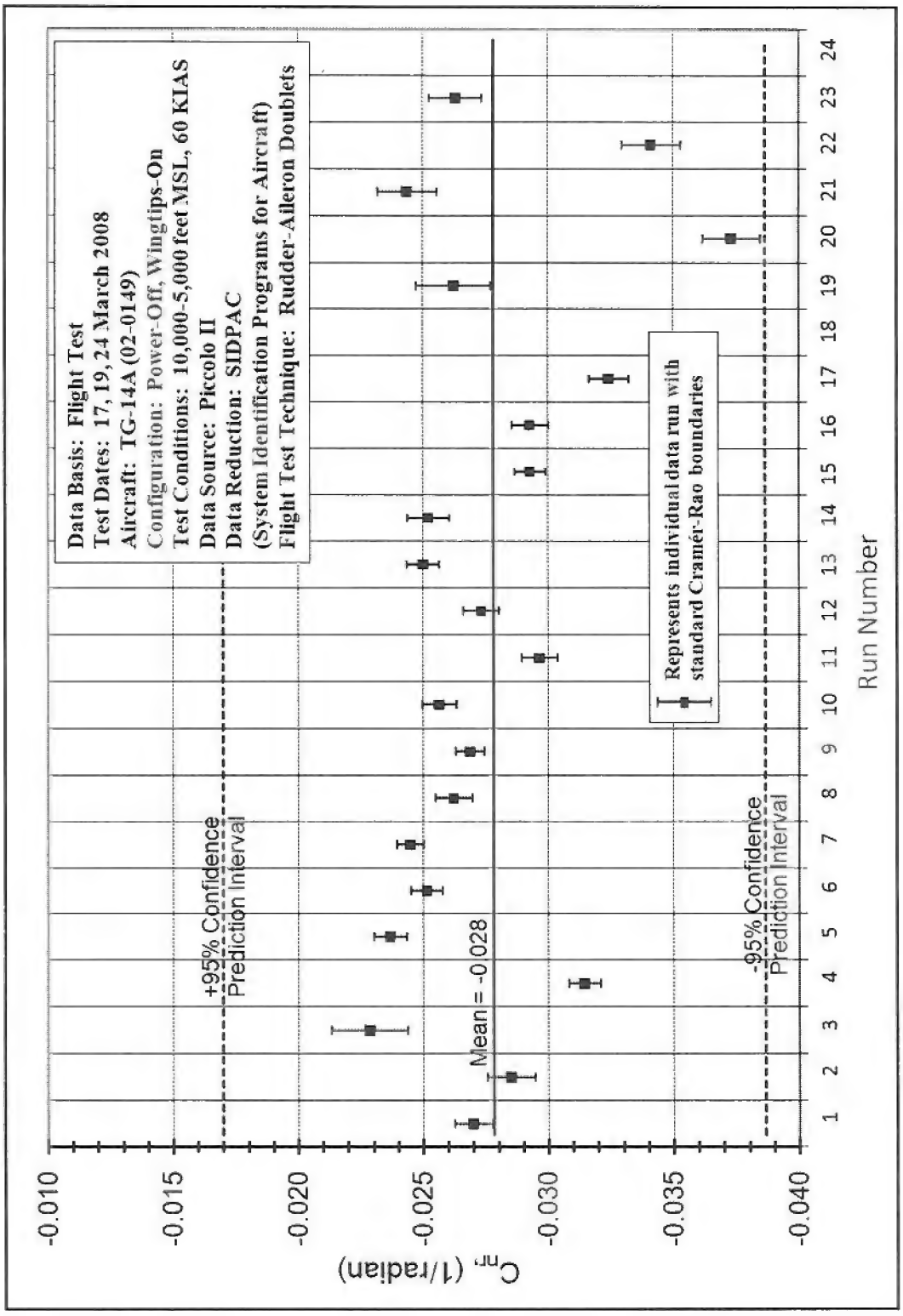

Figure F-27. C_{nr} (Power-Off, Wingtips-On, 60 KIAS)

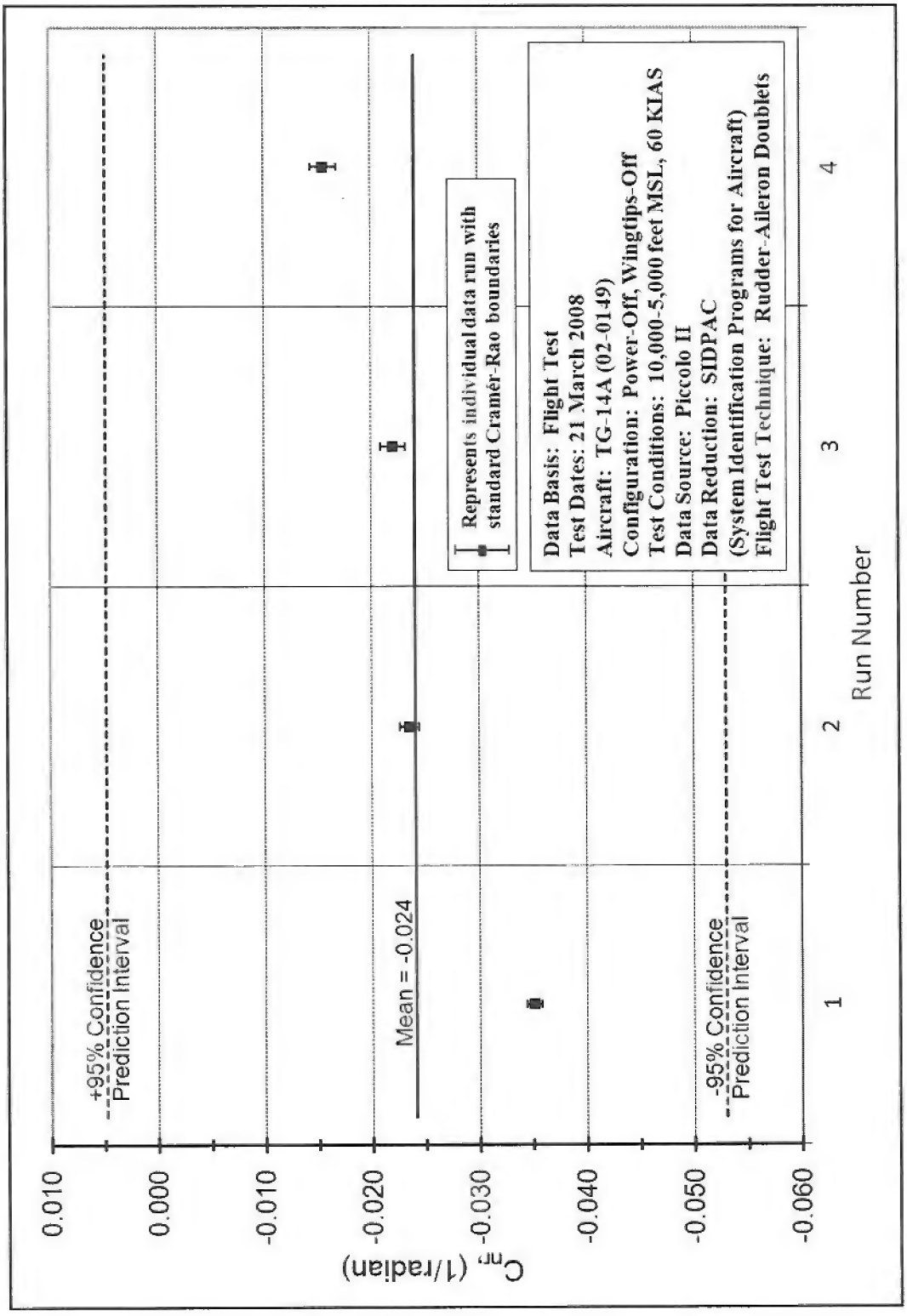

Figure F-28. C_{nr} (Power-Off, Wingtips-Off, 60 KIAS)

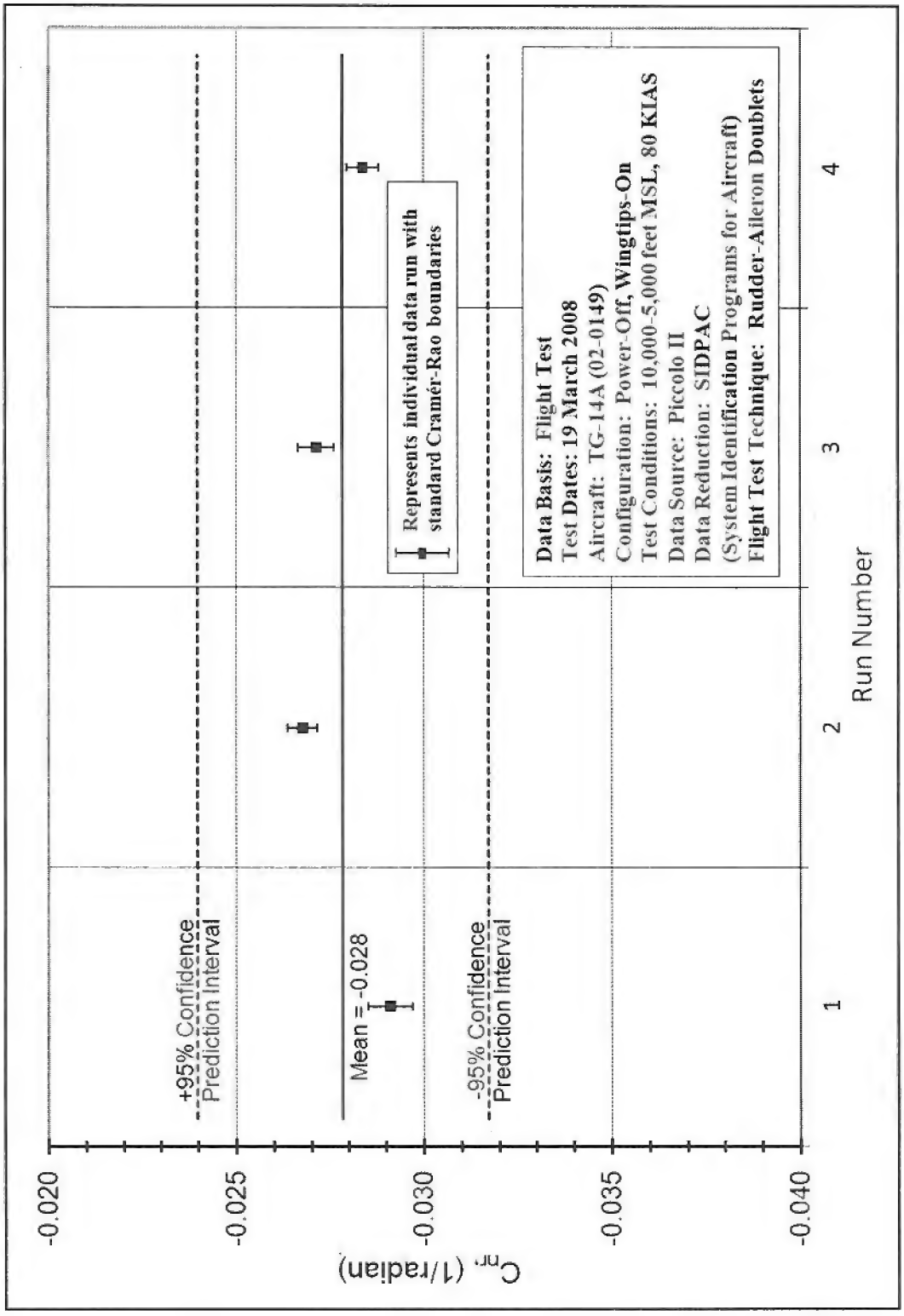

Figure F-29. C_{nr} (Power-Off, Wingtips-On, 80 KIAS)

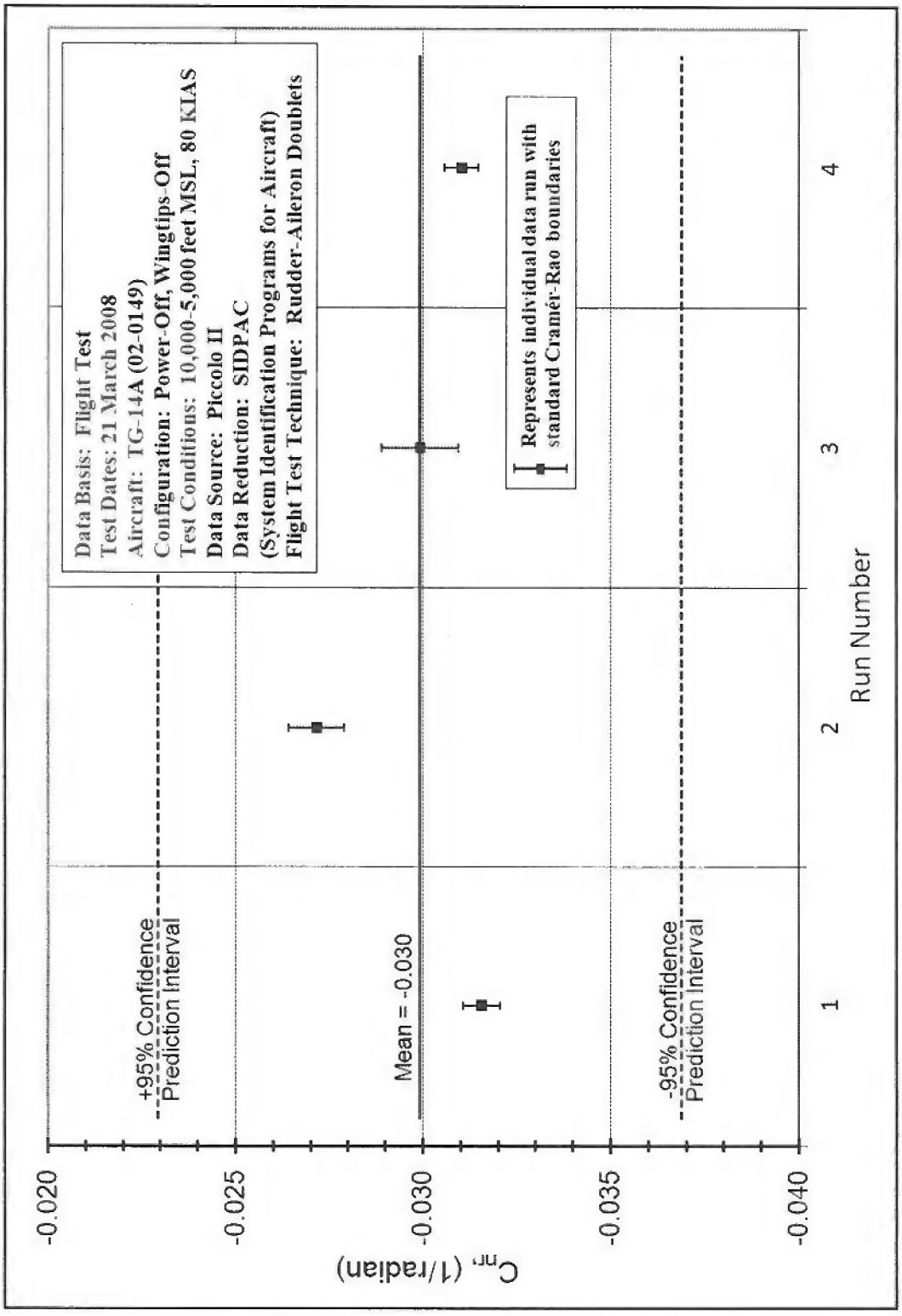

Figure F-30. C_{n_r} (Power-Off, Wingtips-Off, 80 KIAS)

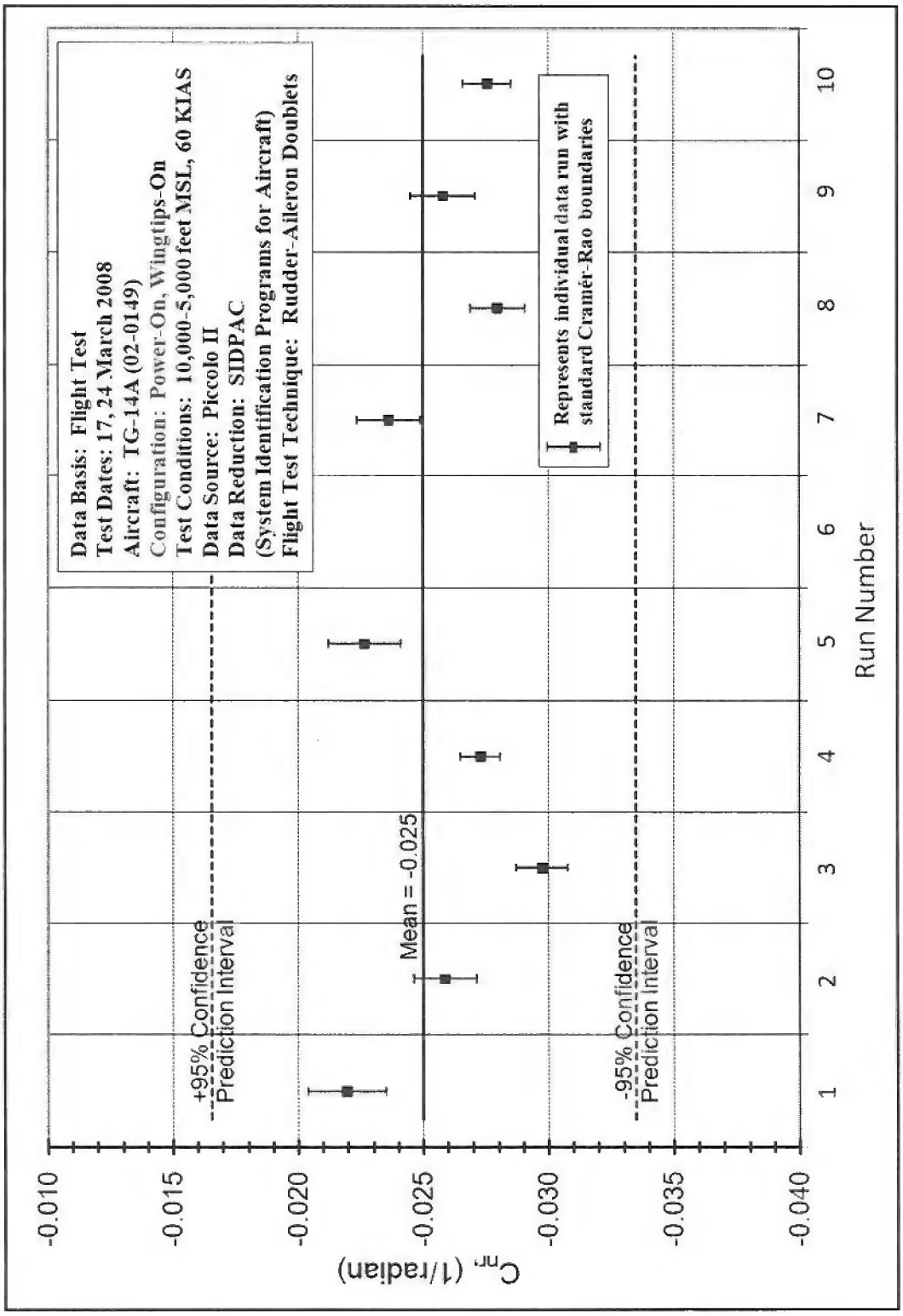

Figure F-31. C_{nr} (Power-On, Wingtips-On, 60 KIAS)

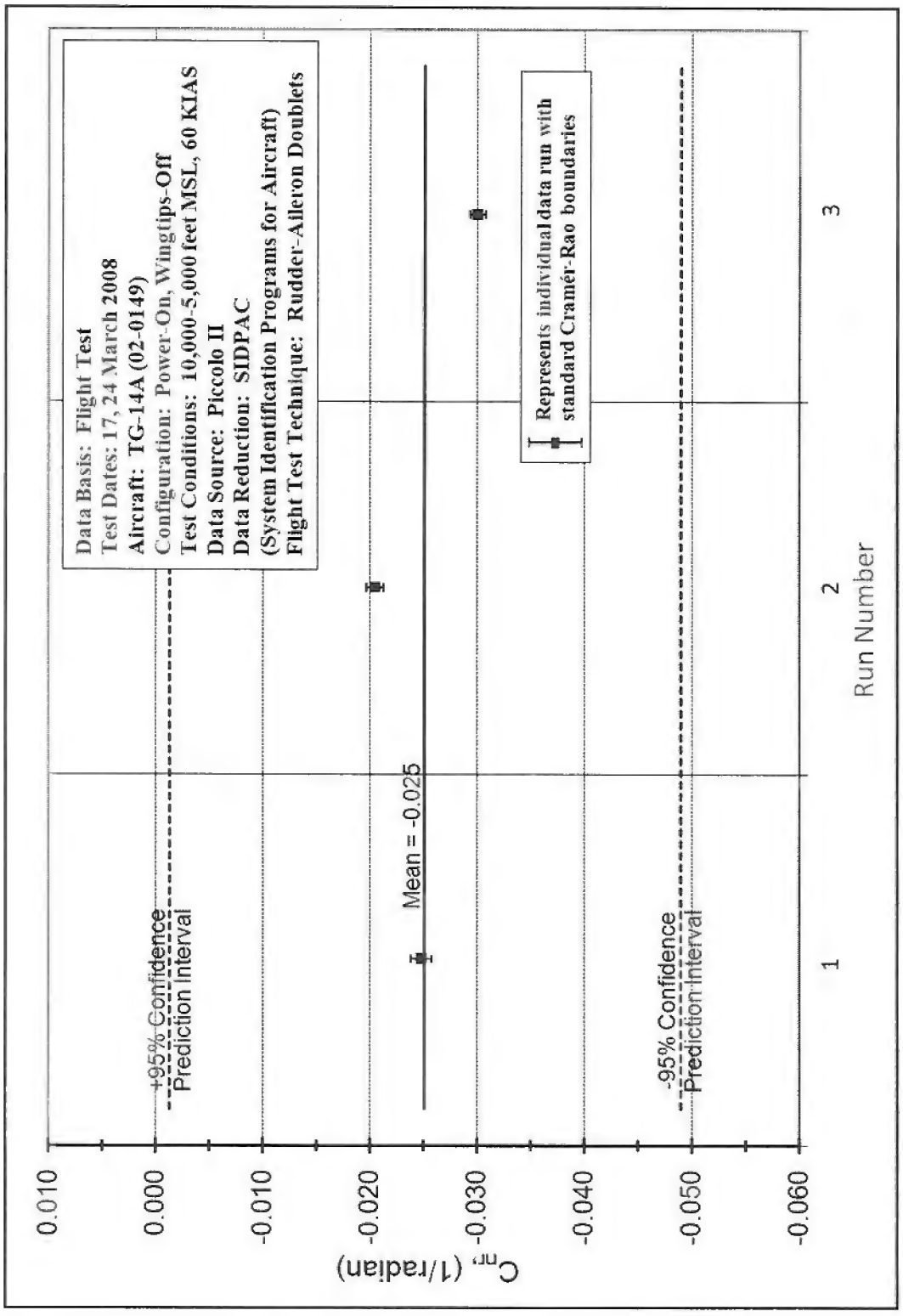

Figure F-32. C_{nr} (Power-On, Wingtips-Off, 60 KIAS)

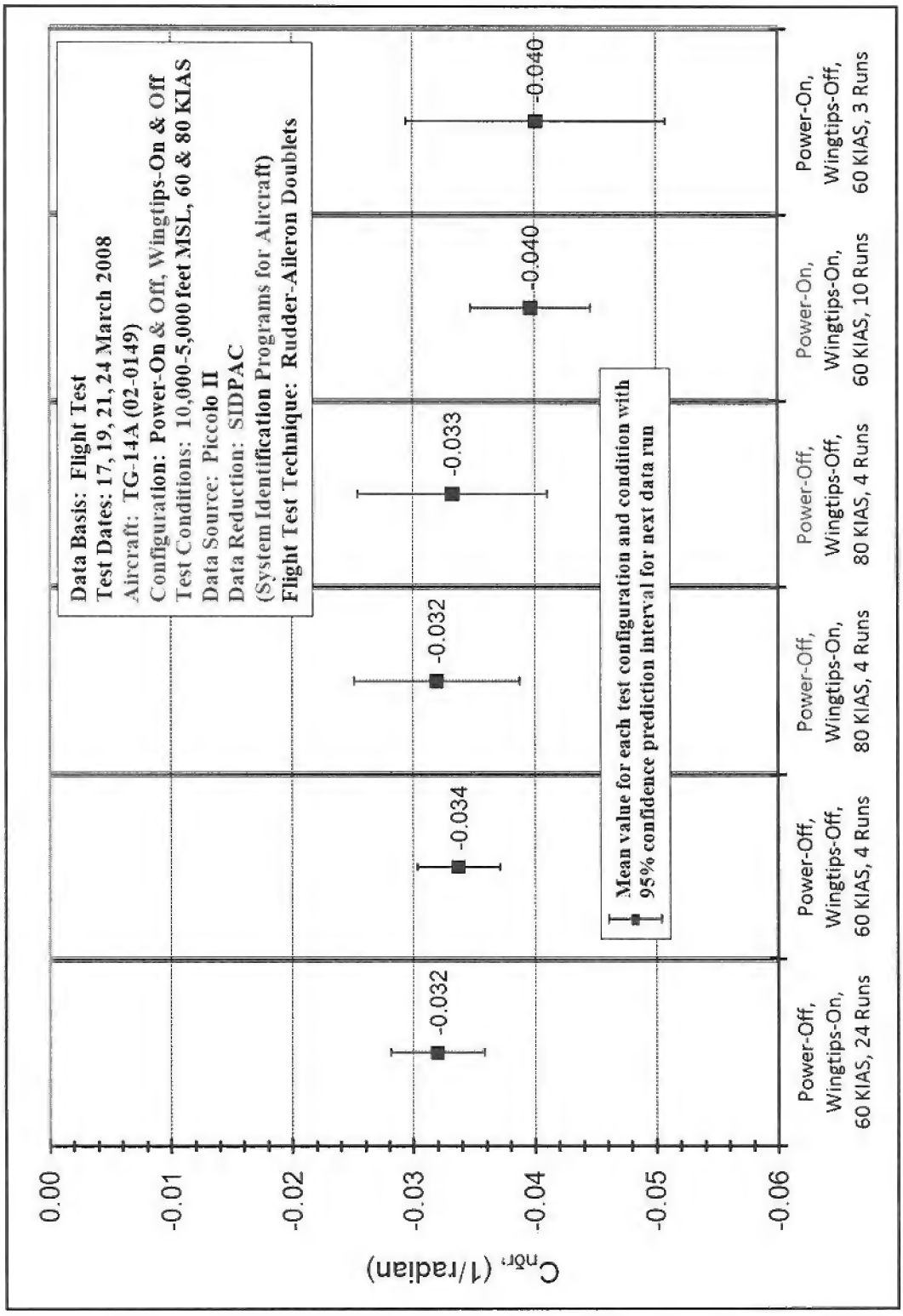

Figure F-33. $C_{n\delta r}$ from all test conditions with 95% confidence intervals

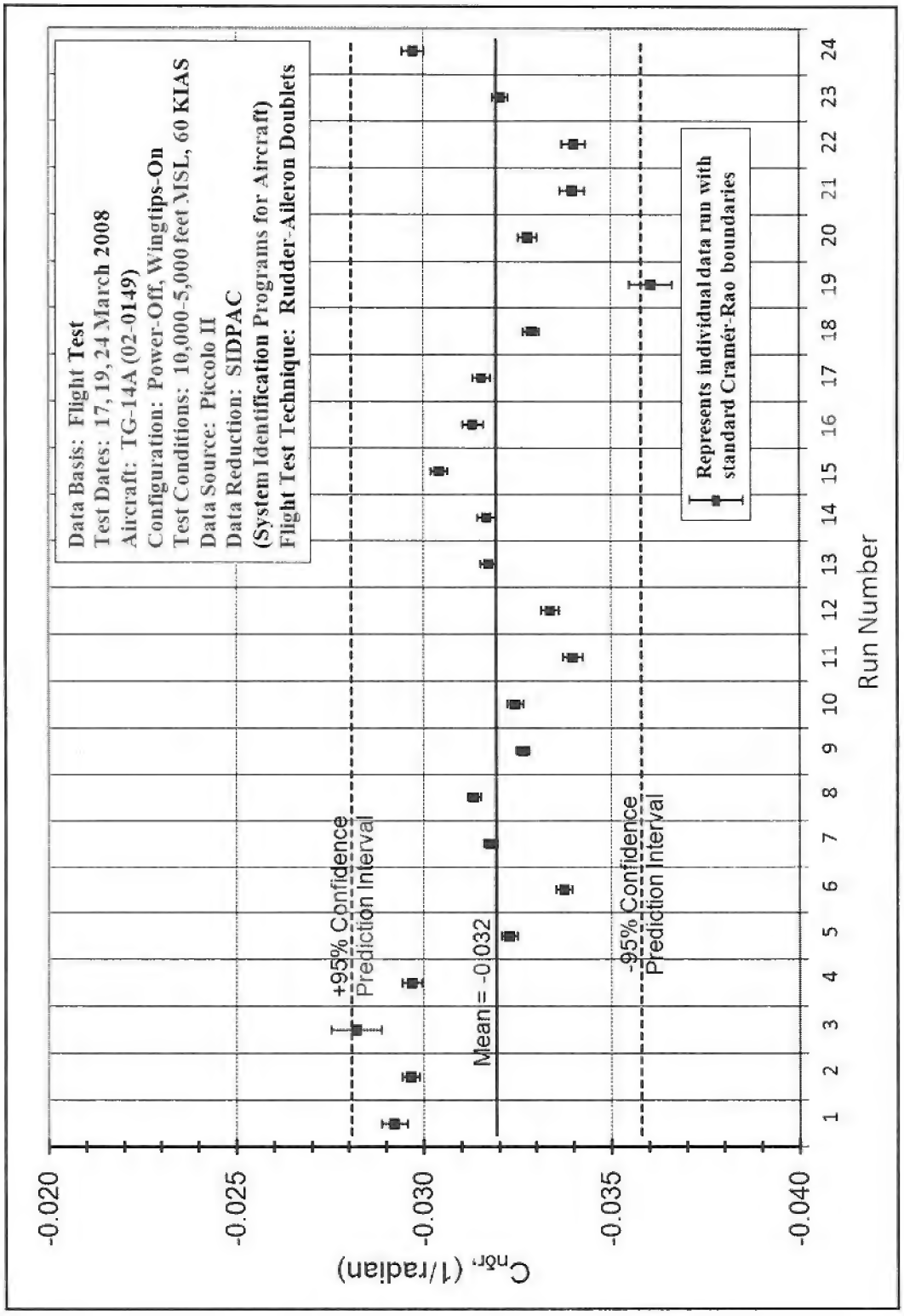

Figure F-34. $C_{n\delta r}$ (Power-Off, Wingtips-On, 60 KIAS)

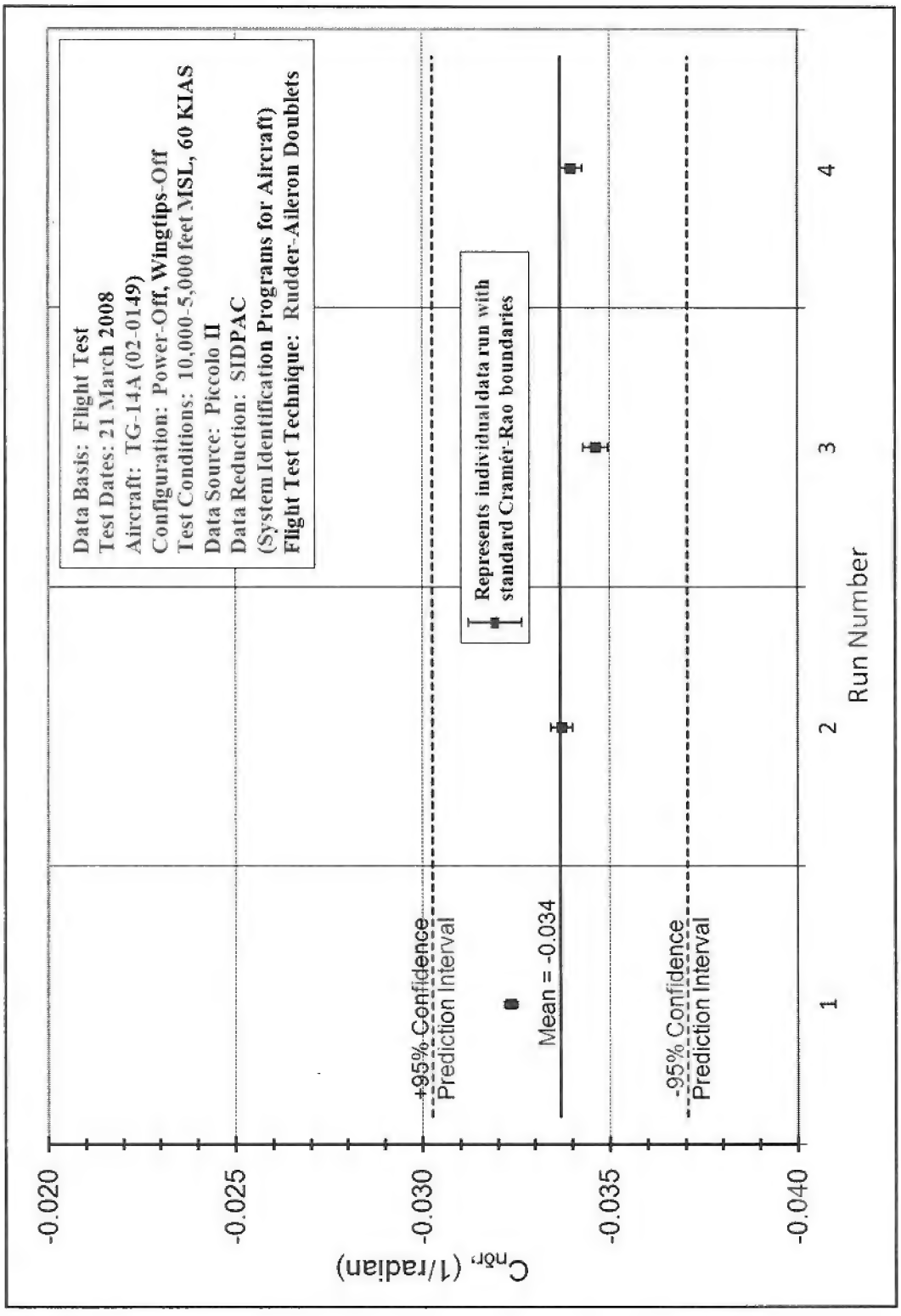

Figure F-35. $C_{n\delta r}$ (Power-Off, Wingtips-Off, 60 KIAS)

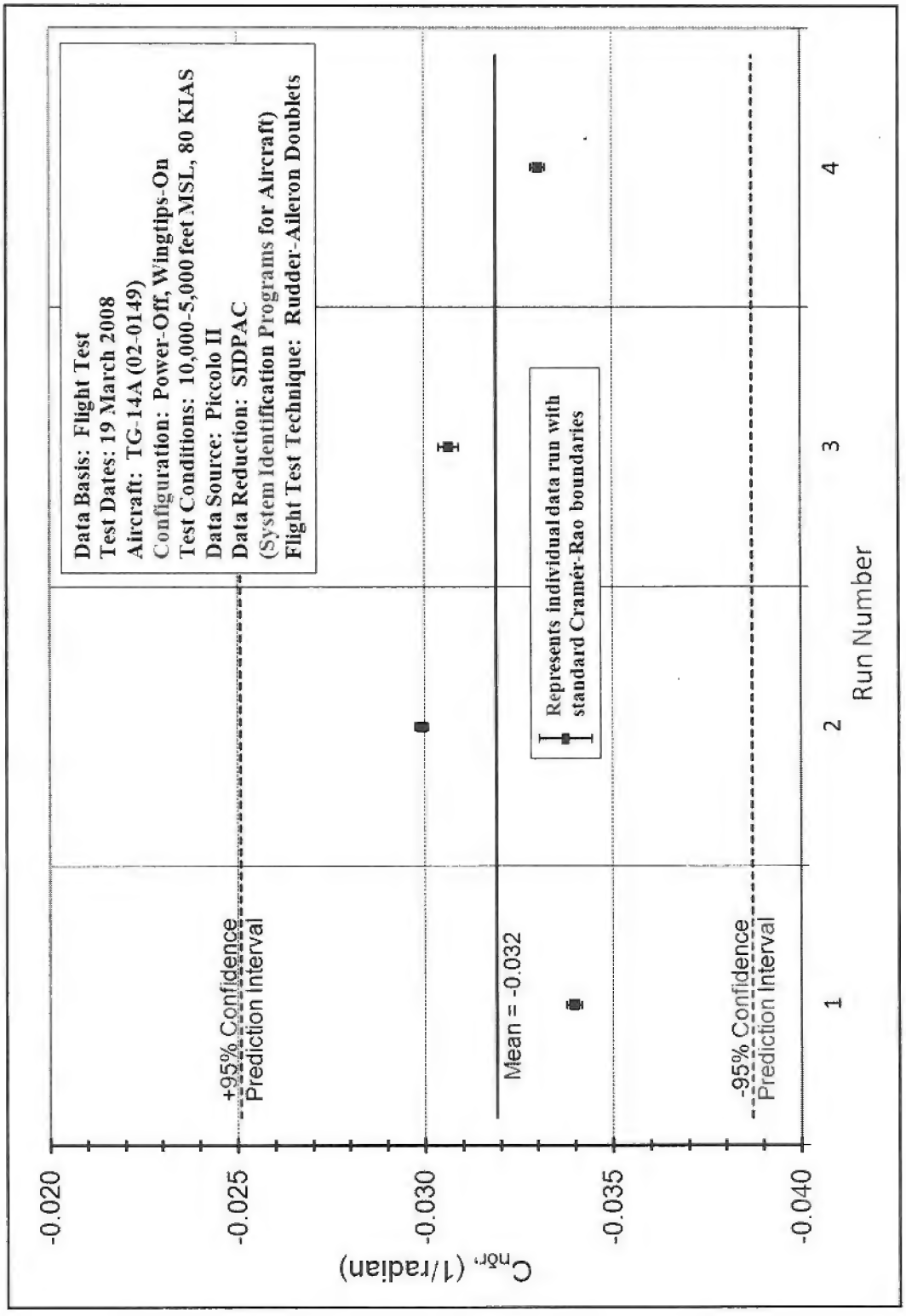

Figure F-36. $C_{n\delta r}$ (Power-Off, Wingtips-On, 80 KIAS)

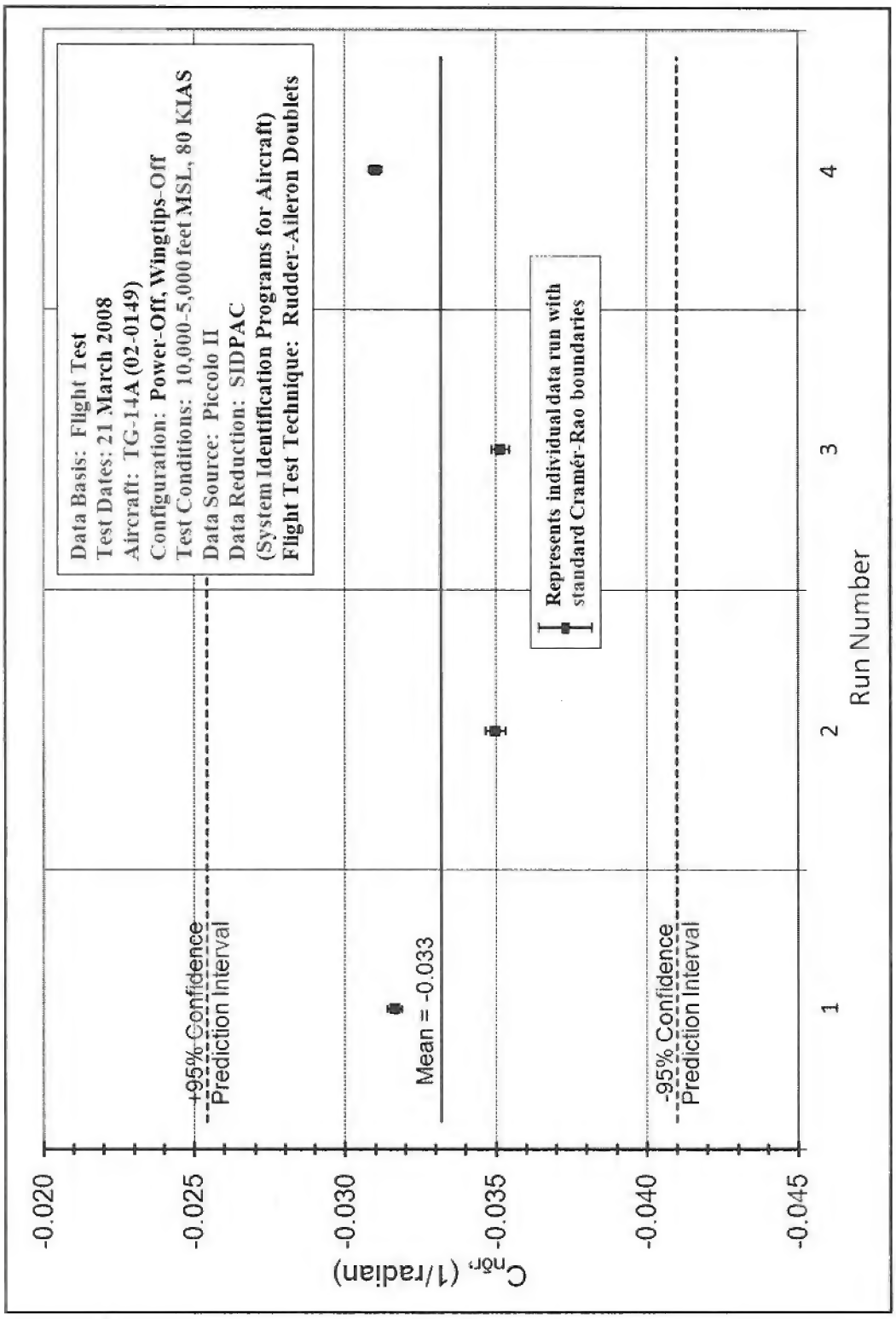

Figure F-37. $C_{n\delta r}$ (Power-Off, Wingtips-Off, 80 KIAS)

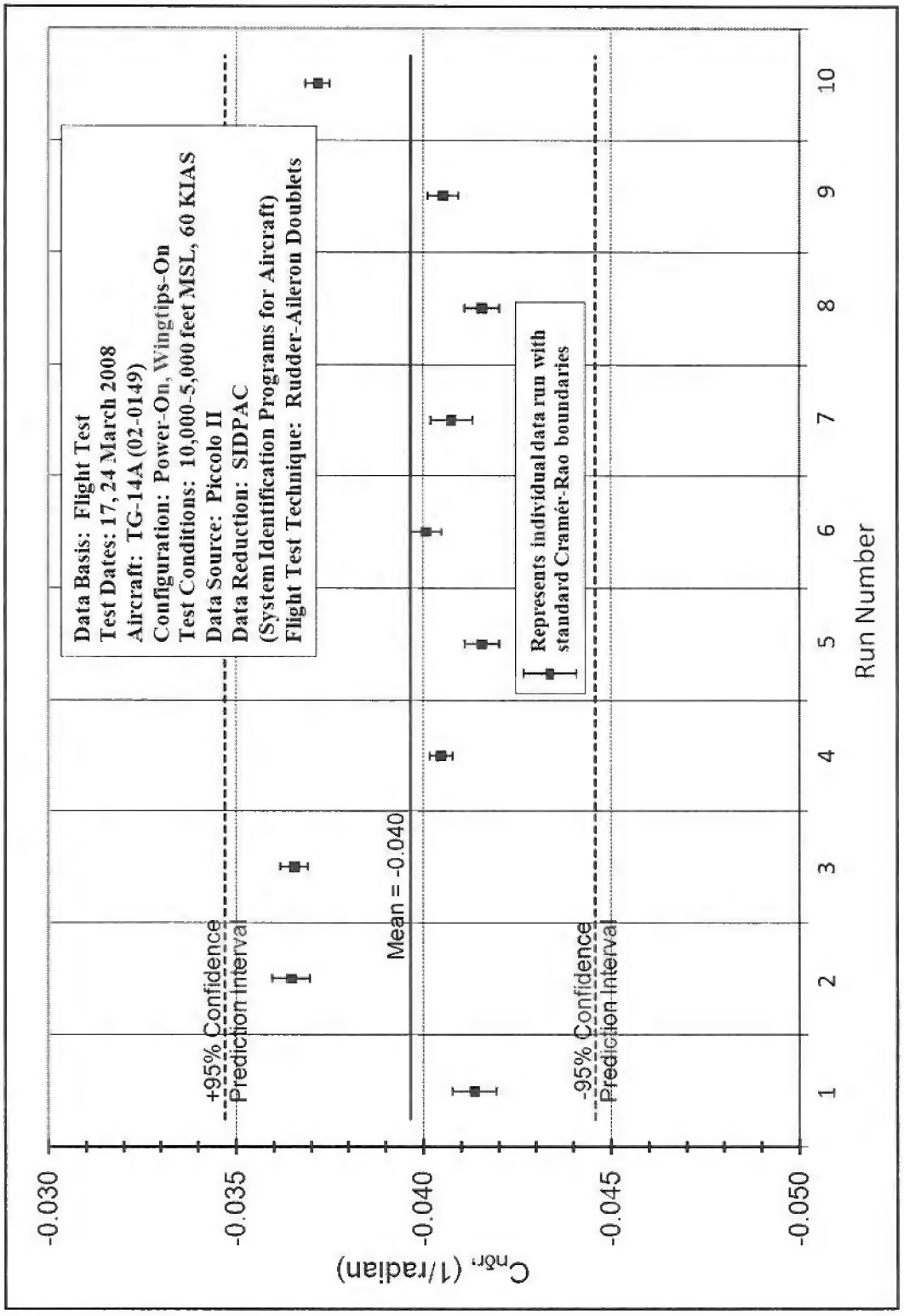

Figure F-38. $C_{n\delta r}$ (Power-On, Wingtips-On, 60 KIAS)

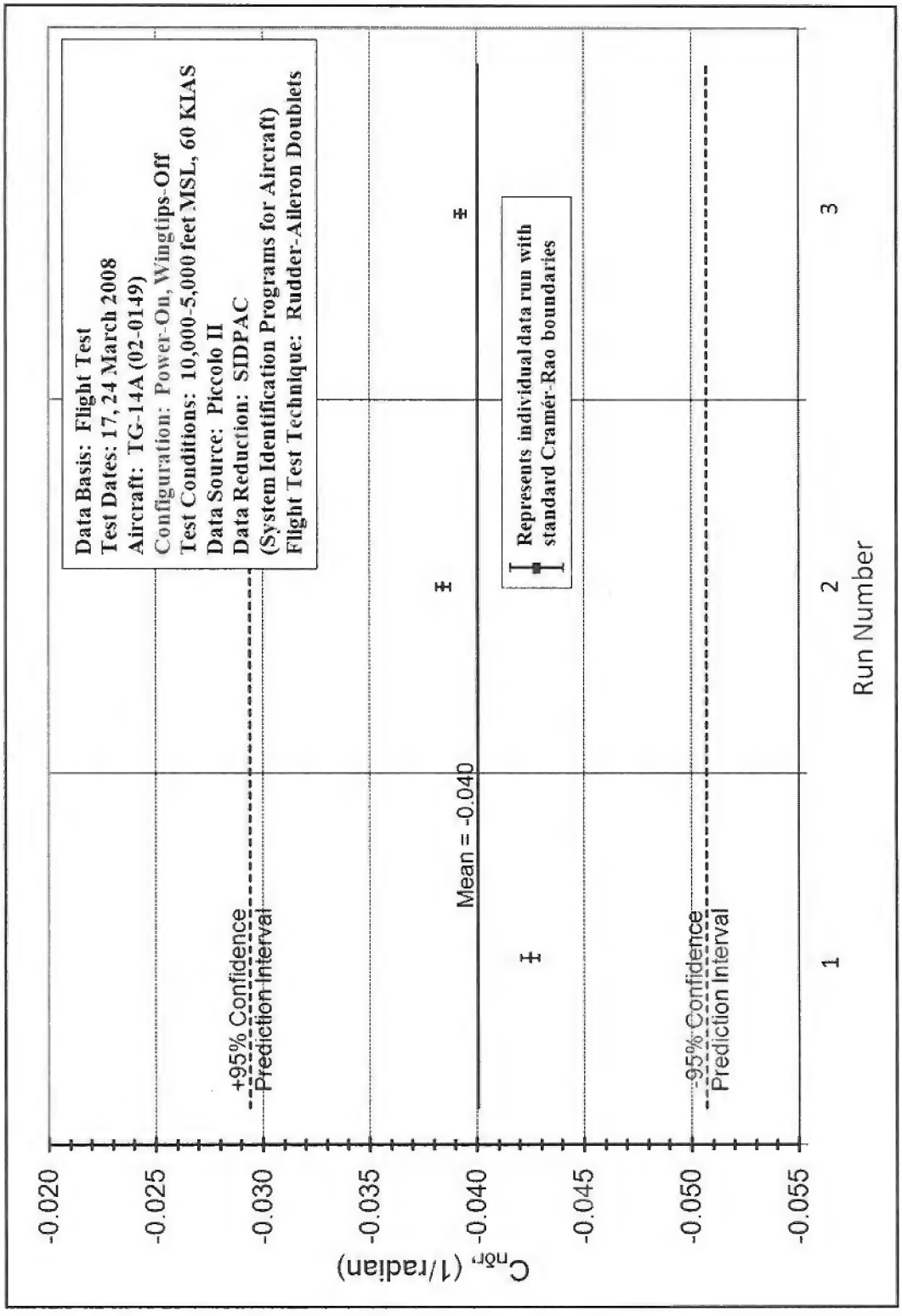

Figure F-39. $C_{n\delta r}$ (Power-On, Wingtips-Off, 60 KIAS)

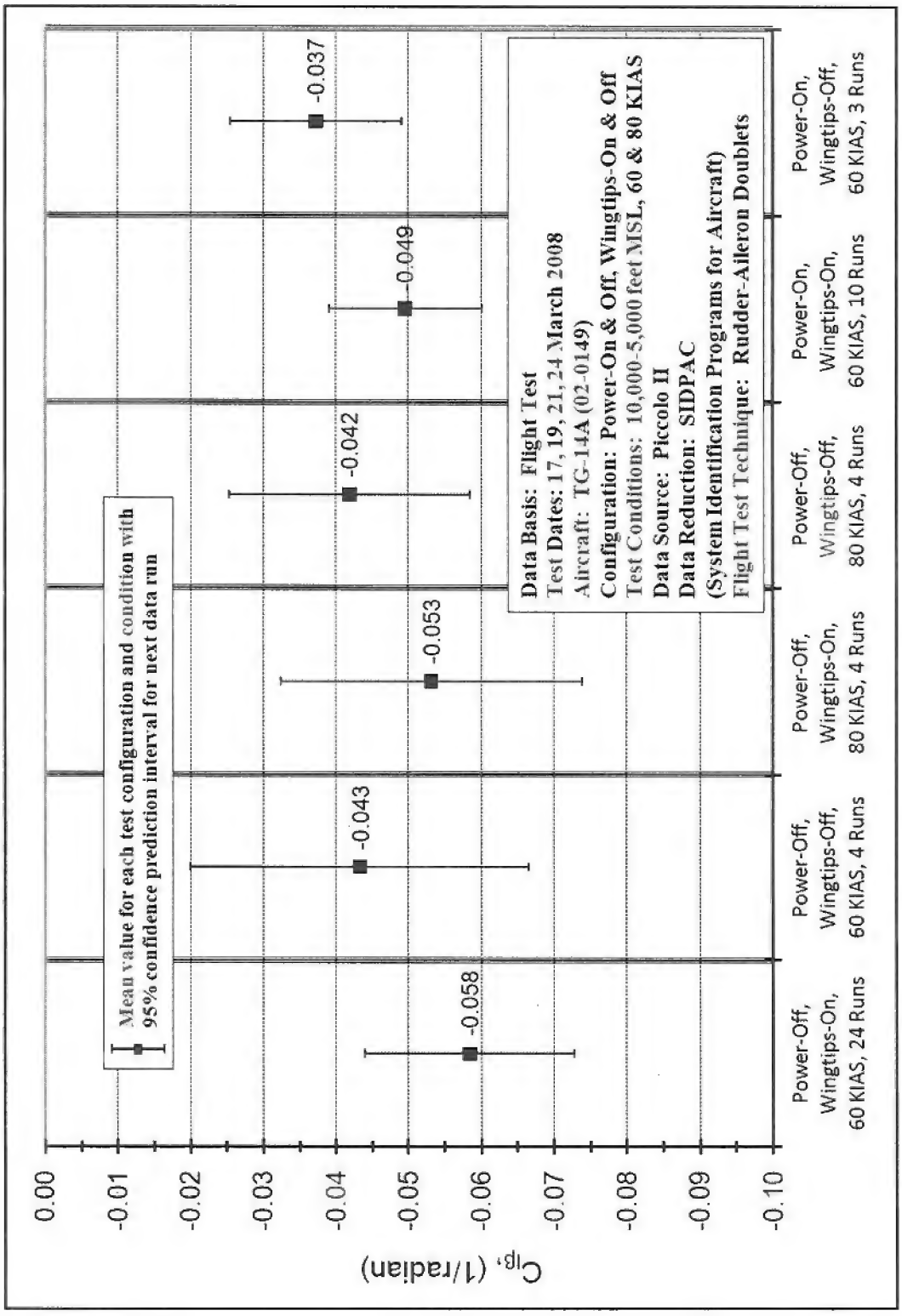

Figure F-40. $C_{l\beta}$ from all test conditions with 95% confidence intervals

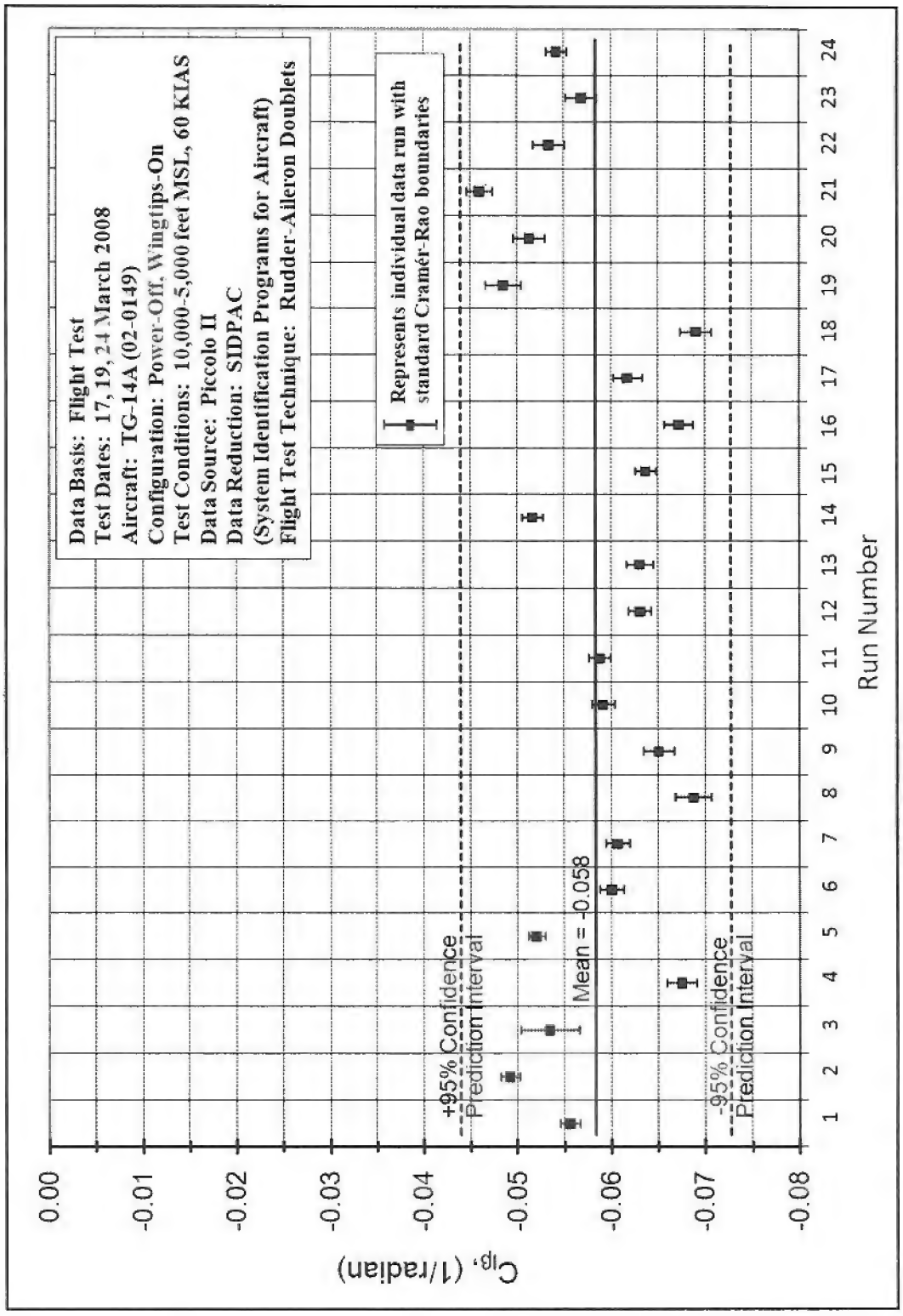

Figure F-41. C_{l_β} (Power-Off, Wingtips-On, 60 KIAS)

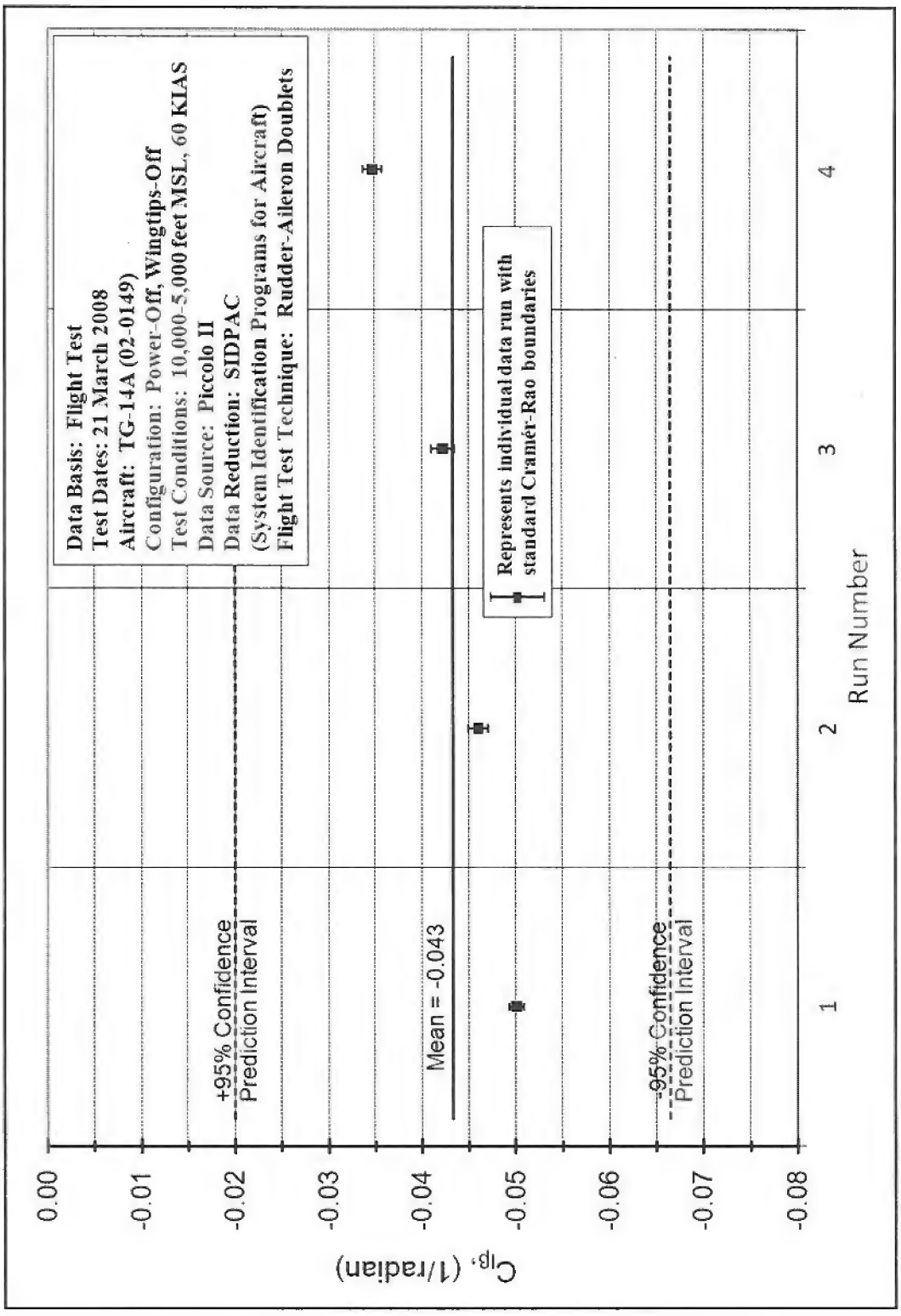

Figure F-42. $C_{l\beta}$ (Power-Off, Wingtips-Off, 60 KIAS)

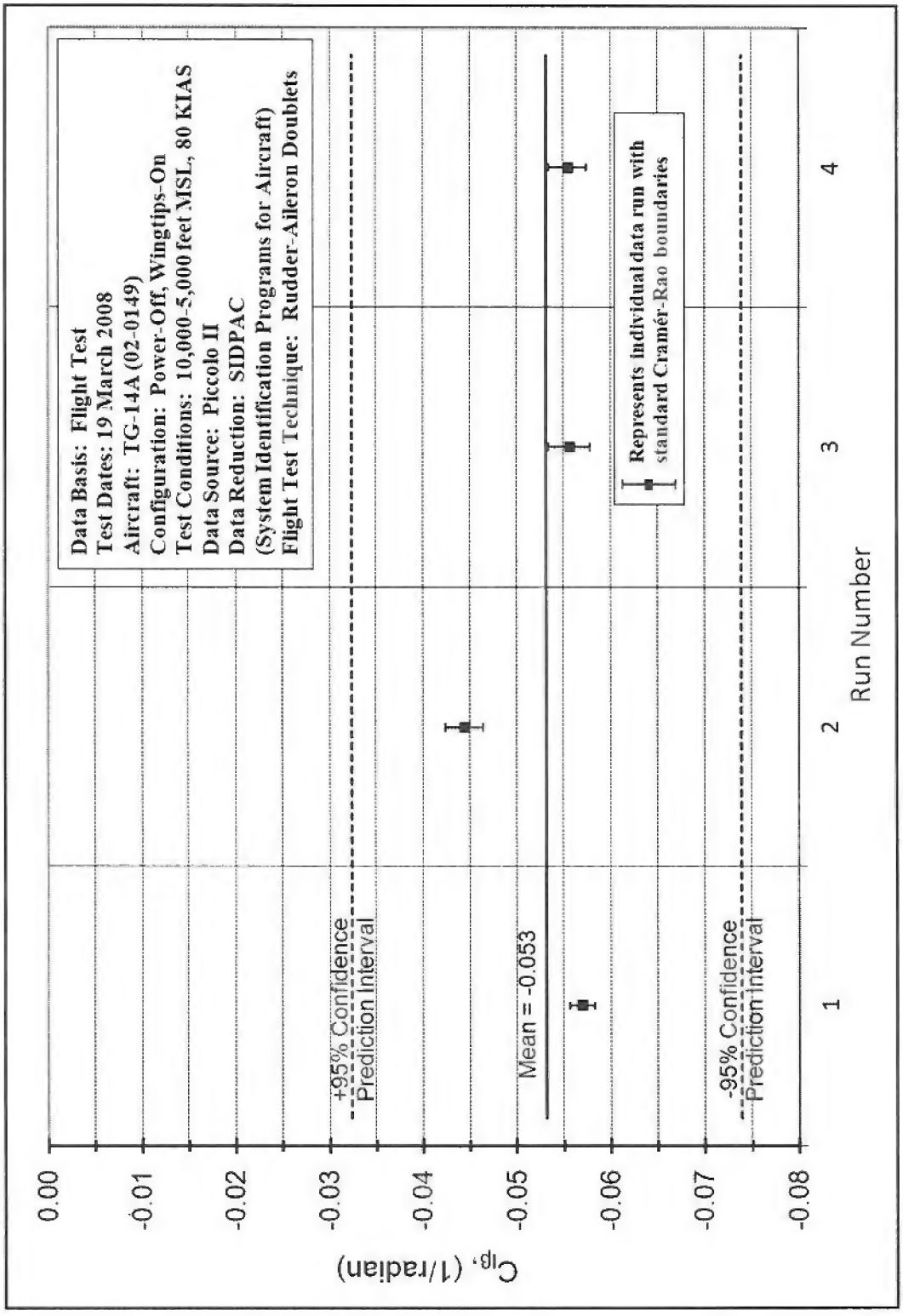

Figure F-43. $C_{l\beta}$ (Power-Off, Wingtips-On, 80 KIAS)

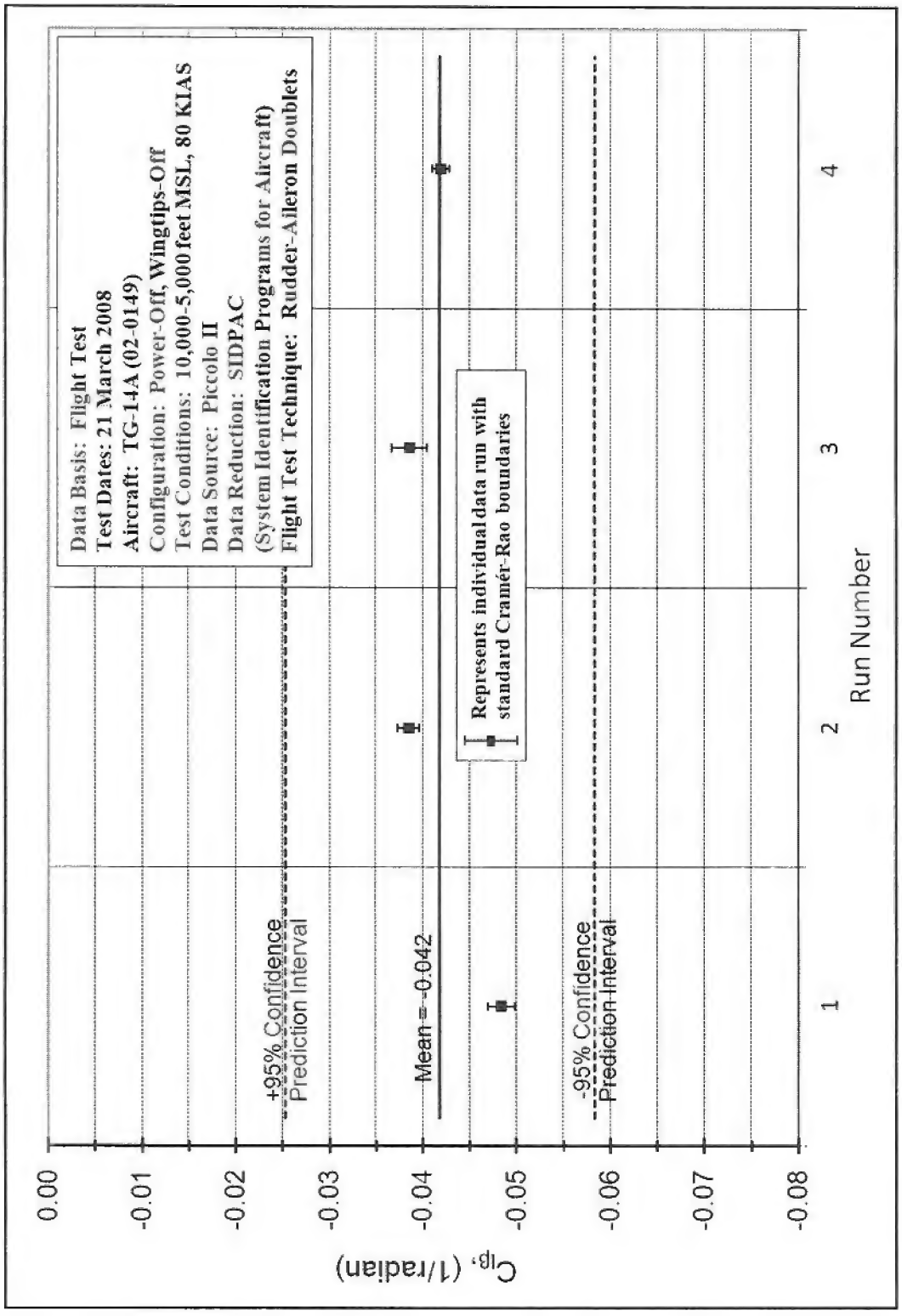

Figure F-44. $C_{l\beta}$ (Power-Off, Wingtips-Off, 80 KIAS)

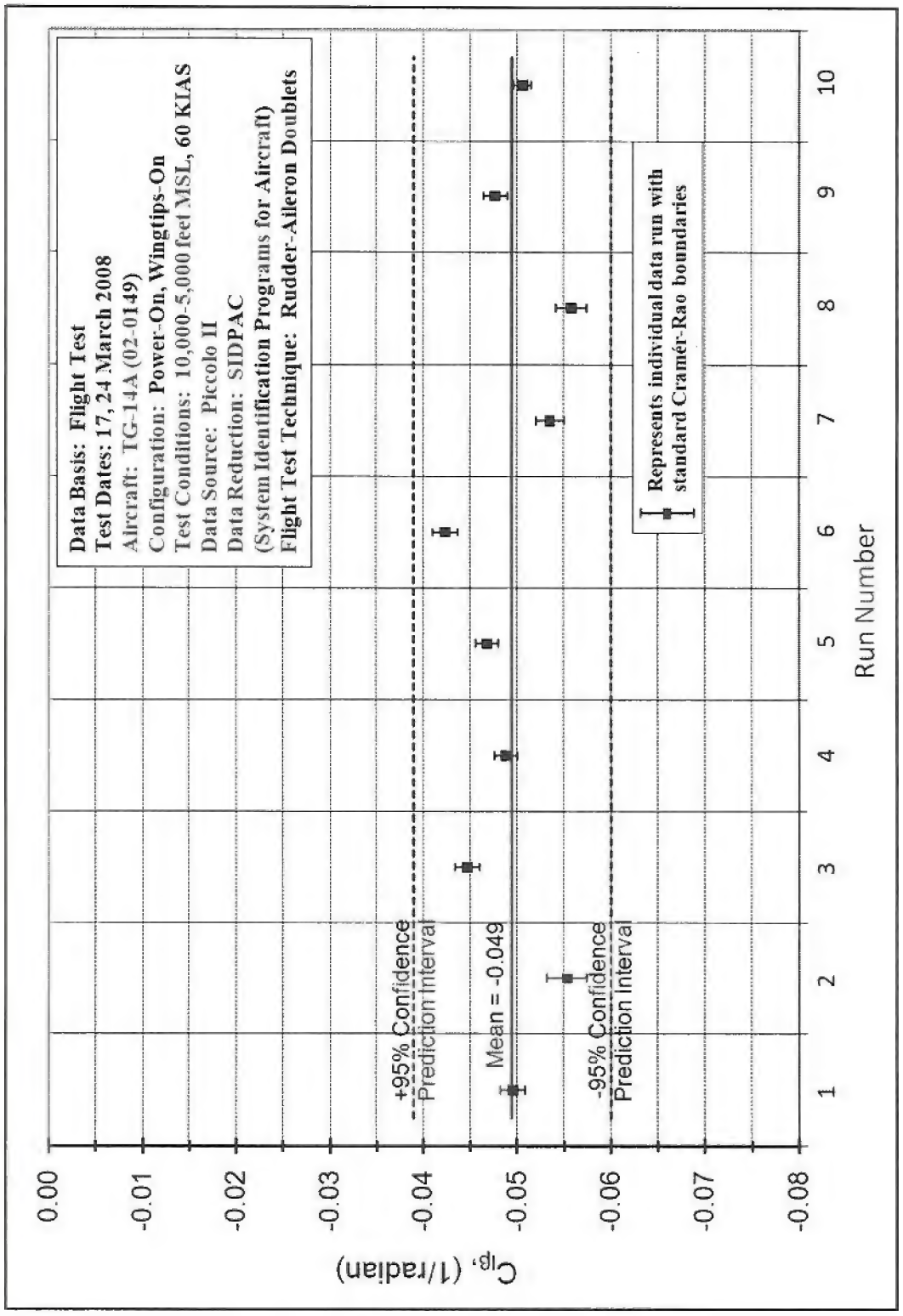

Figure F-45. C_{l_β} (Power-On, Wingtips-On, 60 KIAS)

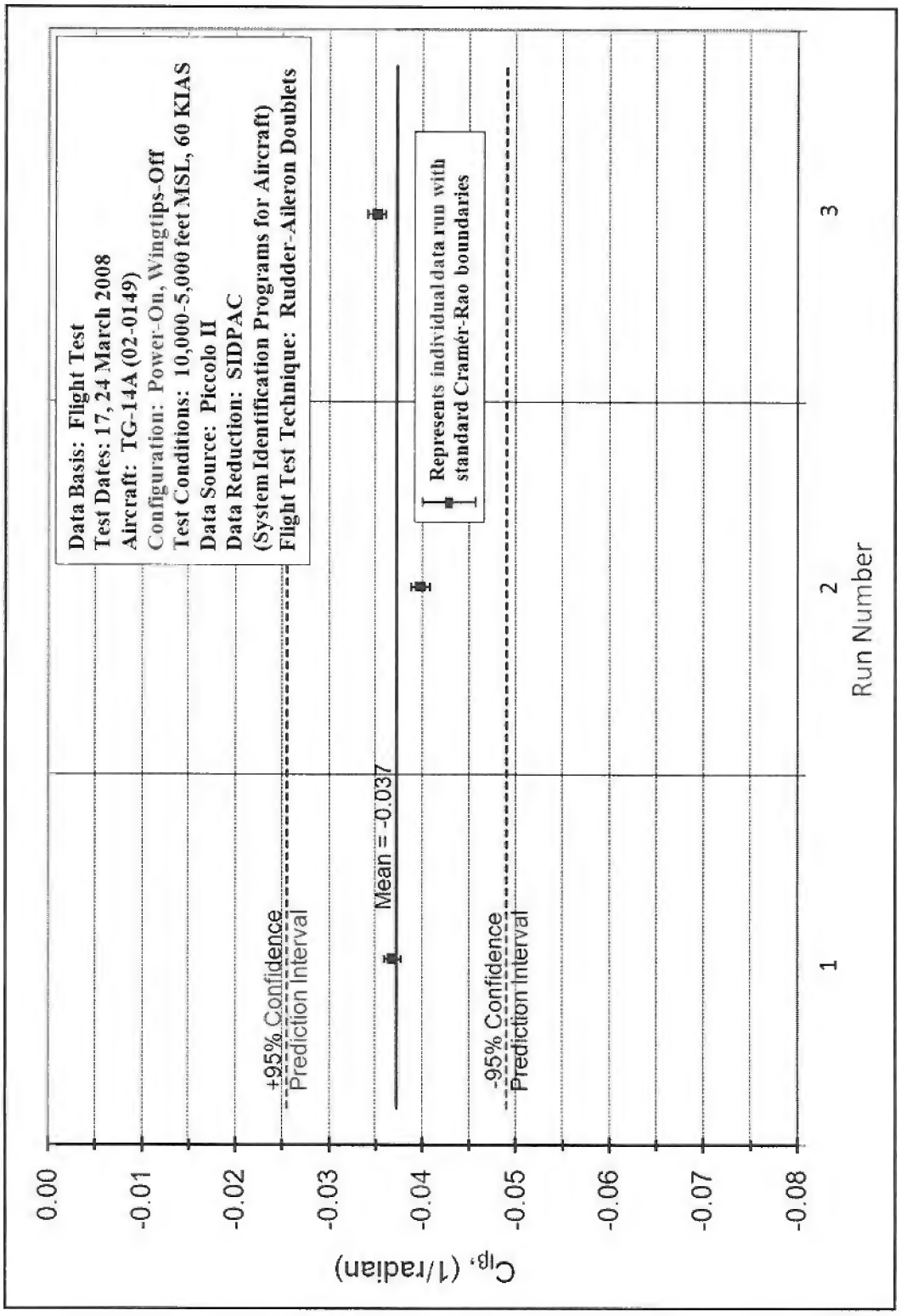

Figure F-46. $C_{l\beta}$ (Power-On, Wingtips-Off, 60 KIAS)

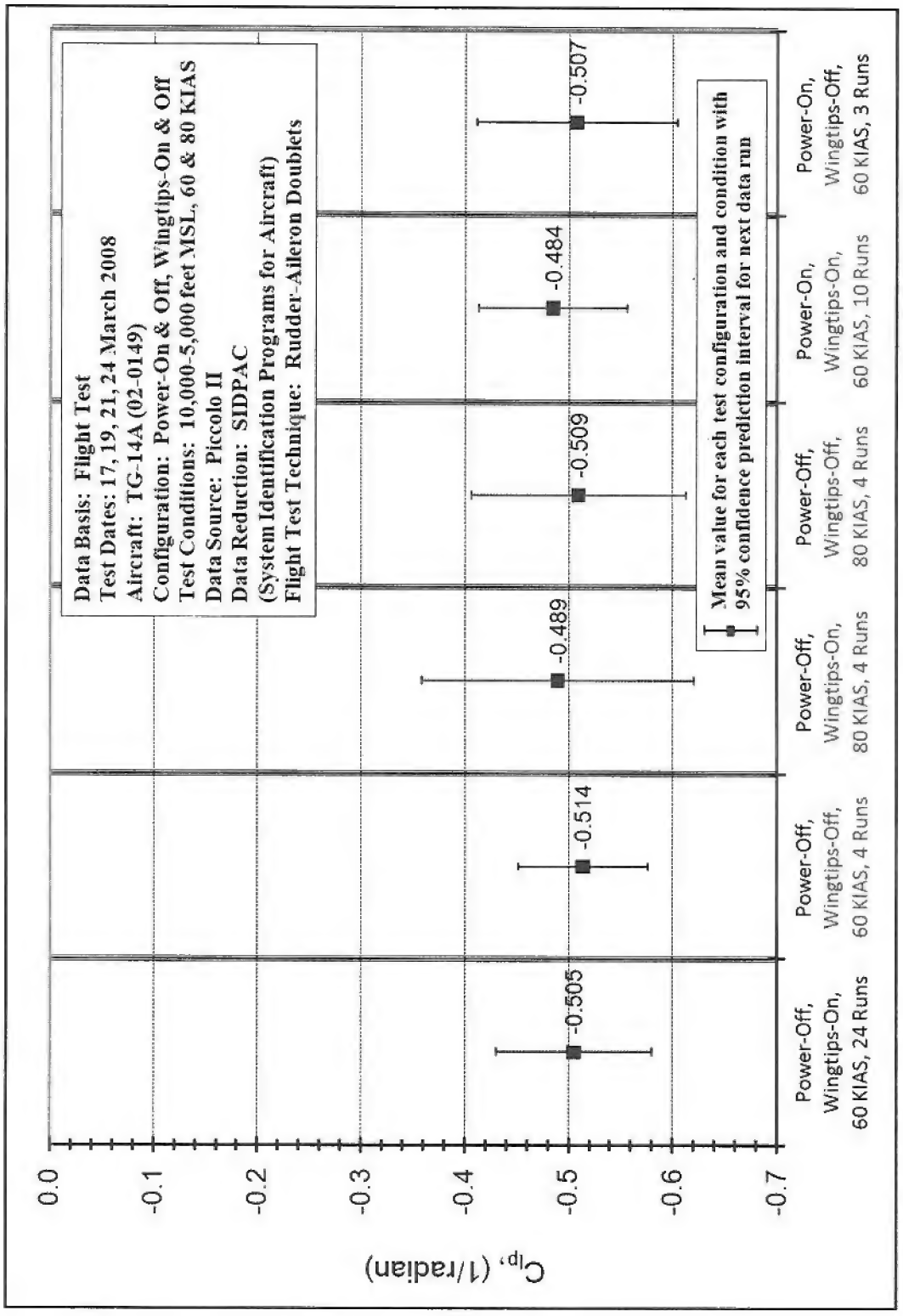

Figure F-47. C_{lp} from all test conditions with 95% confidence intervals

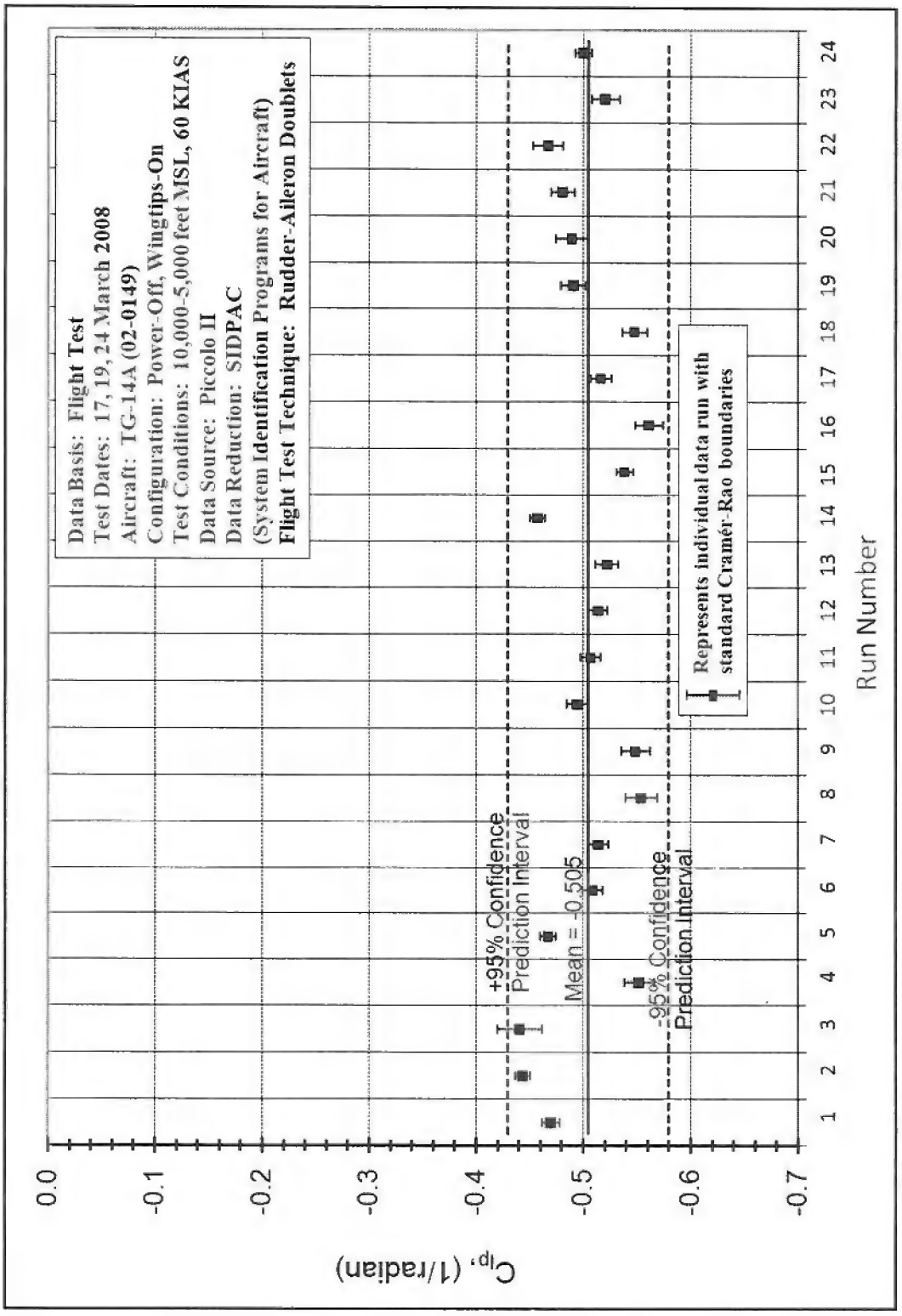

Figure F-48. C_{lp} (Power-Off, Wingtips-On, 60 KIAS)

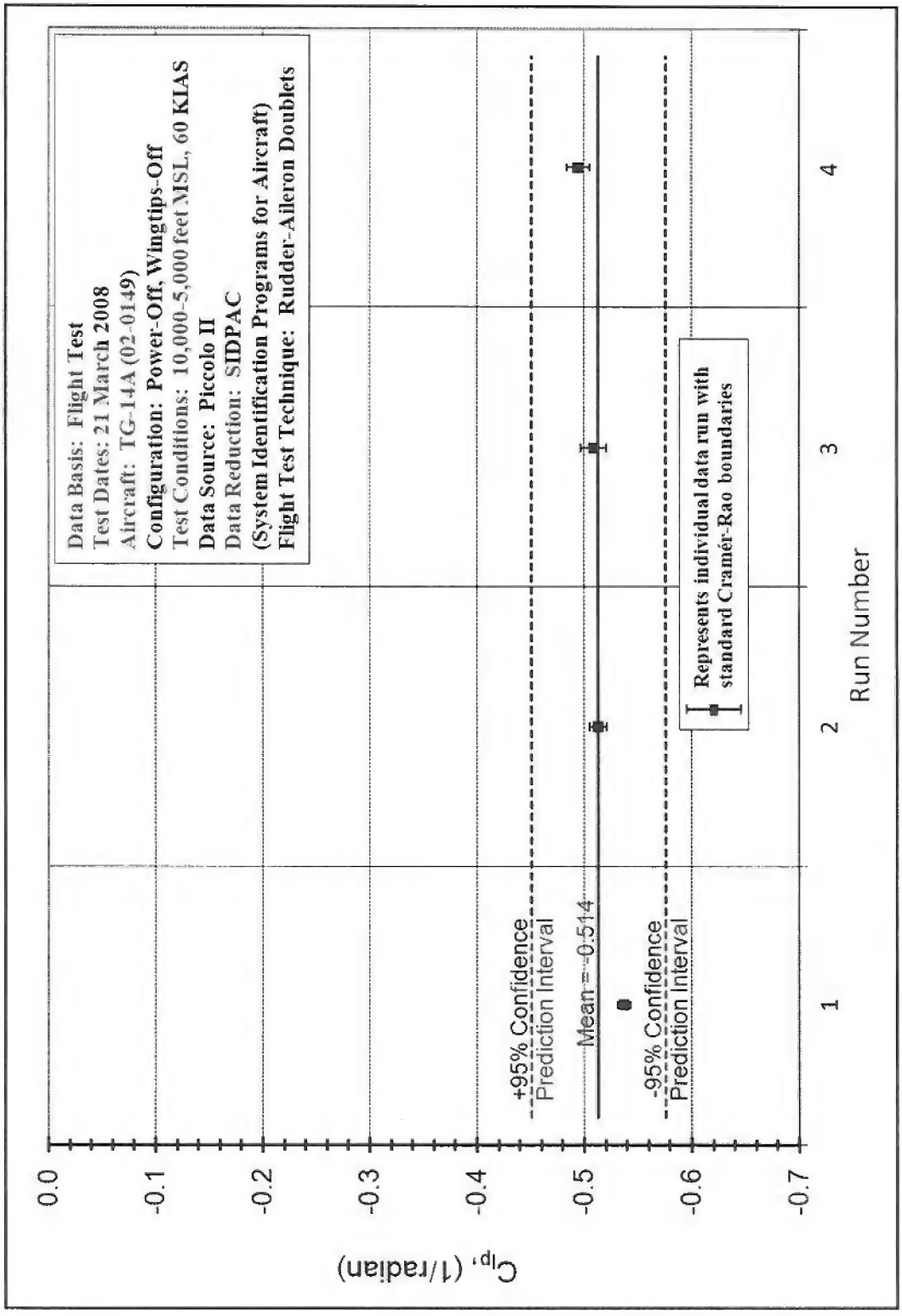

Figure F-49. C_{lp} (Power-Off, Wingtips-Off, 60 KIAS)

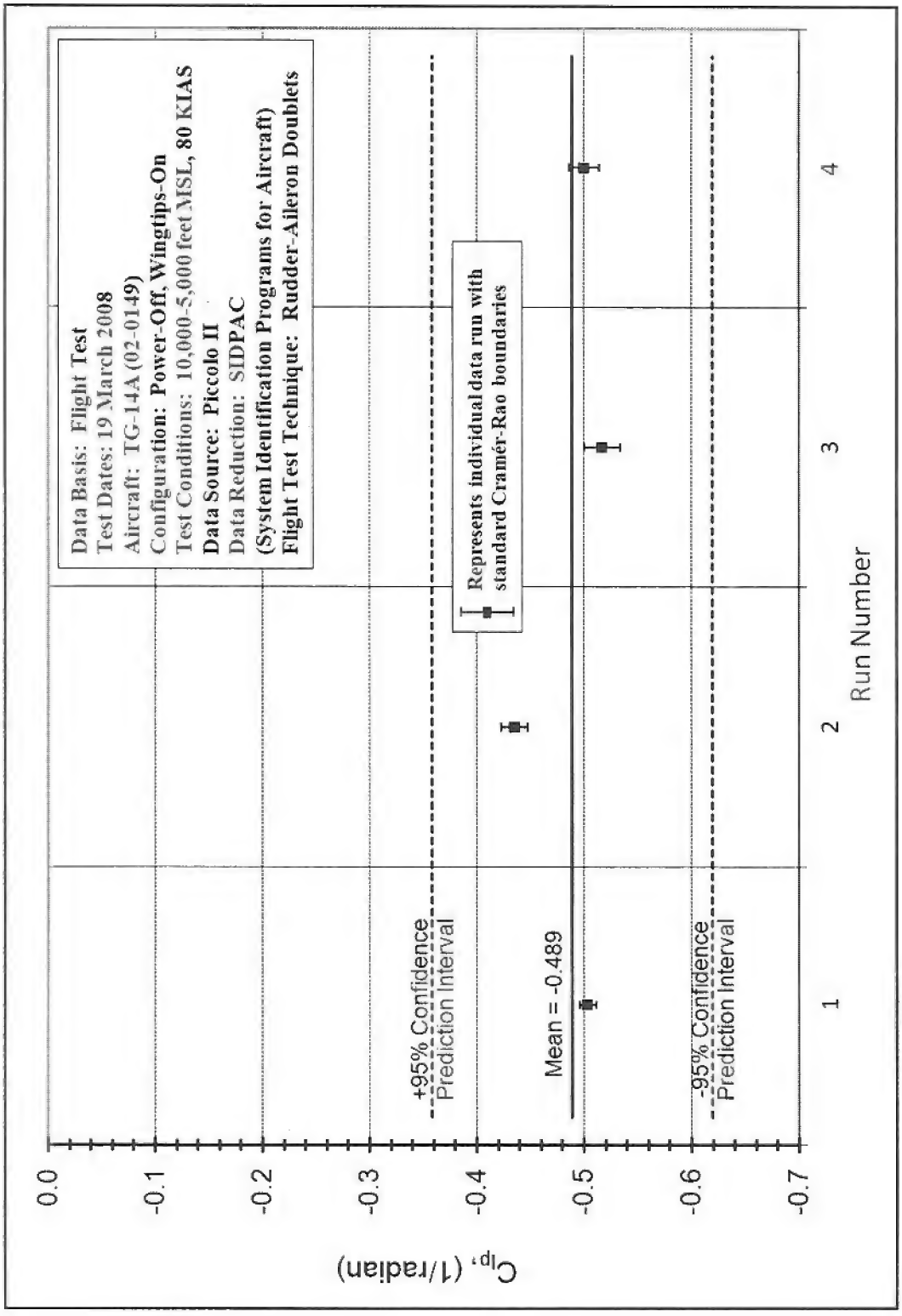

Figure F-50. C_{lp} (Power-Off, Wingtips-On, 80 KIAS)

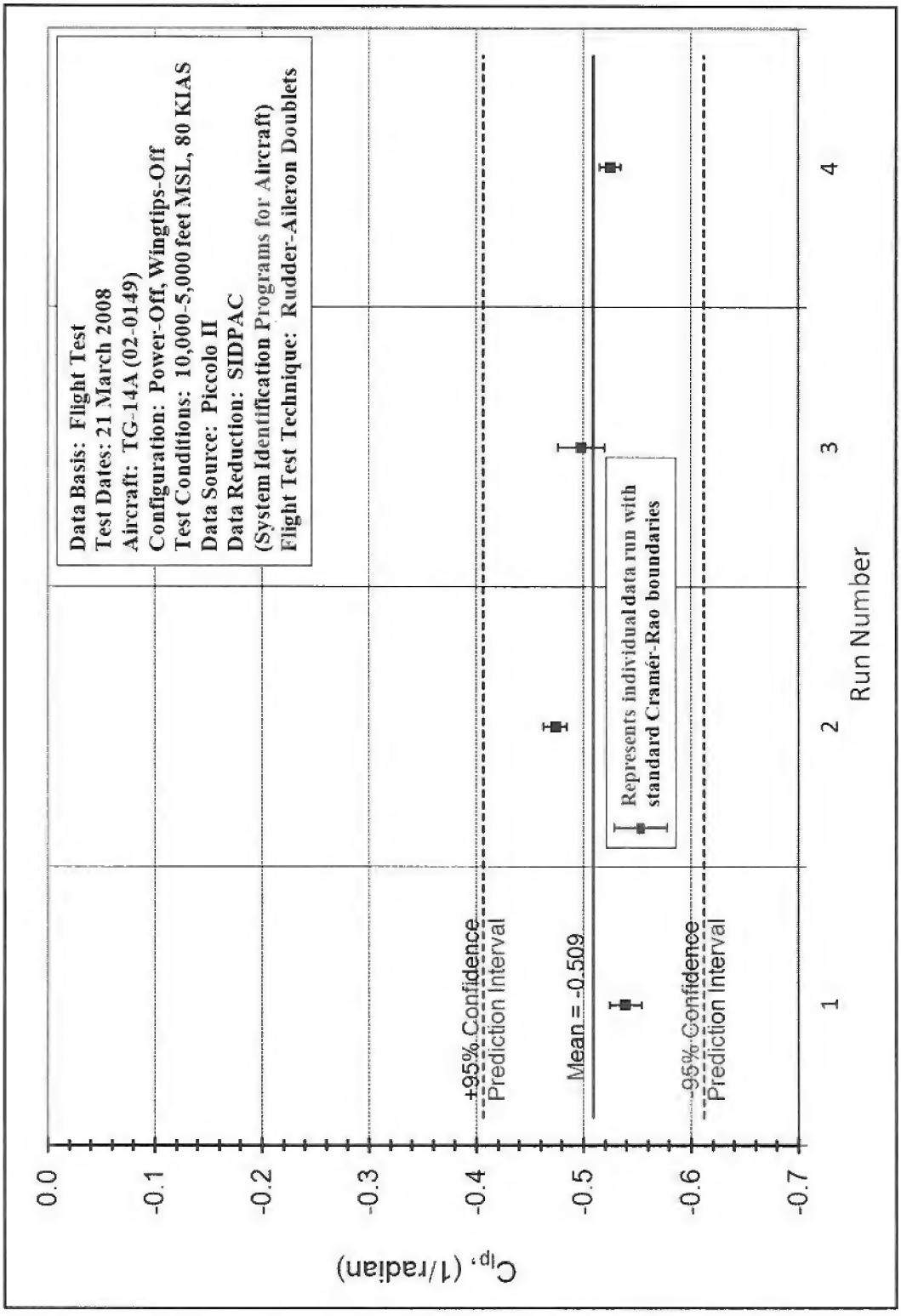

Figure F-51. C_{lp} (Power-Off, Wingtips-Off, 80 KIAS)

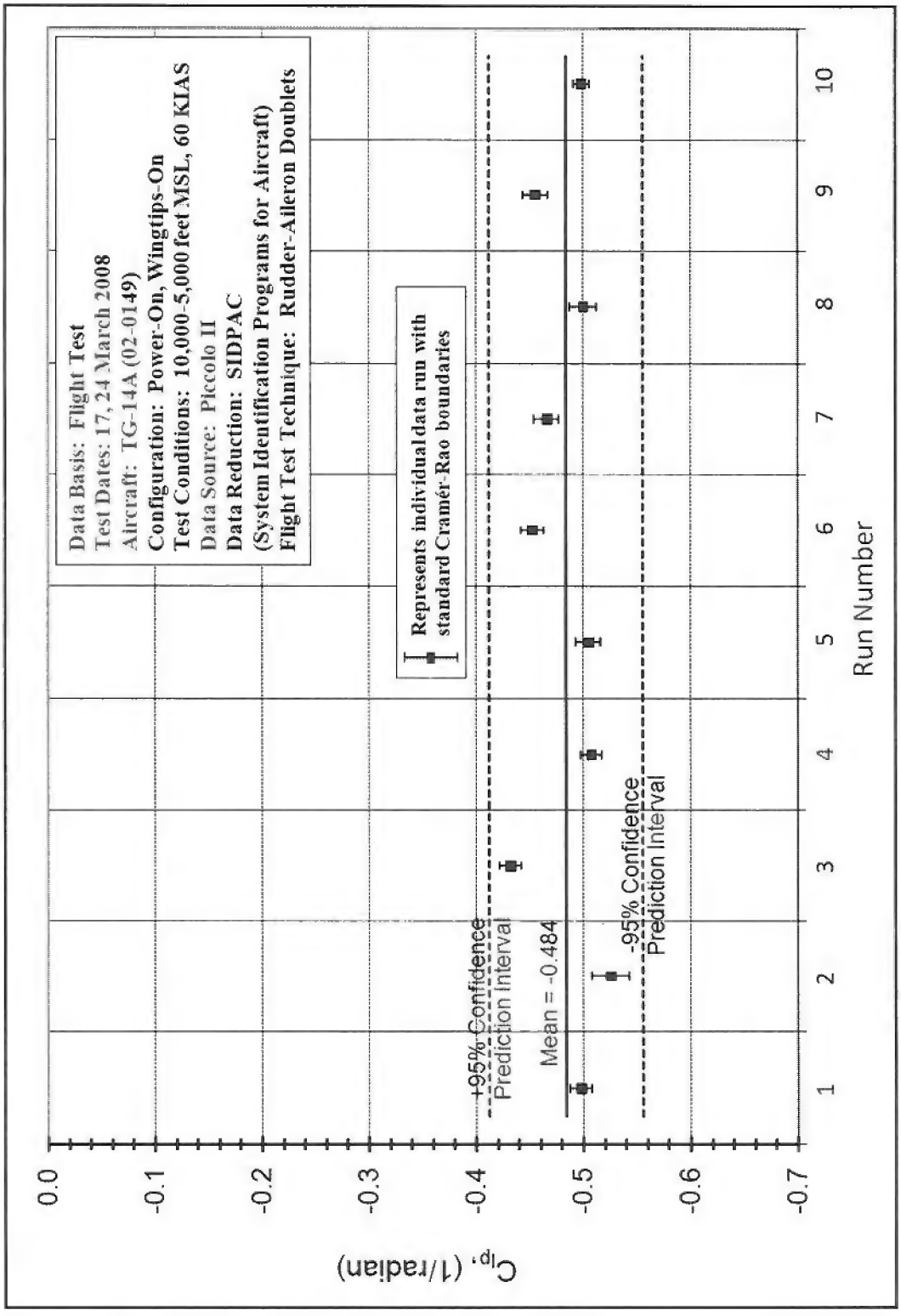

Figure F-52. C_{lp} (Power-On, Wingtips-On, 60 KIAS)

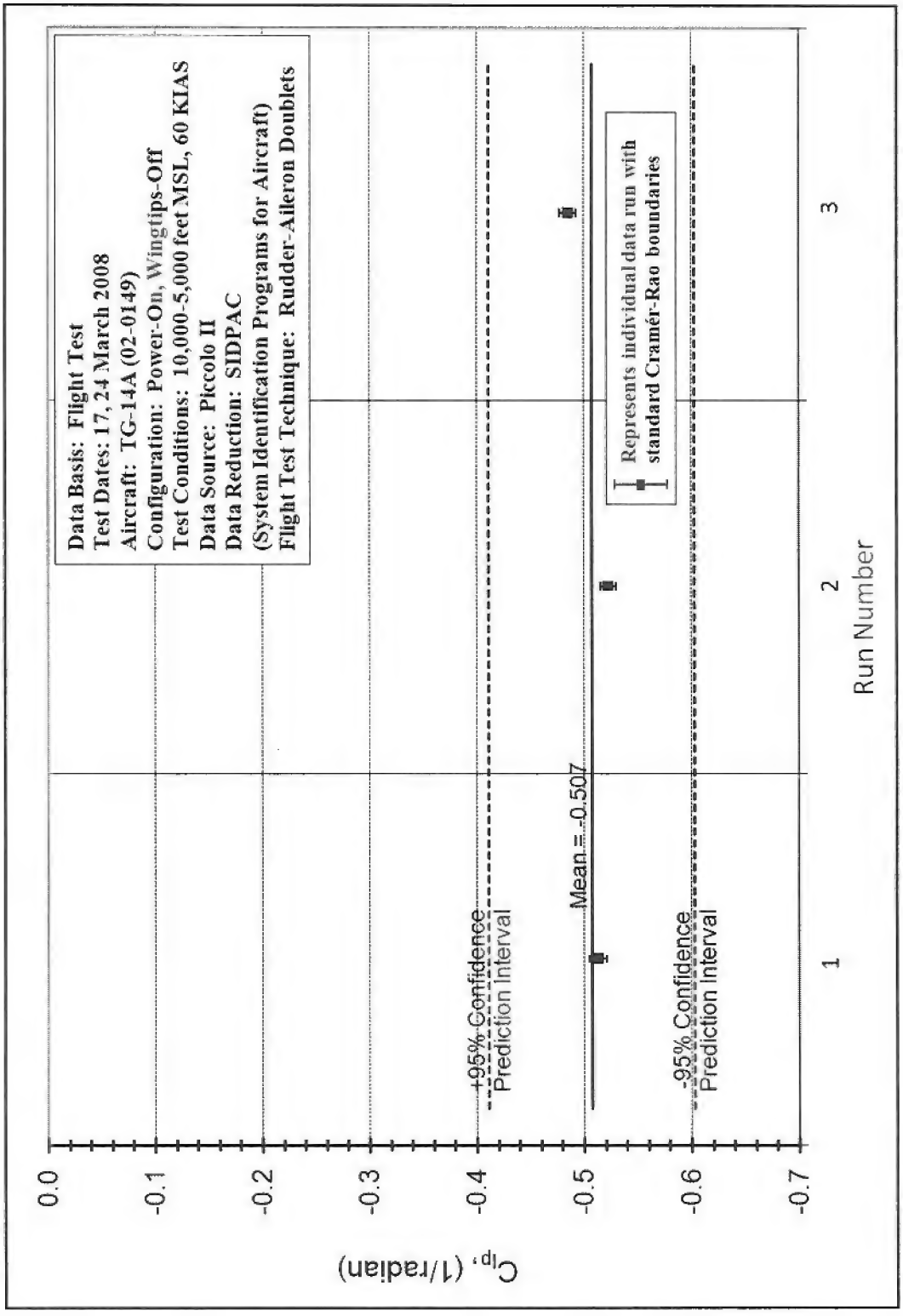

Figure F-53. C_{lp} (Power-On, Wingtips-Off, 60 KIAS)

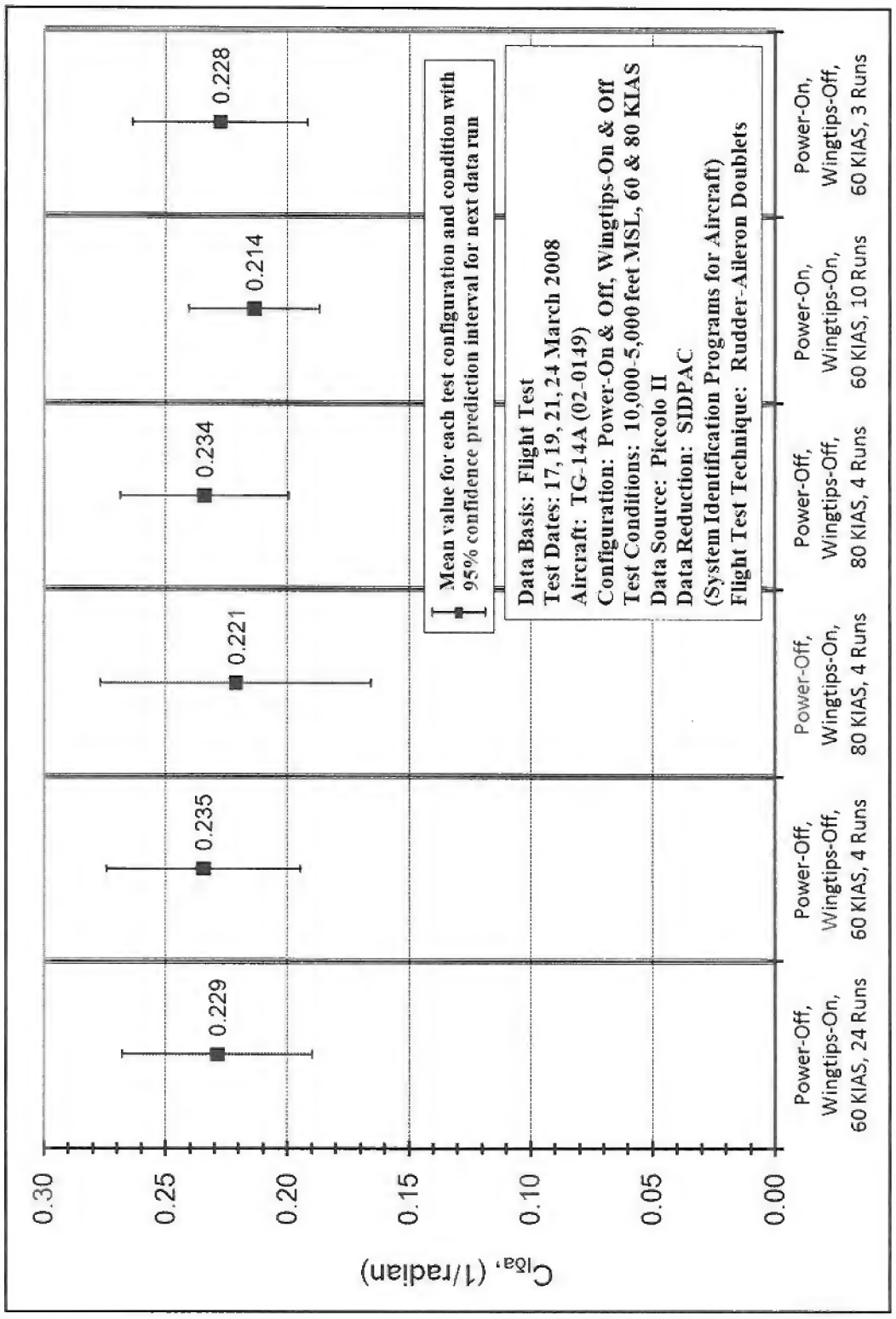

Figure F-54. $C_{l\delta a}$ from all test conditions with 95% confidence intervals

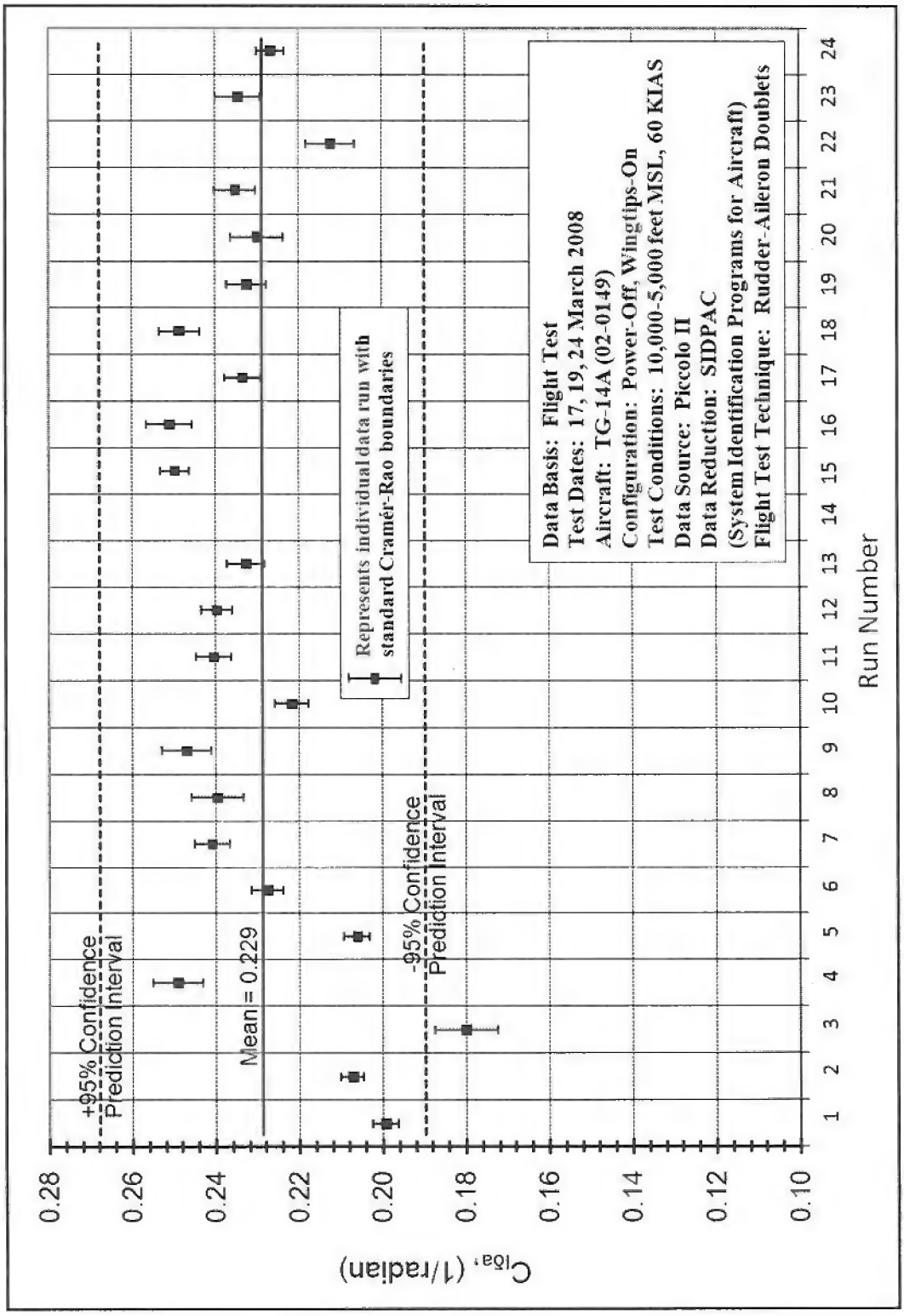

Figure F-55. $C_{l\delta a}$ (Power-Off, Wingtips-On, 60 KIAS)

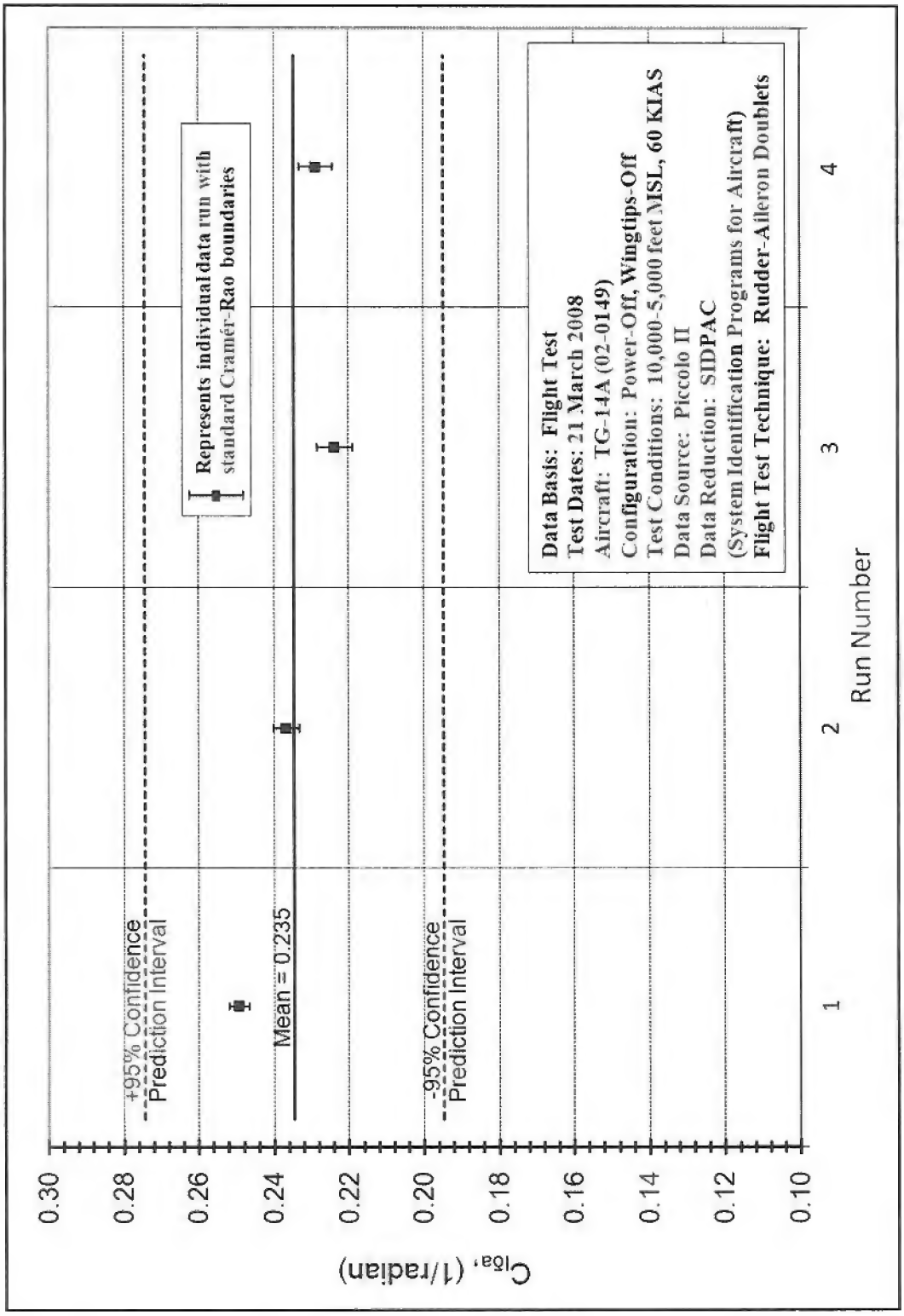

Figure F-56. $C_{l\delta a}$ (Power-Off, Wingtips-Off, 60 KIAS)

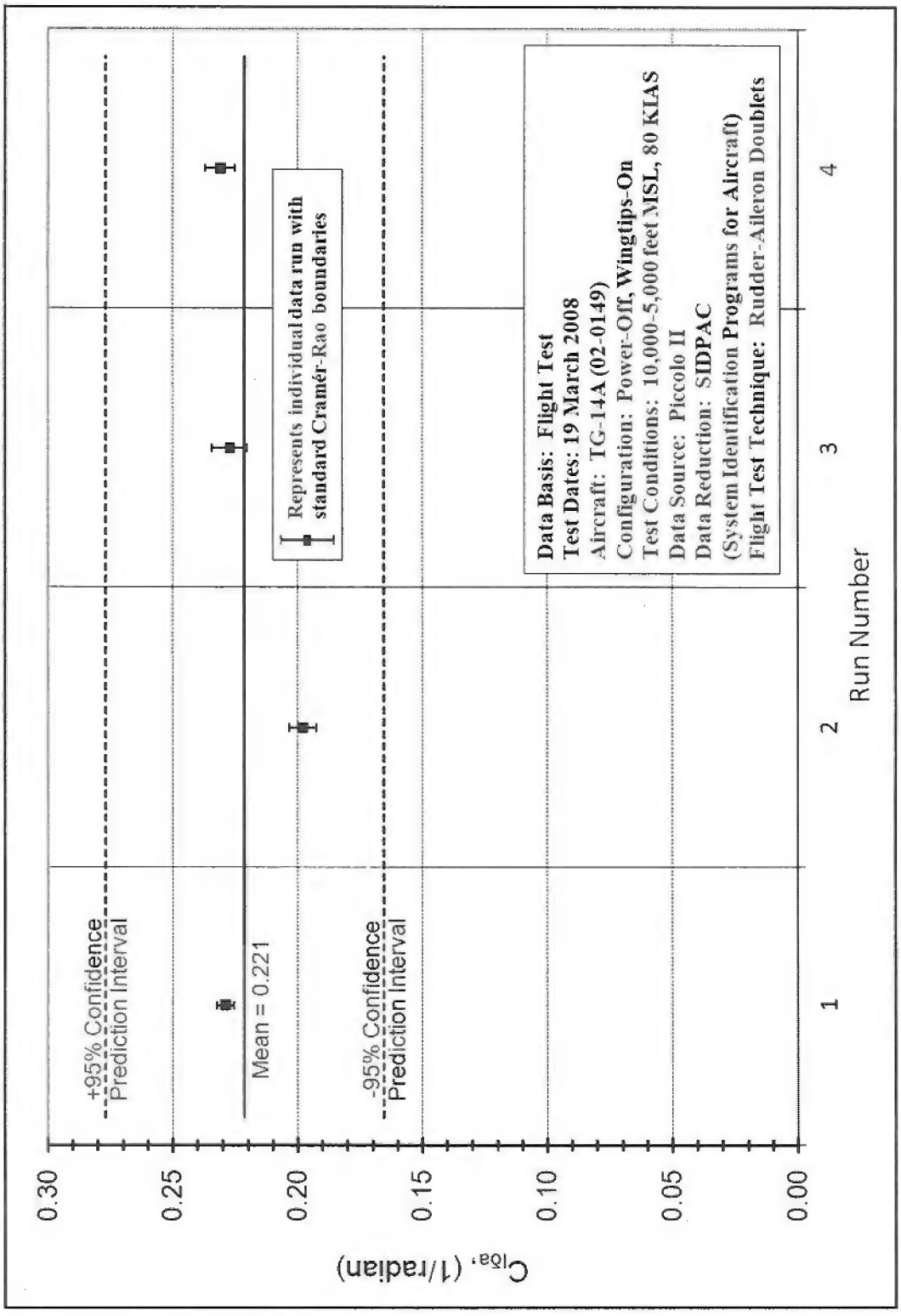

Figure F-57. $C_{l\delta a}$ (Power-Off, Wingtips-On, 80 KIAS)

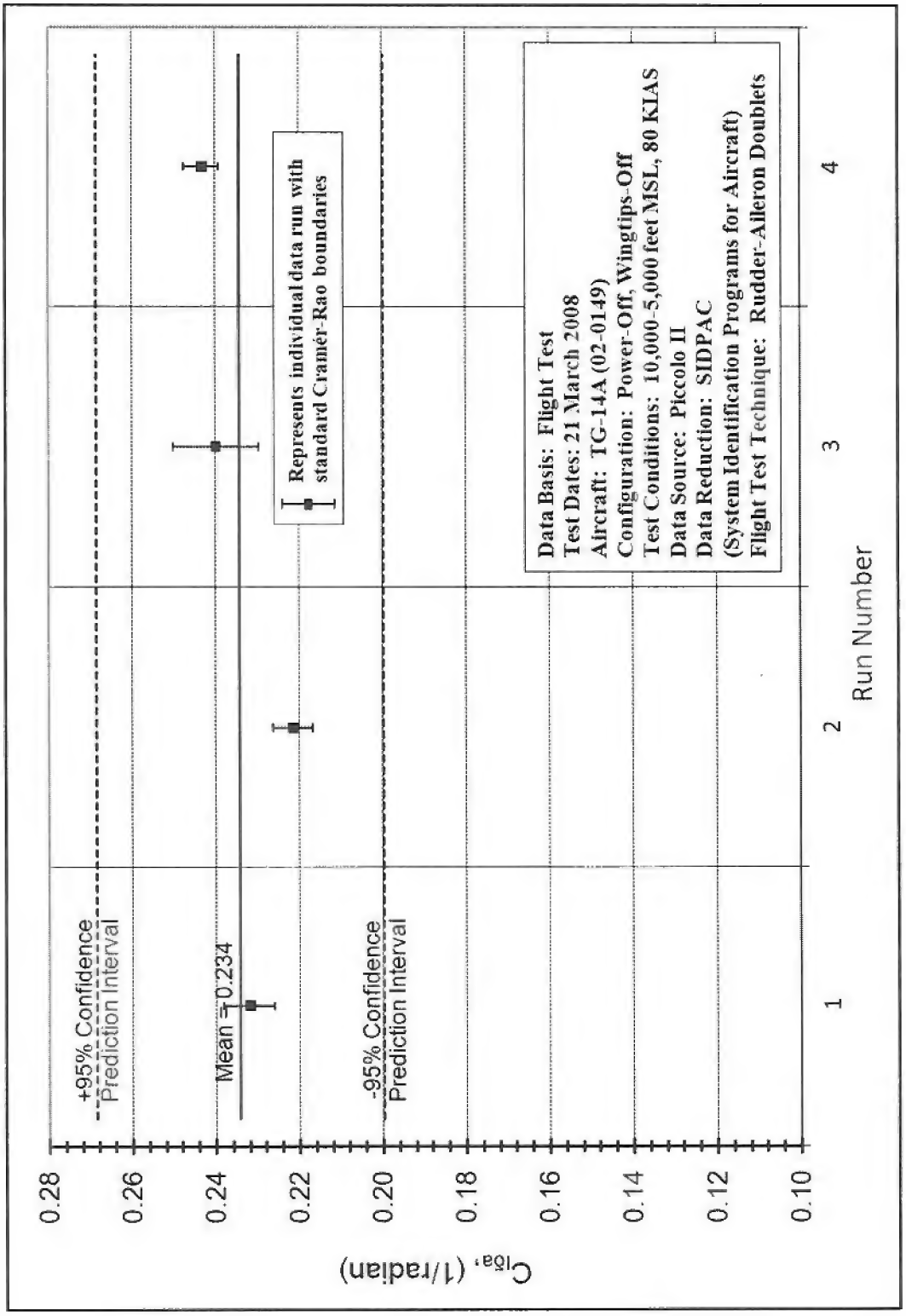

Figure F-58. $C_{l\delta a}$ (Power-Off, Wingtips-Off, 80 KIAS)

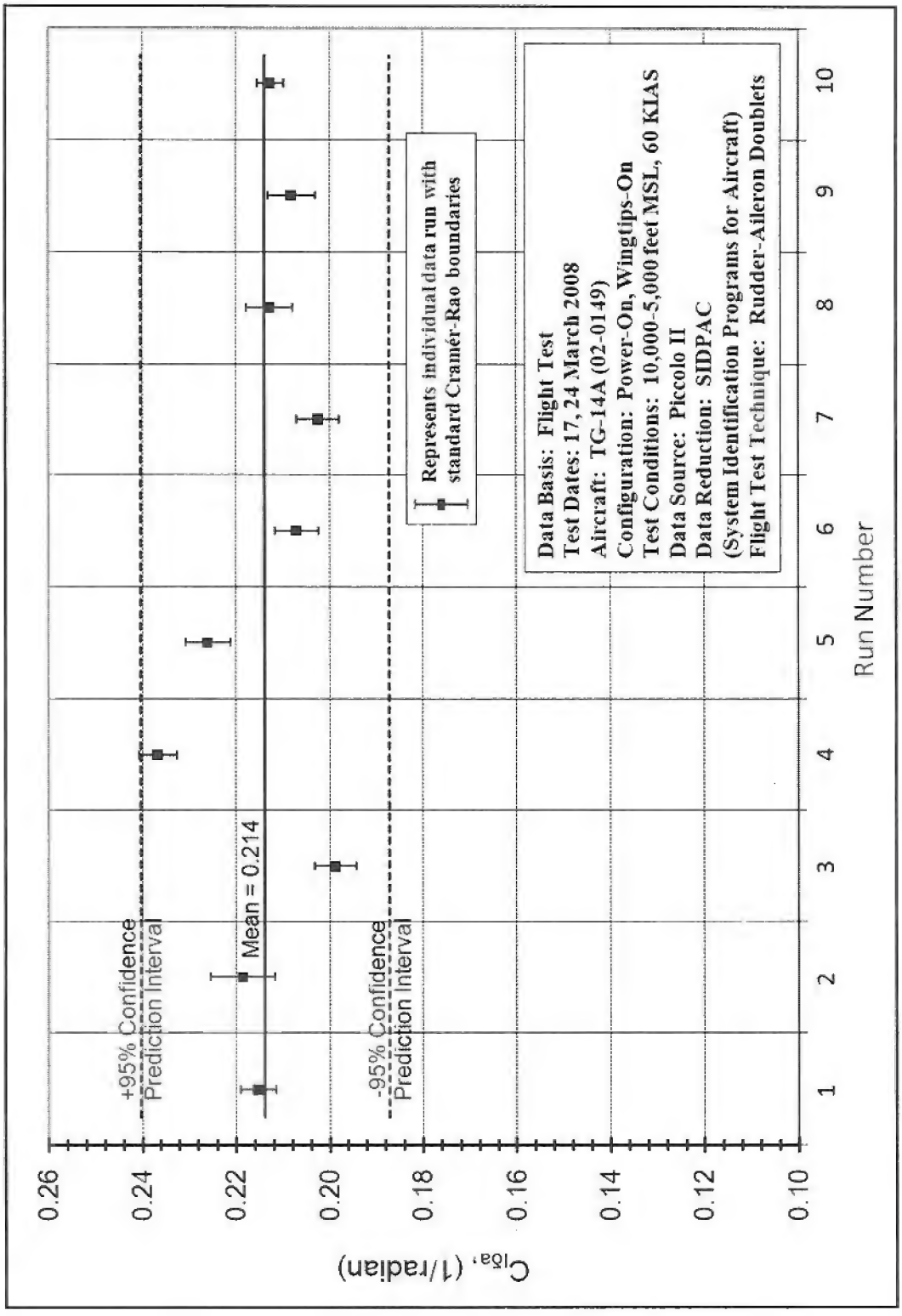

Figure F-59. $C_{l\delta a}$ (Power-On, Wingtips-On, 60 KIAS)

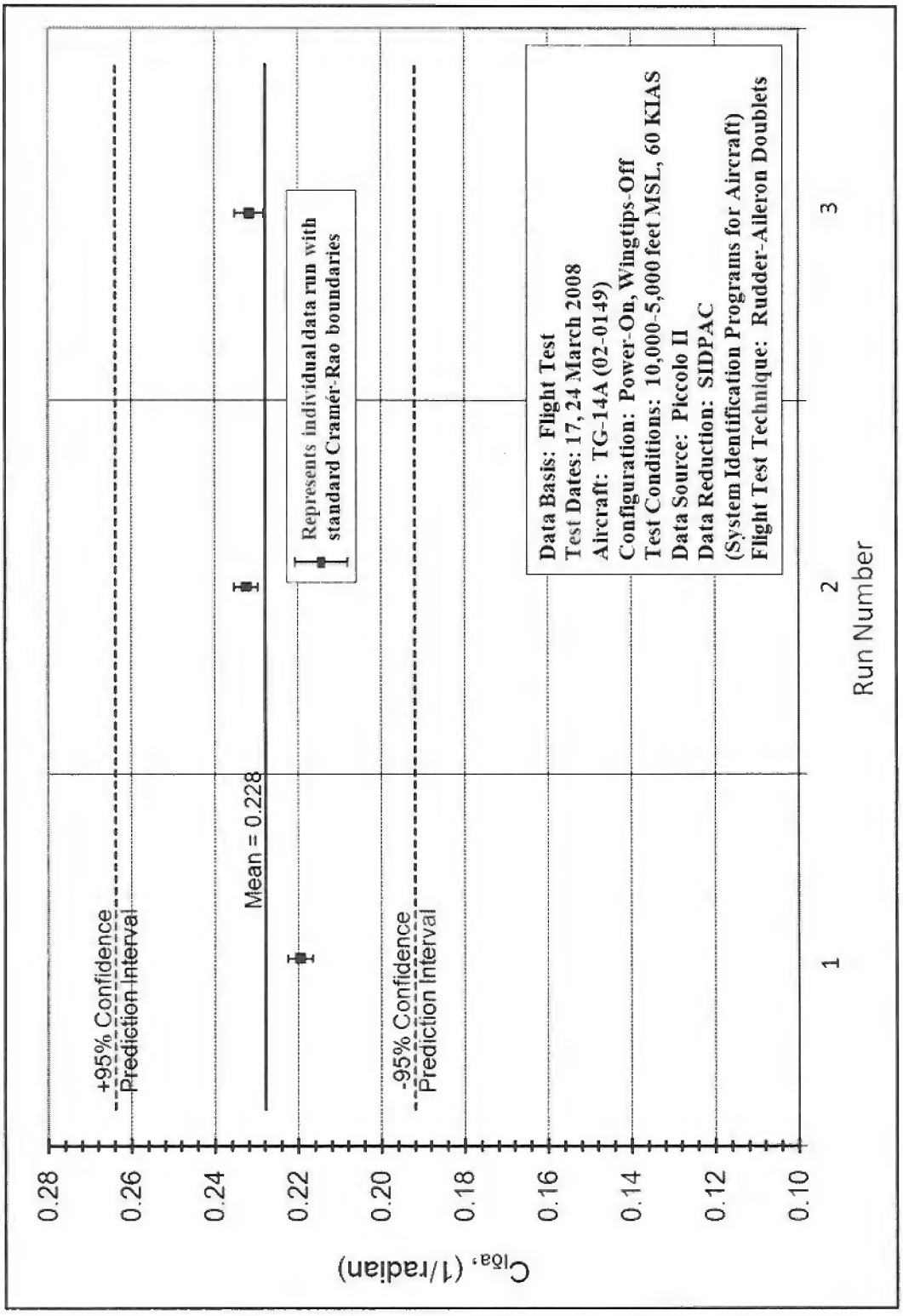

Figure F-60. $C_{l\delta a}$ (Power-On, Wingtips-Off, 60 KIAS)

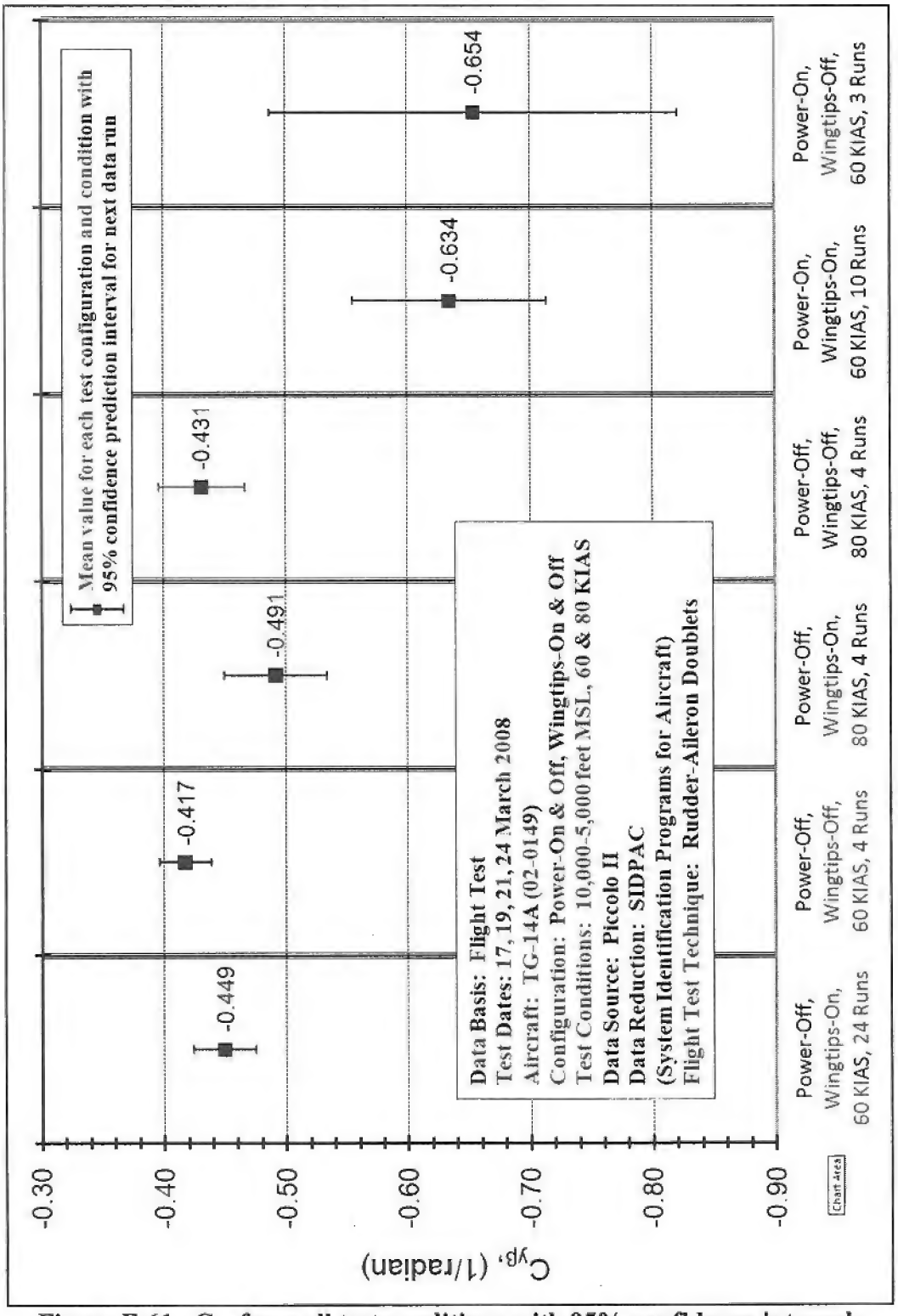

Figure F-61. $C_{y\beta}$ from all test conditions with 95% confidence intervals

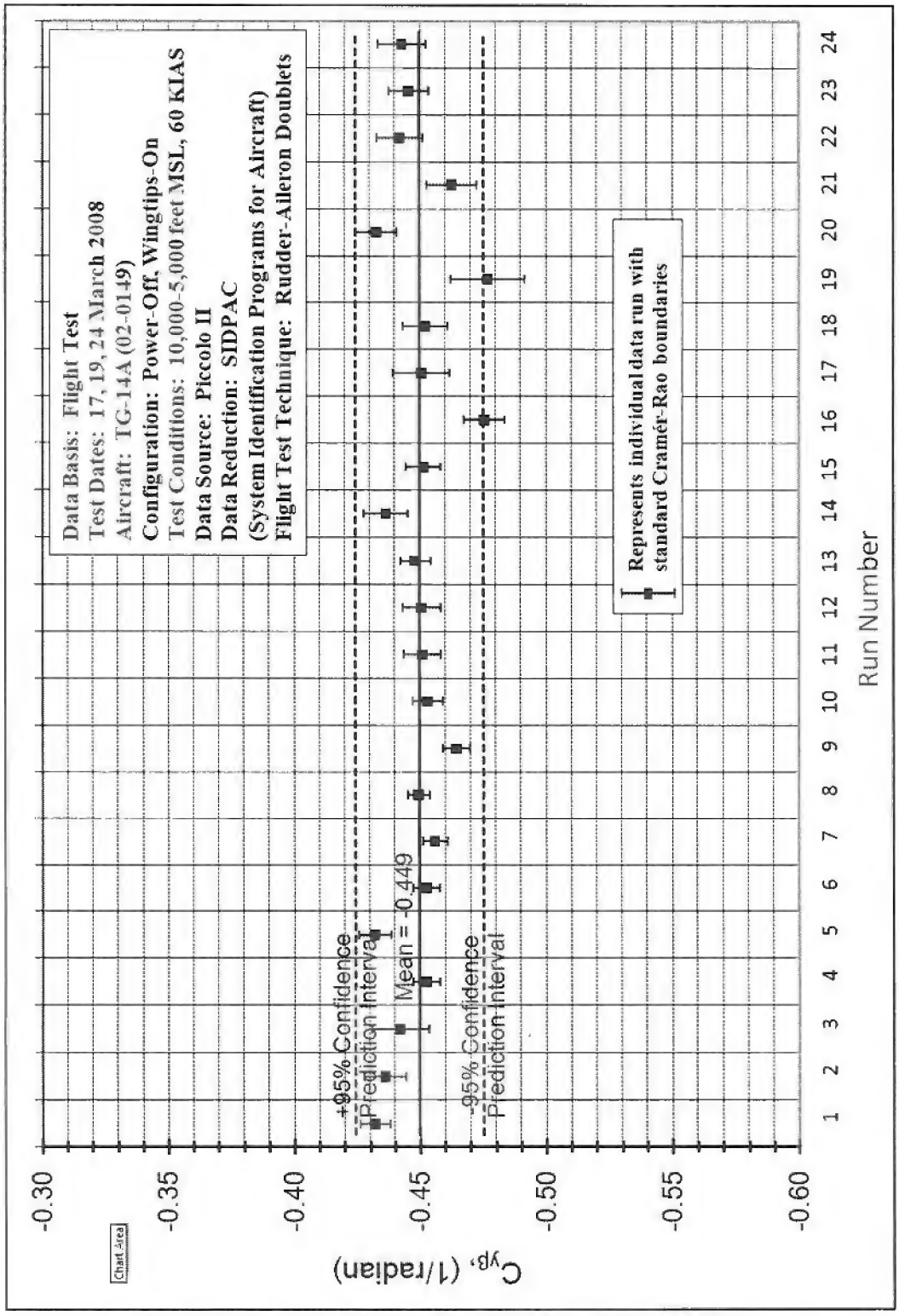

Figure F-62. $C_{y\beta}$ (Power-On, Wingtips-Off, 60 KIAS)

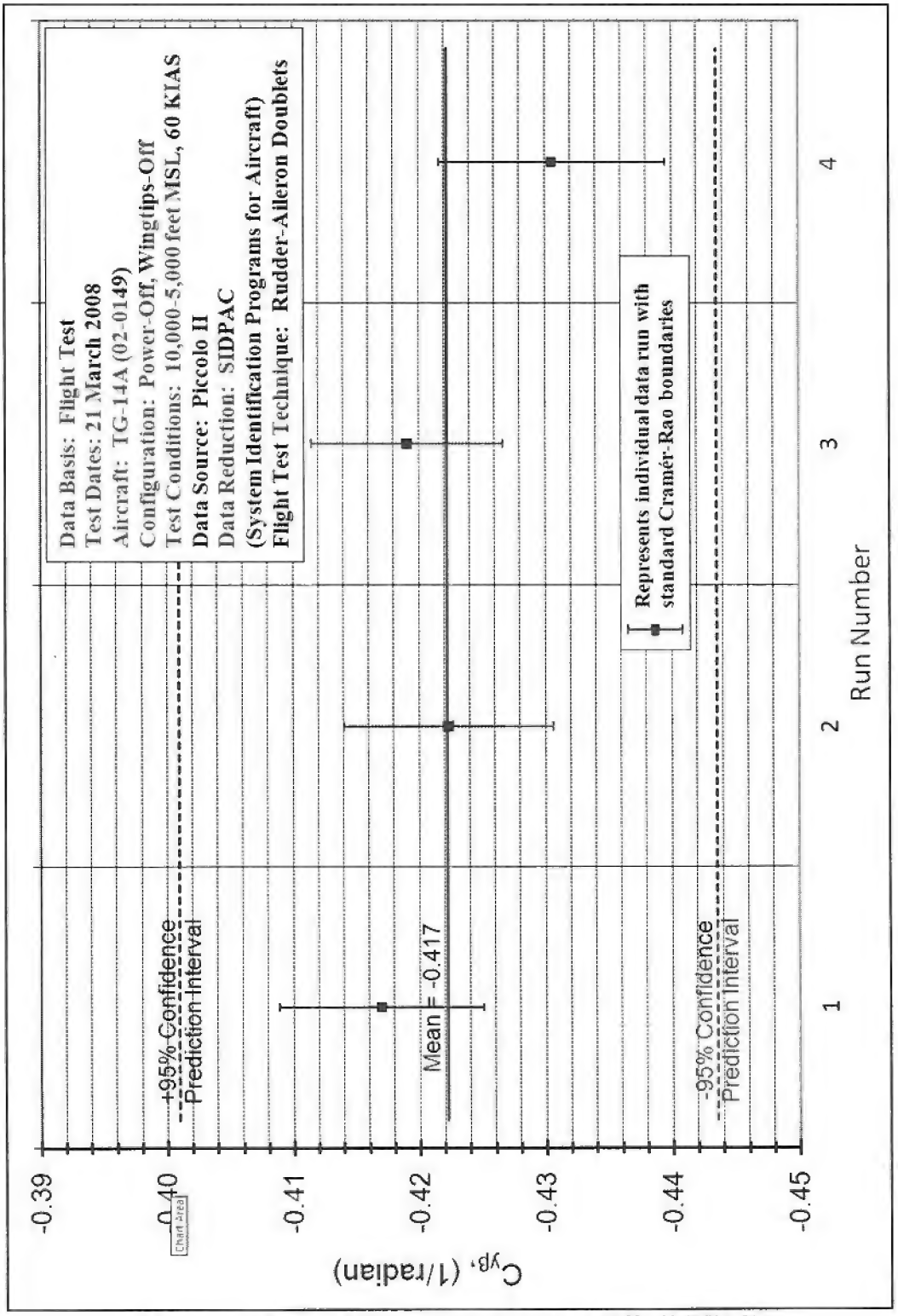

Figure F-63. $C_{y\beta}$ (Power-Off, Wingtips-Off, 60 KIAS)

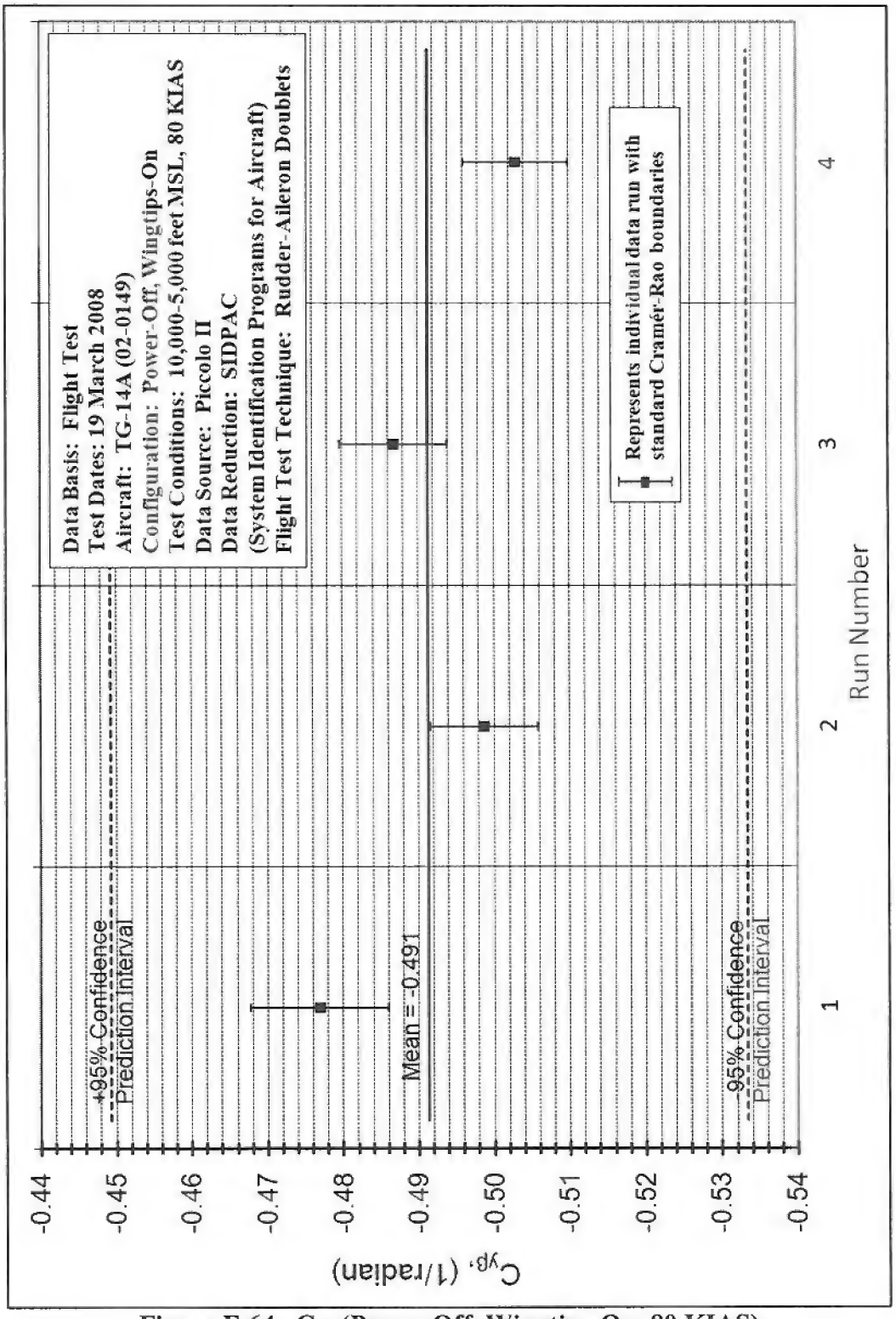

Figure F-64. $C_{y\beta}$ (Power-Off, Wingtips-On, 80 KIAS)

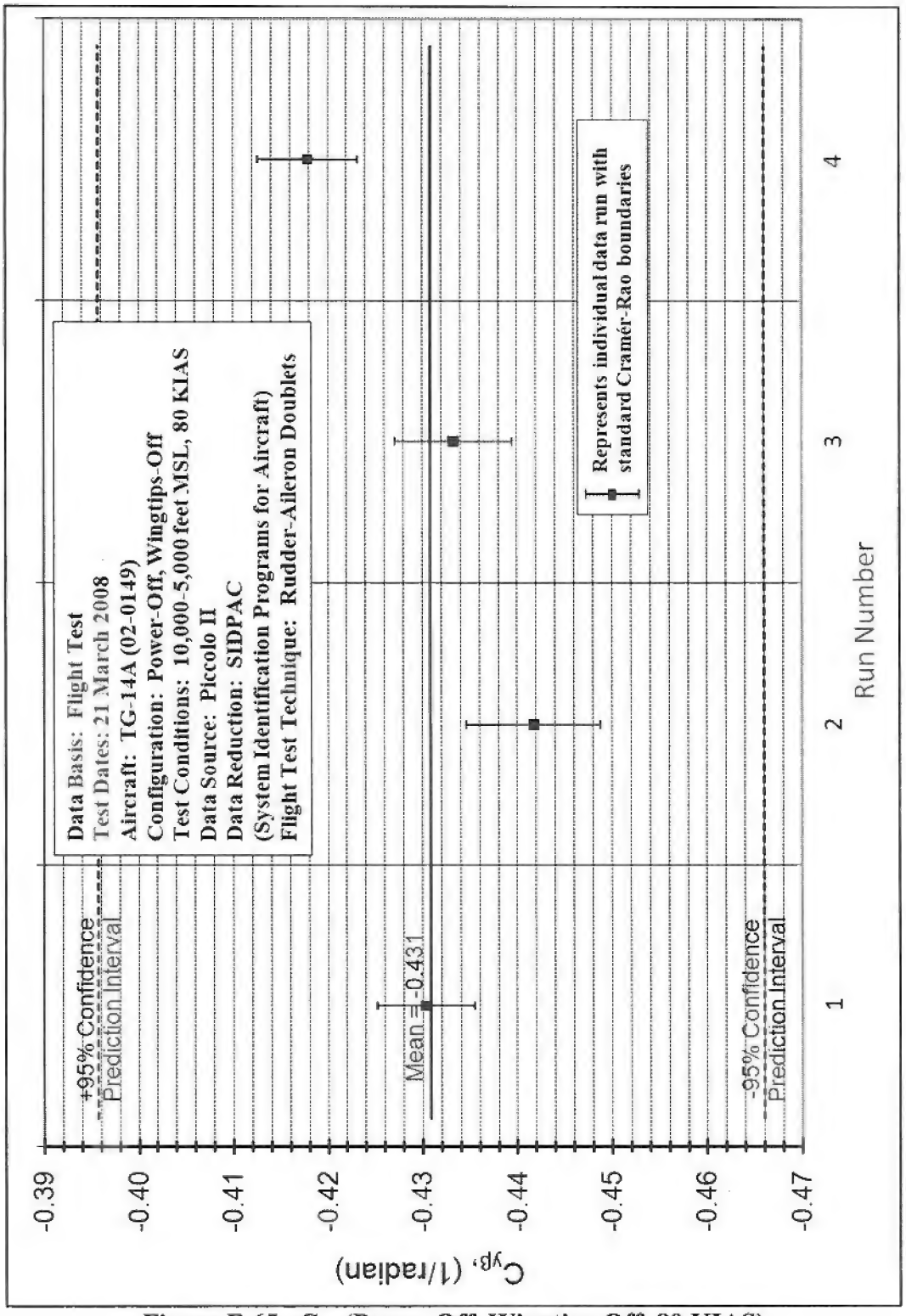

Figure F-65. $C_{y\beta}$ (Power-Off, Wingtips-Off, 80 KIAS)

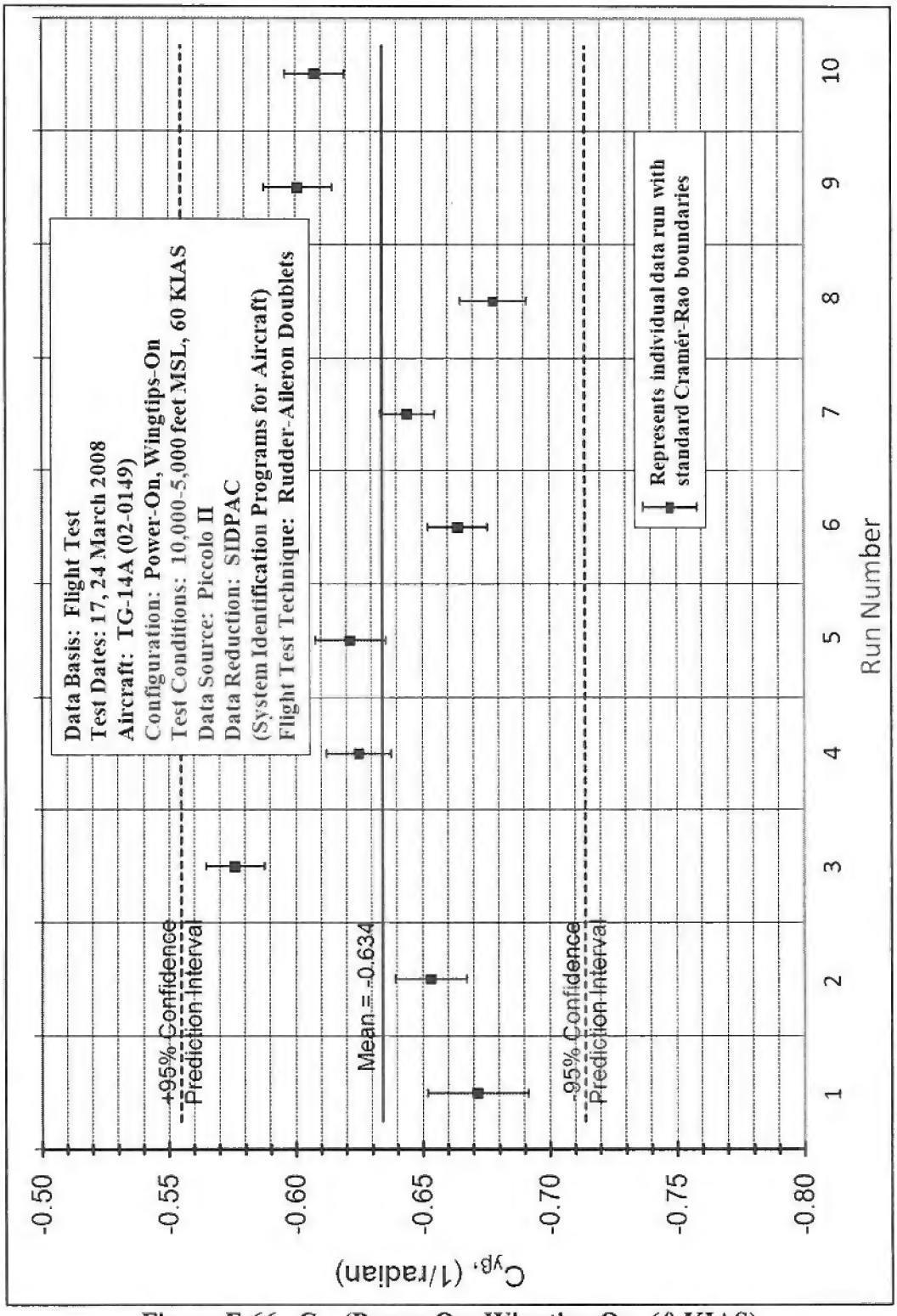

Figure F-66. $C_{y\beta}$ (Power-On, Wingtips-On, 60 KIAS)

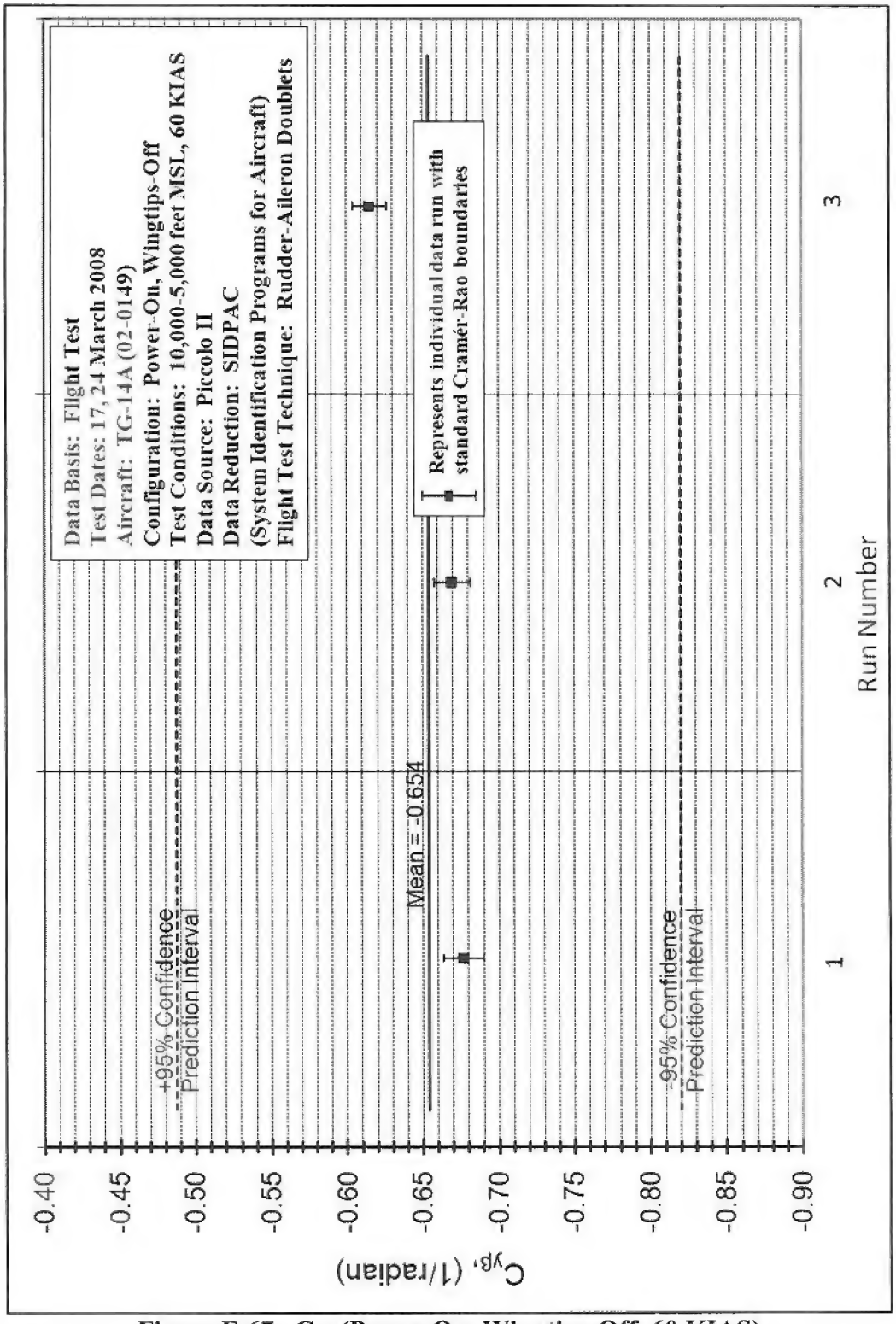

Figure F-67. $C_{y\beta}$ (Power-On, Wingtips-Off, 60 KIAS)

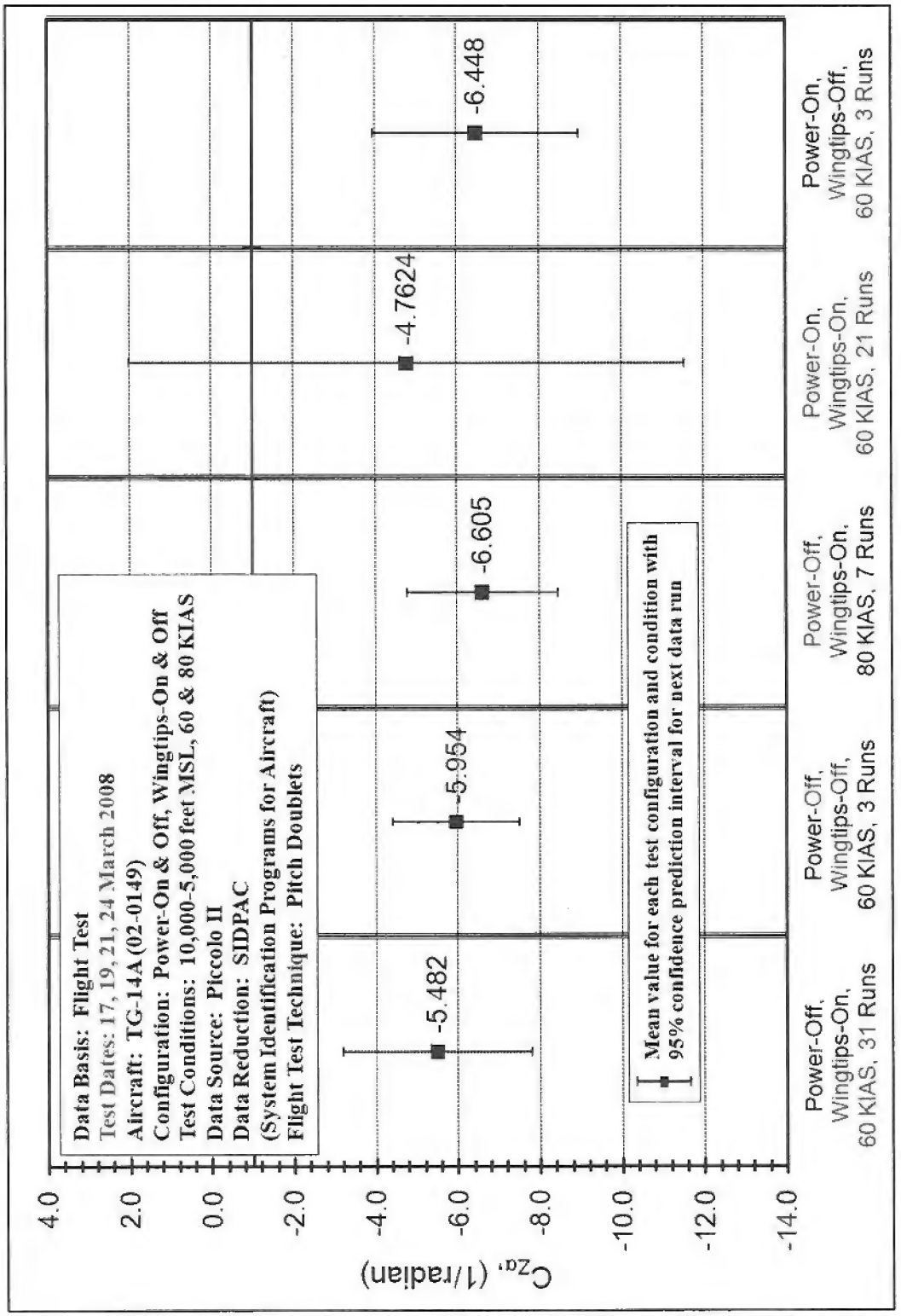

Figure F-68. $C_{z\alpha}$ from all test conditions with 95% confidence intervals

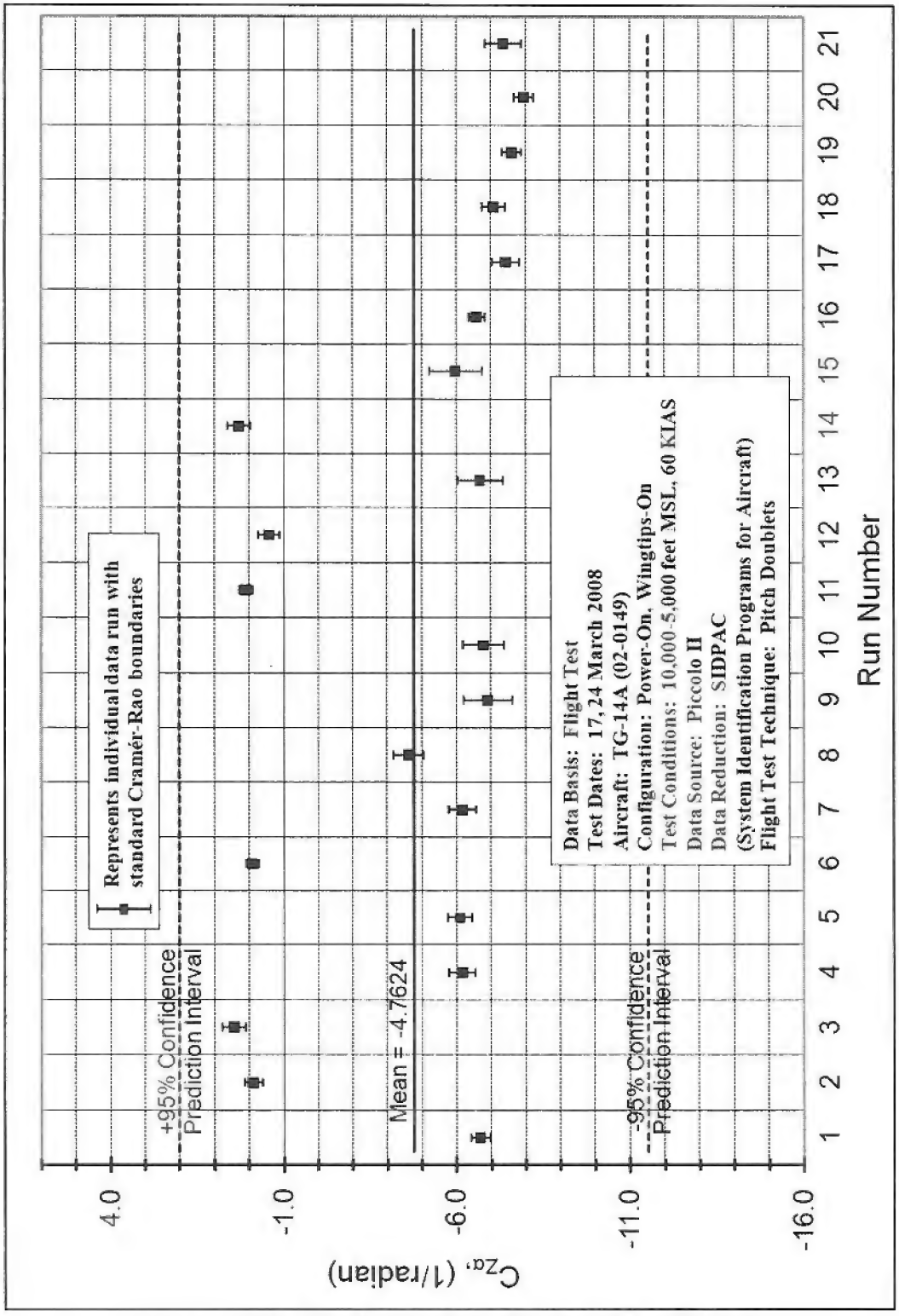

Figure F-69. $C_{z\alpha}$ (Power-On, Wingtips-On,60 KIAS)

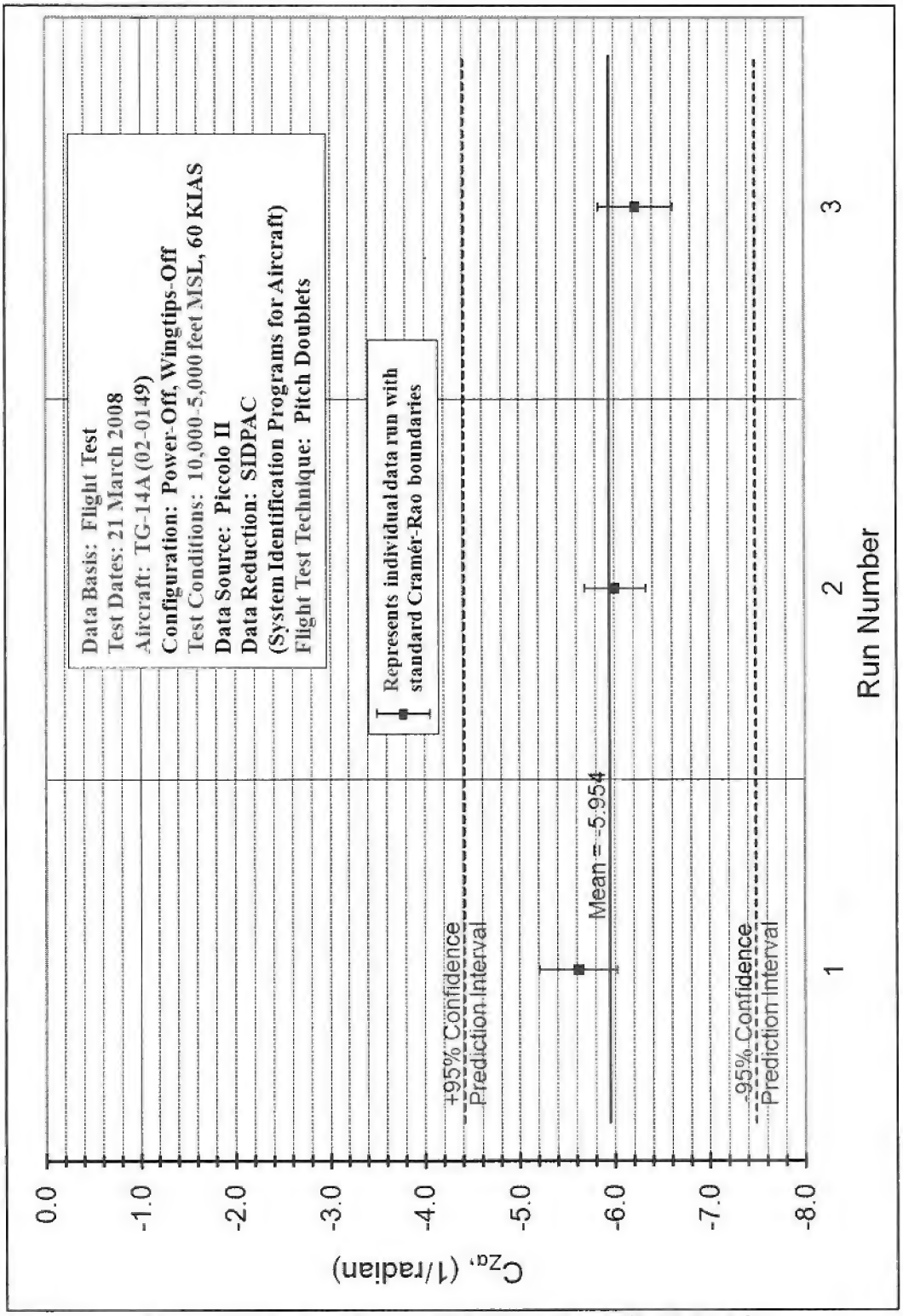

Figure F-70. $C_{z\alpha}$ (Power-Off, Wingtips-Off, 60 KIAS)

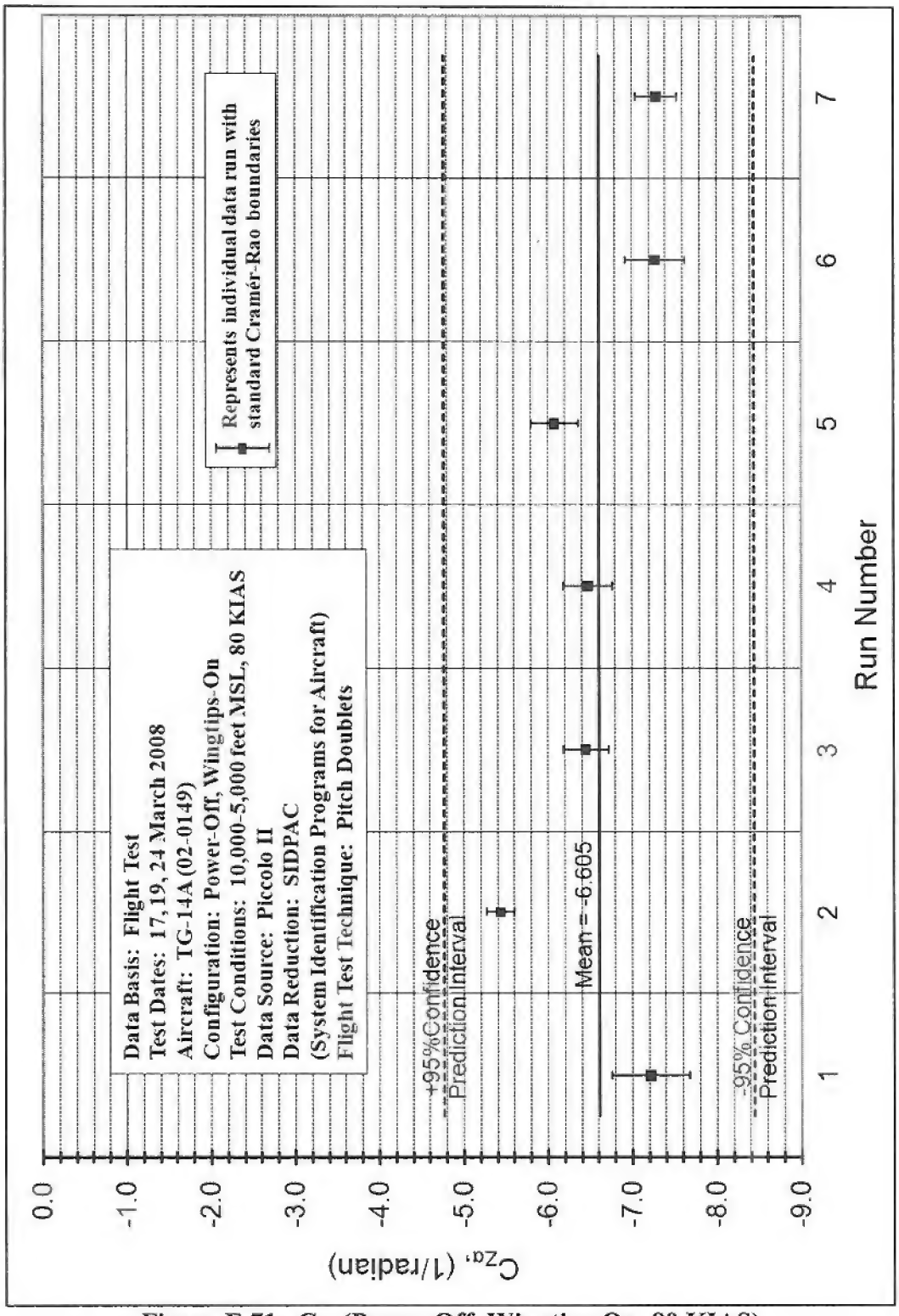

Figure F-71. $C_{z\alpha}$ (Power-Off, Wingtips-On, 80 KIAS)

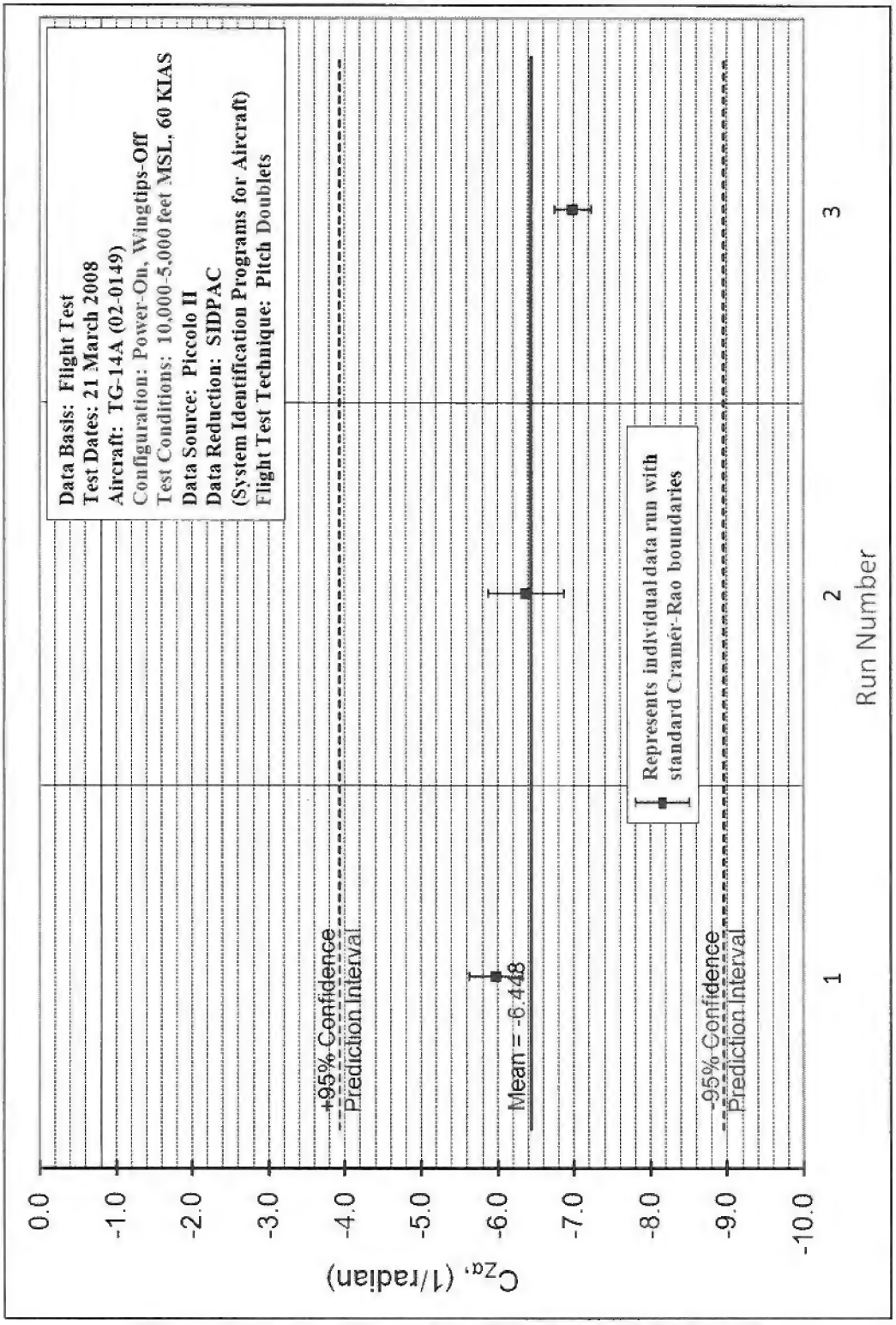

Figure F-72. $C_{z\alpha}$ (Power-On, Wingtips-Off, 80 KIAS)

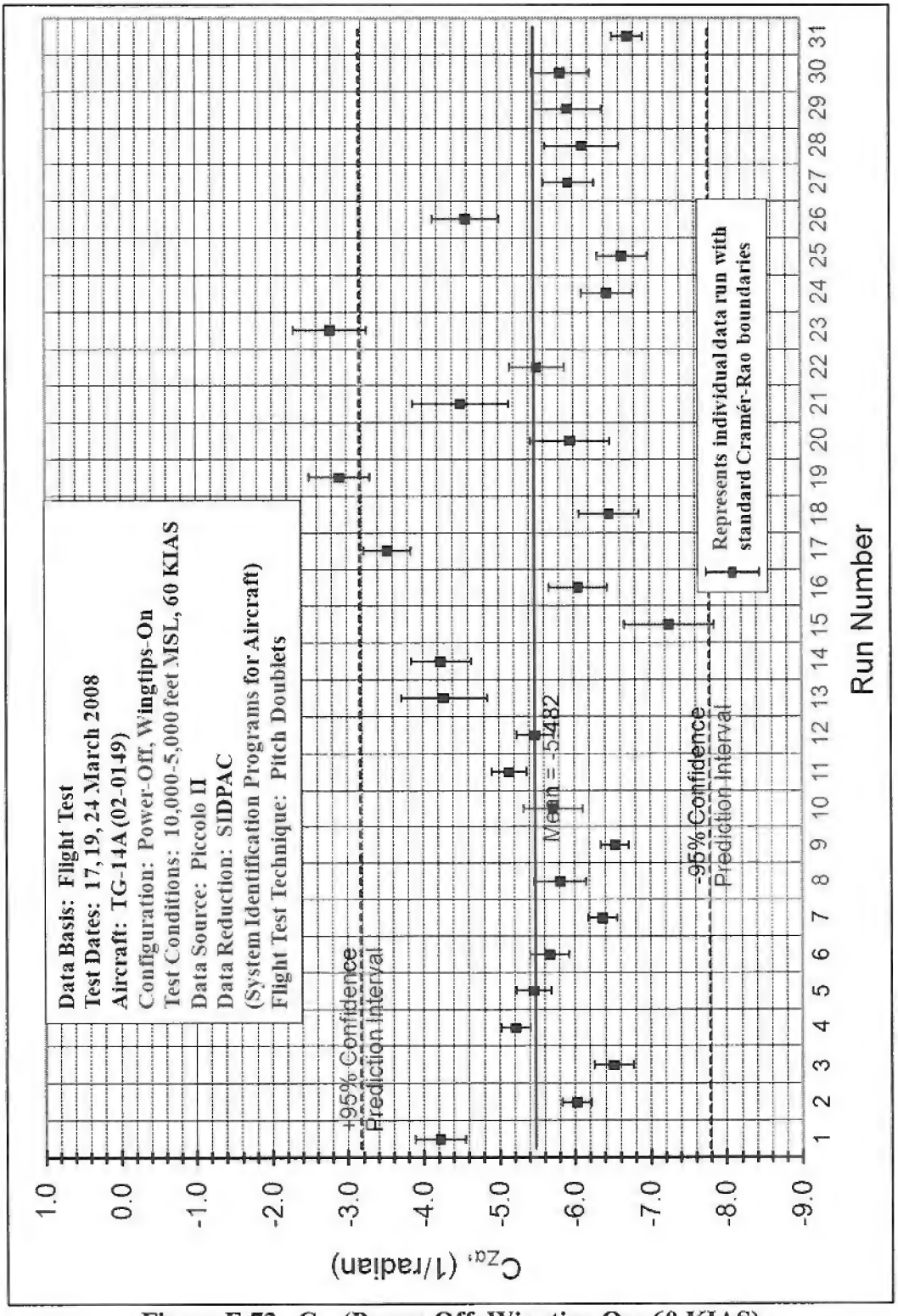

Figure F-73. $C_{z\alpha}$ (Power-Off, Wingtips-On, 60 KIAS)

APPENDIX G –PREDICTED RESPONSE

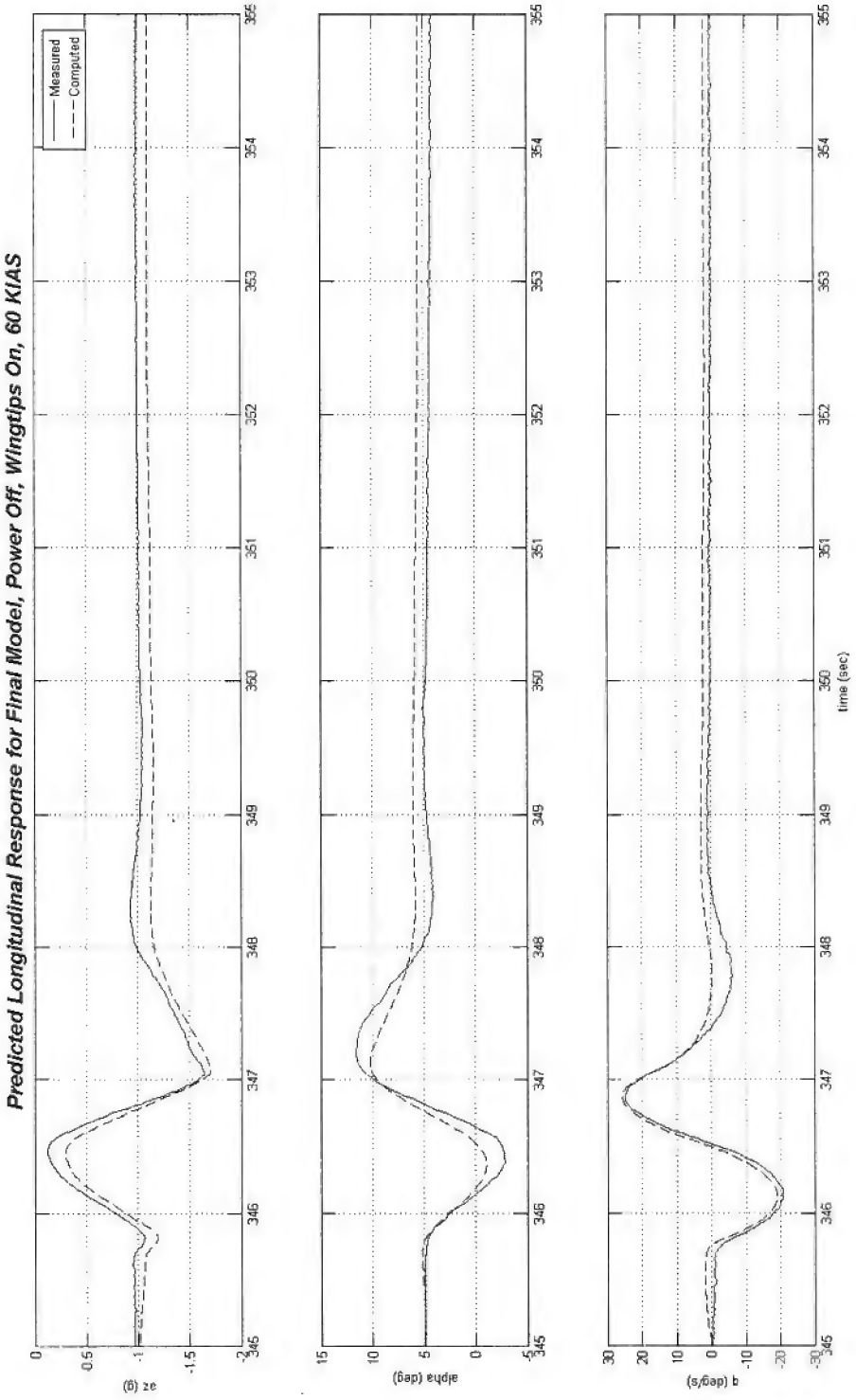

Figure G-1. Predicted Longitudinal Response (Power-Off, Wingtips-On, 60 KIAS)

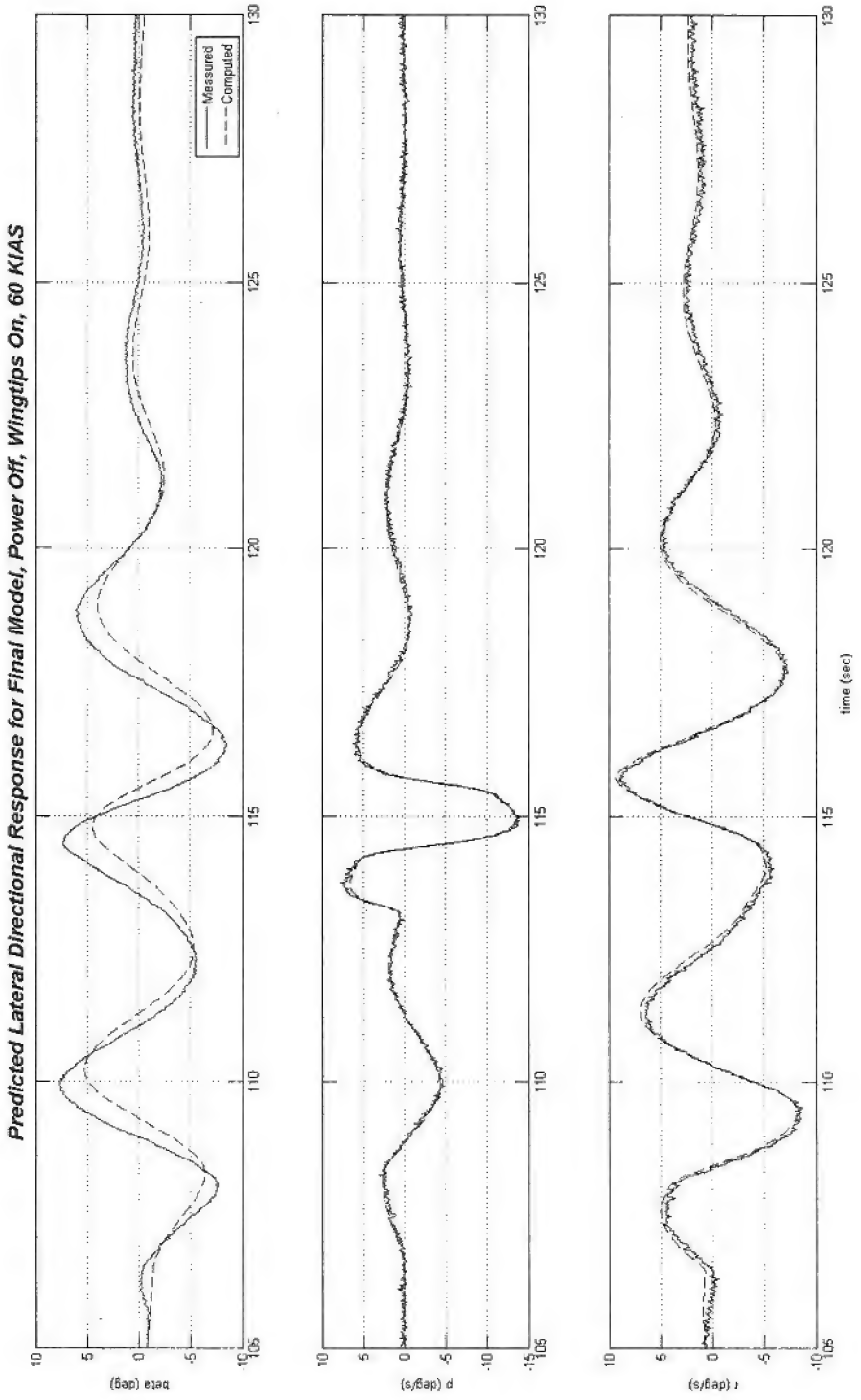

Figure G-2. Predicted Lateral Response (Power-Off, Wingtips-On, 60 KIAS)

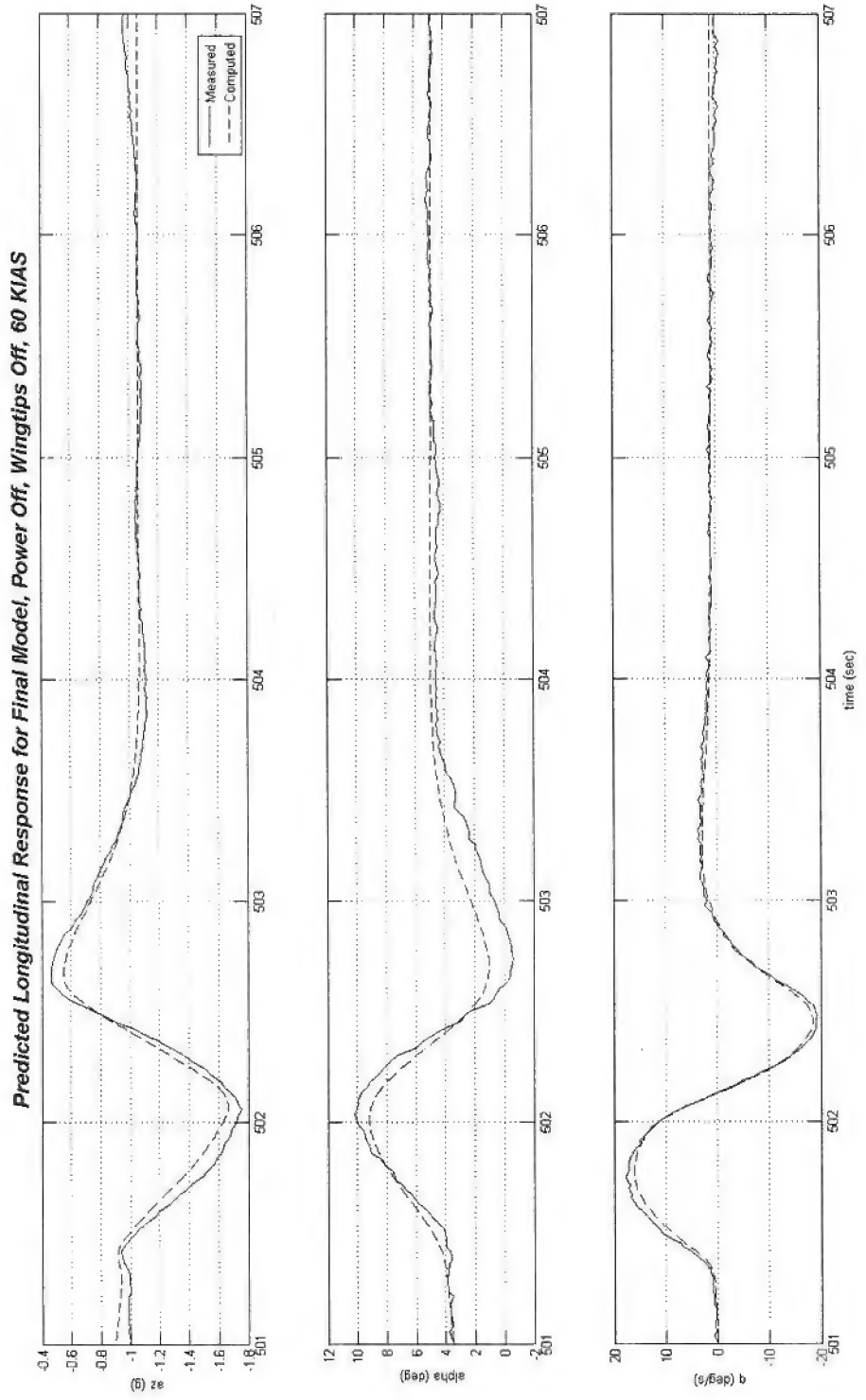

Figure G-3. Predicted Longitudinal Response (Power-Off, Wingtips-Off, 60 KIAS)

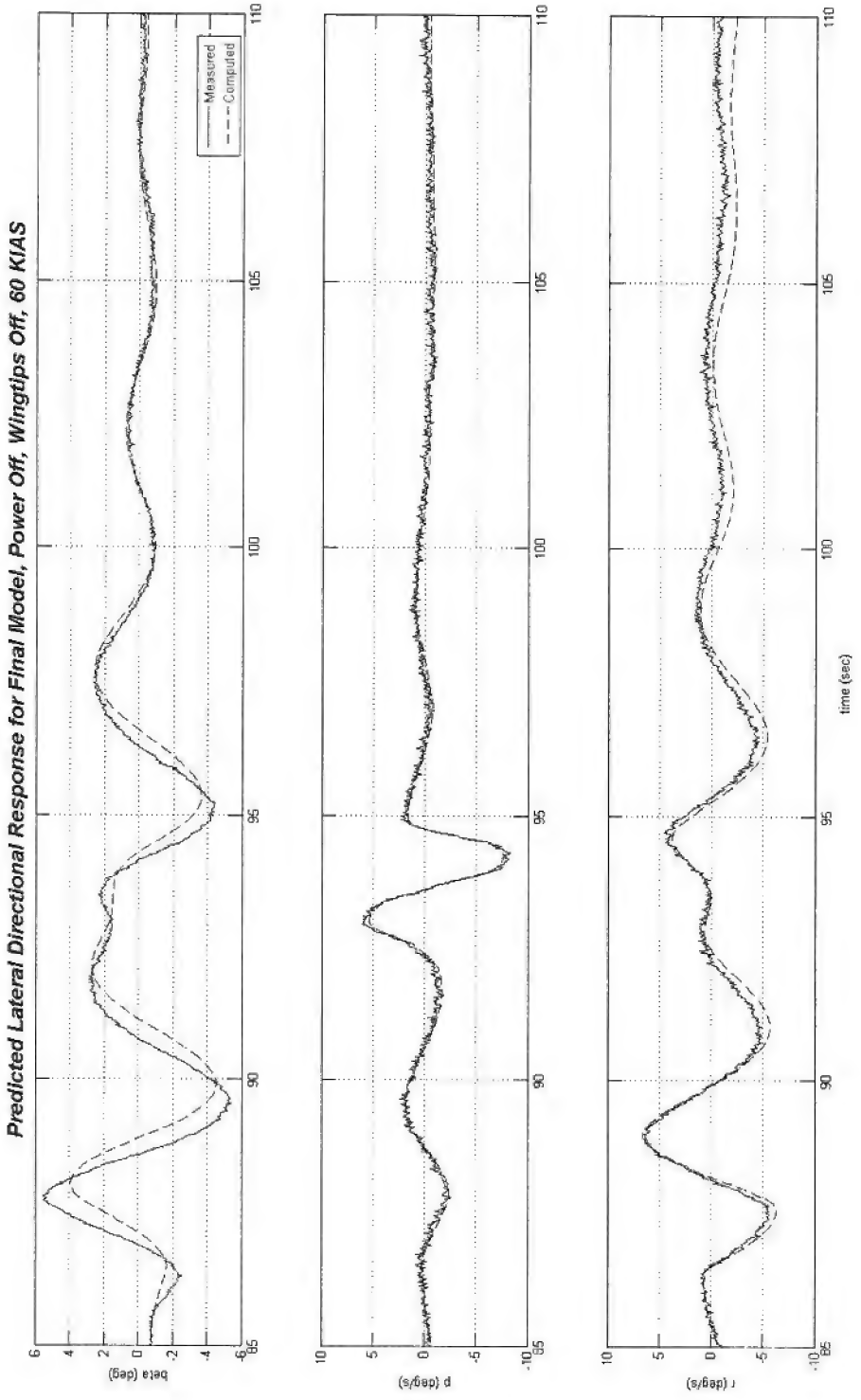

Figure G-4. Predicted Lateral Response (Power-Off, Wingtips-Off, 60 KIAS)

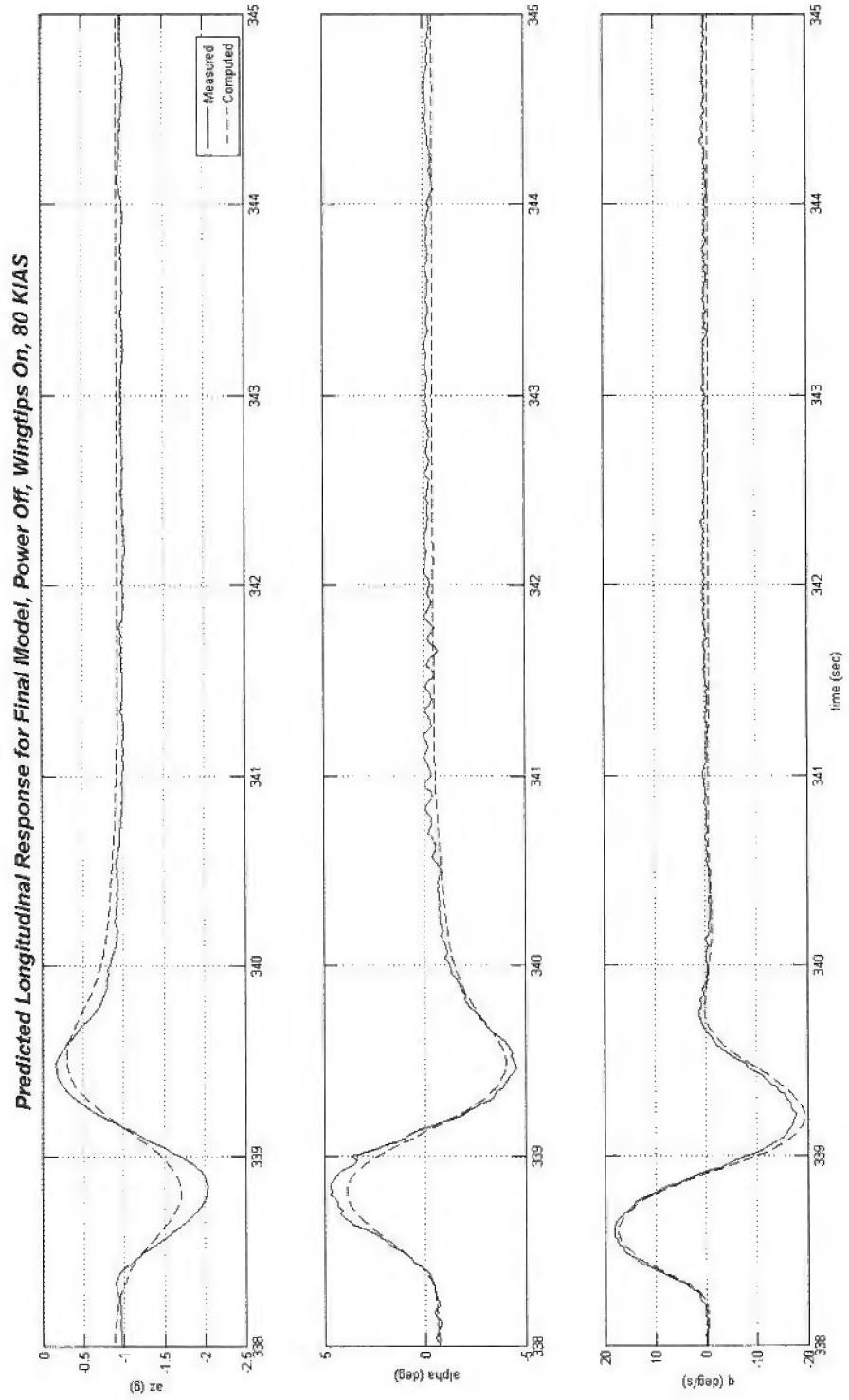

Figure G-5. Predicted Longitudinal Response (Power-Off, Wingtips-On, 80 KIAS)

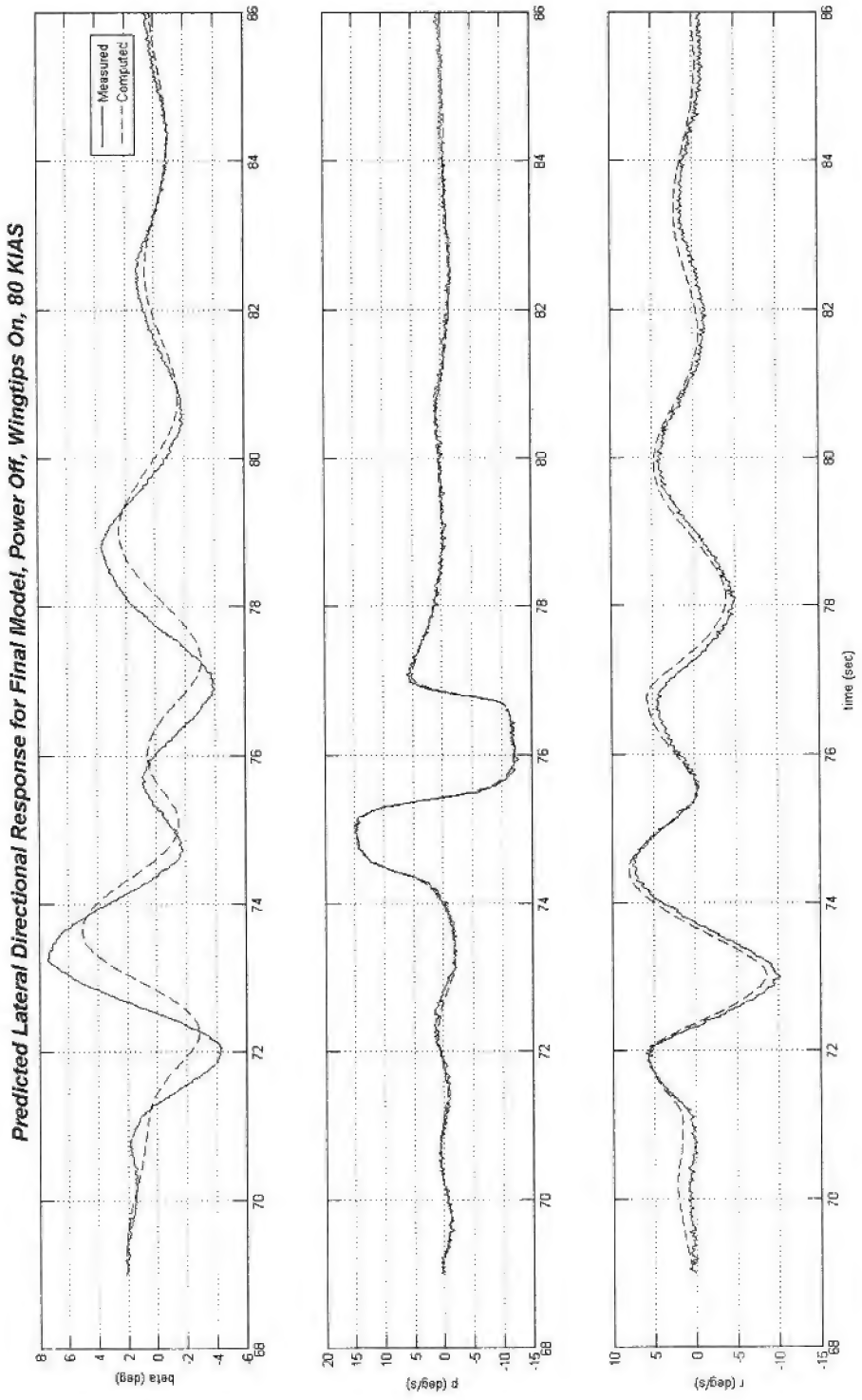

Figure G-6. Predicted Lateral Response (Power-Off, Wingtips-On, 80 KIAS)

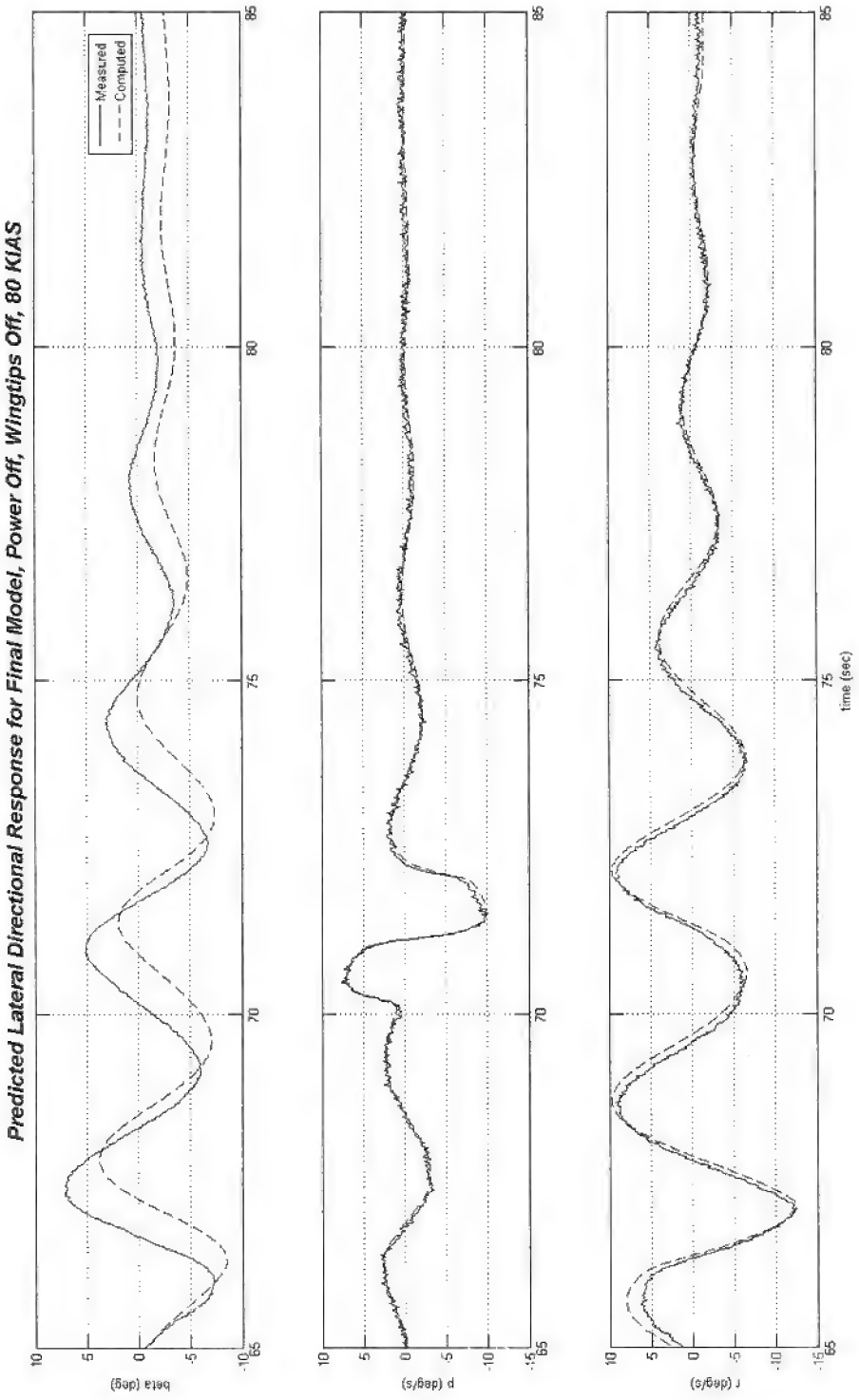

Figure G-7. Predicted Lateral Response (Power-Off, Wingtips-Off, 80 KIAS)

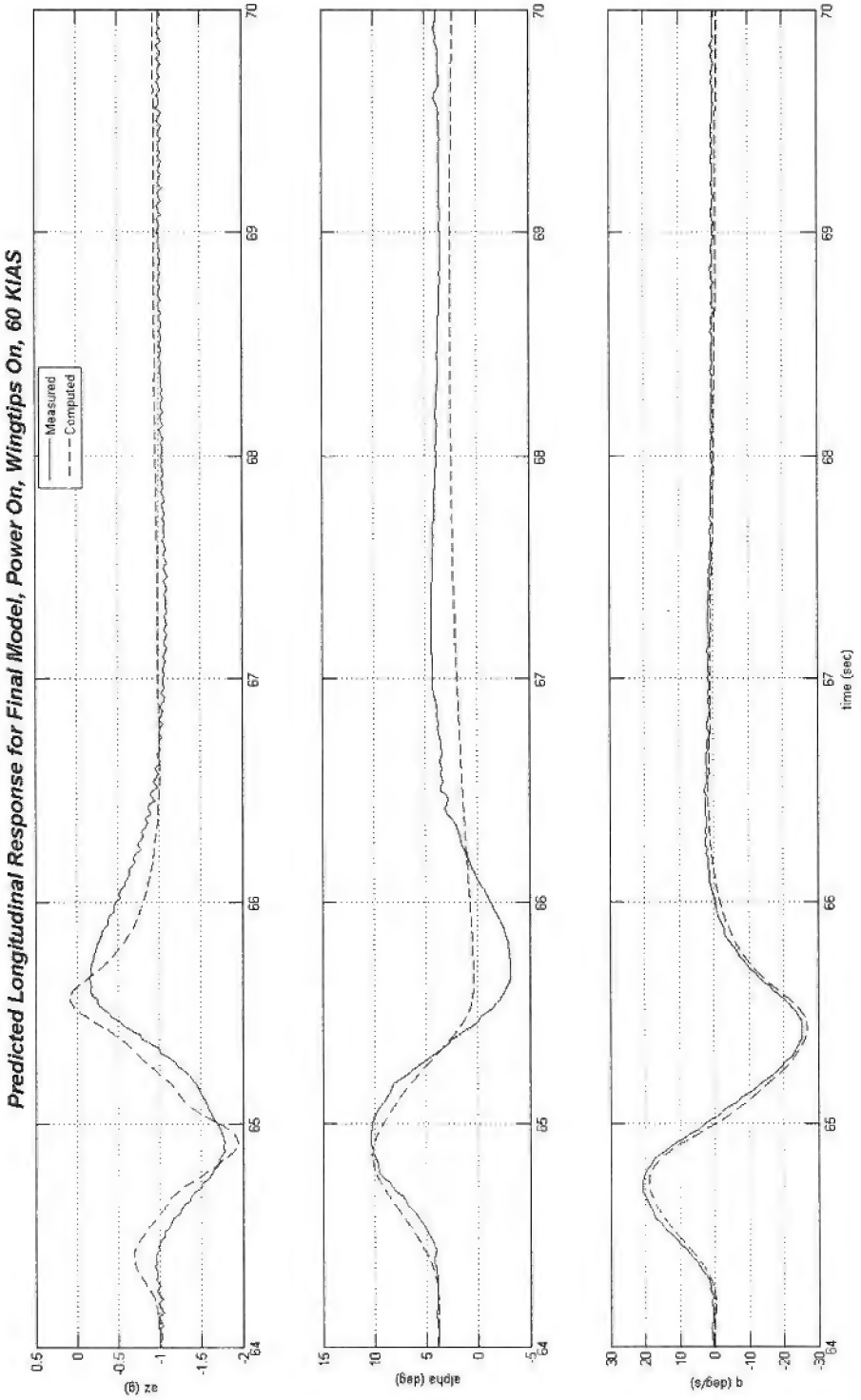

Figure G-8. Predicted Longitudinal Response (Power-On, Wingtips-On, 60 KIAS)

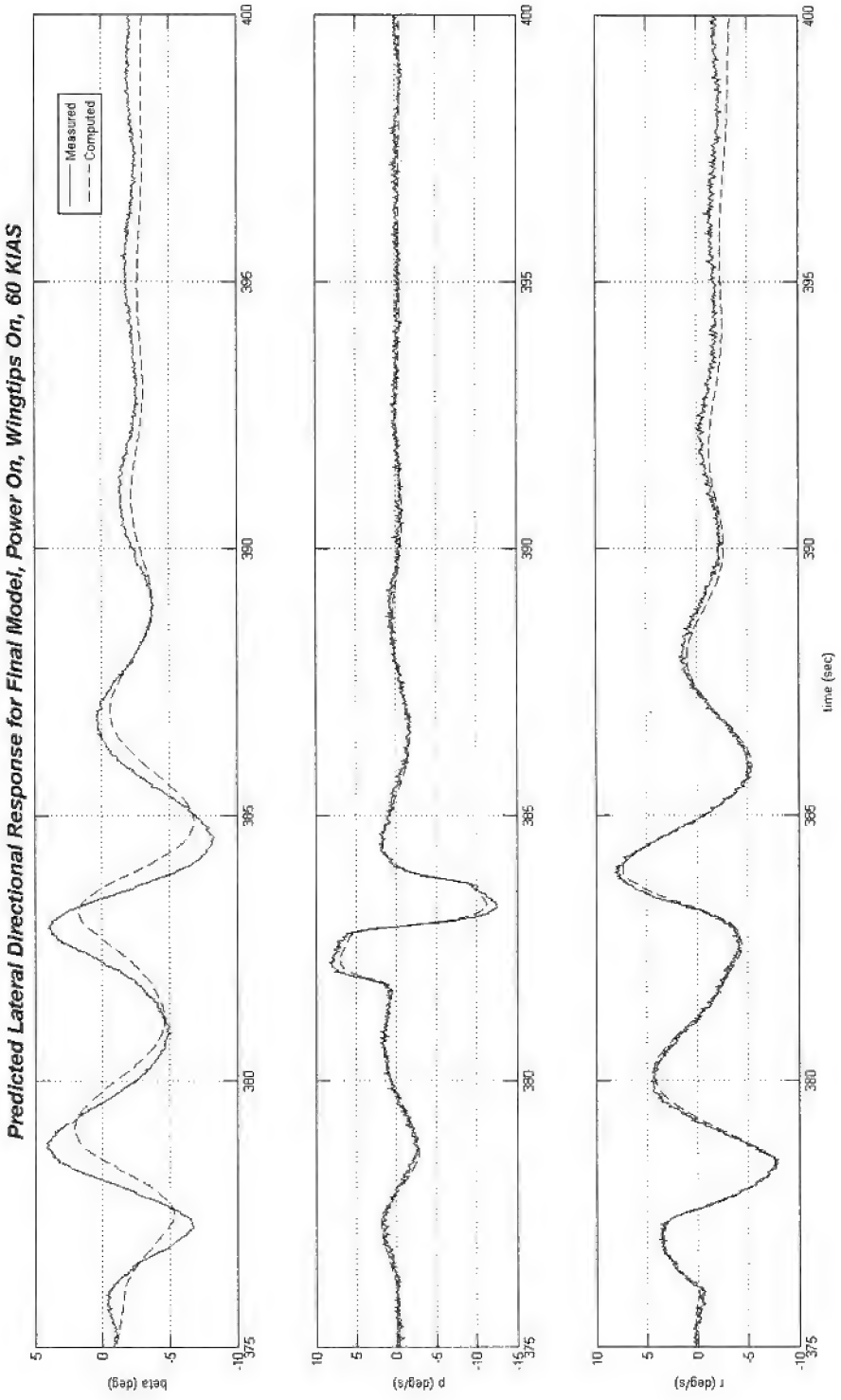

Figure G-9. Predicted Lateral Response (Power-On, Wingtips-On, 60 KIAS)

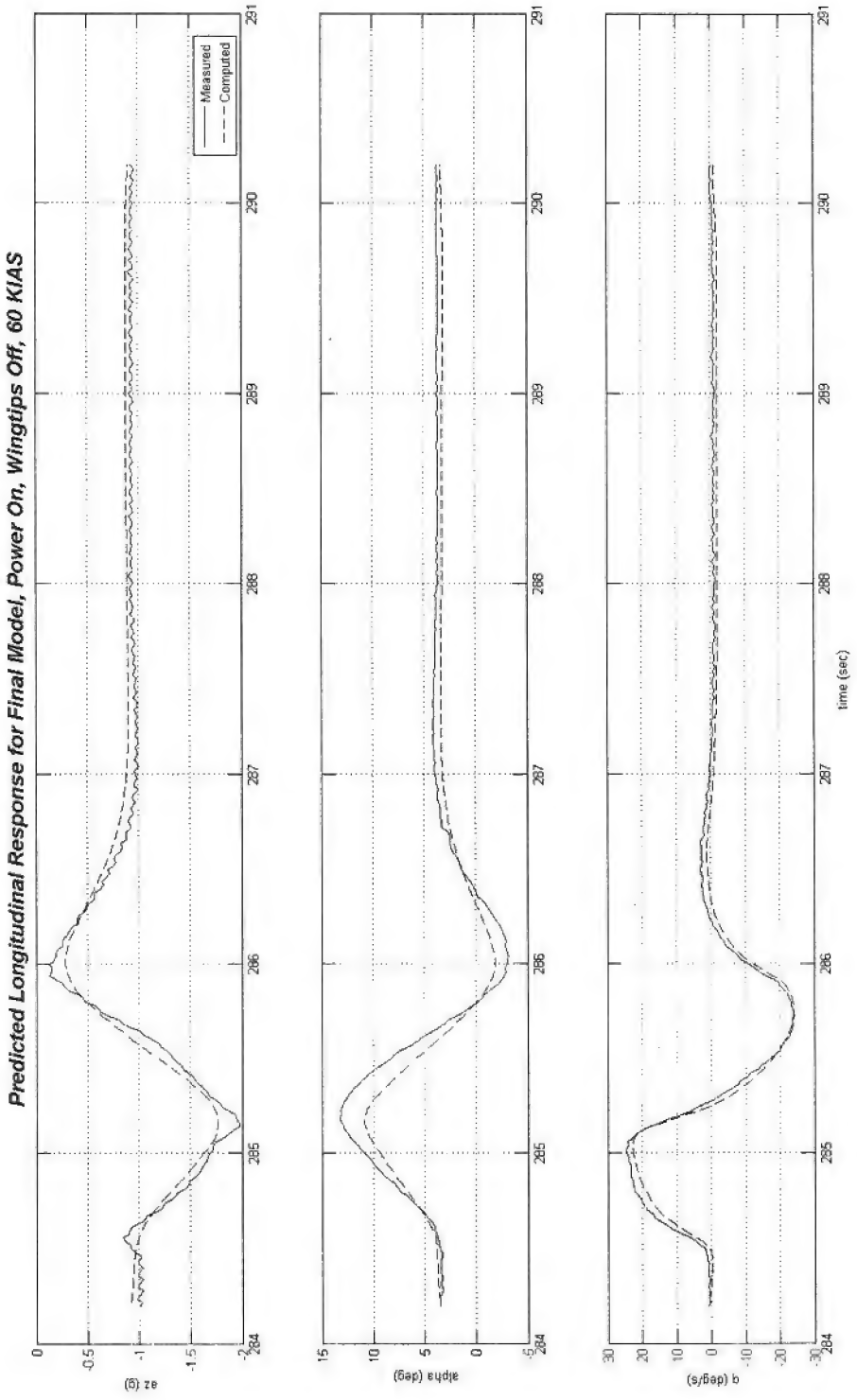

Figure G-10. Predicted Longitudinal Response (Power-On, Wingtips-Off, 60 KIAS)

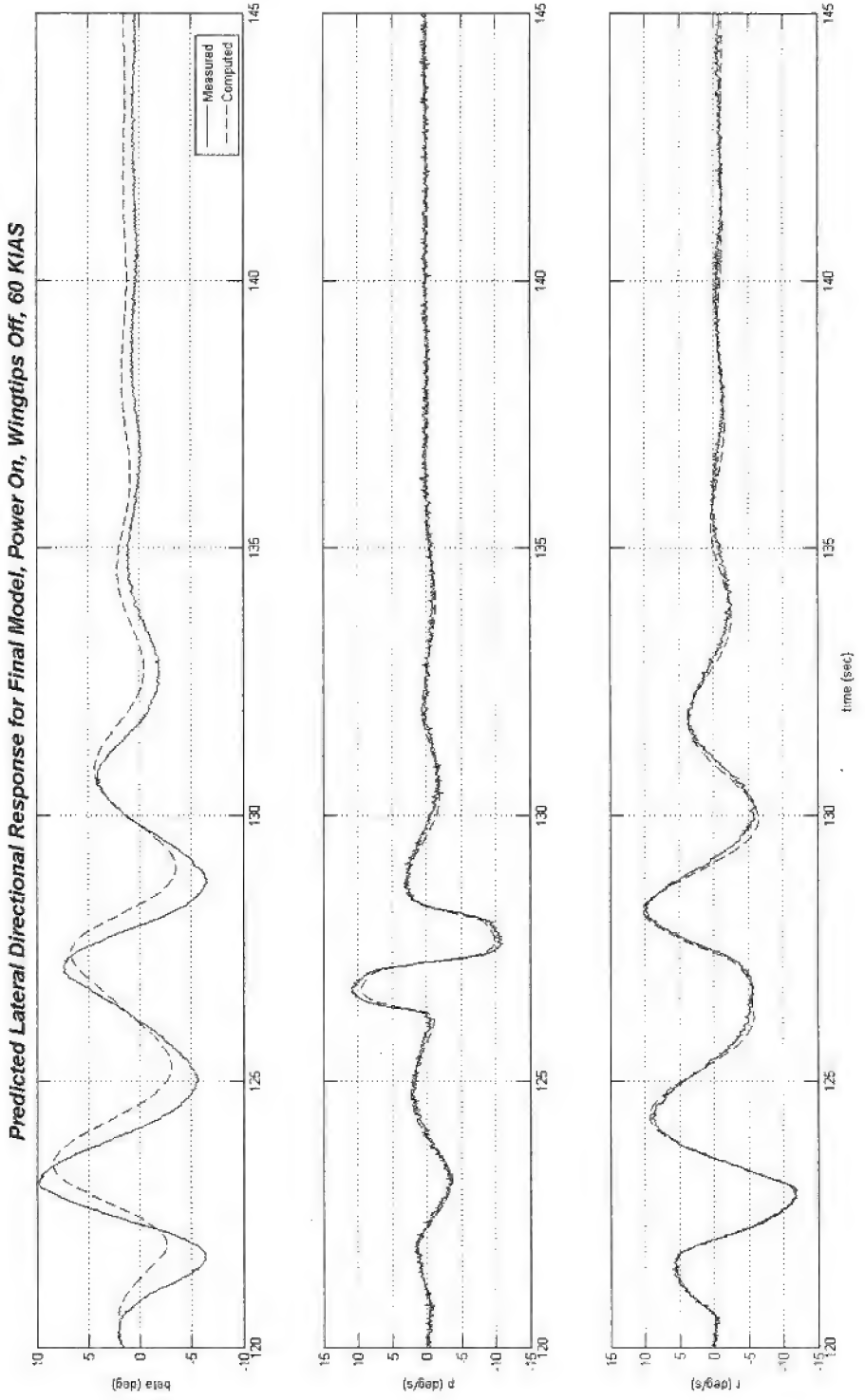

Figure G-11. Predicted Lateral Response (Power-On, Wingtips-Off, 60 KIAS)

APPENDIX H – FLIGHT LOG

Date	Aircrew	Test Points Flown
14-Mar	Maril, Leigh	Instrumentation Checkout, verification of Piccolo installation. Tower Flyby at 60 and 90 KIAS; Low Altitude Speed Course at 60 and 90 KIAS
17-Mar	Maril, Leigh	Cloverleaf FTT at 9,000 ft and 50, 60, 70, 80, 90 KIAS, Wingtips On
17-Mar	Maril, Leigh	Pitch Doublets at 10,000-8,000 ft, 60 KIAS, Wingtips On, Power Off
17-Mar	Traynor, Singh	Tower Flyby at 50, 60, 70, 80, 90 KIAS, Low Altitude Speed Course at 50, 60, 70, 80, 90, 100 KIAS, Wingtips On.
17-Mar	Traynor, Singh	Pitch Doublets at 10,000-7,000 ft, 60 KIAS Power On and Off, Wingtips On
18-Mar	Traynor, Singh	Yaw Roll Doublets at 10,000-7,000 ft, 60 KIAS Power On and Off, Wingtips On
19-Mar	Traynor, Singh	Pitch and Yaw Roll Doublets, 60 KIAS Power On and Off, Wingtips On
19-Mar	Traynor, Singh	Pitch and Yaw Roll Doublets, 60 KIAS Power On and Off and 80 KIAS Power Off, Wingtips On
19-Mar	Maril, Leigh	Pitch and Yaw Doublets, Level, 50,60,70,80,90 KIAS Power On, Wingtips On, 9,000 ft.
19-Mar	Maril, Leigh	Yaw Roll Doublets, 60 and 80 KIAS Power Off, 60 KIAS Power On, Wingtips On.
21-Mar	Traynor, Leigh	Cloverleaf FTT, Low Altitude Speed Course 50, 60, 70, 80, 90, 100 KIAS , 9,000 ft, Wingtips Off.
21-Mar	Traynor, Leigh	Pitch and Yaw Roll Doublets Wingtips Off 60 and 80 KIAS Power Off and 60 KIAS Power On, Wingtips Off.
24-Mar	Traynor, Leigh	Pitch and Yaw Roll Doublets Wingtips On 60 and 80 KIAS Power Off and 60 KIAS Power On, Wingtips On.
24-Mar	Traynor, Marlin	Cloverleaf FTT at 50-90 KIAS and 5,000-10,000 ft, Wingtips On
24-Mar	Traynor, Marlin	Cloverleaf FTT at 50-90 KIAS and 5,000-10,000 ft, Wingtips On
25-Mar	Maril, Marlin	Pitch and Yaw Roll Doublets at 10,000-7,000 ft, 60 KIAS Power Off and Wingtips On
25-Mar	Maril, Marlin	Pitch and Yaw Roll Doublets at 10,000-7,000 ft, 60 KIAS Power Off and Wingtips On
27-Mar	Traynor, Marlin	Pitch and Yaw Roll Doublets at 10,000-7,000 ft, 60 KIAS Power Off and Wingtips On
28-Mar	Maril, Marlin	Cloverleaf FTT at 55-65 KIAS and 5,000-10,000 ft, Wingtips On
28-Mar	Maril, Marlin	Cloverleaf FTT at 55-65 KIAS and 5,000-10,000 ft, Wingtips On

APPENDIX I – LIST OF ABBREVIATIONS, ACRONYMS, AND SYMBOLS

Abbreviation	Definition	Units
AFOSR	Air Force Office of Scientific Research	--
a_x	X acceleration	ft/s2
a_y	Y acceleration	ft/s2
a_z	Z acceleration	ft/s2
C_l	Roll moment coefficient	--
C_{lp}	Roll damping	1/rad
$C_{l\beta}$	Dihedral	1/rad
$C_{l\delta a}$	Aileron Control Power	1/rad
C_{l0}	Roll Moment Bias	--
C_m	Pitching Moment Coefficient	--
C_{mq}	Pitch Damping	1/rad
$C_{m\alpha}$	Longitudinal Static Stability	1/rad
$C_{m\delta e}$	Elevator Control Power	1/rad
C_{m0}	Pitching Moment Bias	--
C_n	Yawing Moment Coefficient	--
C_{nr}	Yaw Damping	1/rad
$C_{n\beta}$	Weathercock Stability	1/rad
$C_{n\delta r}$	Rudder Control Power	1/rad
C_{n0}	Yawing Moment Bias	--
C_x	Chord Force Coefficient	--
C_y	Side Force Coefficient	--
C_{yp}	Change in Sideforce due to Roll Rate	1/rad
C_{yr}	Change in Sideforce due to Yaw Rate	1/rad
$C_{y\beta}$	Change in Sideforce dur to Sideslip	1/rad
C_{y0}	Side Force Bias	--
C_z	Normal Force Coefficient	--
C_{zq}	Change in Normal Force Due to Pitch Rate	1/rad
$C_{z\alpha}$	Normal Force due to Angle of Attack	1/rad
$C_{z\delta e}$	Normal Force due to Elevator	1/rad
C_{z0}	Normal Force Bias	--
FTT	Flight Test Technique	--
PPCL	Propeller Pitch Control Lever	--
PTI	Programmed Test Input	--
p	Roll Rate	deg/s
q	Pitch Rate	deg/s
r	Yaw Rate	deg/s
SIDPAC	System Identification Programs For Aircraft	--
TMP	Test Management Project	--
TPS	Test Pilot School	--
V	Airspeed	ft/s
α	Angle of Attack	deg
β	Angle of Sideslip	deg

Abbreviation	Definition	Units
ΔH_{pc}	Altitude Position Correction	ft
ΔV_{pc}	Airspeed Position Correction	knots
θ	Pitch Attitude	deg
φ	Roll Angle	deg
ψ	Heading Angle	deg

APPENDIX J – DISTRIBUTION LIST

For "onsite" distribution:

812 TSS/ENTL 307 E Popson Ave, Bldg 1400, Rm 110 Edwards AFB CA 93524-6630	3
USAF TPS/EDT Attn: Mr Gary Aldrich 220 S Wolfe Ave, Bldg 1220 Edwards AFB CA 93524-6485	2
USAF TPS/CS Attn: Ms Dorothy Meyer 220 S Wolfe Ave, Bldg 1220 Edwards AFB CA 93524-6485	2
Maj Chad Ryther PSC Box 1998 20 W Popson Edwards AFB CA 93524	1
James Murray NASA DFRC M/S D-2228 Edwards, CA 93523	1
Maj Rotem Maril 23 Eagle Ct Edwards AFB CA 93523	1
Maj Devin Traynor 40 Blackbird Edwards AFB CA 93523	1
Wg Cdr Gyandeep Singh 30 Hercules St Edwards AFB CA 93523	1
Capt Elliott Leigh 27 Eagle Ct Edwards AFB CA 93523	1

Capt Michael Marlin
1038 Lovell Way
Edwards AFB CA 93523 1

For "offsite" distribution:

Dr. Hermann F. Fasel
The University of Arizona
Aerospace and Mechanical Engineering
PO Box 210119
Tucson AZ 85721-0119 1

AFRL/AFOSR
Attn: Dr. John Schmisseur
875 N Randolph St
Ste 325 Rm 3112
Arlington VA 22203 1

Defense Technical Information Center (DTIC)
8725 John J. Kingman Rd, Ste 0944
ATTN: Willis Smith (DTIC-OCA)
Fort Belvoir, VA 22060-6218 1